Evaluation of the GLAST-CreERT2/loxP system to knock out receptor proteins in mouse astrocytes

Dissertation

zur Erlangung des akademischen Grades
des Doktors der Naturwissenschaften (Dr. rer. nat.)
der Medizinischen Fakultät, Institut für Physiologie
der Universität des Saarlandes

vorgelegt von

Hannah Maria Jahn
geboren in Braunschweig

Homburg
Februar 2015

First referee: Frank Kirchhoff
Professor of Molecular Physiology
Department of Molecular Physiology
Institute of Physiology
University of Saarland
Building 58
66421 Homburg, Germany
Email: frank.kirchhoff@uks.eu

Second referee: Alexei Verkhratsky
Professor of Neurophysiology
Faculty of Life Sciences
The University of Manchester
1.124 Stopford Building
Oxford Road
Manchester M13 9PT, UK
Email: alex.verkhratsky@manchester.ac.uk

Declaration

I hereby declare that this thesis “Evaluation of the GLAST-CreERT2/loxP system to knock out receptor proteins in mouse astrocytes” has been written independently, with no other aids or sources than quoted by me.

Homburg, February 2015

Table of contents

List of Figures

Introduction

Results

Part I

Part II

Discussion

Material and Methods

Supplments

List of Tables

Abbreviations

AB	Antibody
ACSF	artificial cerebral spinal fluid
ADPβS	adenosine 5′-O-2-thiodiphosphate
BLBP	brain lipid-binding protein
bp	base pair(s)
BSA	bovine serum albumin
bs	brainstem
Ca^{2+}	calcium
cb	cerebellum
Cc	corpus callosum
CNP	2',3'-cyclic-nucleotide 3'-phosphodiesterase
CNS	central nervous system
CNQX	6-cyano-7-nitroquinoxaline-2,3-dione
ctx	cortex
DG	dentate gyrus
DNA	deoxyribonucleic acid
dpi	days post (first) injection of tamoxifen
ECL	enhanced chemiluminescence
EDTA	ethylenediaminetetraacetic acid
ENDX	endoxifen
ER	estrogen receptor
EGFP	enhanced green fluorescent protein
EtOH	ethanol
EYFP	enhanced yellow fluorescent protein
FACS	fluorescence activated cell sorting
GC	granule cell
GDNF	Glial cell line-derived neurotrophic factor
GFAP	glial fibrillary acidic protein
GS	glutamine synthase
hp	hippocampus
HPLC-MS	high-performance liquid chromatography mass spectrometry
HRP	horseradish peroxidase
HSP	heat shock protein
IL-6	interleukin-6
IP	intraperitoneal
IP_3	Inositol 3 phosphate
4-OHT	4-hydroxytamoxifen
kb	kilo base pairs
kDa	kilodalton
LoxP	locus of crossover of the bacteriophage P1
mpi	month post (first) injection
2-ME	β-mercaptoethanol
MBP	myelin basic protein
2-MeSATP	2-Methylthioadenosine triphosphate tetrasodium salt
MRS 2365	[[(1*R*,2*R*,3*S*,4*R*,5*S*)-4-[6-Amino-2-(methylthio)-9*H*-purin-9-yl]-2,3-dihydroxybicyclo[3.1.0]hex-

	1-yl]methyl] diphosphoric acid mono ester trisodium salt
MRS 2179	2'-Deoxy-N^6-methyladenosine 3',5'-bisphosphate tetrasodium salt
MRS 2279	(1*R**,2*S**)-4-[2-Chloro-6-(methylamino)-9*H*-purin-9-yl]-2 (phosphonooxy)bicycle [3.1.0]hexane-1-methanol dihydrogen phosphate ester diammonium salt
MRS 2500	(1*R**,2*S**)-4-[2-Iodo-6-(methylamino)-9*H*-purin-9-yl]-2-(phosphonooxy)bicycle [3.1.0]hexane-1-methanol dihydrogen phosphate ester tetraammonium salt
n	number
Na^+	sodium
NG2	nerve/glia antigen-2
NFkb	nuclear factor kappa-light-chain-enhancer of activated B cells)
Na_2HPO_4	disodiumhydrogenphosphate
NaH_2PO_4	sodiumdihydrogenphosphate
NH_4Ac	ammonium acetate
NDMT	N-desmethyltamoxifen
NMDA	*N*-Methyl-D-aspartic acid
NMDAR	*N*-Methyl-D-aspartic acid receptor
n.s	non-significant
ob	olfactory bulb
opt. n.	optic nerve
$P2Y_1R$	$P2Y_1$ receptor
PB	sodium phosphate buffer
PBS	phosphate buffered saline
PBS-T	PBS-tween-20
PCR	polymerase chain reaction
PDGFR	platelet-derived growth factor receptor
PIPES	piperazine-N,N0-bis(ethanesulfonic acid); 1,4-piperazinediethanesulfonic acid
PPADS	pyridoxalphosphate-6-azophenyl-2',4'-disulfonic acid
SDS-PAGE	SDS-polyacrylamide gel electrophoresis
SEM	standard error of the mean
SVZ	subventricular zone
TAM	tamoxifen
TgH	transgenic by homologous recombination
TgN	transgenic by non-homologous recombination
TNFα	tumor necrosis factor α
UBP141	(2*R**,3*S**)-1-(Phenanthrenyl-3-azine-2,3-dicarboxylic acid
VGlut1	vesicular glutamate transporter I
WT	wild-type

1 Summary

Astrocytes express a variety of transmitter receptors. To clarify their function *in vivo* cell type specific knockout models have been generated which enable the ablation of targeted receptors. To faithfully correlate an observed phenotype to a specific brain region and cell type the efficiency and specificity of recombination of floxed sequences is of high relevance.

In the current study we investigated in a quantitative manner recombination events of the astrocyte-specific and inducible GLAST-CreERT2 mouse line (Mori et al., 2006) throughout the brain. In the cerebellum and cortex, we quantified the increase of recombined receptor genes and determined that three injections of tamoxifen and 21 days are efficient to achieve maximum DNA recombination. Subsequently we quantified the loss of intact alleles after induction of Cre activity. Two floxed receptor alleles (*p2ry1*, *gabbr1*) and the tdTomato reporter allele showed no significant differences in regard to DNA recombination efficiencies and no difference between genders. For one targeted receptor allele (*grin1*) we observed significantly less recombination events independent of the age of injected mice and distance between LoxP sites. Furthermore, the same locus displayed efficient recombination by use of an oligodendrocyte-specific Cre driver line. In conclusion the GLAST-CreERT2/loxP system was highly efficient to recombine floxed sequences but epigenetic regulations, like silencing leading to closed chromatin structures and difficulties for the Cre enzyme to access loxP sites have to be investigated for each floxed target gene individually.

However, GLAST+ cells were equated as astrocytes and the recombination efficiencies as a quantitative measure of astrocytes in the respective brain regions. We concluded that in a brain of a young adult mouse 20 % in the brainstem, 8 % in the cerebellum, 22 % in the cortex, 30 % in the hippocampus and 31 % in the optic nerve account for astrocytes.

In addition, we confirmed by use of the tdTomato reporter mice that predominantly astrocytes are targeted and the difficulty to investigate brain regions affected by adult neurogenesis because here GLAST+ progenitor cells differentiate into granule cells and interneurons. Furthermore FACS sorting of tdTomato reporter cells revealed a higher and lower fluorescent population, which could be appointed to astrocytes and microglia respectively.

In the second part we addressed the role of astroglial NMDA receptors with special emphasis on the cortex by generating conditional mutants where the obligatory GluN1 subunit is ablated. Efficient reduction of GluN1 mRNA was determined in isolated cortical astrocytes by FACS sorting. Furthermore, synaptically evoked currents of patched cortical astrocytes lacking the GluN1 subunit showed no sensitivity to NMDA receptor antagonists. Under physiological conditions astrocytes expressed NMDA receptors in low densities. Expression was upregulated after brain injury suggesting an important role for astroglial NMDA receptors under pathological conditions. In addition we provided further evidence at the mRNA and protein level that the astroglial NMDA receptor incooperates the GluN2C subunit.

Finally we investigated the function of purinergic astroglial $P2Y_1$ receptors in the brain by generating conditional knockout mice where the receptor could be efficiently ablated in a timely controlled manner. Our findings suggest that astrocytes are the predominat cell type in the brain expressing the $P2Y_1$ subtype. In the cerebellum $P2Y_1$ receptor expression is not restricted to young ages, but is disposable for Purkinje cell-parallel fiber synapse formation or maintenance.

Zusammenfassung

Astrozyten exprimieren eine Vielzahl an Transmitterrezeptoren. Um die funktionelle Bedeutung *in vivo* zu untersuchen, wurden Zelltyp-spezifische knock-out Modelle generiert. Diese erlauben eine kontrollierte Exzision von Genabschnitten von Rezeptoren. Um den beobachteten Phenotyp auf eine bestimmte Hirnregion und Zelltyp zurückführen zu können, ist Effizienz und Spezifität der DNA Rekombination von hoher Bedeutung.

In dieser Studie wurden Rekombinationsereignisse durch die Astrozyten-spezifische und Tamoxifen-induzierbare GLAST-CreERT2 Mauslinie (Mori et al., 2006) quantitativ untersucht. Im Cerebellum und Cortex wurde die Zunahme von rekombinierten Rezeptorgenen quantifiziert und festgestellt, dass drei Injektionen von Tamoxifen und 21 Tage ausreichen, um eine maximale Rekombinationseffizienz zu erreichen. Im Folgenden wurde die Abnahme von intakten Allelen nach Induktion der Cre Aktivität bestimmt. Zwei untersuchte Rezeptorgene (*p2ry1*, *gabbr1*) und das tdTomato Reportergen zeigten keine signifikanten Unterschiede in Bezug auf DNA Rekombiationseffizienzen bzw. Unterschiede zwischen Geschlechtern. Bei einem gefloxtem Rezeptorgen (*grin1*) wurde eine geringere Rekombinationseffizienz beobachtet unabhängig von dem Alter der injizierten Mäuse oder dem Abstand zwischen den loxP Stellen. Weiterhin zeigte derselbe Genlocus effiziente Rekombinationsereignisse wenn eine oligodendrozytenspezifische Cre Maus Linie benutzt wurde. Daraus kann abgeleitet werden, dass das GLAST-CreERT2/loxP System äußerst effizient gefloxte Genabschnitte in Astrozyten rekombiniert. Epigenetische Regulationen, wie posttrankriptionelles Gen-silencing das zu einer geschlossenen Chromatin Struktur und Schwierigkeiten für die Cre DNA Rekombinase den Lokus zu betreten führt, müssen für jedes gefloxte Gen individuell untersucht werden.

GLAST+ Zellen wurden mit Astrozyten gleichgesetzt und die Rekombinations-effizienz als quantitatives Maß für die Anzahl von Astrozyten per Hirnregion angenommen. In einer erwachsenen Maus besteht der Hirnstamm somit zu 20 %, das Cerebellum zu 8 %, der Cortex zu 22 %, der Hippocampus zu 30 % and der optische Nerv zu 31 % aus Astrozyten.

Zusätzlich wurde mit Hilfe der tdTomato Reporter Maus bestätigt, dass hauptsächlich Astrozyten von der DNA Rekombination betroffen sind und es schwierig ist Regionen der adulten Neurogenese zu untersuchen, da hier GLAST+ Vorläuferzellen rekombiniert werden und zu Interneuronen und Körnerzellen differenzieren. Weiterhin wurde bei FACS Experimenten mit tdTomato Reportermäusen zwei fluoreszente Populationen entdeckt, wobei die schwächer fluoreszente Population als Mikroglia und die stärker fluoreszente als Astrozyten identifiziert wurde.

Im zweiten Teil der Studie wurde die Rolle von astroglialen NMDA Rezeptoren mit Schwerpunkt auf dem Cortex untersucht. Dafür wurde in konditionalen Mausmutanten die obligatorische GluN1 Untereinheit inaktiviert. Eine effiziente Reduktion der GluN1 mRNA wurde in FACS sortierten kortikalen Astrozyten nachgewiesen. Zusätzlich zeigten gepatchte knockout Astrozyten keine Sensitivität gegenüber NMDA Rezeptor Antagonisten. Unter physiologischen Bedingungen exprimierten Astrozyten eine geringe Dichte an NMDA Rezeptoren. Die Expression war nach einer Hirnverletzung hochreguliert, was auf eine stärkere Rolle von NMDA Rezeptoren unter pathologischen Bedingungen hinweist.

Zusätzlich wurden weitere Indizien gefunden, dass astrogliale NMDA Rezeptoren die Untereinheit GluN2C inkooperieren.

Letztlich wurde die Funktion von purinergen astroglialen $P2Y_1$ Rezeptoren durch die Generierung eines konditionalen Mausmodells untersucht. Es konnte gezeigt werden, dass Astrozyten der primäre Zelltyp für die Expression von $P2Y_1$ Rezeptor mRNA im Gehirn darstellen. Im Kleinhirn wurde gezeigt, dass die Expression von $P2Y_1$ Rezeptoren nicht auf junges Alter limitiert ist. Desweiteren sind $P2Y_1$ Rezeptoren nicht an der Bildung bzw. Erhaltung von Purkinjezell-Parallel Faser - Synapsen beteiligt.

2 Introduction

The mammalian central nervous system (CNS), consisting of brain and spinal cord, is comprised of a heterogeneous population of cell types, classified into neurons and glia cells. Glial cells are divided into two groups the macro- and microglia. Astrocytes, oligodendrocytes and NG2 cells are considered as macroglia, derived from neuroepihelial cells.

Microglia derive from hematopoietic stem cells and migrate in early development to brain and spinal cord. They are phagocytic cells, constantly monitoring their environment, eliminating pathogens and apoptotic cells and mediate the initial immune responses after injury. They are referred to the resident immune cells of the CNS (Kettenmann et al., 2013).

Oligodendrocytes isolate electrically nerve cells from each other by wrapping myelin sheats around their axons, thereby controlling conduction velocity and contributing indirectly to synaptic plasticity and higher brain function. In addition, oligodendrocytes support and maintain long-term axonal integrity and survival, also independent of myelination probably through support of their associated axons with metabolites and tropic factors (Funfschilling et al., 2012; Lee et al., 2012). The underlying axon-glia support mechanisms are still not well understood (Saab et al., 2013).

NG2 glia are considered as oligodendrocyte precursor cells (OPCs), giving rise to oligodendrocytes throughout life (Huang et al., 2014). A subpopulation of NG2 glia in the immature brain also generates protoplasmic astrocytes. Even the neuronal fate of NG2 cells is debated. Besides their stem cell character a large population of NG2-expressing cells remains in the mature CNS and displays unique physiological properties, like synapse to neurons (Sakry et al., 2011).

Astrocytes were labeled as silent cells, since they do not communicate via electrical signals, bound to be simple supporting cells for neurons. Indeed astrocytes are metabolically coupled to neurons, providing them with lactate as a source of energy, maintaining their ionic environment, recycling their neurotransmitters and providing structural support. But they also respond to neuronal activity and sensory stimuli with spatially defined changes in the intracellular calcium and sodium concentration. Further they are able to modulate synaptic transmission through the release of gliotransmitters and control synapse formation. They regulate the blood flow and are an essential part of the blood brain barrier (Verkhratsky et al., 2014).

Neurons integrate input information and convey these signals in a precise manner within the neuronal network. This spatially and temporally controlled communication between millions of neurons is the scaffolding of movement, emotions, consciousness, memory and learning and also simply appearing functions like breathing. To manage this task, neurons are physically connected through specialized communication compartments, the synapses. At the presynapse electrical signals from the cell body are converted into chemical signals that are transferred and recognized by the postsynapse of a neighboring neuron. The connectome (connections of neurons via synapses) is built up during development of the CNS, but stays dynamic throughout the whole lifespan.

Taken together, glial cells still hold the job of the neuron supporting cells but nowadays their function is assumed to be far more complex and essential for proper brain function. Neurons

need their energy to transfer information via long distances throughout the brain. Glial cells seem within these processes more specialized and dynamic, showing multitasking abilities in responding to the demand of neurons, like provision of metabolites and transmitters and the modulation of the information process itself. In case of emergency/brain injury it's also glia cells which protect the more sensitive neurons and it has been shown that they are activated in neurodegenerative diseases, like Alzheimer's and Parkinson's disease (Charron et al., 2014; Lim et al., 2014). There is a growing recognition for the important role of glia in the normal and pathological brain. For each glial cell type immense research is needed to clarify their function within the complex system of the CNS.

2.1 Astrocytes, heterogeneity and information processing

Our research focuses on astrocytes, their receptor expression profile and its function in the physiological and pathological brain. Astrocytes have specialized perisynaptic astroglial processes (PAPs) surrounding synapses for modulation of synaptic transmission. In numerous studies it could be highlighted how essential these PAPs are for effective and reliable information processing at synapses (Hirrlinger et al., 2004; Perez-Alvarez et al., 2014; Reichenbach et al., 2010). Therefore astrocytic processes were added to the known picture of the synapse and the term tripartite synapse was created (Araque et al., 1999; Perea et al., 2009; Perez-Alvarez and Araque, 2013) (see Figure 1).

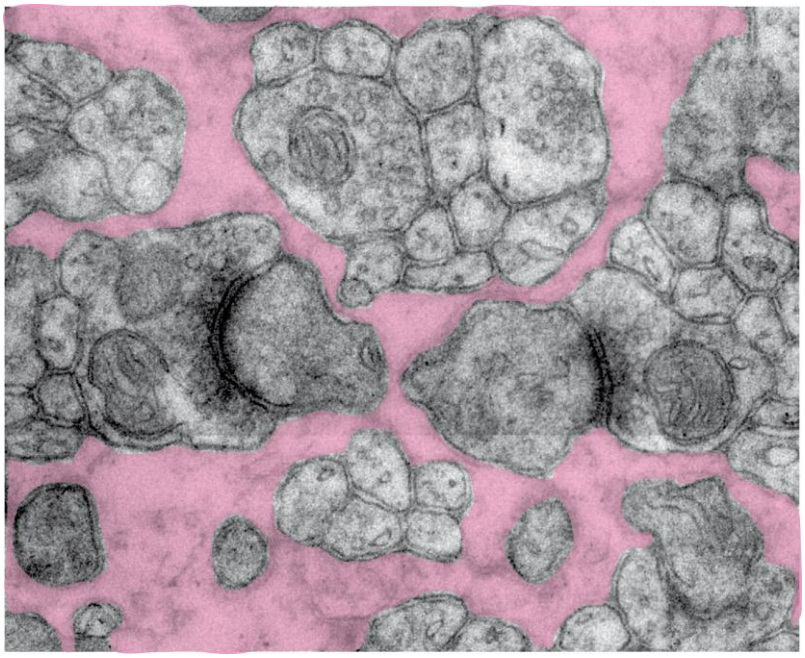

Figure 1 The tripartite synapse
The electron micrograph shows two synapses surrounded by Bergmann glial appendages (PAPs) (pink colored) in an ultrathin section (50 nm) in the molecular layer of the cerebellum. The presynaspe, postsynapse and astroglial processes symbolize the so called tripartite synapse. In these microdomains neurons and glial cells communicate via receptors to implement brain function.

Individual astrocytes tend to occupy distinct, non-overlapping domains and their processes can envelop approximately 40.000 synapses (Bushong et al., 2002; Volterra and Meldolesi, 2005) (see Figure 2 a). This immediate proximity places them in a unique situation to be able to listen and respond to neurons throughout the brain. For sensing neuronal activity

astrocytes are equipped with transmitter and peptide receptors, like glutamatergic AMPA and NMDA receptors, purinergic receptors like P2Xs and P2Ys as well as gabaergic receptors like $GABA_{B1}$ (Charles et al., 2003; Fischer et al., 2009; Franke et al., 2012; Lalo et al., 2006; Oka et al., 2006; Saab et al., 2012; Terunuma et al., 2015). Interestingly the expression of these receptors is rather diverse and heterogeneous during development, but also in different brain regions (Höft et al., 2014; Sun et al., 2013). Astrocytes show also different morphologies depending on the brain region, gray or white matter and health status of the brain tissue. Protoplasmic astrocytes are in the grey matter and have many fine processes (approx. ~50 µm long), which are extremely elaborated and complex (see Figure 2 a-c). Fibrous astrocytes are present in the white matter. Their processes are long (up to 300 µm) and much less elaborated as compared to protoplasmic astroglia. The second big group of astroglial cells is the radial glia, which are bipolar cells each with an ovoid cell body and elongated processes. Radial glia are a common feature of the developing brain and play an important role in the adult neurogenesis They usually have two main processes, one of them forming endfeet at the ventricular wall and the other at the pial surface (Kimelberg, 2010). They are the first cells to develop from neural progenitors; from very early embryonic stages radial glia also form a scaffold, which assists in neuronal migration. After maturation, radial glia disappear from many brain regions and transform into astrocytes, although radial glial cells remain in the retina (Müller cells*).* Further a subpopulation is thought to serve as neuronal stem cells in the adult brain throughout life giving rise to neuroblasts which integrate in the hippocampus and olfactory bulb (Bonfanti and Peretto, 2007; DeCarolis et al., 2013; Dimou and Gotz, 2014).

The cerebellum contains specialized semi-radial glia called Bergmann glia. They have relatively small cell bodies (~10 µm in diameter) and three to six processes that extend from the Purkinje cell layer to the pial surface (see Figure 2 d). They arise from radial glial cells and their shafts provide scaffolding for granule cells (Altman, 1975; Hatten and Mason, 1990) and direct growth of Purkinje cell dendrites (Lordkipanidze and Dunaevsky, 2005; Yamada et al., 2000). After the bulk of granule cell migration is complete, lateral processes emerge from Bergmann glial cell shafts, coincident with the expansion of the Purkinje cell dendritic trees and synaptogenesis (Grosche et al., 1999; Lippman et al., 2008; Yamada et al., 2000). Bergmann glial surface expands by an estimated 50-fold during the first three postnatal weeks in mice after which most excitatory synapses in the cerebellar cortex are ensheathed by Bergmann glial cells (Grosche et al., 2002). On average there are eight Bergmann glial cells to every Purkinje cell.

After brain injury astrocytes are activated and increase synthesis of glial fibrillary acidic protein (GFAP). During the severe astrogliosis, reactive astrocytes proliferate and display hypertrophic morphology, resulting in pronounced overlapping of reactive astrocytes and formation of a dense and compact glial scar (Sofroniew, 2005, 2009). Neuropathological potentials are known for all glial cells but particular astrocytic function seems to play an important role in neurodegenerative diseases, like Alexander's-, Alzheimer's- and Parkinson's disease and multiple sclerosis (Charron et al., 2014; Verkhratsky et al., 2013).

Astrocytes appear as highly specialized cells particularly tailored to act within the spatio-temporal activity map of the healthy and diseased brain. They express various receptors, but the particular function of each individual one in neuronal networks is mainly unclear. Astrocytes use calcium (Ca^{2+}) as a signaling device

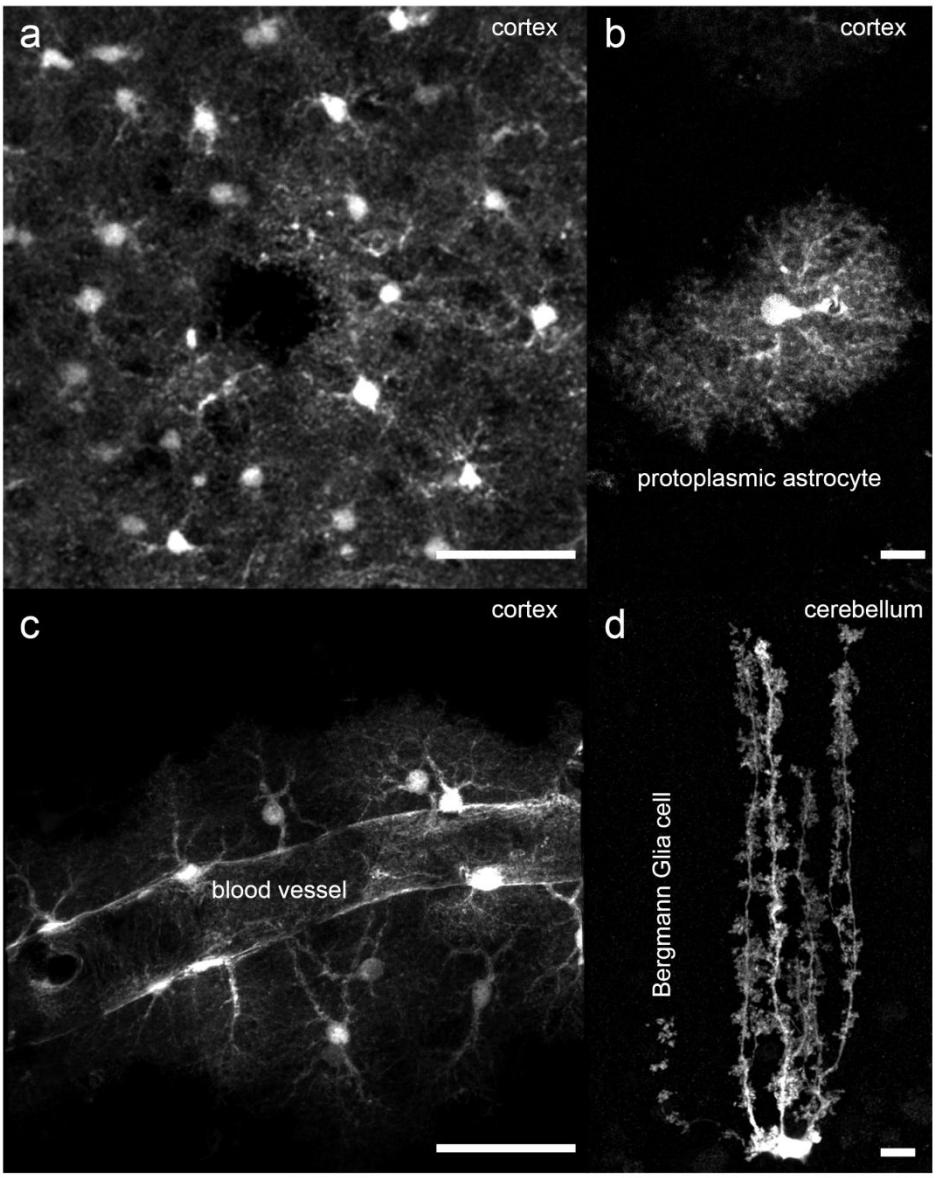

Figure 2 Astrocytes in the cortex and cerebellum
a) Protoplasmic astrocytes in the cortex. Cells express the red reporter protein tdTomato (**a**-**c**) or EGFP (**d**) after tamoxifen application. In the middle a single, not recombined astrocyte leaves a defined space, demonstrating his non overlapping domain. (**b**) Protoplasmic astrocytes have many fine processes which are extremely elaborate and complex. The processes can also contact blood vessels, forming so called perivascular endfeet (**c**) and form multiple contacts with neurons. (**d**) The astrocytes in the molecular layer of the cerebellum are radial glia cells, so called Bergmann glia cells (BG). They extend their processes through the molecular layer and ensheat the dendritic tree of a Purkinje neuron. The scale bar in **a** and **c** corresponds to 50 µm and in **b** and **d** for 10 µm.

They respond to brain activity with an intracellular Ca^{2+} rise, demonstrating that they are able to sense activity in their surroundings (Volterra et al., 2014; Zorec et al., 2012). Astrocytes are also able to convey signals to a network of other astrocytes via gap junctions (Orellana and Stehberg, 2014). Both forms of Ca^{2+} signaling can occur also independent of neuronal

activity, so called spontaneous Ca^{2+} oscillations. Further these Ca^{2+} signals can occur within the whole cell, soma and processes or are propagated within defined microdomains. As a response, astrocytes are able to release transmitters, like D-Serine, ATP and glutamate which can act back on neighboring neurons, astrocytes and other cell types (Araque et al., 2014). Neuromodulatory processes of astrocytes are likewise complex as in neurons and depend on the kind of transmitter, the site of release and the type of activated receptor. Nowadays special emphasis is placed on the establishment of imaging techniques for the diverse astroglial Ca^{2+} signals in brain slices and anesthetized as well as awake mice. Associated are the development and testing of various Ca^{2+} indicator dyes and transgenic mouse models, which express genetically encoded calcium indicators, like GCaMPs (Jiang et al., 2014; Paukert et al., 2014). Nowadays also changes in sodium (Na^+) concentrations are considered as an indicator for communications events in astrocytes. Cytosolic Na^+ concentrations are tightly controlled by Na^+-dependent transporters to preserve ion homeostasis of potassium, glutamate and also Ca^{2+} (Rose et al., 2009). Further Na^+ transients control metabolic neuronal-glial signaling, stimulating lactate production which on release from astrocytes can be taken up and utilized by nearby neurons (lactate shuttle) (Pellerin et al., 2007; Pellerin and Magistretti, 1994). Transmitters, most notably glutamate, and excitatory neuronal activity evoke long-lasting sodium transients in astrocytes, which properties are distinctly different from those of activity-related glial Ca^{2+} signals. Further also ligand gated receptors are permeable for Na^+ ions. In summary, understanding the intracellular fluctuations of the even more abundant cation Na^+ is a new emerging field in glial signaling research (Kirischuk et al., 2012; Rose and Karus, 2013). In the future the interplay of both ions has to be observed in astrocytic signaling processes.

2.2 The Cre/loxP site DNA recombination system

In order to investigate the relevance of the astroglial receptors *in vivo*, genetically modified mouse lines were generated in which receptor genes were conditionally deleted by use of the Cre/loxP system (Gu et al., 1993; Lewandoski, 2001; Rajewsky et al., 1996). The concept of the Cre/loxP mediated cell type specific mutation is based on the generation of two mouse lines. In the first mouse line the Cre recombinase (causes recombination) (Abremski et al., 1983; Sauer and Henderson, 1989) is expressed under a cell type specific promoter. The Cre recombinase (38 kDa) was isolated from the bacteriophage P1 and belongs to the family of site-specific tyrosin integrases. In mice of the second mouse line the target gene is flanked by loxP sequences (locus of crossover x of the bacteriophage P1). Crossbreeding of both mouse lines gives rise to genetically modified offspring, which expresses the Cre recombinase and carry genes flanked by loxP sites. The Cre recombinase catalyzes the recombination of DNA between the loxP sequences (Hamilton and Abremski, 1984; Hoess and Abremski, 1984; Sternberg and Hamilton, 1981) by binding of two molecules of the Cre recombinase to specific binding sites (Grindley et al., 2006; Guo et al., 1997; Mack et al., 1992).

To allow next to the cell type specificity a temporal control of the Cre activity, a ligand regulated form of the Cre recombinase was developed. The Cre recombinase was hereto fused with a mutated ligand binding domain (LBD) of the estrogen receptor (Brocard et al., 1997; Feil et al., 1996; Metzger and Chambon, 2001; Metzger et al., 1995; Schwenk et al.,

1998). After expression, the fusion protein is bound to two molecules of the heat shock protein HSP90 in the cytosol and prevented from the transport to the nucleus. Only after application and binding of the appropriate ligand (tamoxifen), the fusion protein is released and translocated to the nucleus, where the enzyme can cut the floxed gene sequence (see Figure 3).

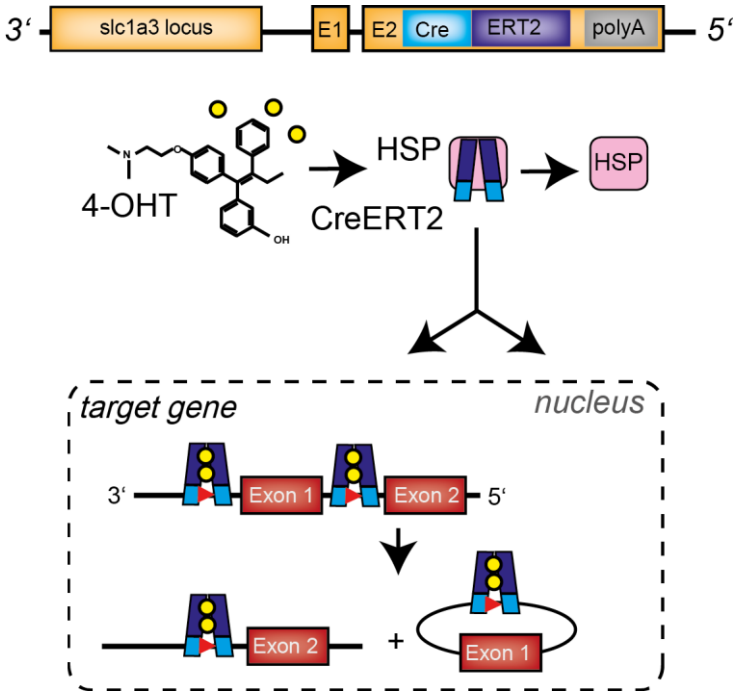

Figure 3 Generation of mouse strains with astroglial-specific genomic recombination
At top the genetic modified gene section of the mouse line used for selective and inducible depletion of target genes is illustrated. The genetic information for the CreERT2 fusion protein replaces the GLAST (gene symbol: *slc1a3*) wildtype allele. The GLAST promoter region is followed by the CreERT2 construct with the polyadenyl sequence for complete processing of mRNA. CreERT2 remains bound to the heat shock protein (HSP90) in the cytosol. After binding of 4-hydroxytamoxifen (4-OHT), respectively the complex is released and CreERT2 is transported to the nucleus. There two molecules bind to each loxP site (red arrow heads) and the floxed gene sequence, here exon1, is excised, respectively. After recombination the respective gene is inactivated (Mori et al., 2006).

Different versions of CreERT were developed to decrease their nuclear translocation in the absence of the inducer, while increasing their sensitivity to tamoxifen and their recombination efficiency. To evaluate the physiological role of astroglial receptors in the complex neuronal network the improved tamoxifen inducible Cre recombinase fused to the human hormone receptor ERT2 was used, which has a triple mutation of human ER-LBD (Feil et al., 1997; Indra et al., 1999; Seibler et al., 2003). CreERT2 is currently the best characterized and most frequently used system for inducible gene modifications. The fusion protein is insensitive to endogenous 17β-estrogen, but responsive to the synthetic estrogen antagonist 4-hydroxytamoxifen (4-OHT). In the liver tamoxifen is converted to the more active form 4-OHT. CreERT2 is expressed under the control of the astrocyte-specific GLAST (L-glutamat/L-aspartate transporter) locus. For that purpose the CreERT2 construct was cloned by homologous recombination in embryonic stem cells into the locus of the GLAST. (Mori et al., 2006). The advantage of the so called knock-in approach is that the CreERT2 expression is controlled by all endogenous regulatory elements. It is essential to use mice

heterozygous for the transgene, to maintain expression of the transporter. At the same time only one allele is functional to generate physiological levels of the transporter. The majority of the Cre driver lines were generated by the less time intensive approach where the transgenic construct integrates randomly into the genome. Here the promotor region is part of the transgene (Hirrlinger et al., 2006).

In the current study mouse lines carrying floxed target genes for the NMDA receptor subunit GluN1 (gene symbol *grin1)* (Bannerman et al., 2012; Tsien et al., 1996b), the $P2Y_1$ receptor (*p2ry1*) (Leon et al., 1999), the GABA receptor subunit B1 (*gabbr1*) (Haller et al., 2004) and the AMPA receptor subunit GluA4 (*gria1*) (Fuchs et al., 2007) were used.

To monitor recombination events, reporter mice can be introduced like the Rosa26-CAG-tdTomato reporter mouse (Madisen et al., 2010). This mouse expresses a red reporter protein tdTomato, where a floxed STOP cassette separates the CAG promoter from the reporter gene. tdTomato expression only occurs when the floxed STOP cassette is eliminated by the Cre recombinase and serves therefore as a recombination control. The red fluorescent protein tdTomato is a genetic fusion of two copies of the tdTomato gene. The tandem dimer structure is responsible for the bright fluorescence. It has an excitation maximum at 554 nm and emits light at 582 nm (Shaner et al., 2007).

Finally, for investigation of receptor function in different brain regions the described mouse lines have to be crossbred so that animals are generated which express astrocyte-specifically CreERT2, are usually homozygous floxed and carry at least one receptor gene.

2.2.1 Tamoxifen metabolism in mice and humans

Tamoxifen (TAM) is for more than 30 years the endocrine therapy of hormone dependent breast cancer in the postmenopausal woman. The effects of tamoxifen and the metabolism have been intensively studied in clinical trials with humans. Tamoxifen is a prodrug and undergoes oxidation in the liver by cytochrome P450 isoforms to several primary and secondary metabolites with variable potencies toward the estrogen receptor. Major tamoxifen metabolites include N-desmethyltamoxifen (NDMT), 4- hydroxytamoxifen (4-OHT) and endoxifen (ENDX) (see Figure 4) (Caldas and Tannock, 2013; Goetz et al., 2008; Stearns and Rae, 2008).

CYP2D6 appears to be the rate-limiting enzyme converting the pharmacologically inactive metabolites (tamoxifen and NDMT) to endoxifen, and additionally contributes to the formation of 4-OHT. The CYP2D6 gene is highly polymorphic, currently with 63 different major alleles known, many of which are associated with increased, decreased or abolished function of the final gene product. The CYP2D6 phenotypes associated with these different alleles include poor, intermediate, extensive and ultrarapid metabolizers. These genotypes correlate as well with the success or failure of the breast cancer therapy (Goetz et al., 2008; Mahgoub et al., 1977; Mürdter et al., 2011; Nebert et al., 1996; Stearns and Rae, 2008).

4-OHT possesses a much higher affinity for estrogen receptors (ER) and is 30- to 100-fold more potent than TAM in suppressing estrogen-dependent cell proliferation (Borgna and Rochefort, 1981; Jordan et al., 1977; Robertson et al., 1982). But 4-OHT represents less than 10 % of TAM primary oxidation (Lonning, 1992, Desta 2004). For this reason 4-OHT was considered to be the active metabolite of tamoxifen.

However, newer data suggested that endoxifen has identical properties, like ER-binding affinity and suppression of estrogen-dependent cell growth and potency as 4-OHT, but is present in concentrations up to 10-fold higher than 4-OHT (Johnson et al., 2004; Stearns et al., 2003). The conversion of tamoxifen by N-demethylation to N-desmethyltamoxifen, catalyzed primarily by CYP3A, contributes to ~92 % of tamoxifen metabolism (Desta et al., 2004; Kiyotani et al., 2012; Stearns et al., 2003). In humans, the final serum concentrations of 4-OHT and ENDX exhibit substantial variability that is partially explained by genetic in CYP2D6 enzyme activity (Madlensky et al., 2011).

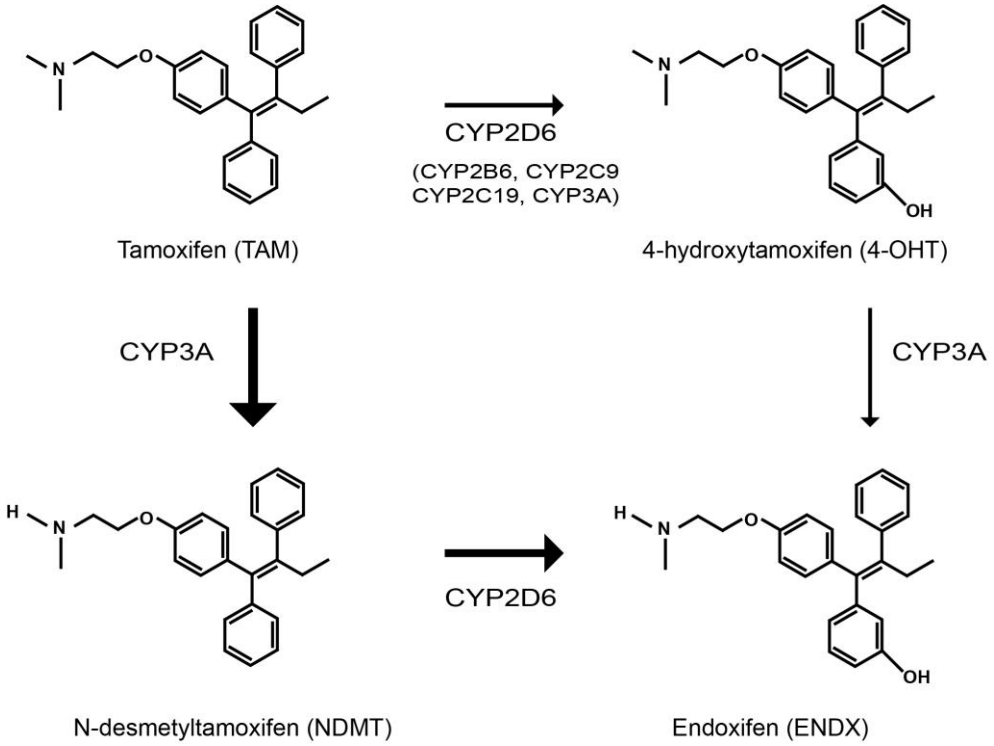

Figure 4 Tamoxifen biotransformation in humans
Tamoxifen (Tam) is predominantly N-demethylated by the CYP3A enzyme to N-desmethyltamoxifen (NDMT), which is a major primary tamoxifen metabolite. This metabolite undergoes multiple oxidations including 4-hydroxylation by CYP2D6 to endoxifen. Tamoxifen 4-hydroxylation via multiple CYPs to 4-hydroxytamoxifen (4-OHT) represents a minor primary metabolic route of tamoxifen. A small portion of endoxifen serum concentrations appears to result from CYP3A-catalyzed N-demethylation of 4-hydroxytamoxifen (Borges et al., 2006).

In mice pharmacokinetics of tamoxifen are not as well established as in humans. Differences are likely due to the lower expression of CYP2D and CYP3A enzymes in mice compared to humans (McLaughlin et al., 2008) and differences in P450-catalyzed metabolism of TAM. CYP2D6 was originally characterized as debrisoquine hydroxylase in rat and human liver, but does not appear to be homologous to the P450 enzyme that catalyzes debrisoquine hydroxylation in mice since it is not inhibited by an antibody against purified rat liver CYP2D that inhibits debrisoquine hydroxylase activity (Jordan and Allen, 1980; Löfgren et al., 2004; Masubuchi et al., 1997). However, the main metabolites, TAM, NDMT, 4-OHT and ENDX can also be detected in mice serum and tissue after administration of tamoxifen. But, although NDMT is the major metabolite, levels were equivalent to those of TAM itself,

whereas 4-OHT levels were higher than in human patients (Kisanga et al., 2003; Robinson et al., 1991; Robinson et al., 1989). ENDX levels were lower than 4-OHT concentrations in serum of mice (Reid et al., 2014). In contrast, rats showed a similar metabolite profile as human patients (Lien et al., 1991b; Robinson et al., 1991; Robinson et al., 1989).

2.2.2 Astrocyte-specific glutamate transporter

One of the major functions of astrocytes within the CNS is glutamate uptake from the synaptic cleft, which influences excitatory neurotransmission and prevents excitotoxicity. Next to GLAST (EAAT-1) astrocytes predominantly express the glutamate transporter-1 (GLT1/EAAT-2).

The pattern and strength of expression differs among GLAST and GLT1 in regard to brain regions. Early immunohistochemical studies in rats (Chaudhry et al., 1995; Danbolt et al., 1992; Lehre et al., 1995; Storck et al., 1992) and a promoter study where BAC (bacterial artificial chromosome) transgenic mice were generated which express fluorescent proteins under the control of the natural GLT1 or GLAST BAC promoters (Regan et al., 2007) revealed that GLAST is expressed primarily in radial glia as well as cortical astrocytes during development. In adulthood expression persists in the Bergmann glial cells of the cerebellum, fibrous astrocytes of the ventral white matter tracts of the spinal cord, as well as progenitor cells of the subgranular layer of the dentate gyrus and subventricular zone. At late-embryonic and postnatal stages, radial glial cells give also rise to the neural stem cells responsible for adult neurogenesis. In contrast, GLT1 is the predominant glutamate transporter expressed in the adult brain and highly active in both protoplasmic and fibrous astrocytes accounting for 90 % of glutamate uptake in the CNS.

The combination of reporter gene expression and functional analysis of transporter currents in BAC transgenic mice demonstrated that two populations of astrocytes exist with either GLAST or GLT1 as the strongly dominant expressed transporter. By in situ hybridization the majority of brain astrocytes were determined to simultaneous express both GLAST and GLT1 mRNA, albeit at different levels (Berger and Hediger, 1998). Also immunohistochemical studies showed localization of both transporters in the membrane of an individual cell (Chaudhry et al., 1995; Lehre et al., 1995).

In general GLAST and GLT1 consist of 8 transmembrane domains with intracellular carboxyl and amino termini (Koch and Larsson, 2005; Sheldon and Robinson, 2007). The transport is sodium (Na^+) dependent; with each glutamate/aspartate molecule three Na^+ ions and one proton are co-transported. Simultaneously one potassium ion is counter-transported, so that the glutamate binding site is again accessible for glutamate molecules (Rose et al., 2009; Zerangue and Kavanaugh, 1996). The transporters show an uneven distribution on astrocytes, with an enriched occurrence on astrocytic processes that face nerve terminals, axons and spines compared to those that face capillaries, pia or stem dendrites (Chaudhry et al., 1995; Rothstein et al., 1994). Intracellular uptake of glutamate by astrocytes leads to its metabolization into glutamine, mediated by the ATP-dependent, astrocyte specific glutamine synthetase (GS). Glutamine transporters release the glutamine into the extracellular space where it is taken up by neurons and converted into glutamate (Hertz et al., 1999; Rose et al., 2013). Knockout models of GLAST (Watase et al., 1998) and GLT1 (Tanaka et al., 1997) clearly demonstrated the importance of glutamate transporters in the healthy brain. Animals

without GLAST and GLT1 show motor incoordination and seizures, followed by death at the age of 6 weeks, respectively. Further expression of glutamate transporters is changed in animal models of neurologic diseases, like ALS, stroke, Huntingon's and Alzheimer's disease (Maragakis and Rothstein, 2004).

2.3 Astrocytic receptor knockout mice as a tool to study the tripartite synapse

The main aim of astrocyte-specific knockout animals is to reveal the *in vivo* function of the respective receptor in the neuronal network. As described earlier, it is a difficult task to dismantle Ca^{2+} and Na^{+} signals in astrocytes and to match them with a specific receptor. Besides neurons and astrocytes also other cell types, like microglia and oligodendrocytes express the same set of receptor proteins. Therefore traditional pharmacological approaches act on the respective protein in all cell types. To differentiate between neuronal and glia specific contribution to information processes we developed mouse models to knock out receptor proteins specifically in astrocytes in the living animal (see 2.2). We thereby influence astrocytes in the process of information uptake. The intracellular Ca^{2+} and Na^{+} fluctuations induced by $P2Y_1$ and NMDA receptors are prevented in conditional knock out animals (cKO). Hereby, we aim to see differences in the signaling behavior of astrocytes and to reveal consequent changes in modulation processes, like gliotransmitter release and changes in neuronal signaling itself. By knocking out astroglial NMDA and $P2Y_1$ receptors we interfere with glutamatergic and purinergic signaling in the CNS.

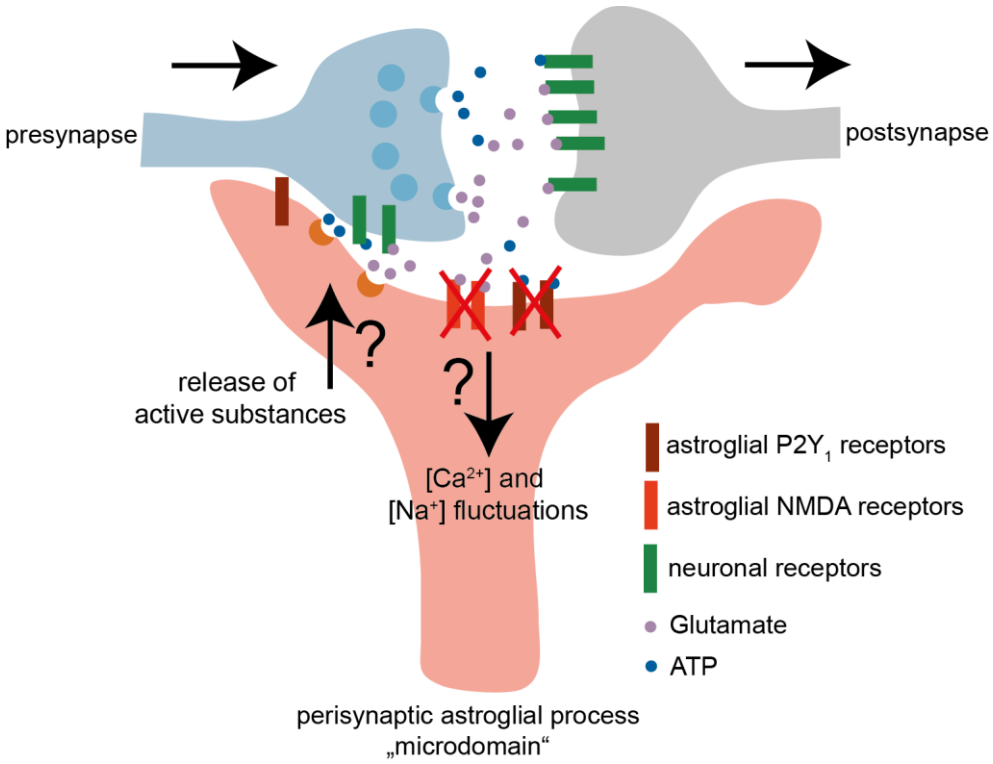

Figure 5 Glutamatergic and purinergic signaling at the tripartite synapse
The presynaptic neuron releases glutamate and ATP that activate receptors on the postsynapse. In parallel, $P2Y_1$ and NMDA receptors located on astroglial processes are activated and mediate Ca^{2+} release from internal stores and ion influx, respectively. However, the physiological impact of astroglial $P2Y_1$ and NMDA receptor activation for neuron-glia communication and brain function is still unclear.

2.3.1 Relevance to study astroglial purinergic $P2Y_1$ receptors

Extracellular purines (adenosine, ADP and ATP) and pyrimidines (UDP and UTP) are important signaling molecules that mediate diverse intracellular pathways. They are considered as the major gliotransmitter, integrating neuron-glia network in the brain and astroctyes are suggested to be the main source for physiologically released ATP in the CNS (Coco et al., 2003). They release ATP to communicate with each other, with other types of glia and neurons by stimulating purinoceptors on neurons, microglia, oligodendrocytes and blood vessels (Butt, 2011; Verkhratsky and Burnstock, 2014; Verkhratsky et al., 2009).

The purinergic receptor family consists of two different subgroups, the P1 and P2 receptors. P1 receptors are responsive to adenosine and G-protein-coupled, whereas the P2 receptors are subdivided likewise in G-protein-coupled and ligand-gated ion channels, so called P2Y and P2X receptors respectively. Here we concentrate on the metabotropic P2Y receptors. To date eight mammalian receptor subtypes have been identified with different ligand preferences: $P2Y_1$: ADP; $P2Y_2$: ATP/UTP; $P2Y_4$: UTP; $P2Y_6$: UDP; $P2Y_{11}$: ATP; $P2Y_{12}$: ADP; $P2Y_{13}$: ADP and $P2Y_{14}$: UDP-glucose and other nucleotide sugars (Fields and Burnstock, 2006; Franke et al., 2012).

Murine and rat astrocytes express $P2Y_1$, $P2Y_2$, $P2Y_4$, $P2Y_6$, $P2Y_{11}$, $P2Y_{12}$, $P2Y_{13}$ and $P2Y_{14}$ receptors verified by immunohistological, mRNA or functional analysis (Fields and Burnstock, 2006; Franke et al., 2012; Verkhratsky et al., 2009). And there is compelling evidence that among these subtypes, $P2Y_1$ is the prominent subtype expressed on murine astrocytes and responsible for modulatory effects of neuronal networking in health and disease, reinforced by more than 100 publications.

Due to the fact that P2Y subtypes are activated by rather the same antagonists with different potencies specific synthetic agonists (ADPβS, 2-MeSADP, 2-MeSATP, MRS 2365) and antagonists (MRS 2179, MRS 2216, MRS 2279, MRS 2500) for $P2Y_1$ and other subtypes were constructed. It improved the possibility to correlate specific function with a specific receptor subtype unlike the broad spectrum agonist ADP and antagonists, like suramin and PPADS which block non-selective all P2Y subtypes (Burnstock, 2007; von Kügelgen, 2006).

In general, $P2Y_1$ receptors ($P2Y_1$Rs) are expressed throughout the brain (Morán-Jiménez and Matute, 2000) and the receptor couples via G_q-proteins to stimulate predominantly phospholipase C (PLC) which in turn leads to an increase in inositol triphosphates (IP_3) and mobilization of Ca^{2+} from intracellular stores. Ca^{2+} as a second messenger consequently activates different pathways and e. g. triggers apoptosis (Sellers et al., 2001) or proliferation (Franke et al., 2009). $P2Y_1$R agonists, like ADP, strongly promote astrogliosis and the upregulation of GFAP expression after brain injury (Franke et al., 2003; Franke et al., 2004; Kuboyama et al., 2011). Astrocytes react to ATP with hypertrophy, swelling of the cell body and main processes and proliferation with subsequent formation of the glial scar (Franke and Illes, 2014; Franke et al., 2003; Franke et al., 2001; Lecca et al., 2012; Tu and Wang, 2009; Washburn and Neary, 2006). In addition, astrocytic $P2Y_1$R activation induces the release of proinflammatory cytokines, like IL-6 (Fujita et al., 2009; Kuboyama et al., 2011; Noguchi et al., 2013) and GDNF (Sun et al., 2008) which act back on surrounding cells during acute injury, like trauma and ischemia. Thus, $P2Y_1$Rs on astrocytes transduce neuroinflammatory responses when activated by ATP released or leaked from damaged neurons or glial cells.

Main findings in regard to astroglial $P2Y_1R$ function under physiological conditions were investigated *in vitro* and *in situ* experiments at perforant path-granule cell synapses in the dentate gyrus of the hippocampus. Simultaneous activation of astroglial TNFα (tumor necrosis factor) and $P2Y_1$ receptors by TNFα and ATP, respectively, triggers the fusion of glutamate vesicles in astrocytes facing presynaptic NMDA receptors, thereby increasing the excitatory synaptic activity (Domercq et al., 2006; Jourdain et al., 2007; Santello et al., 2011). In cell culture experiments, hippocampal microglia were activated with LPS, a proinflammatory molecule, which recruited astrocytes by activation of $P2Y_1R$ upon ATP release. Activation of $P2Y_1Rs$ stimulated astrocytes to release glutamate, which modulates neuronal activity through metabotropic glutamate receptors (Pascual et al., 2012).

On the other hand, *in vitro* experiments could show that after applying a neurotoxicant the microglial recruitment of astrocytes via $P2Y_1Rs$ is part of a neuroprotective response due to IL-6 release by astrocytes (Noguchi et al., 2013). It was further demonstrated in different *in vivo* brain injury studies, like trauma and ischemia, that $P2Y_1R$ mediated Ca^{2+} release from the endoplasmic reticulum leads to an increase of mitochondrial Ca^{2+} levels and an increased production of ATP in astrocytes. Higher ATP levels could then be used for any energy-dependent astroglial function which led to reduced neuronal damage and cell death (Talley Watts et al., 2013; Zheng et al., 2013). In contrast another study showed that after *in vivo* traumatic brain injury astroglial $P2Y_1R$ antagonism reduced post-traumatic hippocampal cognitive deficits in mice (Choo et al., 2013). In line, another study clearly demonstrated that also the blockade of $P2Y_1R$ mediated signaling ($P2Y_1R$ knockout (KO) mice or a $P2Y_1R$ specific antagonist) ameliorated the cognitive deficits induced by a focal cerebral stroke (MCAO) (Chin et al., 2013). A different *in vivo* investigation revealed that after cerebral ischemia, inhibition of the astrocytic $P2Y_1Rs$ resulted in cytokine/chemokine transcriptional suppression and cerebroprotection via the rapid acting transcription factor NF-kB (Kuboyama et al., 2011).

In a recent analysis astroglial $P2Y_1Rs$ could directly be linked to the progression of Alzheimer's disease (AD). They revealed that astroglial hyperactivity is reduced after P2 purinoreceptor blockade or nucleotide release through connexin hemichannels, but was augmented by increasing cortical ADP concentrations. Inhibition of $P2Y_1Rs$, which were strongly expressed by reactive astrocytes surrounding the plaques, completely normalized astrocytic hyperactivity. Data suggested that astroglial network dysfunction is mediated by purinergic signaling in reactive astrocytes, and that intervention aimed at $P2Y_1R$ or hemichannel-mediated nucleotide release may help to ameliorate network dysfunction in AD (Delekate et al., 2014).

The data summarized here do not have to be necessarily contradictory but rather reflect multiple Ca^{2+} targets within astrocytes as well as differential Ca^{2+} responses related to e.g. duration or location of the Ca^{2+} signal. It is important to understand the pathological potential of $P2Y_1Rs$ in controlling and fine-tuning of astrocytic responses to identify possible therapeutic principles to treat acute and chronic CNS diseases.

Further it is also important to understand the interplay of $P2Y_1Rs$ with other P2Y subtypes or other purinoreceptors in the same cell, also in regard to the brain region. $P2Y_1R$ play the major role in generating and maintaining propagating Ca^{2+} waves in hippocampal cultured astrocytes (Bowser and Khakh, 2007). In cultured cortical astrocytes $P2Y_1$ and $P2Y_{14}$

receptors were identified to be responsible for the Ca^{2+} response (Fumagalli et al., 2003). In cultured spinal cord astrocytes, however, ATP-mediated propagating Ca^{2+} waves required $P2Y_1$ and $P2Y_2$ receptors, as pharmacological inhibition of either of them eliminated the wave propagation (Fam et al., 2003; Gallagher and Salter, 2003). In astrocytes of the spinal cord acute inhibition of Cx43 synthesis resulted in downregulation of $P2Y_1$Rs and in an increase of $P2Y_4$ receptor expression, which in turn modified the mode of Ca^{2+} wave propagation (John et al., 1999; Suadicani et al., 2003). In addition a high level of co-localisation between A_1 and $P2Y_1$ receptors at glutamatergic synapses and surrounding astrocytes have been demonstrated as well as the functional interaction between these receptors in the hippocampus (Tonazzini et al., 2007).

Further, it was convincingly shown that astroglial $P2Y_1$Rs play a role in the developing brain in cortex and cerebellum and in adult neurogenesis in the subgranular and subventricular zone. Radial glia generate and then guide newborn neurons into the cortical plate. Like in spinal cord astrocytes, radial glial Ca^{2+} waves occur spontaneously and require connexin hemichannels, $P2Y_{1s}$R and intracellular IP_3-mediated Ca^{2+} release. Furthermore, it was shown that wave disruption decreases proliferation in the ventricular zone during the peak of embryonic neurogenesis (Weissman et al., 2004).

Studies also suggested that purinergic signaling promotes the proliferation of rapidly dividing cells and transit-amplifying cells in the SVZ niche through the $P2Y_1$Rs (Suyama et al., 2012). Lineage tracing experiments performed in GLAST-CreERT2xEYFP (enhanced yellow fluorescent protein) reporter mice demonstrated that ADPβS promoted proliferation of GLAST+ progenitors and their progression toward the generation of rapidly dividing progenitors (Boccazzi et al., 2014). Also in adult neurogenesis in the hippocampus it was found that the purinergic system crucially affects progenitor activities directly and through the involvement of reactive astrocytes. ATP secretion by astrocytes even at basal level promoted NSC proliferation in the adult hippocampus through $P2Y_1$R activation (Cao et al., 2013).

Of note, until today there is rather evidence against $P2Y_1$R expression in human astrocytes (Moore et al., 2000), but has to be addressed in more detail.

2.3.2 Relevance to study astroglial NMDA receptors

The majority of studies on NMDA receptors (NMDARs) were performed to reveal neuronal NMDARs function in mice and rats. The CA1-CA3 synapse in the hippocampus served hereby as the most used model system (Nakazawa et al., 2004; Neves et al., 2008). Just a few studies investigated expression and functional aspects in astrocytes (Lalo et al., 2011b; Schipke et al., 2001; Verkhratsky and Kirchhoff, 2007).

NMDA receptors (NMDARs) are a class of ionotropic glutamate receptors (iGluRs) that are essential for neuronal development, synaptic plasticity, learning and cell survival. In general several features distinguish NMDARs from other iGluRs, like AMPA and kainate receptors and underlie the crucial roles NMDARs play in nervous system physiology (Glasgow et al., 2014). They display slow deactivation kinetics, are highly Ca^{2+} permeable apart to Na^+ and potassium (K^+), possess a glutamate- and/or glycine/D-serine-binding site and require depolarization to relieve channel block by external Mg^{2+} ions, thereby making them effective coincidence detectors. Specifically, NMDAR activation requires postsynaptic depolarization (to relieve the Mg^{2+} block) that coincides with presynaptic release of glutamate and glycine

that bind the respective subunits. This remarkable feature of coincidence detection of NMDRs is essential for synaptic plasticity as well as the strength and stability of synaptic connections (Jacobs et al., 2014; Shimizu et al., 2000; Tsien, 2000).

But the mentioned properties and others differ among NMDAR subtypes, which are defined by the subunits that compose the receptor. Functional NMDARs are tetramers composed of different subunits (GluN1, GluN2A-D, GluN3A-B) (Ciabarra et al., 1995; Hollmann and Heinemann, 1994; Ishii et al., 1993; Monyer et al., 1992; Sucher et al., 1995). Typically, NMDARs are di-heteromers comprising two GluN1 subunits and two GluN2 or GluN3 subunits, which assemble as a dimer of dimers (Paoletti et al., 2013).

The GluN1 subunit, which exists in 8 different variants upon alternative splicing, is the obligatory subunit to form a functional NMDAR complex and contains the glycine-binding site (Flores-Soto et al., 2013; Moriyoshi et al., 1991). The GluN2 subunit contains the glutamate-binding site and there are four different isoforms: GluN2A-D. The majority of NMDARs is composed of two GluN1 and GluN2 subunits and hence requires both glycine and glutamate for receptor activation. The type of the GluN2 subunit in the receptor complex critically defines the biophysical and pharmacological properties of the receptor e.g. open probability, single-channel conductance, deactivation time, sensitivity to active modulators and intracellular signaling complexes (Cull-Candy and Leszkiewicz, 2004; Dingledine et al., 1999; Sanz-Clemente et al., 2013).

However, NMDARs are also able to assemble as tri-heteromers (Das et al., 1998; Pilli and Kumar, 2012) (e. g.: GluN1/GluN2B/GluN3A). Both di- and tri-heteromers can differ during development and adulthood (Al-Hallaq et al., 2007; Brothwell et al., 2008)

And further, receptor compositions of GluN1 and GluN3 subunits alone result in a glycine receptor that is resistant to the Mg^{2+} block (Chatterton et al., 2002). The role of the excitatory glycine (NMDA) receptors in the CNS is not well understood but described to functionally exist in neurons as well as in oligodendrocytes (Pachernegg et al., 2012; Piña-Crespo et al., 2010).

The direct link between the described properties of neuronal NMDARs and astrocytes are glycine and D-serine which are required for NMDAR activation, occupying a binding site present in the GluN1 subunit. Both amino-acids are apart from neurons derived from astrocytes and studies indicated that LTP mediated by activation of GluN2A-NMDARs at hippocampal synapses, depends on astroglial released D-serine. In contrast NMDARs located presynapticly are mainly activated by glycine. Here, NMDARs contain the GluN2B subunit, making them 10 fold more sensitive to glycine as an agonist (Henneberger et al., 2010; Oliet and Mothet, 2009; Panatier et al., 2006). Further, neurotransmitter clearance from the synaptic cleft is likewise a major function of astrocytes. They possess transporters to remove the agonist glutamate and the co-agonist glycine (Anderson and Swanson, 2000; Harsing and Matyus, 2013). Conversely, astrocytes may also provide glutamate to extrasynaptic NMDARs. Astrocytes precisely control hereby the regulation of agonist and co-agonist supply to NMDARs at different locations at the synapse and critically influence synaptic NMDAR function, at least in the hippocampus (Papouin et al., 2012). It is tempting to conclude that astrocytes control their responses to synaptic activity likewise by NMDARs. The subcellular localization of NMDAR subunits in humans and mice on astrocytes was determined in distal processes suggesting that NMDARs contribute to monitoring of

glutamate in the extracellular space (Conti et al., 1999; Conti et al., 1996; Conti et al., 1997; Schipke et al., 2001). But exactly in the hippocampus astroglial NMDAR expression is under debate and astrocytes were rather reported to lack NMDAR expression (Matthias et al., 2003) demonstrating that astroglial NMDAR function is far from being understood.

However, astroglial NMDARs provide an example of regional heterogeneity, which expression has been reported doubtless in cortical astrocytes. Bergmann glial (Müller et al., 1993; Shao and McCarthy, 1997) expression is likewise questioned as the expression in the spinal cord (Ahmed et al., 1990; Ziak et al., 1998) and hippocampus (Cai and Kimelberg, 1997; Höft et al., 2014; Latour et al., 2001; Seifert and Steinhäuser, 1995; Shelton and McCarthy, 1999). Most compelling evidence for functional NMDARs exists for cortical astrocytes. It was shown that NMDARs mediate transmembrane currents in cortical astrocytes that were activated upon physiological synaptic transmission, so called glial synaptic currents (GSCs) (Lalo et al., 2011a; Lalo et al., 2006; Palygin et al., 2011; Palygin et al., 2010; Schipke et al., 2001).

There is one fundamental difference between astroglial and neuronal NMDARs: astroglial receptors are insensitive or just weakly sensitive to extracellular Mg^{2+}, which makes physiological sense. Astrocytes are unable to produce the substantial depolarization needed to remove the Mg^{2+} block. This means that the receptors are operational also at negative resting membrane potential (-80 to -85 mV) (Verkhratsky and Kirchhoff, 2007). This property arises already the question of subunit composition differences. NMDARs which are not sensitive to physiological concentrations of Mg^{2+} have integrated a GluN3 subunit next to two obligatory GluN1 subunits. Integration of a GluN3 subunit was further supported by the fact that glycine and D-serine alone were able to evoke a small current. In addition NMDAR mediated astroglial currents were sensitive to GluN2C/D subunit-selective antagonists UBP141 and memantine at physiological concentrations of Mg^{2+}. Further astroglial NMDARs showed 5 times higher affinity to memantine as neurons. The success of memantine in the treatment of Alzheimer's disease has revived interest in the therapeutic use of NMDAR antagonists (Lipton, 2006; Palygin et al., 2011). Supportive for these findings are mRNA studies from isolated astrocytes, showing enrichment particular of the GluN2C subunit (Cahoy et al., 2008; Zhang et al., 2014). The NMDA evoked currents of GSCs in cortical astrocytes are age dependent, the highest evoked currents could be determined in 6 months old mice, the lowest in 1 month and in 18 month old mice, respectively. In conclusion, in the course of CNS maturation the density of NMDARs increases followed by a decrease in the course of aging (Lalo et al., 2011a).

Further NMDARs are inextricable related to excitotoxicity which is thought to contribute to the cell death associated with certain neurodegenerative diseases, stroke, epilepsy and traumatic brain injury. High levels of glutamate activate NMDARs; the resulting Ca^{2+} influx activates signaling pathways which are detrimental for the cell survival. Targeting NMDARs therapeutically is complicated by the fact that signaling downstream is complex and can promote depending on the strength cell survival and plasticity as well as excitotoxicity (Lai et al., 2014; Parsons and Raymond, 2014). Also for this process the localization of NMDA receptors at the synapse or outside of the synapse and the respective different impact are under discussion. Recent publication showed that astroglial NMDARs are involved in exciotoxicity. Astrocytes downregulate the postassium channels K_{ir} 4.1 in response to

overexposure of glutamate and neuronal death in the process of astrogliosis. This process is correlated to swelling and pathogenesis of serveral CNS disorders. NMDAR blocker, among them mementine, could inhibit the decrease of postassium channels in a mouse model of acute liver failure which is accompanied with glutamatergic dysfunction, brain odema and reduced K_{ir} 4.1 expression in the cortex (Cauli et al., 2009; Obara-Michlewska et al., 2014).

In summary these data designate astroglial NMDARs as tri-heteromeric receptors (GluN1/GluN3AorB/GluN2CorD) with different expression strength in different brain regions, which are interesting targets for the development of novel therapeutic agents specifically targeting glial signaling. There is an emerging field of research for specialized functions of NMDARs in regard to their subunit compositions. Of note, astroglial NMDARs are also expressed on human astrocytes (Lee et al., 2010; Nishizaki et al., 1999).

3 Aims of the study

The first aim of this study (Part I) is the evaluation of the GLAST-CreERT2/loxP system in regard to reliability and efficiency to knock out receptor proteins in mouse astrocytes in different brain regions like cerebellum, cortex, hippocampus, brainstem and optic nerve. Therefore we will mate GLAST-CreERT2 mice with mice carrying floxed alleles (*p2ry1*$^{fl/fl}$, *gria1*$^{fl/fl}$, *gabbr1*$^{fl/fl}$, *stop*$^{fl/fl}$*tdTomato*).

We will investigate tamoxifen metabolism in young adult wild type mice to determine an optimal injection protocol achieving maximum DNA recombination of target genes and minimum health burden for experimental animals. Concentrations of tamoxifen and 4-hydroxytamoxifen in serum and brain will be determined by HPLC-MS. Efficiency of DNA recombination of the two target genes *p2ry1*$^{fl/fl}$ and *gria1*$^{fl/fl}$ after different injection protocols will be determined by qRT-PCR quantifying recombined alleles. Data obtained in this study are essential for the tamoxifen treatment of mice in all following experiments.

Subsequently, DNA recombination of the reporter gene tdTomato will be evaluated by qRT-PCR by quantifying intact floxed alleles. Potential differences between male and female mice will be considered. qRT-PCR results will be verified likewise in a quantitative manner by immunohistological methods. Further, we will investigate the loss of two floxed receptor genes (*p2yr1* and *gabbr1*) in the same way as reporter mice and compare results. Experimental animals are in general one month old at the time of injection and analyzed the latest 21 days after the first injection.

Efficiency and especially specificity of the GLAST-CreERT2 system will be evaluated by immunohistological methods at different time points after injection of tamoxifen in young and old (6 months) reporter mice. We will highlight advantages and disadvantages of the system in regard to the brain region of interest.

In addition we will take advantage of the red fluorescent signal of recombined cells in the tdTomato reporter mice and establish FACS sorting for astrocytes (GLAST+ cells). We hereby provide a manifold adaptable method to analyze conditional knockout and control cells at the single cell level.

In summary, we will precisely evaluate the astrocyte-specific GLAST-CreERT2/loxP system in the murine brain by establishing methods best adapted to receptor knockout models. They can serve as a workflow template to obtain more trustful data from knockout models, considering complexity of individual brain regions.

Secondly (Part II), we will apply and transfer established methods to two novel receptor knockout animals, the inducible astrocyte-specific $P2Y_1$ and NMDA receptor knockout mouse lines. We will obtain first data in regard to recombination efficiencies at the DNA, mRNA and protein level. Further we will perform functional studies of astroglial NMDA receptors by immunohistological and electrophysiological methods with particular emphasis on the cortex. Astroglial $P2Y_1$ receptors will be additionally investigated at the ultrastructural level with focus on the cerebellum.

.

4 PART I: Evaluation of the GLAST-CreERT2/loxP system in mouse astrocytes

Hannah M. Jahn[1], Carmen V. Bohn[1], Andreas Helfer[2], Julian Michely[2], Aiman S. Saab[1, 3], Hans H. Maurer[2], Alexei Verkhratsky[4], Anja Scheller[1] and Frank Kirchhoff[1]

(1) Department of Molecular Physiology, University of Saarland, Homburg, Germany

(2) Department of Experimental und Clinical Toxicology, University of Saarland, Homburg, Germany

(3) Institute of Pharmacology and Toxicology, University of Zürich, Zürich, Switzerland

(4) Faculty of Life Sciences, University of Manchester, Manchester, UK

The following study received support from the mentioned colleagues and collaborations. Results will be submitted to a peer-reviewed journal.

4.1 Evaluation of tamoxifen pharmacokinetics in wild type mice

For the generation of astrocyte-specific knockout mice the tamoxifen inducible variant of the Cre DNA recombinase CreERT2 was inserted into the locus of the glutamate aspartate transporter (GLAST) (Mori et al., 2006). After tamoxifen injection the Cre DNA recombinase is translocated into the nucleus where the enzyme recombines the floxed gene sequences.

Tamoxifen (TAM) is a selective estrogen receptor modulator and a prodrug, metabolized in the liver by a cytochrom of the P450 superfamily to active metabolites, like 4 -hydroxytamoxifen (4-OHT), which possesses ~100 fold higher affinity to estrogen receptors as tamoxifen itself in humans and mice. Estrogen receptors are modulators of various physiological functions, including formation of sexual characteristics. The drug is not specific for the mutated ligand binding domain of the estrogen receptor of the Cre fusion protein (CreERT2); it also binds to endogenous estrogen receptors. In addition, TAM is not soluble in aqueous solutions and has to be injected intraperitoneal dissolved in oil. To maintain physiological conditions it is crucial to control the dosage of the drug very carefully. At the same time the dosage has to be high enough to achieve the maximum number of recombined alleles. To find the best protocol we firstly asked how much of the injected TAM can be found in the brain? How much is metabolized to 4-OHT? And how long are TAM and its metabolite 4-OHT detectable in the serum and brain of wild type mice after injection?

Mice were intraperitoneally (IP) injected once with TAM according to the following formula:

100 mg/kg bodyweight/ concentration of solution (0,01 mg/µl) , e.g: a 20 g mouse received 200 µl TAM; 2 mg TAM in total. Blood and whole brain samples were collected 8 hours (h), 1 day (d), 2 d, 5 d, 7 d, 14 d and 21 d post injection (pi) and processed for HPLC-MS analysis to determine the concentrations of TAM and 4-OHT (see Figure 4. 1 A; B: serum, C: brain, Table 17 in the supplementary). Per time point 3 animals were used. 8 h after injection maximum TAM and 4-OHT concentrations were measured in serum with 779 (± 93) ng/ml and 483 (± 36) ng/ml and brain with 5749 (± 668) ng/ml and 1006 (± 170) ng/ml for TAM and 4-OHT, respectively. 4-OHT concentrations in serum and brain are lower as TAM concentrations, in the serum a 1.6 fold difference and for the brain a 5.7 fold difference could

be detected. In addition, a 7.4 and 2.1 fold higher concentration for TAM and 4-OHT has been determined in the brain as in the serum. Already after 1 dpi TAM and 4-OHT concentrations decreased to half of the initial values, this statement counts for serum and brain (serum: TAM 330 (± 39) ng/ml; 4-OHT: 285 (± 32) ng/ml, brain: TAM 2250 (± 485) ng/ml; 4-OHT 516 (± 99) ng/ml. Further, 2 dpi TAM concentrations decreased again by 8.5 and 7.3 fold to 40 (± 29) ng/ml and 309 (± 197) ng/ml for serum and brain, respectively.

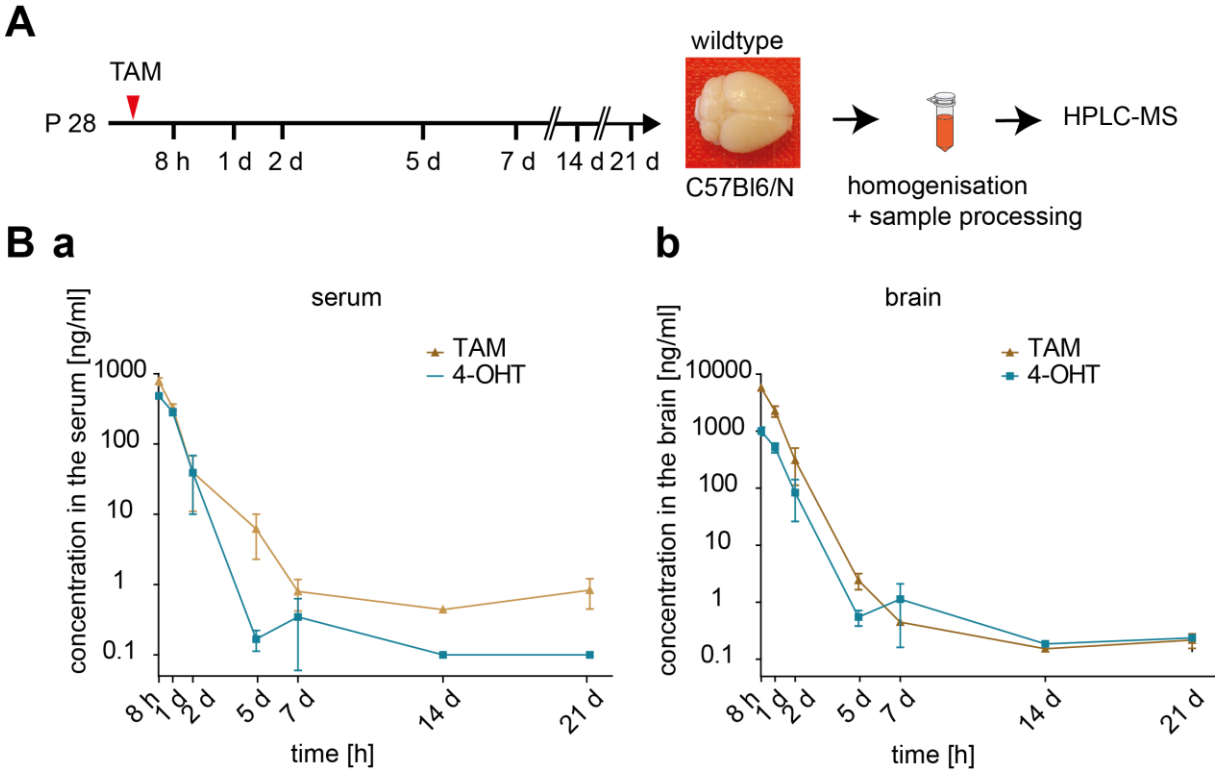

Figure 4. 1 [TAM] and [4-OHT] in serum and brain depending on time post injection
A: Mice were injected at the age of 28 days and blood and brain samples were collected 8h, 1d, 2d, 5d, 7d, 14d and 21d after the first injection (n=3). **B:** Samples were processed and analyzed via HPLC-MS. **a (serum)**, **b (brain)**: The determined TAM and 4-OHT concentration (y) are plotted against the time (x). Values are shown with $\log_{10}$ scale to visualize low concentrations after day 2. Data are shown ± SEM.

4-OHT was reduced by 7.3 and 6.2 fold to 39 (± 29) ng/ml and to 83 (± 57) ng/ml for serum and brain, respectively. At the following time point, 5 dpi, it was difficult to detect TAM (serum: 6 (± 4) ng/ml; brain 2 (± 1) ng/ml) and the metabolite 4-OHT was almost undetectable. At the later time points, 7 d, 14 d and 21 dpi, the concentrations were vanishingly low. Values are shown logarithmized to see minor differences (Figure 4. 1 B a b). Maximal concentrations (C_{max}) were present 8 h after injection or quite likely before that time point. Values at following time points were decreased, so peak concentrations could not be determined. If we assume C_{maxTAM} and $C_{max4\text{-}OHT}$ 8 h after injection, half lifes in the serum were 22.3 h and 26.8 h for TAM and 4-OHT, respectively. In the brain it took 20.9 h and 25.3 h till concentrations of TAM and 4-OHT, respectively, are decreased half of initial concentrations.

In summary the results show, that on average a single injection of 1.65 (± 2.85 SD) mg TAM can be detected as long as 5 dpi in serum and brain homogenates, but already 1 dpi concentrations are halved. TAM and 4-OHT possess fast half lives in the hour range.

4.2 Quantification of recombination events after tamoxifen injection

We investigated two target genes, floxed *p2ry1* and *gria1* gene loci in the cerebellum (cb) and cortex (ctx). These genes code for the $P2Y_1$ receptor and AMPA receptor subunit GluA1, respectively (see Figure 4. 2 A a). Mice were injected once with TAM at the age of 28 days and were analyzed 8 h and 21 d after injection, respectively, for changes of the floxed loci by quantitative real time PCR (qRT-PCR) for genomic recombination. Primers flank both loxP sites. After successful recombination they approach each other and PCR products can be amplified. Therefore the PCR quantifies DNA recombination events. In addition we injected mice twice, three and five times with TAM at consecutive days and analyzed the samples 21 d later (note in all experiments with more than one injection dpi means days post first injection). Further, we waited for 200 d after three injections for a final analysis. Additionally, we injected mice three times with TAM with an interval of two days in between injections, since 4-OHT concentrations dropped already 2 dpi to baseline level. Again analysis took place 21 dpi. Per experiment at least three animals were used and data were normalized to the mean value of the five times injection time point (see Figure 4. 2 A b c). The results are depicted in Figure 4. 2 B (b: ctx, c: cb).

An important observation, three injections and five injections of TAM did not show significant differences in the quantity of recombined *p2ry1* and *gria1* alleles 21 dpi in cortex and cerebellum, respectively. The same applied for three injections and a waiting period of 200 d before analysis (compare Figure 4. 2 B 4, 5, 6). However, we can conclude that 3 injections and a period of 21 d are sufficient to complete recombination process of floxed genes. Noteworthy, there is a tendency of higher number of floxed alleles after 5 injections of TAM.

After 8 h (Figure 4. 2 B 1) 15 % (± 1 %) and 5 % (± 1 %) of floxed *p2ry1* and *gria1*, respectively, alleles are recombined in the cortex. In the cerebellum already 39 (± 2) % and 37 (± 2) % of *p2ry1* and *gria1* alleles, respectively, are recombined. After 21 d (Figure 4. 2 B 3) number of recombined alleles increased in the cortex to 43 (± 6) % and 23 (± 4) % for *p2ry1* and *gria1*, respectively. In the cerebellum recombined alleles of *p2ry1* and gria1 also increased to 58 (± 4) % and 75 (± 1) %, respectively. Interestingly, 2 injections did not significantly increase the number of recombined alleles neither in the cerebellum nor in the cortex (Figure 4. 2 B 4 3). Three injections of TAM on the other hand significantly increased the number of recombined alleles to 86 (± 5) % and 85 (± 5) % for *p2ry1* and *gria1*, respectively. In the cerebellum 3 injections led to 96 (± 3) % and 94 (± 4) % for *p2ry1* and *gria1*, respectively. As mentioned earlier after TAM injections on 5 consecutive days maximum recombination events could be measured by qRT-PCR for both genes and brain regions (ctx: *p2ry1*: 100 (± 7) %, *gria1*: 100 (± 5) %; cb: *p2ry1*: 100 (± 4) %, *gria1*: 100 (± 4) %). They were considered as 100 %.

Based on the decreased levels of TAM concentration after 24 h in serum and brain we investigated as well an interval protocol. Mice were injected 3 times with tamoxifen but with a break of 2 days in between injections

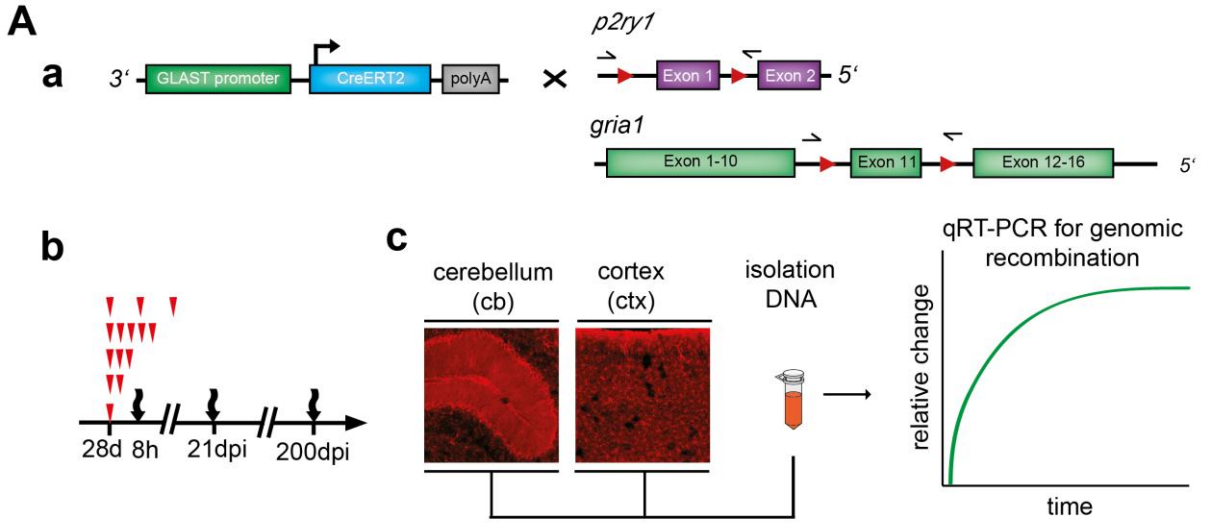
A
a
3'
GLAST promoter
CreERT2
polyA
×
p2ry1
Exon 1
Exon 2
5'
gria1
Exon 1-10
Exon 11
Exon 12-16
5'
b
28d 8h
21dpi
200dpi
c
cerebellum (cb)
cortex (ctx)
isolation DNA
qRT-PCR for genomic recombination
relative change
time

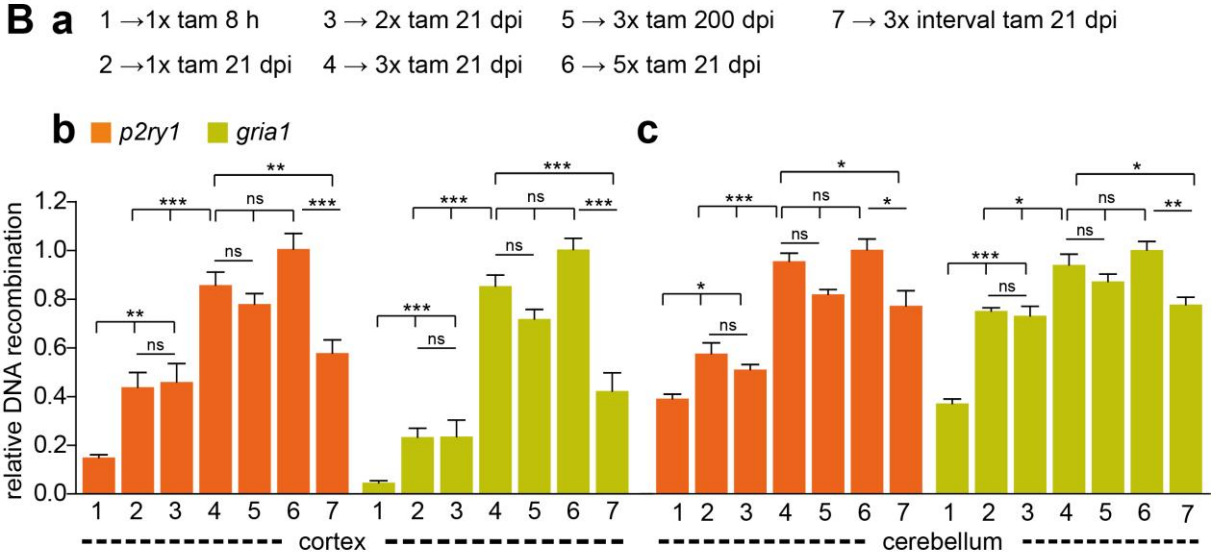
B a
1 →1x tam 8 h
2 →1x tam 21 dpi
3 → 2x tam 21 dpi
4 → 3x tam 21 dpi
5 → 3x tam 200 dpi
6 → 5x tam 21 dpi
7 → 3x interval tam 21 dpi
b
p2ry1
gria1
c
relative DNA recombination
cortex
cerebellum

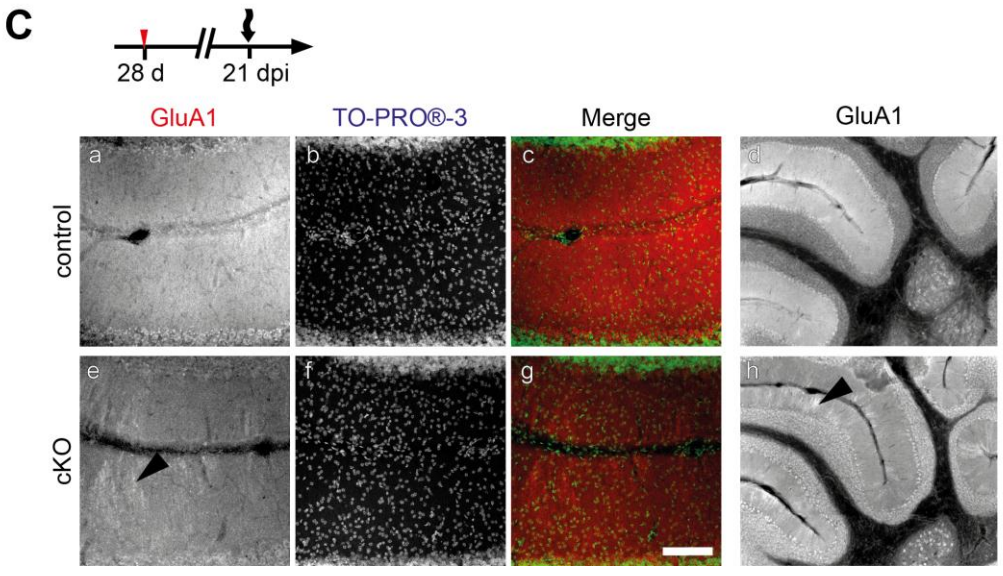
C
28 d
21 dpi
GluA1
TO-PRO®-3
Merge
GluA1
control
cKO

.

Figure 4. 2 3 TAM injections are sufficient to achieve maximum DNA recombination
A: For the analysis GLAST-CreERT2 x P2Y1$^{fl/fl}$x GluA1$^{fl/fl}$ mice were used (**a**). Mice received TAM with 7 different protocols (see **b** and **B a**) and were sacrificed 8 h, 21 and 200 dpi, respectively. Ctx and cb were homogenized and DNA isolated for qRT-PCR. Primers span for the *p2ry1* and *gria1* gene both loxP sites, after recombination primers converge and the flanked sequence can be amplified (**c**). **B:** Quantification of recombination events of the floxed *p2ry1* and *gria1* locus in ctx (**b**) and cb (**c**) after Cre induction. Per protocol 3 mice were analyzed. ΔC_T-values of animals were normalized to the mean value of animals which received 5x TAM. **C:** Vibratom slices of the cerebellum showed the reduction of GluA1 protein in cKO animals injected with a single TAM injection 21 dpi (**e-h**) compared to the control animal (**a-d**). The arrow head point to remaining protein. Scale bar in (**g**) corresponds to 100 µm. The error bars correlate to the SEM of the natural replicates (n=3, *p<0,05, **p< 0.01, ***p<0.001, unpaired t-test).

The results clearly showed that an interval protocol is not as efficient as consecutive injections: in the cortex 58 (± 4) % *p2ry1* and 42 (± 8) % *gria1* alleles and in the cerebellum 77 (± 6) % *p2ry*1 and 77 % (± 3) % *gria1* alleles were recombined.

In summary, the target genes *p2ry1* and *gria1* showed different recombination kinetics, in the initial hours after one injection (compare Figure 4. 2 B 1 and 2) but equilibrated to same values after 3 and 5 injections of TAM, respectively. The floxed *p2ry1* locus showed faster kinetics as *gria1* in the cortex after one or two injections. In the cerebellum the same number of *p2ry1* and gria1 alleles is recombined after 8 h, but after 21 d *gria1* showed a 20 % higher efficiency as *p2ry1*. In general, the cerebellum showed faster recombination kinetics as the cortex after one injection and between 8 h and 21 d.

The next question, after successful recombination, is the extent of the protein knock down. We injected astrocyte-specific control and GluA1 cKO mice (GLAST$^{CreERT2/+}$ x GluA1$^{fl/fl}$) once with tamoxifen and checked for GluRA expression in the molecular layer of the cerebellum 21 d after injection (see Figure 4. 2 C). At the DNA level we determined 75 (± 1) % recombination events. Immunohistochemical staining of the targeted protein demonstrated definite reduction of GluA1 expression. Just single Bergmann glia cells still showed GluA1 expression. This experiment showed that also on protein level about 75 % (not quantified) of BG glia cells lost their expression after one injection of tamoxifen. A detailed investigation of protein degradation of the GluA1 and GluA4 AMPAR subunits after 5x TAM injection are investigated in Saab et al., 2012.

4.3 Evaluation of reliability of DNA reombinantion induced by the GLAST-CreERT2 system

To evaluate the reliability of the Glast-CreERT2 driver line, recombination efficiencies of one reporter gene (tdTomato$^{fl/fl}$) and two floxed receptor genes (p2yr1$^{fl/fl}$, gabbr1$^{fl/fl}$, which codes for the GABA receptor subunit B1.) were investigated (see Figure 4. 3 B). Mice were genotyped, grouped in control and conditional knock out (cKO) animals and injected for three days once a day with TAM. Animals were 4 weeks old at the first day of injection. 21 d after induction of Cre activity (see Figure 4. 3 A a), DNA was isolated from different brain regions (see Figure 4. 3 A b), like brainstem (bs), cerebellum (cb), cortex (ctx), hippocampus (hp) and optic nerve (opt.n.).

Quantity of intact loxP sites were determined by qRT-PCR for DNA recombination. Primers flank one of the loxP sites for each respective gene. The reduction of the fluorescent signal in

cKO animals indicates a reduction of intact floxed alleles resulting from successful recombination; in contrast to the PCR strategy discussed in 4.2 which quantified recombined alleles. In addition the reporter mouse line was analyzed for potential sex differences at the mRNA level by qRT-PCR for mRNA expression and at the protein level by immunohistochemical methods.

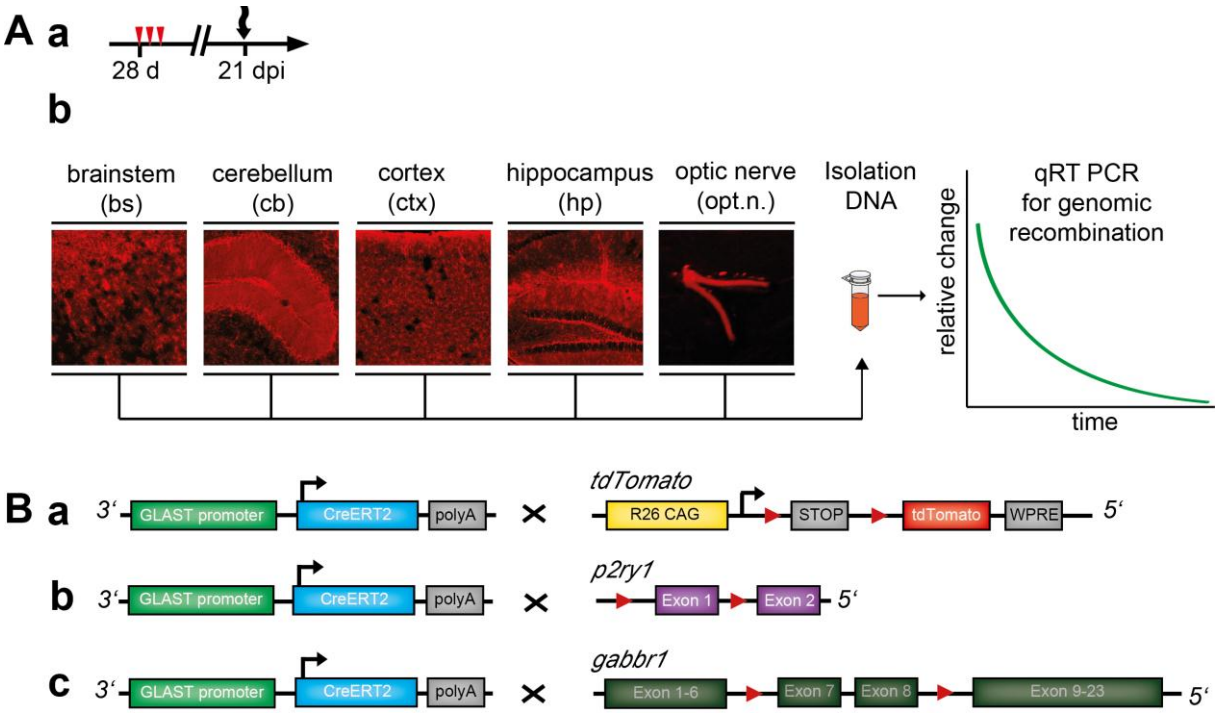

Figure 4. 3 Schematic overview of experimental design
A: Mice were injected at the age of 28 d and analyzed 21 dpi. **B:** Heterozygous GLAST-CreERT2 mice were crossbred to mice carrying the floxed stop codon downstream of the expression sequence of the reporter protein tdTomato (**a**), the floxed exon1 of the $P2Y_1R$ gene (*p2ry1*) (**b**) and the floxed exons 7/8 of the $Gaba_{B1}$ gene (*gabbr1*) (**c**). The extent of genomic recombination of the floxed genes was determined by qRT-PCR for different brain regions (bs, cb, ctx, hp and opt. n.). The primers are designed to result in a decreased signal in recombined animals.

4.3.1 Evaluation of GLAST-CreERT2 driven DNA recombination at the reporter level

It is common practice to investigate functionality of a Cre driver line by crossbreeding it to a reporter mouse line. After onset of Cre activity, recombined cells express a fluorescent protein, visualizing the successful recombination process. Here we used a reporter mouse which expresses after successful recombination of a floxed stop cassette; the red fluorescent protein tdTomato (Madisen et al., 2010). Mice were grouped in male and female, reporter and control mice. Controls are homozygously floxed for the tdTomato locus but lack CreERT2 expression. Mice were injected at the age of 28 d. The analysis took place 21 d after the first injection (see Figure 4. 4 A a, b).

Females showed higher fluorescent intensity of the reporter protein tdTomato as depicted in representative epifluorescent sagittal brain slices of a female and male. The quantification of fluorescent signals revealed a reduction to 82 (± 2) % in males compared to female littermates (100 %) (Figure 4. 4 B a, b, c, d) per cell.

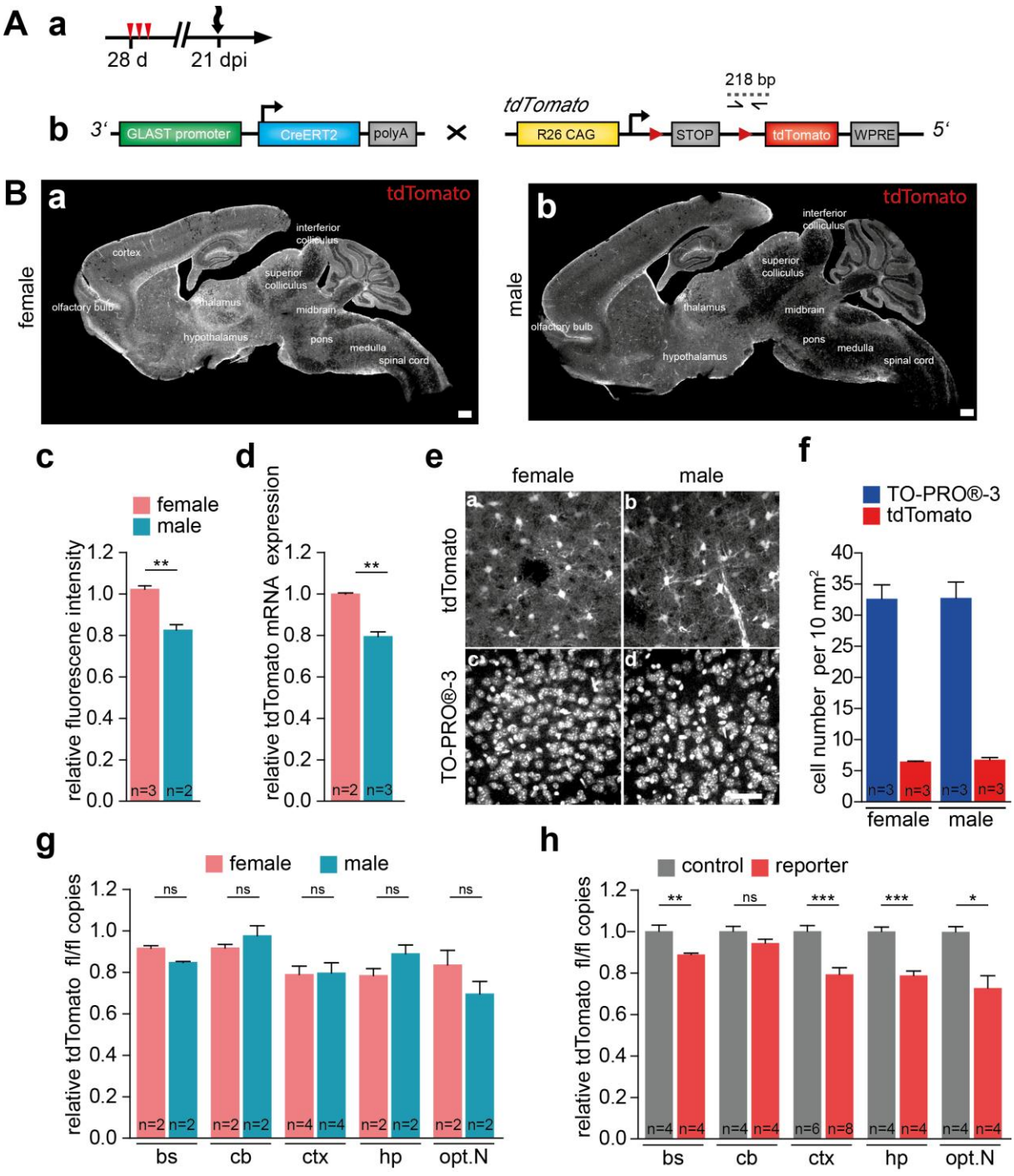

Figure 4. 4 Females and males show similar recombination efficiencies

A: The injection/analyzing scheme and modified gene sequences of the GLAST-Cre$^{ERT2/+}$ x stop$^{fl/fl}$ tdTomato mice is shown in **a** and **b,** respectively. **B:** Two representative sagittal overviews of a GLAST$^{CreERT2/+}$ x stop$^{fl/fl}$tdTomato female (**a**) and male (**b**) show decreased fluorescent tdTomato intensities in males quantified in (**c**). Quantification of tdTomato mRNA by qRT-PCR determined, in line with the IHC results, a 20 % decrease of tdTomato mRNA expression in male compared to female mice (**d**). The number of recombined cells in female and male mice is not different. Counting of TO-PRO-®-3+ and tdTomato+ cells in cortices of ♀/♂ GLAST$^{CreERT2/+}$ x stop$^{fl/fl}$ tdTomato vibratom slices showed no significant difference (**f**). Quantification of floxed non-recombined alleles in bs, cb, ctx, hp and opt.n by qRT-PCR in female and male animals showed no significant differences (**g**). In conclusion qRT-PCR results of males and females were combined (**h**). The scale bar in **B** and **e**, **d** corresponds to 2.5 cm and 50 µm, respectively. The error bars correlate to the SEM of the natural replicates (n=as indicated, *p<0.05, **p< 0.01, ***p<0.001, unpaired t-test).

We also compared mRNA expression of tdTomato in both gender and could determine 21 (± 2) % reduction of tdTomato mRNA expression in male mice. A higher intensity can be explained by a higher number of recombined cells in females or different regulation of the R26 locus, resulting in more protein.

The actual pattern of recombined astrocytes looks similar in cortex, olfactory bulb, thalamus and hypothalamus in both genders but less dense in medulla, pons, midbrain, superior and inferior collicullus of male brains. The impression of gender differences of the pattern of recombined astrocytes could be slightly displaced since the exact same depth of sagittal slices has to be compared. Being able to pool female and male mice for further experiments is an advantage considering breeding capacities and unreasonable killing of male or female littermates, respectively.

We counted tdTomato positive (+) cells and normalized them to TO-PRO-3®+ cells in detailed confocal images of female and male cortices. The results show no significant differences in the number of recombined cells that could count for differences between male and female mice. In a cortical area of 10 mm^2 7 (± 1) % and 7 (± 1) % cells in female and males, respectively, are tdTomato+ (see Figure 4. 4 B e, f). In line, qRT-PCR for DNA recombination determined no significant differences in the quantity of loxP sites in cortices male and female reporter mice. In both genders, the same number of stop codons were cut off by the cre recombinase, the same applied for the brainstem, cerebellum, hippocampus and optic nerve (see Figure 4. 4 B g).

In conclusion qRT-PCR results for males and females were combined (see Figure 4. 4 B h). Primers amplified floxed non-recombined alleles and revealed therefore significant reductions of floxed *p2ry1* alleles in homogenates of reporter mice (positive recombination events). In brainstem 11 (± 1) %, cerebellum 6 (± 1) %, hippocampus 22 (± 2) % and in optic nerve 27 (± 5) % of cells were recombined.

In the cortex qRT-PCR revealed 21 (± 3) % of recombined cells. As mentioned earlier, tdTomato+ cells were also counted in the cortex, here 21 (± 3) % of all cells (TO-PRO-3®+) were tdTomato+. These results clearly demonstrate, that the qRT-PCR approach to determine the quantity of loxP sites, correlate to the actual number of recombined cells. The recombination efficiency roughly reflects the percentage of GLAST-positive glia (astrocytes) in the respective brain regions.

4.3.2 Evaluation of GLAST-CreERT2 driven DNA recombination efficiency of target genes

Recombination efficiencies at the reporter level looked promising so we analyzed two actual target genes *p2ry1* (see also 4.2) and *gabbr1*. We followed the same protocol as with the tdTomato reporter mice. Mice were injected at the age of 28 days for 3 consequetive days. Brainstem, cerebellum, cortex, hippocampus und optic nerve were analyzed 21 days later in a quantitative manner for the loss of floxed gene sequences by qRT-PCR for DNA recombination. Primers flank 3'- loxP site and the 5'- loxP site of the *gabbr1* and *p2ry1* gene, respectively (see Figure 4. 5 a, b).

Values of cKO are normalized to the values of the respective control animals. Results for the target gene *p2ry1* are shown in Figure 4. 5 b. cKO animals showed in the brainstem a reduction of 23 (± 3) %, in the cerebellum of 6 (± 1) %, in the cortex of 20 (± 2) %, in the hippocampus of 33 (± 4) % and in optic nerve of 32 (± 1) %.

The results for the *gabbr1* gene are depicted in Figure 4. 5 c**,** here cKO animals showed a reduction of floxed alleles of 25 (± 1) % in the brainstem, of 14 (± 4) % in the cerebellum, of 25 (± 6) % in the cortex, of 29 (± 7) % in the hippocampus and of 38 (± 4) % in optic nerve.

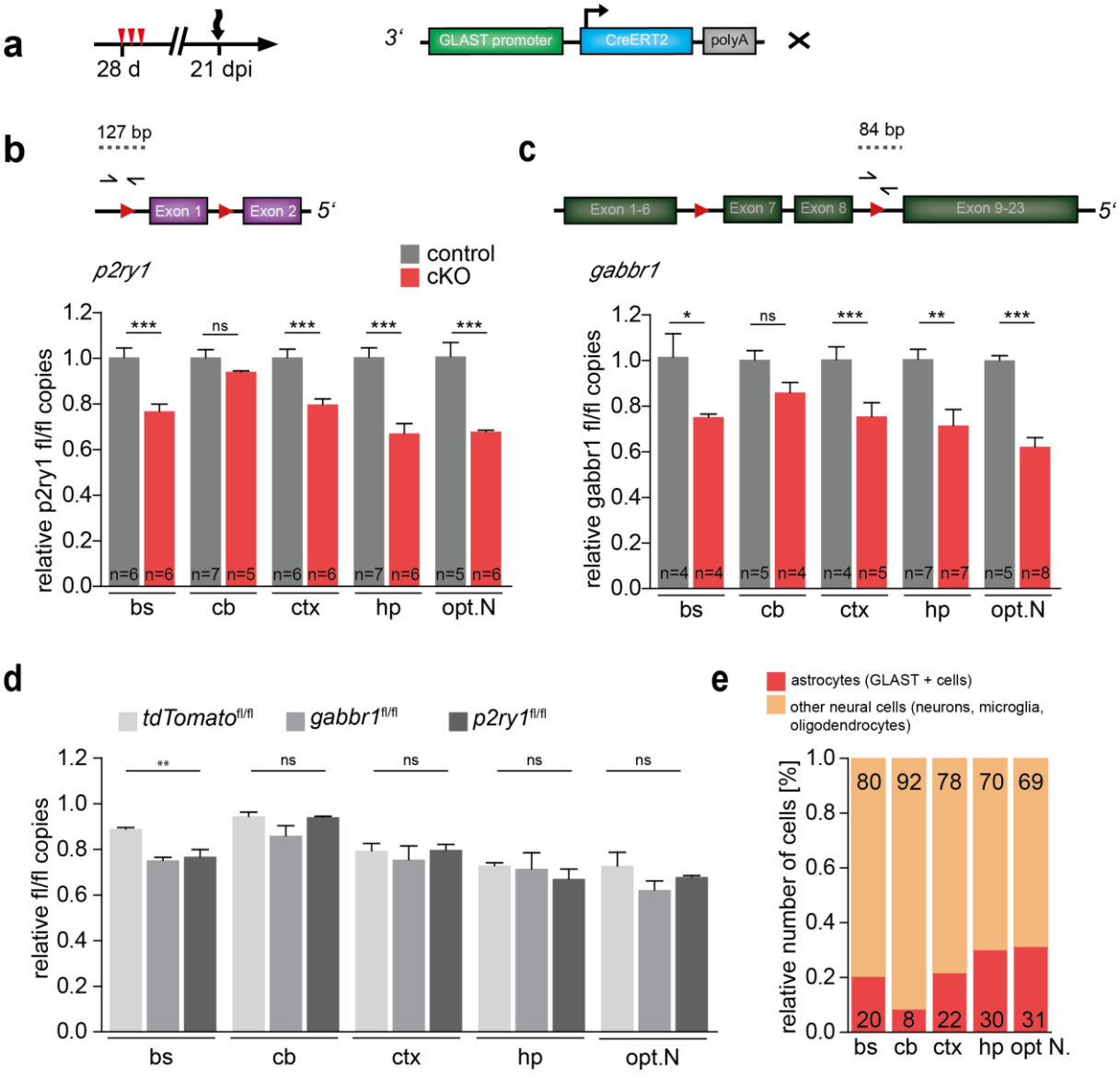

Figure 4. 5 Recombination efficiencies are stable for target genes and reporter
a: Animals were injected with 28 d and analyzed 21 dpi. Primers for qRT-PCR were designed in close vicinity of the 3' loxP site for the *p2ry1* gene (**b**) and of the 5' loxP site for the *gabbr1* gene (**c**). ΔC_T-values of cKO animals were normalized to the mean of the respective control animals. The reduction of the fluorescent signal in cKO mice indicates a reduction of intact loxP sites, resulting from successful recombination. Direct comparison of cKO values showed no significant differences in recombination efficiencies in cb, ctx, hp and opt. n. between three target genes. Only the reporter gene showed significant less recombination events in the brainstem (**d**). The recombination efficiency reflects the percentage of GLAST+ glia (astrocytes) in the respective brain regions (**e**). Data are shown as mean ±SEM of the natural replciates (n=as indicated, *p<0.05, **p< 0.01, ***p<0.001, unpaired t-test).

Values of cKO animals are summarized in Figure 4. 5 d to show the direct comparison of the two investigated target genes and the reporter gene (see 4. 3). For the cerebellum, cortex, hippocampus and optic nerve no significant difference was detected. Meaning that the floxed

stop codon, floxed exon1 of *p2ry1* and floxed exon 7-8 of the *gabbar1* gene are recognized by the cre recombinase and recombined in the same quantitative manner. Only in the brainstem a significant difference between reporter and target genes has been observed. Nonetheless, the GLAST locus seemed to be reliable to induce Cre activity and to recombine different floxed loci to the same extent. We pooled the data for all investigated brain regions (see Figure 4. 5 e) considering that no differences between males and females and floxed loci exist (see Figure 4. 4 B g). We equate GLAST+ cells as astrocytes and the quantified loss of floxed alleles as a measure for astrocytes in a given brain tissue. We conclude that in a brain of a young adult mouse in the brainstem 20 (± 2, n=14) %, in the cerebellum 8 (± 2, n=13) %, in the cortex 22 (± 2, n=19) %, in the hippocampus 30 (± 3, n=16) % and in the optic nerve 31 (± 2, n=17) % account for astrocytes.

4.4 Evaluation of DNA recombination specificity of the GLAST-CreERT2/loxP system

We further analyzed the efficiency of the GLAST-CreERT2 system and investigated if DNA recombination is restricted to astrocytes by immunohistochemical methods. An overview of the experimental design is depicted in Figure 4. 6 A. The red boxes indicate the position, were confocal images of sagittal vibratom slices have been taken. In B and C representative images of the cerebellum (a, b), cortex (c, d), hippocampus (e, f) and brainstem (g, h) of $GLAST^{CreERT2/+}$ x $stop^{fl/wt}$ tdTomato animals, 3 d and 21 d after first injection, are shown. By comparisan of the two time points it became obvious that two injections and 3 days of waiting period are not sufficient to recombine 100 % of GLAST+ cells in the cerebellum, cortex and brainstem. These results are in line with the recombination efficiencies determined at DNA level for the cerebellum and cortex (see 4.2). In the hippocampus it was difficult to distinguish differences between 3 and 21 d after the first injection in regard to the quantity of recombined cells in 2D images. But it was already visible that also radial glia/granule cell precursor cells recombine in the dentate gyrus (DG) of the hippocampus. They show different morphologies as protoplasmic astrocytes. They have a pyramidal shaped soma and long fine processes (see Figure 4. 6 B f, C f).

In Figure 4. 7 A and B we investigated at tdTomato+ cells 3.5 and 5 months (m), respectively, after the first injection (mpi). The pattern and morphology of tdTomato+ cells in cerebellum, cortex and brainstem did not change between 3.5 and 5 mpi and compared to 21 d after the first injection. These results showed that 3 injections of TAM and 21 d are sufficient to recombine the maximum number of cells. Again, results are in line with data obtained by qRT-PCR for DNA recombination (see 4.2 and 4.3). We also injected mice at the age of 6 month and investigated tdTomato+ cells 3.5 mpi. Also here the number of recombined cells did not seem to increase compared to younger injected mice in the cerebellum, cortex and brainstem (compare Figure 4. 7 A a-d, g, h and C a-d, g, h).

Importantly, the hippocampus did show a different pattern of recombined cells 3.5 and 5 mpi compared to 3 and 21 dpi (Figure 4. 7 A, B, e, f). The number of tdTomato+ differentiated granule cells increased, considering the visible axons in the dentate gyrus. Predominantly these neurons were visible. If we injected older mice and waited as well 3.5 mpi until analysis, rather recombined astrocytes with the common morphology were tdTomato+ in the

dentate gyrus and CA3 and CA1 regions. At the same time the number of radial glial/granule cells neurons decreased (see Figure 4. 7 C e, f).

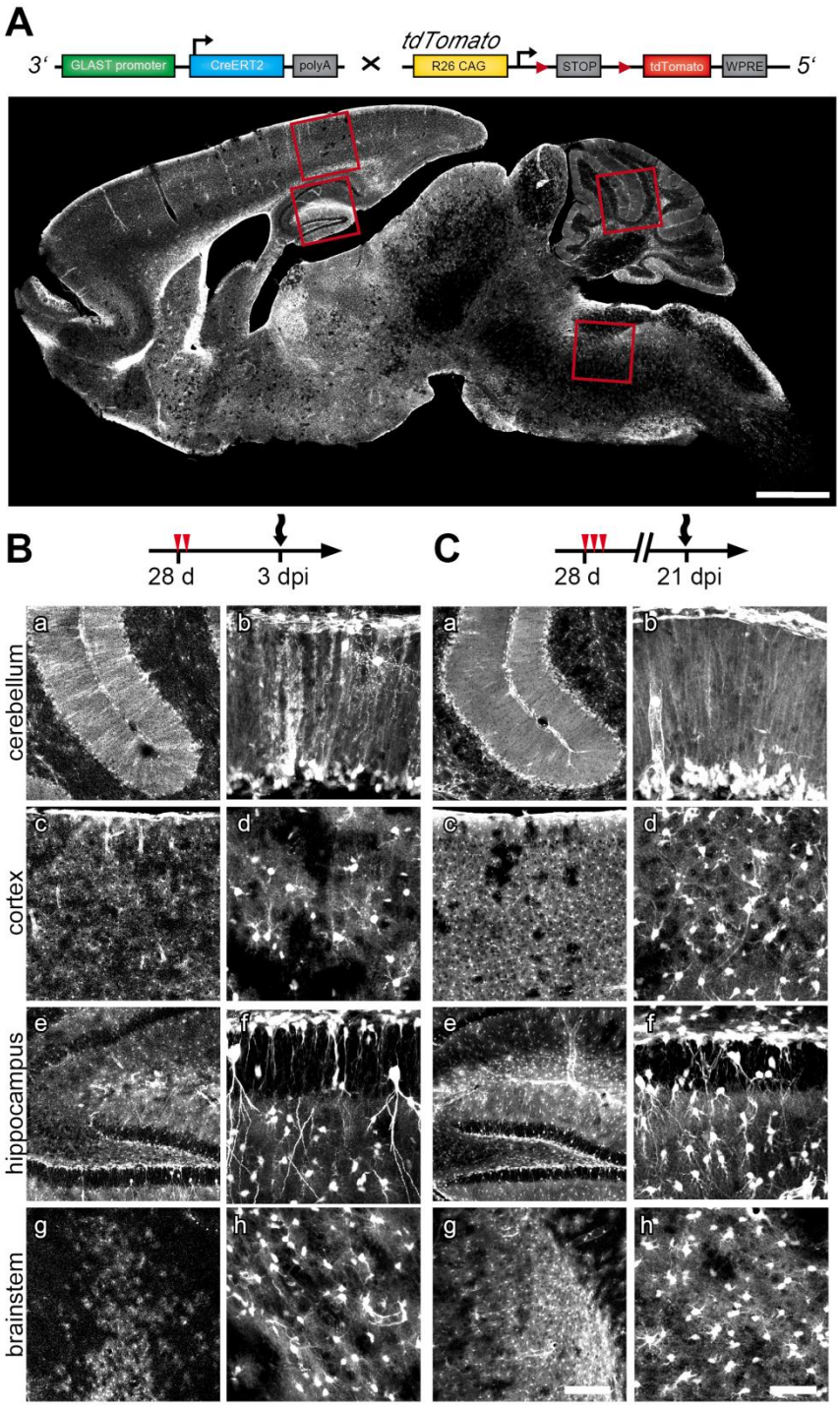

Figure 4. 6 DNA recombination 3 and 21 days after TAM injections at the reporter level in young mice

A: Overview of a sagittal vibratom slice of a GLAST$^{CreERT2/+}$ x stop$^{fl/wt}$ tdTomato animal 21 d after the first injection of tamoxifen. Fluorescent cells are recombined and express the red reporter protein. Red boxes indicate the position in bs, cb, ctx and hp where confocal images have been taken for further analysis (see **B**, **C** and figure 4. 7). **B**, **C:** Confocal images show tdTomato expression in the cb (**a**, **b**) ctx (**c**, **d**), hp (**e**, **f**) and bs (**g**, **h**) 3 dpi and 21 dpi after the first injection, respectively. An increase of recombined cells can be observed 21 dpi compared to 3 dpi. The scale bar in (**C: g**) corresponds to 200 µm and applies for images (**B**, **C**: **a**, **c**, **e**, **g**), the scale bar in (**C: h**) corresponds to 50 µm and applies for the images (**B**, **C**: **b**, **d**, **f**, **h**).

To identify recombined cells not only by morphology as astrocytes sagittal slices of injected mice at all mentioned time points were co-stained with the astrocytic markers GFAP (glial fibrillary acidic protein) and glutamine synthetase (GS) (see 3 dpi: Figure 8. 1; 21 dpi: Figure 8. 3 , 3.5 mpi Figure 8. 5, 5 mpi: Figure 8. 7, 6 m + 3.5 mpi: Figure 8. 9) and the neuronal marker NeuN (3 dpi: Figure 8. 2; 21 dpi: Figure 8. 4; 3.5 mpi: Figure 8. 6; 5 mpi: Figure 8. 8; 6 m+3.5 mpi: Figure 8. 10).

In summary, tdTomato+ cells showed as expected either GFAP and/or GS expression in cerebellum, hippocampus and brainstem. Cortical astrocytes were not stained by GFAP but tdTomato+ cells showed GS expression. Noteworthy we determined also tdTomato+ cells which showed neither expression of GFAP or GS. These results support the idea of a heterogeneous population of astrocytes. A marker which stains all astrocytes has not been found yet.

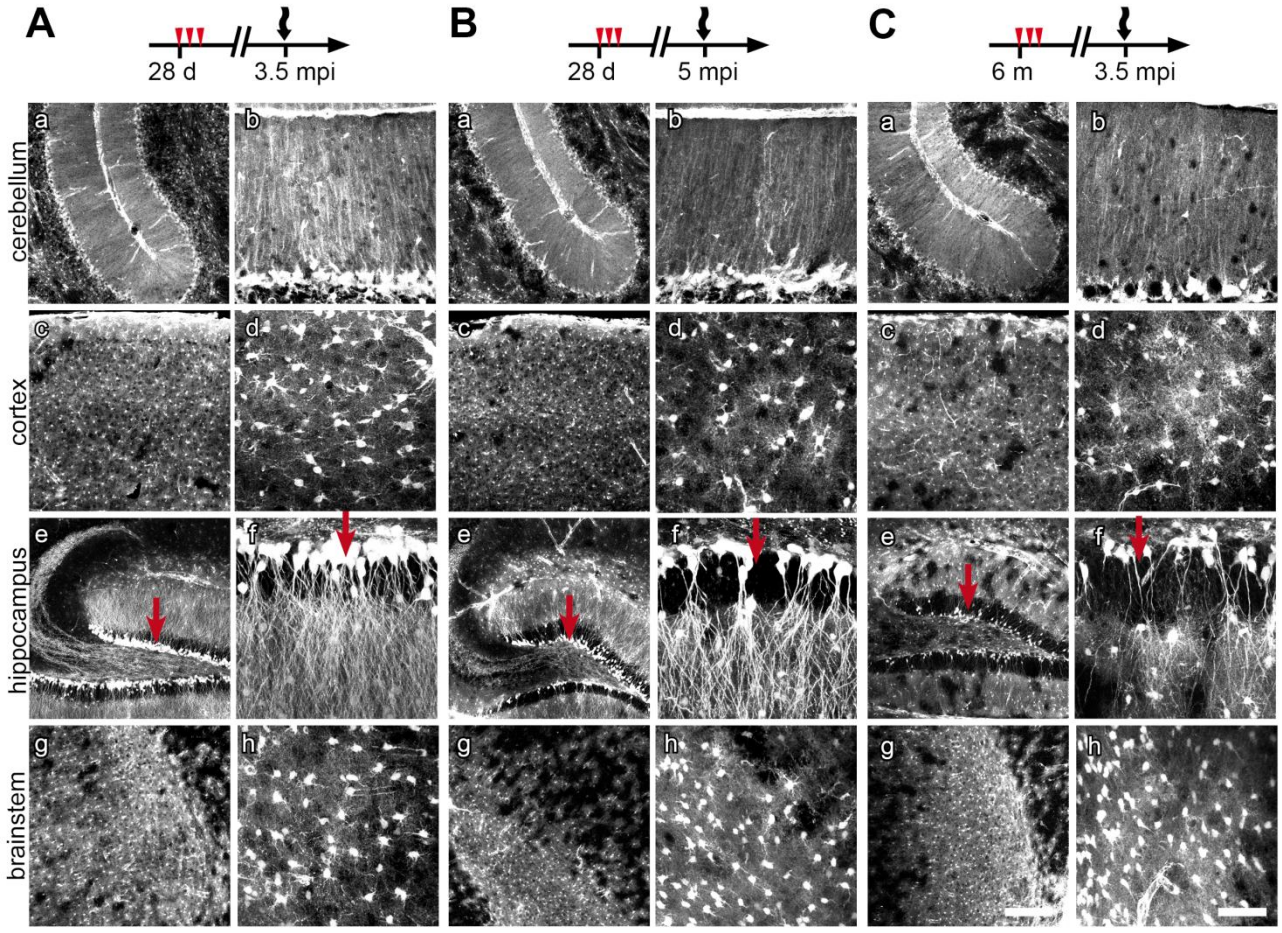

Figure 4. 7 DNA recombination 3.5 and 5 months after TAM injections at the reporter level in young and old mice

A, B: Animals were injected with TAM at 3 consecutive days at the age of 28 d and analyzed 3.5 and 5 mpi, respectively. **C**: Animals were injected with TAM at the age of 6 months and analyzed 3.5 m after the first injection. Confocal images in **A**, **B**, **C** show the reporter protein expression of tdTomato in cb (**A**, **B**, **C**: **a**, **b**) ctx (**A**, **B**, **C**: **c**, **d**), hp (**A**, **B**, **C**: **e**, **f**) and bs (**A**, **B**, **C**: **g**, **h**) after Cre activation at the mentioned time points. Maximum recombination seemed to be achieved already 21 dpi (compare figure 6 C). After 3.5 and 5 mpi tdTomato+ granule cells in the dentate gyrus became more present (red arrow heads), indicating that next to astrocytes GLAST+ progenitor cells are recombined (**B**, **C**). The number of labeled, newly born neurons seems to be reduced in older injected animals (**C**). The scale bar in (**C: g**) corresponds to 200 µm and applies for the images (**A**, **B**, **C**: **a**, **c**, **e**, **g**), the scale bar in (**C: h**) corresponds to 50 µm and applies for the images (**A**, **B**, **C**: **b**, **d**, **f**, **h**).

In all investigated brain regions and time points after injection we could not detect any NeuN+ recombined cells in cerebellum, brainstem and cortex. Exception is again the hippocampus.

Representative confocal images of co-stained GLAST-CreERT2 x stop$^{fl/wt}$tdTomato 3.5 mpi are shown in Figure 4. 8 B (GS), C (NeuN) and Figure 4. 9 B (GS) D (NeuN) for young and old injected mice, respectively.

Furthermore, slices were stained at both later stages after injection against the radial glia marker BLBP (brain lipid-binding protein) (Figure 4. 8 D, Figure 4. 9 G) and the mature oligodendrocyte marker MBP (myelin basic protein) (Figure 4. 8 G, Figure 4. 9 F). In addition young injected mice were investigated for the NG2 (nerve/glia antigen-2) glia marker PDGFRα (platelet-derived growth factor receptor) (Figure 4. 8 F) and for oligodendrocyte lineage marker Olig2 (OL lineage gene) (Figure 4. 8 E). Old injected mice were in addition analyzed for the astrocyte marker S100β (Figure 4. 9 C) and the neuronal marker VGlut1 (vesicular glutamate transporter 1) (Figure 4. 9 E). The in depth analysis was done to exclude that a disregarded GLAST+ subpopulation acts as an progenitor cell and differentiates after TAM application into oligodendrocytes or neurons throughout the brain in other regions apart from the niches of adult neurogenesis (see 6.4).

In all investigated brain regions we found tdTomato+ cells which have been positive for BLBP. As expected Bergmann glia cells in the cerebellum and radial glia, differentiating into granule cells in the DG were positive for the marker but also a subpopulation in cortex and brainstem (Figure 4. 8 D a-d and Figure 4. 9 G a-d, red arrow) showed BLBP expression. tdTomato+ cells did not co-localize with PDGFRα, Olig2, MBP or VGlut1. tdTomato+ cells co-localized with S100β, but not all recombined cells showed expression of the astroglial marker.

In summary, in young and old injected mice astrocytes are predominantly targeted by GLAST promoter induced DNA recombination as seen by GS, S100β and GFAP expression in recombined reporter cells. At both ages GLAST+ cells did not differentiate into neurons or oligodendrocytes 3.5 month after Cre DNA recombination in the cerebellum, cortex and brainstem. In the hippocampus recombined radial glia cells differentiate into granule cell neurons in the dentate gyrus. A subpopulation of tdTomato+ cells in all investigated brain regions expressed the radial glia marker protein BLBP which is also linked to neuronal differentiation. Notably, at no investigated time point co-staining with NeuN occurred in brainstem, cerebellum and cortex. So we conclude, that GLAST promoter activity, at least from postnatal day 28, is not related to neuronal differentiation in the cerebellum, cortex and brainstem.

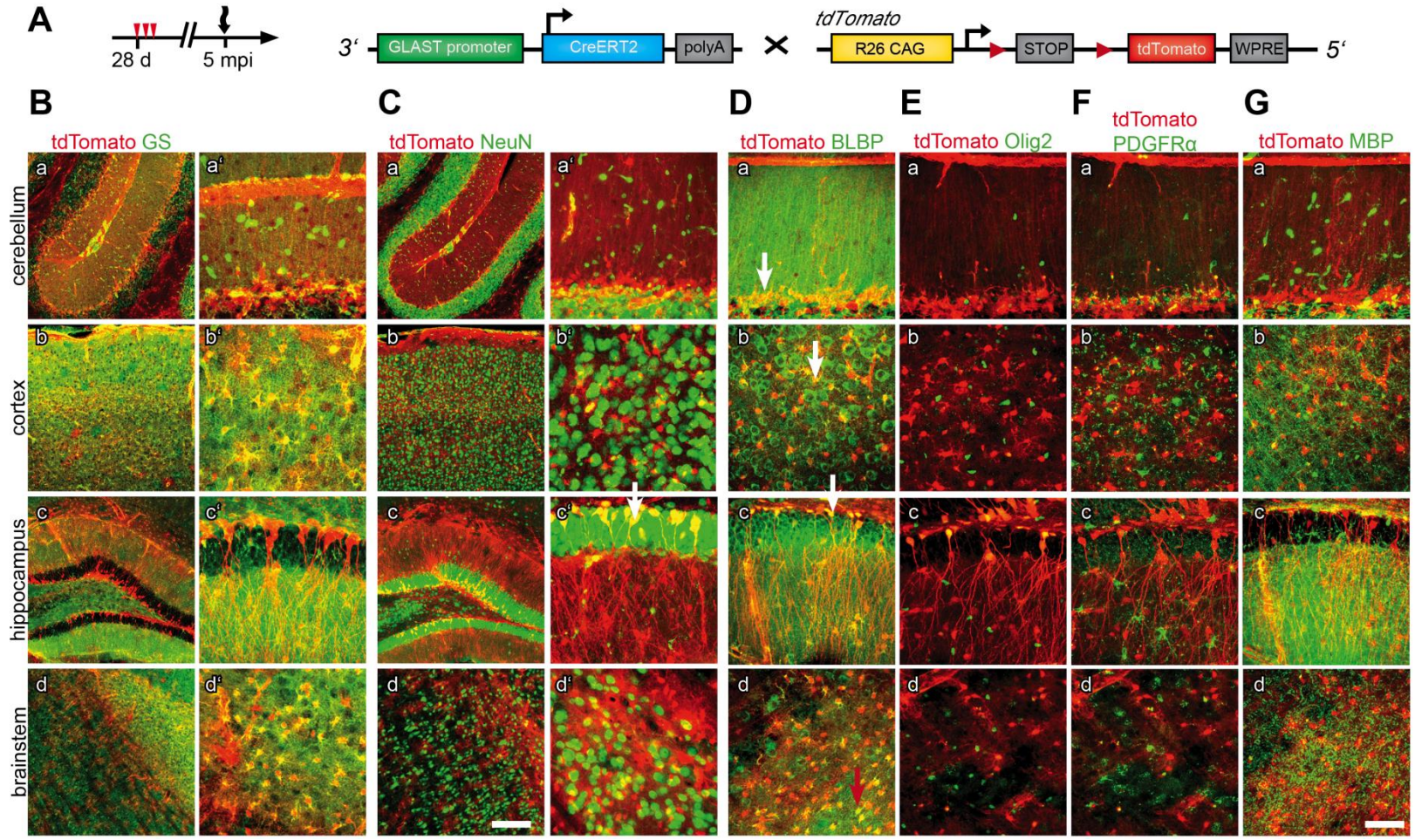

Figure 4. 8 Predominantly astrocytes are targeted by DNA recombination in young mice
Depicted are immunohistochemical stainings against GS (**B**), NeuN (**C**), BLBP (**D**), Olig2 (**E**), PDGFRα (**F**) and MPB (**G**) in cb (**B**, **C**, **D**, **E, F, G: a**, **a’**), ctx (**B**, **C**, **D**, **E, F, G**: **b**, **b’**), hp (**B**, **C**, **D**, **E, F, G**: **c**, **c’**) and bs (**B**, **C**, **D**, **E, F, G**: **d**, **d**’) of animals treated with TAM at p28 and perfused after 5 m. tdTomato+ cells showed a broad overlap with cells positive for the astrocyte marker GS but no overlap with cells positive for the neuronal marker NeuN (except differentiated granule cells), the oligodendrocyte marker Olig2 or the NG2 glia marker PDGFRα. But Bergmann glia in the cb, radial glia in the hp and a subpopulation of astrocytes in cortex and brainstem expressed the radial glial and neuronal differentiation marker BLBP (red arrow). The scale bar in (**C, d**) corresponds to 200 µm and applies for images (**B**, **C**: **a**, **b**, **c**, **d**), the scale bar in (**C, d’**) corresponds to 50 µm and applies for all remaining images.

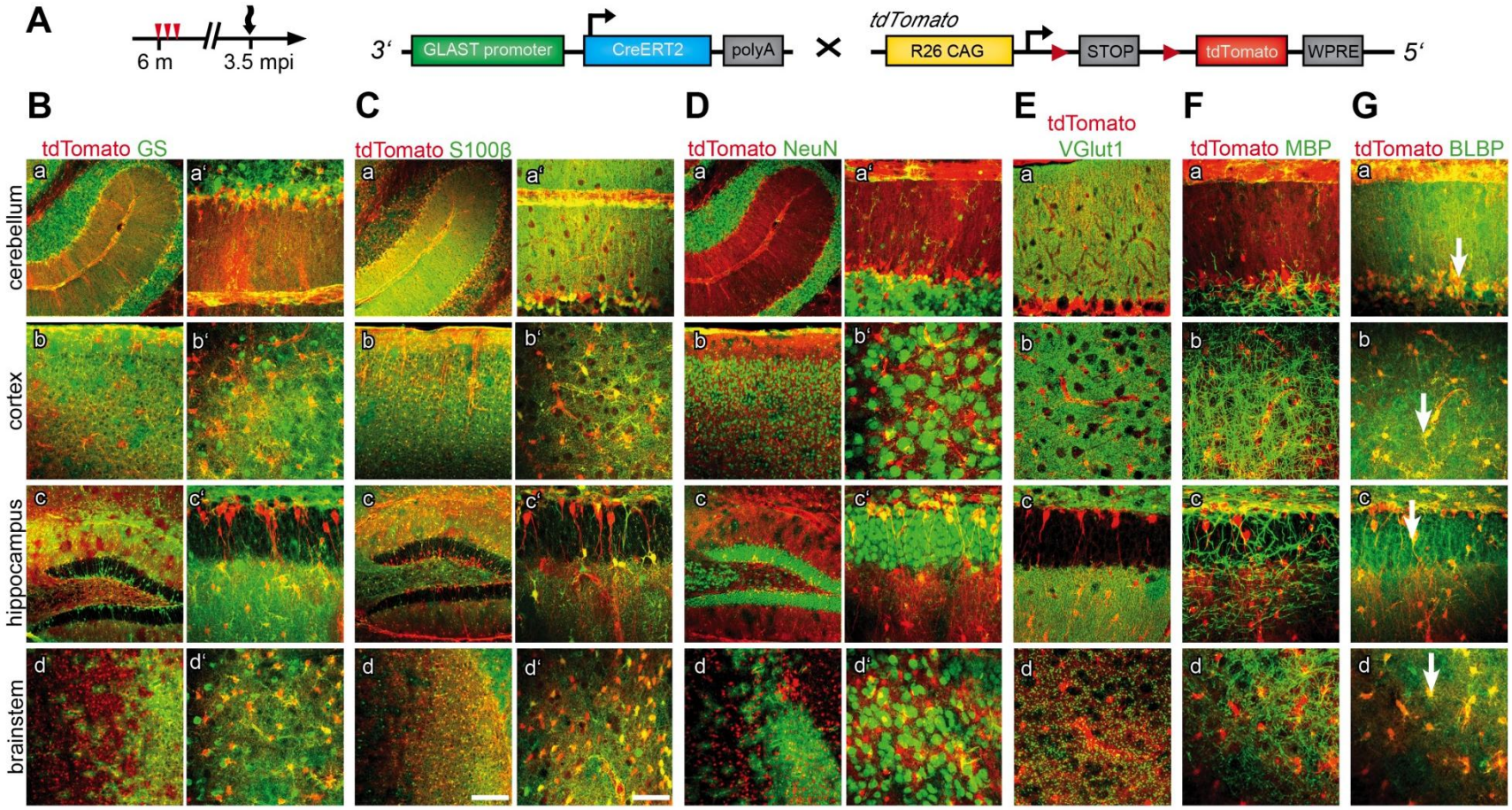

Figure 4. 9 Predominantly astrocytes are targeted by DNA recombination in old mice

Depicted are immunohistochemical stainings against GS (**B**), S100β (**C**), NeuN (**D**), VGlut1 (**E**), MPB (**F**) BLBP (**G**) in the cb (**B**, **C**, **D**, **E, F, G**: **a**, **a'**), ctx (**B**, **C**, **D**, **E, F, G**: **b**, **b'**), hp (**B**, **C**, **D**, **E, F, G**: **c**, **c**') and bs (**B**, **C**, **D**, **E, F, G**: **d**, **d'**) of an animal which has been treated with TAM and perfused 3.5 mpi for staining. As expected, GS and S100β positive cells are positive for tdTomato, but not all tdTomato+ cells are positive for one of the astrocyte markers. tdTomato+ cells do not show co-expression of the neuronal markers, NeuN (except differentiated granule cells), VGlut1 or the oligodendrocyte marker MBP. Like in young injected animals, tdTomato+ cells show an overlap with BLBP (see red arrow). The scale bar in (**C**: **d**) corresponds to 200 µm and applies for images (**B**, **C**: **a**, **b**, **c**, **d**), the scale bar in (**C**: **d'**) corresponds to 50 µm and applies for all remaining images **a b c d**.

4.1 GLAST-CreERT2/loxP system targets progenitor cells in the niches of adult neurogenesis

Today, the continuous neurogenesis in the subventricular zone (SVZ) of the lateral ventricle and the subgranular zone (SGZ) of the hippocampal dentate gyrus (DG) in mammals is accepted. Neuronal progenitor cells (NPCs) in the subventricular zone migrate along the migratory stream to the olfactory bulb (OB) and from the SGZ into the granule cell layer and differentiate into neurons. Radial glia serve as the primary scaffold for these migrating neurons.

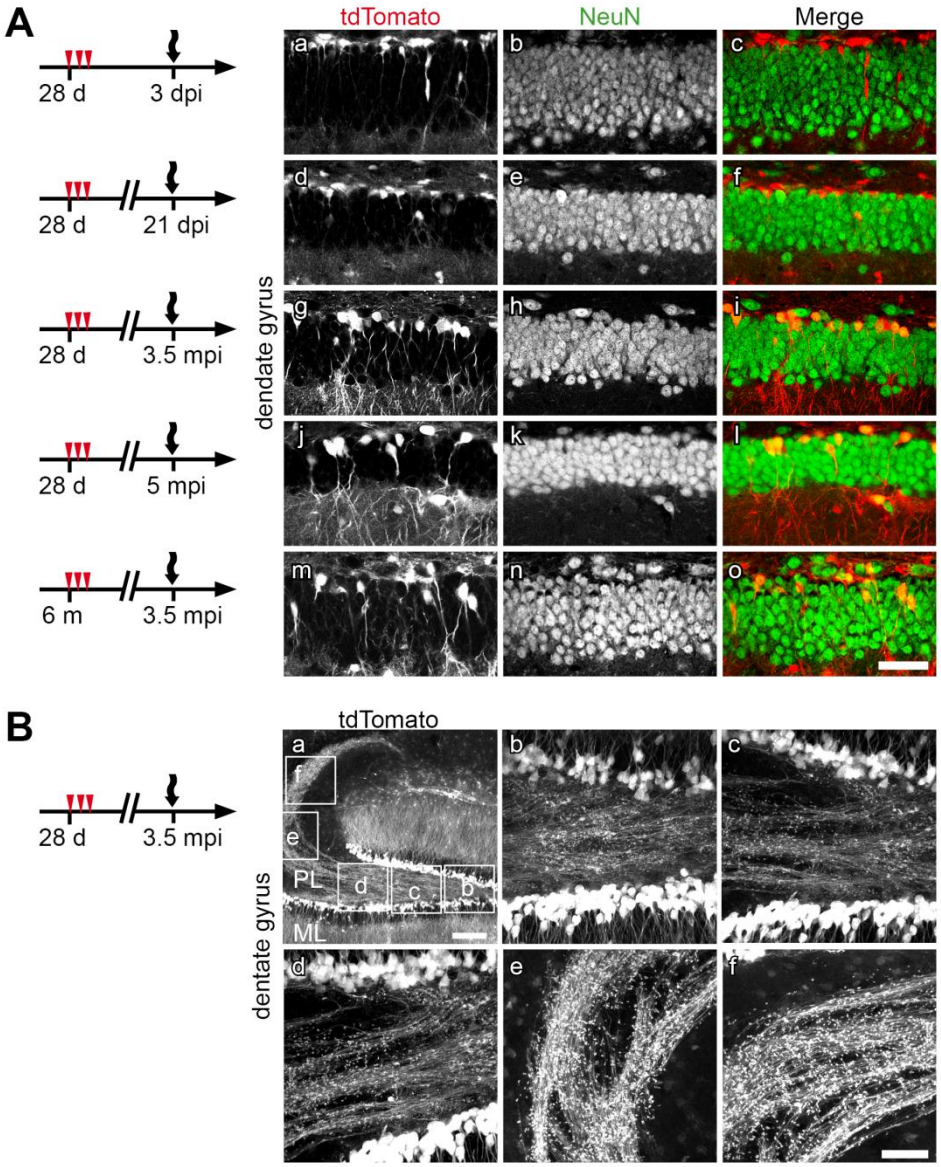

Figure 4. 10 RG in the DG differentiate to functional GC in young and adult mice
A: Representative, detailed confocal images of the DG of tdTomato reporter mice at different time points after TAM treatment (see also figure 6, 7, 8, 9). Brain slices have been stained for NeuN. 3 dpi (**a-c**) and also 21 dpi (**d-f**) recombined cells still showed radial glia character and tdTomato expression but no co-labeling for NeuN. 3.5 and 5 mpi recombined cells changed their morphology and appeared NeuN+ indicating that recombined radial glia cells differentiated into granule cells. They extend dendrites into the molecular layer (ML) and project axons through the polymorphic layer (PL) (**B**). Scale bar in **A**, **o** and **B**, **f** corresponds to 50 µm and holds for all images.

Recent work revealed that radial glia itself also act as neuronal progenitors, producing neurons and glia that will populate the OB and DG. These progenitor/radial glia cells have astroglial characteristics like GFAP and GLAST promoter activity. Therefore we had a detailed look in the dentate gyrus in young injected mice 3 and 21 dpi and 3 .5 and 5 mpi and in old injected mice 3.5 mpi. The results are summarized in Figure 4. 10. Sagittal slices were stained against NeuN to follow the differentation process of radial glia to mature neurons. tdTomato+ cells did not show NeuN expression 3 and 21 dpi suggesting, still radial glia character. In addition cells possessed the typical morphology of radial glia cells, a pyramidal shaped soma and a long fine process. At the later time points (3 and 5 mpi) almost all somas are positive for NeuN (see Figure 4. 10 A), indicating successful differentiation to granule cell neurons. New born cells showed the typical dendrites from the apical surface of the cell body, extending to the molecular layer (ML) of the dentate gyrus and axons emerging from the basal surface collateralizes within the polymorphic layer (PL) (Figure 4. 10 B).

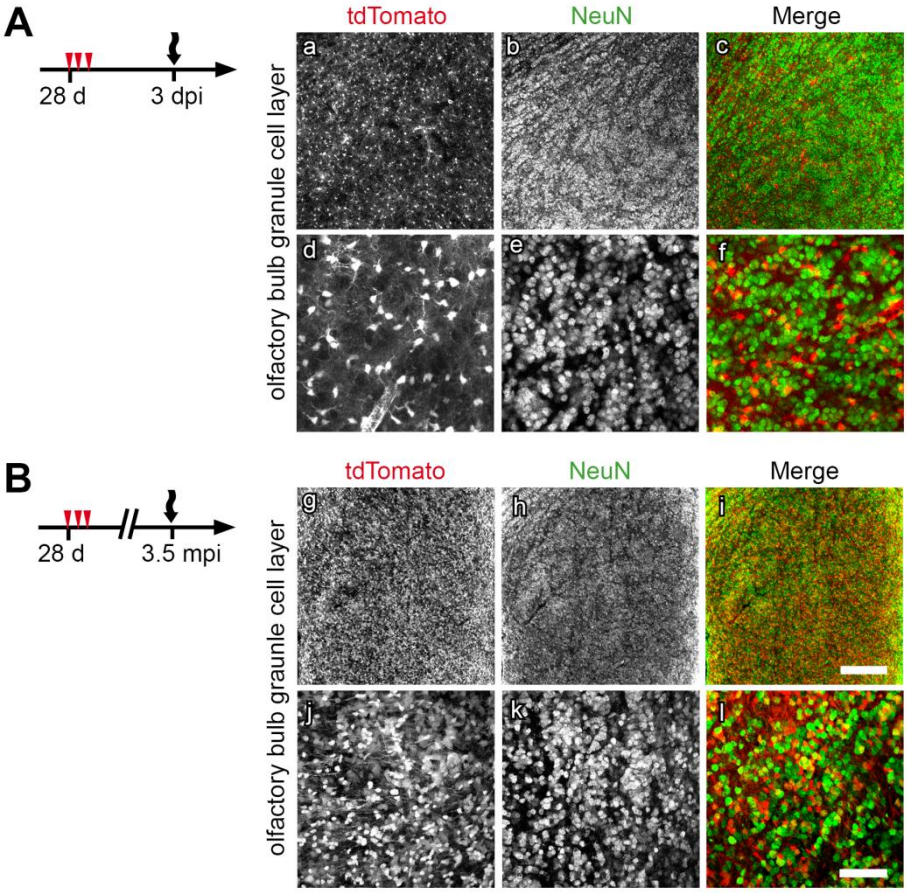

Figure 4. 11 Adult neurogenesis in the olfactory bulb can be visualized in reporter mice
Animals were injected with TAM at the age of 28 days and analyzed 21 dpi (**A**) and 3.5 mpi (**B**). Confocal images of vibratom slices of the olfactory bulb with the endogenous fluorescence of the reporter protein tdTomato+ stained with NeuN. Co-labeled cells increase with time after injection, demonstrating the differentiation of recombined progenitor cells to interneurons in the OB.

In older injected mice (Figure 4. 10 A, m, n, o) just a subpopulation of recombined cells showed NeuN expression, pointing to less radial glia differentiating into granule cell neurons in older mice. In 4.4 we already described morphological and pattern differences of recombined cells based on confocal images of the hippocampus in young and old injected

mice (see Figure 4. 7 A e; B, e , C, e). In adult mammals, neurogenesis is most prominent in the SVZ in the walls of the lateral ventricles. Type B cells give rise to C cells, generating immature neuroblasts (A cells), which migrate in chains to the olfactory bulb where they differentiate into interneurons, granule cells and periglomerular neurons (Sakamoto et al., 2014). Despite their NSC properties, type B cells display ultrastructural characteristics and markers of astroglial cells, including the expression of GFAP, GLAST and other astroglial markers (Platel et al., 2009). So it is not surprising that by use of the GLAST-CreERT2 system, B cells in the SVZ recombine and migrate to the olfactory bulb. Predominantly astrocytes are tdTomato+ in the granule cell layer of OB 3 days after injection of tamoxifen, as seen by the characteristic morphology (see Figure 4. 11 A). At the later time point, 3.5 months after the injection, the OB is populated by new born tdTomato+ neurons. They show NeuN expression and the typical small soma (see Figure 4. 11 B).

4.2 Fluorescence activated cell sorting taking advantage of the red fluorescent reporter protein in recombined astrocytes

Receptor expression in astrocytes is relatively low compared to other neural cell types, like neurons. In astroglia-specific receptor knock out models, it is therefore difficult to determine the knock down of the respective mRNA and protein by qRT-PCR and immunohistochemical methods or Western blotting of brain homogenates. To circumvent this problem, we established fluorescence activated cell sorting (FACS) to isolate astrocytes from brain regions, like cerebellum, hippocampus and cortex (for details see 7.4). We took advantage of the red fluorescent reporter line. Mice were heterozygous for GLAST-CreERT2 and the floxed reporter gene (stop$^{fl/wt}$tdTomato). Recombined cells show a bright red fluorescencent signal in GLAST+ cells and are therefore applicable for FACS. Littermates without Cre activity were considered as control animals. We concentrated at the mRNA level and initially analyzed the reporter line itself (see Figure 4. 12). Later we crossbred the reporter line to floxed receptor mouse lines to characterize cKO cells (see 5.). Mice were injected with tamoxifen at the age of 4 weeks, 21 days later perfused and the cortex was processed for FACS. Representative dot plots of ~ 10.000 events of a control and reporter (GLAST$^{CreERT2/+}$ x stop$^{fl/wt}$tdTomato) cortical single cell suspension are shown in Figure 4. 12 B. The measured side scatter of cells was plotted against fluorescence intensity. As expected the control cortical suspension showed the lowest fluorescent values and is positioned in the left lower corner (black dot) and considered as non-fluorescent. Red dots are representative for a single cell suspension from an injected GLAST$^{CreERT2/+}$ x stop^{flwt}tdTomato animal. Sorting revealed non-fluorescent cells (population I) and two distinguishable fluorescent populations: less fluorescent (population II) and high fluorescent (population III). After dissociation of brain tissue all neural cell types were present in the single cell suspension (see Figure 4. 12 A). The two fluorescent populations were expected to contain astrocytes as the major cell type. To clarify the identity of the populations, 100.000 events per population were collected and RNA was isolated for marker expression analysis by qRT-PCR. Astrocytic specific markers, including aquaporin 4 (Aqp4), excitatory amino acid transporter 2 (GLT1) and glutamine synthetase (GS) exhibited a relative enrichment of 4 to 7 fold in the third population, the highest fluorescent population. Unexpectedly, in the other two, also in the less fluorescent population, astrocytic marker proteins were not depleted but much less expressed.

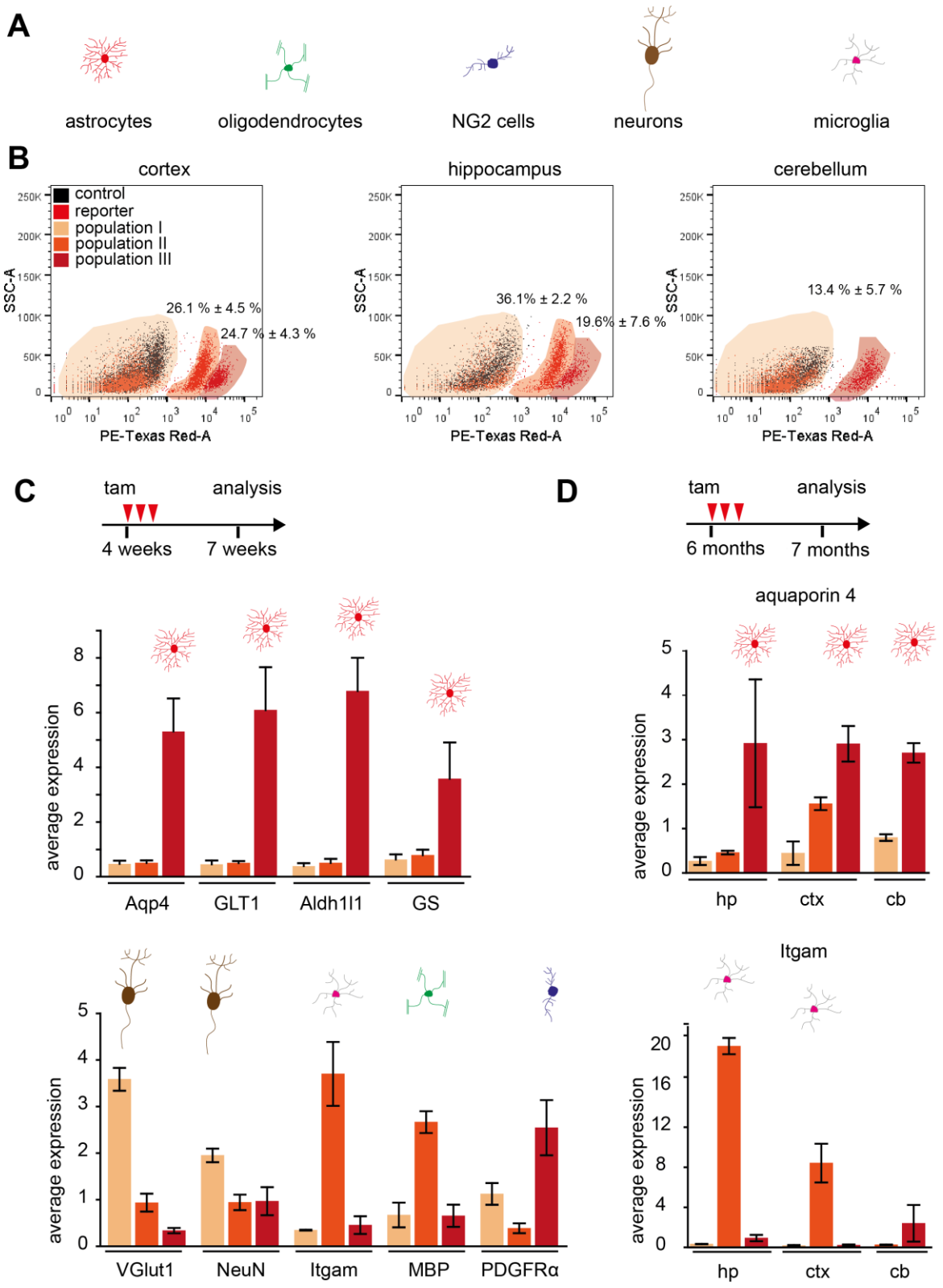

Figure 4. 12 FACS of brain cells of tdTomato reporter mice
A: Schematic drawing of neural cell types. **B:** Representative dot plots of FACS events of single cell suspensions of ctx, hp and cb. Black dot plots indicate tdTomato negative littermates. Cream colored dots indicate non-fluorescent cells (population I), orange colored dots indicate less red fluorescent cells (population II) and red dots indicate highly red fluorescent cells (population III). For the cb, one fluorescent population appeared, for the ctx and hp two. The stated percentages per population are averaged values (ctx n = 26, hp = 3 and cb = 10 ± SD) **C:** qRT-PCR analysis of marker expression in purified mouse cortical control and tdTomato+ populations. Mice have been treated with tamoxifen at

the age of 28 days: Compared to the median of all three populations, astrocytic specific markers including Aldh1l1, Aqp4, GS and the oligodendrocyte precursor marker PDGFRα are enriched in the high tdTomato+ fluorescent population. In the less fluorescent population the microglial marker Itgam and oligodendrocytic marker MBP are enriched and in the non-fluorescent population the neuronal markers VGlut1 and NeuN **C:** qRT-PCR analysis of marker expression in sorted, cortical populations of 6 months old, TAM injected mice revealed the same tendency: the less and high fluorescent population possessed enriched astrocytic markers and microglia marker, respectively. The same accounted for sorted hippocampal populations. In the cb only one fluorescent population could be detected, which showed enriched expression of the astrocyte marker aquaporin 4. Data are shown as mean ± SEM of the natural replicates (n=2-3).

Conversely, in the less fluorescent population II the microglial marker integrin alpha M (Itgam*)* and the oligodendrocyte marker MBP were 4 and 3 fold, respectively, enriched. In the non-fluorescent population expression of neuronal markers, like VGlut1 and NeuN was 3.5 and 2 fold, respectively, increased. The oligodendrocyte precursor marker PDGFRα was only increased in population III only. By means of determined marker expression we identified the highest fluorescent population as astrocytes and to some extent also as oligodendrocytes precursor cells, the less fluorescent population as microglia cells and oligodendrocytes, and the non-fluorescent cells predominantly as neurons. We repeated the experiment with 6 months old mice and here cortex, hippocampus and cerebellum were dissected and processed for FACS (see Figure 4. 12 C). Analysis of cortical single cell suspensions revealed, also in older mice, three populations. Astrocytic marker expression of Aqp4 pointed to the highest fluorescent population as astrocytes. In addition Itgam expression was enriched in the less fluorescent cells, supporting the conclusion, that microglia were predominantly present in population II. Hippocampal single cell suspensions showed next to non-fluorescent cells, also two fluorescent populations (see Figure 4. 12 B). Itgam and Aqp4 expression profiling of these populations indicated population II and III as microglia and astrocytes, respectively. FACS of single cell suspensions of the cerebellum divided cells in just two populations, non- and fluorescent cells. The fluorescent populations showed as expected enriched expression of the astrocyte marker gene Aqp4 and a slight enrichment of the microglial marker Itgam.

We quantified the percentages of the respective fluorescent populations after each sort. For the cortex we pooled in total 26 experiments and of all events 26.1 (±4.5) % and 24.7 (±4.3) % accounted for population II and the astrocytic population III, respectively. Further, in the hippocampus population II accounted for 36.1 (± 2.2) % and the astrocytic population for 19.6 (±7.6) % of all events. In the cerebellum 13.4 (± 5.7) % of all events showed red fluorescence.

In summary we established FACS for brain tissue with young and old mice to isolate astrocytes. Sorting of GLAST$^{CreERT2/+}$ x stop$^{fl/wt}$ tdTomato identified three populations based on their fluorescence intensities in cortex and hippocampus. The population with the highest red fluorescence values was appointed as astrocytes due to enriched astroglial marker gene expression. Conversely, the cerebellum showed only one fluorescent population with enriched astroglial marker expression. Of note, mRNA analysis was performed during the establishment of the sorting procedure, e.g. life and dead cell discrimination was not applied during the gating procedure. Contamination of other cell types in the astrocyte population was later reduced by an improved gating strategy (see Figure 7. 6).

5 PART II: Astroglial NMDA and P2Y$_1$receptors

Hannah M. Jahn[1], Carmen V. Bohn[1], Yuriy Pankratov[2], Ulyana Lalo[2], Xianshu Bai[1], Yvonne Schwarz[1], Anja Scheller[1], Alexei Verkhratsky and Frank Kirchhoff[1]

(1) Department of Physiology, University of Saarland, Homburg, Germany

(2) School of Life Sciences, Unversity of Warwick, Coventry UK

(3) Faculty of Life Sciences, University of Manchester, Manchester, UK

Focus of our research is the clarification of astroglial receptor function in the complex neural network. In Part I we proved the GLAST-CreERT2/loxP system as a reliable tool to investigate gene function, specifically in astrocytes, troughout the brain. In the following part we used this system to knock out astroglial ionotropic NMDA and metabotropic P2Y$_1$ receptors. The study received support from the following colleagues and collaborations.

5.1 Generation of astroglial NMDA receptor knockout mice

To investigate the function of NMDARs in astrocytes conditional mutants were generated by crossbreeding mice carrying the floxed NMDA receptor subunit 1 (GluN1) gene (*grin1*) (Tsien et al., 1996b) with mice expressing CreERT2 recombinase from the GLAST locus. Since GluN1 is the obligatory subunit in the receptor complex, its deletion is sufficient to obtain a complete loss of NMDA receptor function (De Biase et al., 2011; Glass et al., 2008; South et al., 2003; Tsien et al., 1996b). GLAST$^{CreERT2/+}$ x NRFL$^{fl/fl}$ animals are considered as conditional knockout, termed cKO in the following. Control mice were also homozygously floxed, but lacked CreERT2 expression (GLAST$^{wt/wt}$).

We first evaluated the extent of GLAST-CreERT2 mediated DNA recombination by qRT-PCR, amplifying genomic DNA from brainstem, cerebellum, cortex, hippocampus and optic nerve, obtained from 7 weeks old animals that were injected 3 weeks earlier with TAM. We quantified the degree of recombination from the loss of floxed alleles (see Figure 5. 1 A). Although the method was verified to be reliable to determine the extent of recombined alleles (see 4.3) the quantity of floxed *grin1* alleles in cKO animals was not decreased. Also cortical mRNA tested for GluN1 expression showed no significant difference in expression levels in control and cKO animals. Since we investigated expression levels in homogenates where also other cell types like neurons contribute to the respective mRNA level, it was not surprising that no changes in GluN1 mRNA expression in cKOs after TAM treatment could be detected (see Figure 5. 1 A, b).

Lalo et al., 2011 patched cortical astrocytes in 1, 3, 6, 9, 12 and 18-21 months old mice and recorded currents *in situ*. In the pharmacological profile of these so called glial synaptic currents (GSCs) (see also 5.4) a NMDA evoked fraction was identified. Interestingly, the amplitude of this current was age dependent. From 1 to 6 month of age they measured an increase of the amplitude, followed by a decrease from 6 to 21 months of age. We considered these findings and concluded that low currents at 1 month of age correlate to low membrane expression of NMDARs.

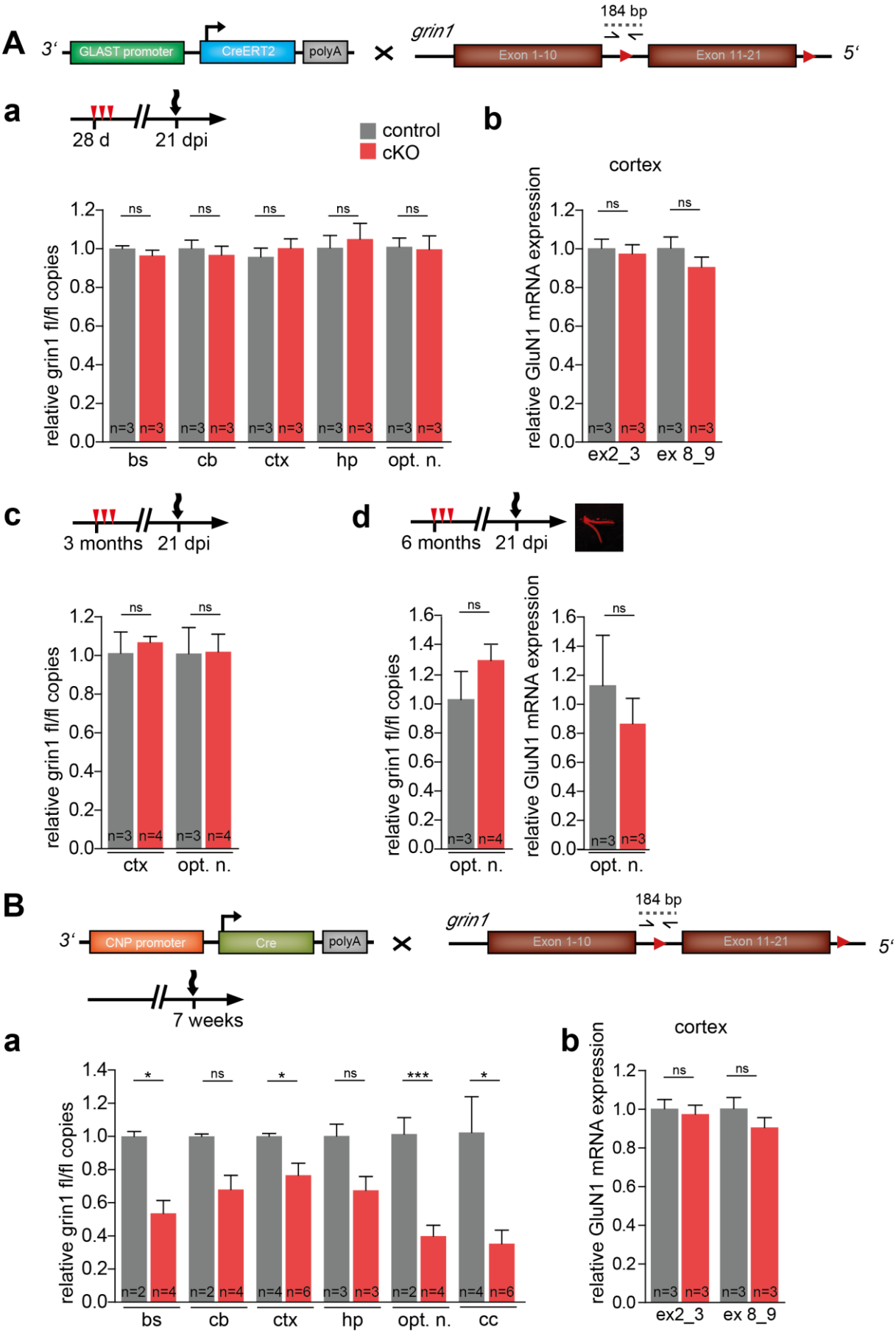
A
3'
GLAST promoter
CreERT2
polyA
grin1
184 bp
Exon 1-10
Exon 11-21
5'
a
28 d
21 dpi
control
cKO
relative grin1 fl/fl copies
ns
n=3
bs
cb
ctx
hp
opt. n.
b
cortex
relative GluN1 mRNA expression
ex2_3
ex 8_9
c
3 months
21 dpi
n=4
d
6 months
21 dpi
B
CNP promoter
Cre
7 weeks
*
***
cc

Figure 5. 1 Changes at the DNA and mRNA level after TAM application in GluN1 cKO mice

A: Conditional mutants were generated by crossbreeding mice carrying the floxed GluN1 subunit gene with mice expressing the Cre recombinase from the GLAST locus. **a**: Cre-mediated recombination of genomic DNA from cb, ctx, hp, bs and opt.n. Depicted is the relative abundance of floxed GluN1 copies normalized to the floxed genomic fragments of ($grin1^{fl/fl}$) controls. Animals were injected at the age of 4 weeks and analyzed 21 dpi. Primers for qRT-PCR were designed in close vicinity of the 5' loxP site. For every brain region no significant difference could be detected. **b**: Analysis of mRNA expression of the NMDA receptor subunit 1 in the cortex revealed no significant difference between cKO and control animals. Primer pairs stretching exon 2/3 and exxo 8/9 were tested. **c**: DNA recombination events were analyzed in cortices and optic nerves of mice injected at the age of 3 months and analyzed 21 dpi. No significant difference in the abundance of floxed GluN1 copies between cKO and control animals could be detected. **d**: Animals were injected at the age of 6 months and analyzed 21dpi. qRT-PCR for DNA recombination and mRNA expression revealed no changes in cKOs relative to control values. **B**: To test functionality of primers CNP-Cre x $grin^{fl/fl}$ animals were investigated for DNA recombination. In all investigated brain regions the quantity of $grin1^{fl/fl}$ copies was reduced in cKO animals. GluN1 mRNA expression is not reduced. Data are shown as mean ± SEM of the natural replicates (n = as indicated; *p<0.05, unpaired t-test).

The efficiency of Cre recombinase might be challenged by accessibility of the *grin1* locus since at this age the locus it is not frequently used for expression in the physiological sense. Therefore we analyzed optic nerves and cortices from 3 months old injected animals (see Figure 5. 1 A c). But also at this age no decrease of intact floxed alleles in cKO animals 21 dpi could be determined. The peak amplitude of NMDA dependant response in cortical astrocytes could be measured in 6 months old animals.

We investigated at this time point optic nerves 21 d after TAM application for DNA recombination and changes in GluN1 mRNA expression (see Figure 5. 1 d). Again, also in 6 months old animals no decrease of floxed alleles and likewise no reduction in GluN1 mRNA expression could be detected. We sequenced the amplified DNA and confirmed the expected nucleotide sequence (data not shown). Recombination efficiency is thought to be dependent on the distance between LoxP sites. Two Cre molecules per LoxP site have to approach each other to form a Holliday junction for successful DNA recombination. LoxP sites of already investigated floxed mice (see Figure 4. 5) flank a sequence of ~1641 bp, ~1150 bp, ~1700 bp and ~900 bp for *p2ry1*, *gabbr1*, *gria1* and the reporter gene tdTomato, respectively. LoxP sites for the *grin1* locus flank ~6800 bp.

To exclude any technical problems and to check if 6800 bp are in general too long for efficient recombination, the same qRT-PCR reaction was tested on DNA isolated from 7 weeks old GluN1 floxed mice crossbred to mice expressing the non-inducible Cre recombinase from the oligodendrocyte-specific 2',3'-cyclic nucleotide 3'-phosphodiesterase (Cnp1) locus (see Figure 5. 1 B a). We determined in brainstem 46 (± 8) %, in cerebellum 32 (± 8) %, in cortex 23 (± 7) %, in hippocampus 33 (± 8) %, in optic nerve 40 (± 7) % and in the corpus callosum 65 (± 8) % loss of floxed alleles compared to control animals. GluN1 mRNA expression was not significantly changed in KO animals (Figure 5. 1 b). These results show that no technical problems with the PCR itself existed and that with the CNP promoter and the non inducible Cre recombinase a floxed 6800 bp sequence can be efficiently recombined.

Further, we considered as well that the CNP promoter is already active early in development independent of TAM application. To exclude that the astrocyte-specific promoter and/or TAM applications were obstructive to recombine a floxed sequence of 6800 bp size, we

investigated likewise the *grin1* locus, but with a different floxed mouse line (Bannerman et al., 2012). In this case, a sequence of only ~ 2400 bp is flanked by loxP sites (see Figure 5. 2 A). We determined a small but not significant decrease in floxed alleles in optic nerve and cortex of cKO animals (see Figure 5. 2 B a). Further, in contrast to the former floxed *grin1* mouse line (Tsien et al., 1996b), we had full access to the transgenic sequence and designed primers to distinguish intact (2897 bp) and recombined alleles (419 bp) (see Figure 5. 2 A, B b). PCR amplified sequences were visualized on an agarose gel.

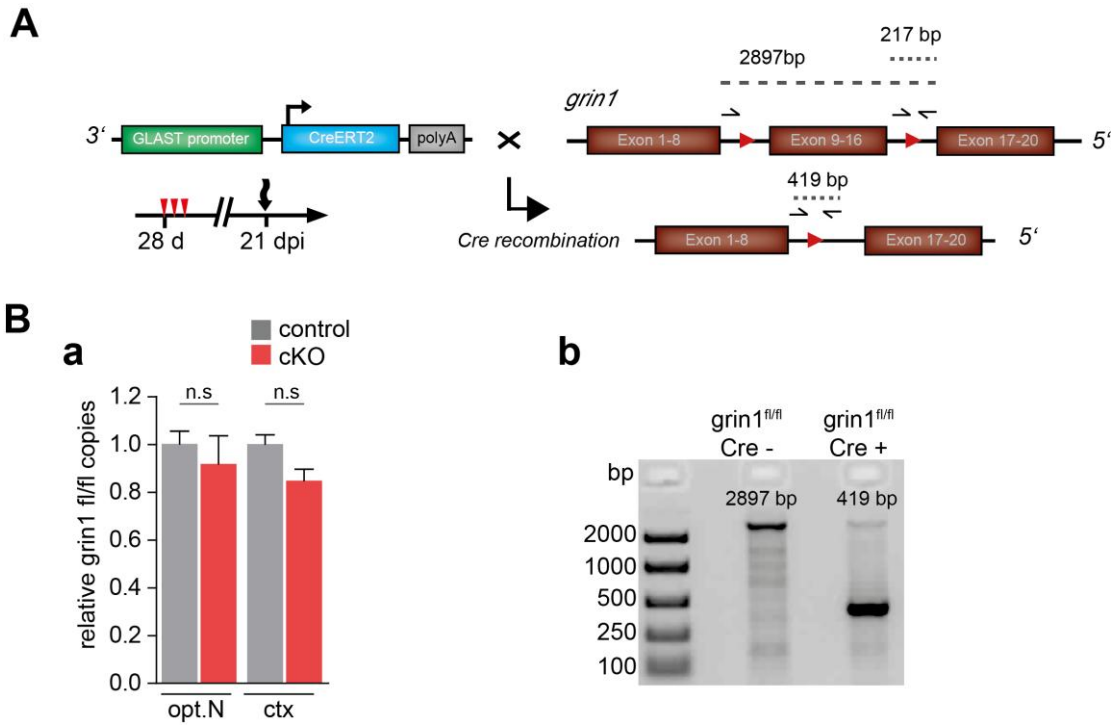

Figure 5. 2 Evaluation of DNA recombination of the *grin1* locus in GluN1 II cKO mice

A: Mice were injected with TAM at the age of 28 days and analyzed 21 dpi. Primers flank the 5' loxP (**B a**) site (217 bp) or are located close to both loxP sites (**B b**)**.** The qRT-PCR documents therefore a decrease of floxed alleles or on increase of recombined alleles. In homogenates of cortex and optic nerve no significant decrease in floxed allels in cKOs relative to controls was detected (**B a**). But DNA recombination still occurred verified by the PCR product of 419 bp in the agarose gel in cKO animals (**B b**)**.** Data are shown as mean ± SEM of the natural replicates (n = 3, unpaired t-test).

As expected, with and without Cre recombinase only the recombined alleles and intact floxed alleles were amplified, respectively (see Figure 5. 2 B b). We conclude from the series of these experiments that the floxed *grin1* locus with GLAST-CreERT2 LoxP/system is recombined, but not as efficient as for other floxed genes (*p2ry1*, *gabbr1* and *tdTomato*).

5.2 Astrocytes express low densities of NMDA receptors

In the following section we investigated NMDAR expression on astrocytes. We co-stained sagittal slices of 8 weeks old mice which express the green fluorescent protein EGFP (enhanced green fluorescent protein) under the control of the astrocyte-specific GFAP promoter (Nolte et al., 2001) with an antibody against the GluN1 subunit. In Figure 5. 3 representative images of the cerebellum (a-c), brainstem (d-f) and cortex (g-i) are shown. An overlap between the punctuated receptor staining and astroglial processes and soma was in none of the brain regions clearly detectable

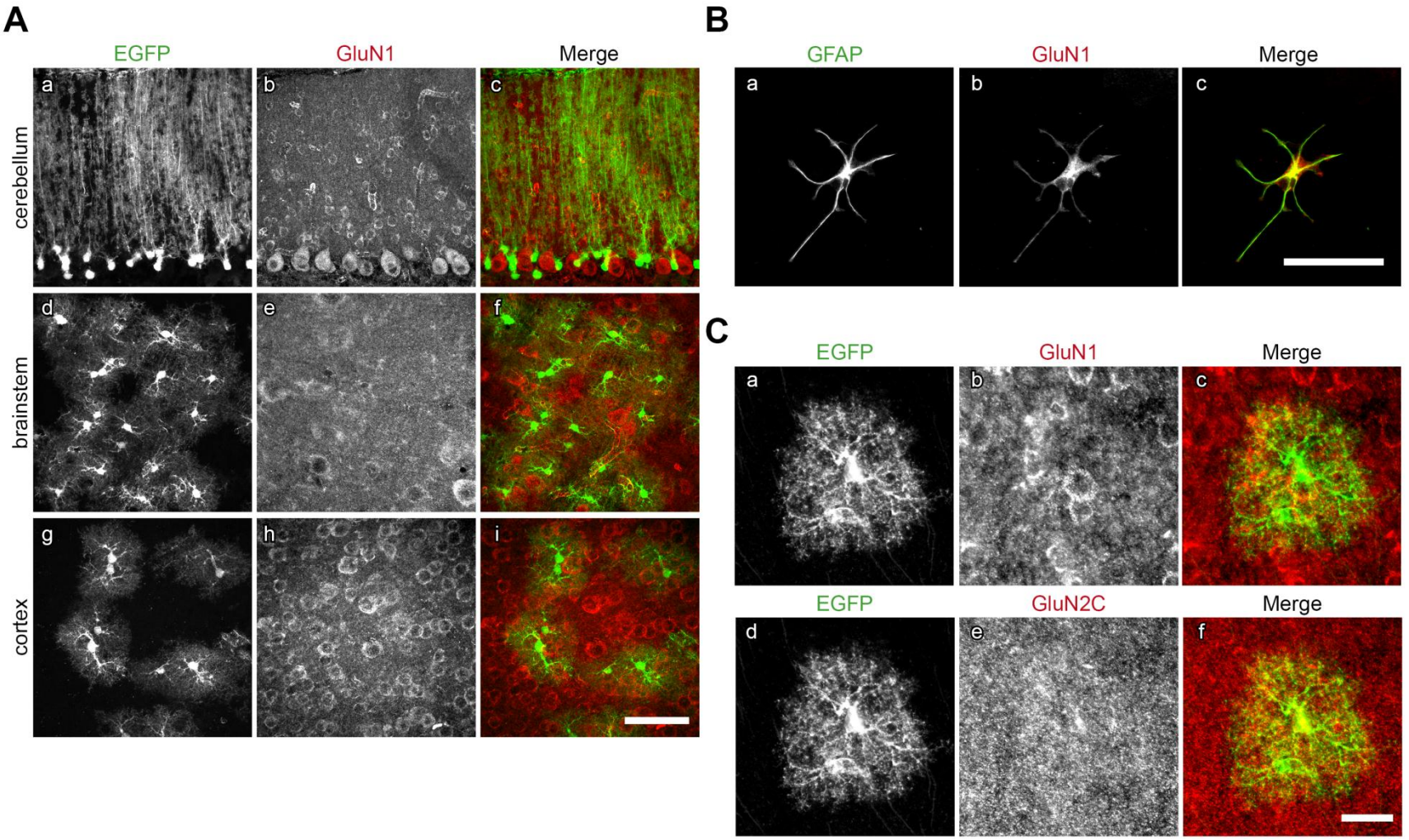

Figure 5. 3 Astrocytes express NMDA receptors in low densities

A: Immunohistological analysis of NMDAR (**b**, **e**, **h**) expression in vibratom slices of hGFAP-EGFP mice, which showed endogenous green fluorescent astrocytes (**c**, **f**, **i**) in cb (**a**, **b**, **c**), bs (**d**, **e**, **f**) and ctx (**g**, **h**, **i**). Slices were stained against GluN1. The merge revealed little or no co-localization of GluN1 in astrocytes in all investigated brain regions. The scale bar in (**i**) corresponds to 50 µm and holds for all illustrated images **B:** Hippocampal astrocytes in culture show a high density of receptors at soma and processes. The scale bar in **c** correlates to 20 µm, applies for **a**, **b** as well. **C:** A detailed view in the cortex demonstrated that astrocytes express almost no GluN1 subunits at the soma, rather at the processes. Stainings against the GluN2C subunit showed a different pattern (**e**) with clear co-localizations at the soma and processes (**c**, **f**). The scale bar in **f** corresponds to 20 µm and holds for all illustrated images.

In contrast, somata of neurons, e.g. Purkinje cells in the cerebellum could be clearly identified. We also stained primary cultured hippocampal astrocytes (see Figure 5. 3 B) against GluN1 and GFAP. Here, GluN1 subunits co-localize with astrocytic processes and the soma, demonstrating definite differences between astrocytic *in vivo* and *in vitro* NMDAR expression. In Figure 5. 3 C detailed images of cortical green fluorescent astrocytes are shown co-stained for the GluN1 (C, b) and GluN2C (C, e) subunit, respectively. Also here, astrocytic structures almost lacked GluN1 subunit expression. In contrast the GluN2C subunit was localized in soma and processes. We also stained parasagittal slices for the astrocytic marker S100β and GluN1. The rare expression of the GluN1 subunit on astroglial processes was present in all cortical layers (1-6) and not region specific (see Figure 5. 4).

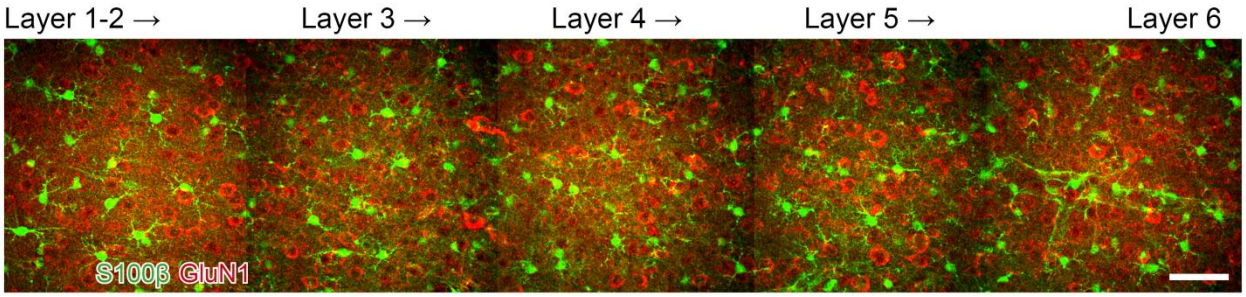

Figure 5. 4 NMDA receptor expression in the cortex (layer 1-6)

Vibratom slices were stained against GluN1 and the astrocyte marker S100β. Based on the merge of both fluorescent signals co-localization of GluN1 and EGFP was difficult but rather detected at the processes than at the soma. It showed no preferred astrocytic NMDA receptor expression in a specific layer of the cortex. The scale bar corresponds to 50 µm.

In addition, Western blot analysis was performed and immuno probed for GluN1 and α-tubulin (see Figure 5. 5 a). Blotted protein amounts of GluN1 were determined by densitometric quantification of band intensities (Figure 5. 5 b). Variability in loaded protein amounts was minimized by normalizing each sample to its own endogene (α-tubulin). Subsequently band intensities of cKO animals were normalized to the mean of control animals. We could not detect changes in protein expression after induction of recombination in cKO animals compared to control animals.

Figure 5. 5 Western blot analysis of GluN1 protein expression in ctx and hp

Representative Western blots are depicted in **a,** showing the protein amounts of GluN1 expressed in cKOs 21 days after the first injection of TAM, compared to control animals in hippocampus and cortex. Histogram in **b** shows the results of the densitometric quantification. α-tubulin was used as a loading control. No significant differences could be detected. Error bars correlate to the SEM of the natural replicates (n = 4, unpaired t-test).

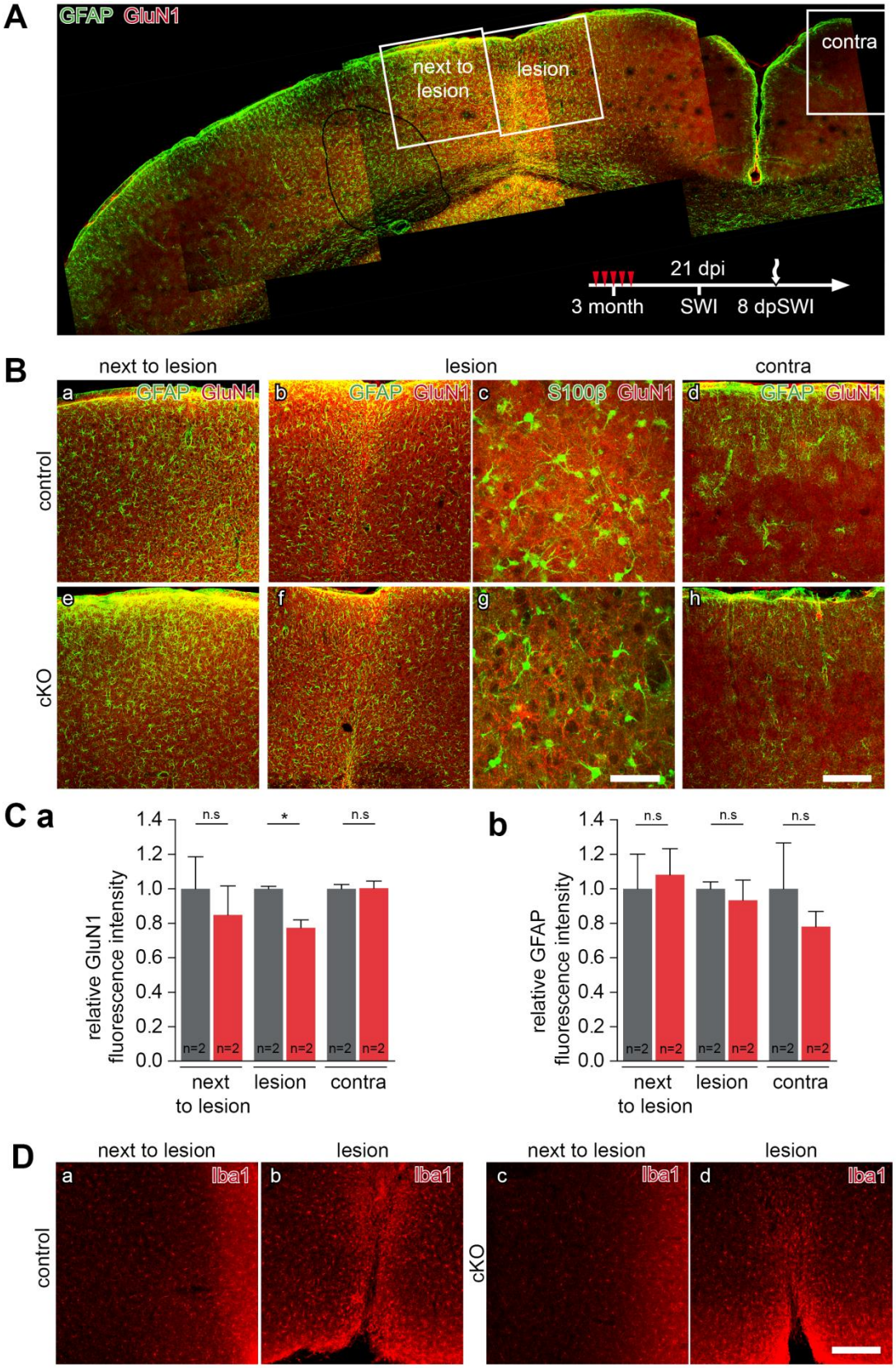

Figure 5. 6 Stab wound injury revealed reduced GluN1 expression in cKO animals

The image shows an overview of a coronal section of the cortex stained against GluN1 and GFAP, including the lesion side. White boxes demonstrate the positions where confocal images (**B**) were taken for densitometric quantification of GluN1 and GFAP fluorescence intensities (**C a**, **b**). The scale bar in **g** corresponds to 50 µm and in **h** to 200 µm. Data are shown as mean ± SEM of the natural replicates (n = 2; *p<0.05, unpaired t-test). **D:** Representative images of Iba1 staining, no difference between cKO and control could be observed.

Immunohistochemical and Western blot analysis of wildtype, control and GluN1 cKO animals demonstrated minor expression of GluN1 subunits on astrocytes under physiological conditions. In the following we tested cKO and control animals under pathophysiological conditions and performed a cortical stab wound experiment. We injected 3 months old mice for five consecutive days with TAM starting 21 d before the injury and analyzed 8 d post injury as shown in **Error! Reference source not found.** A. Coronal slices were stained gainst GFAP, GluN1 and the microglial marker gene, ionized calcium-binding adapter molecule 1 (Iba1). Representative confocal images of the stab wound and surrounding cortical areas showed an increase of GluN1 expression in the lesion area compared to more ipsilateral and contralateral parts. We quantified the fluorescence intensity in the mentioned three regions in cKO and control animals. We could not detect significant differences in GluN1 expression next to the lesion and on the contralateral side, but we could detect in cKO animals a decrease to 77 (± 5) % GluN1 fluorescence intensity compared to fluorescence intensities measured in control mice (100 (± 1) %). In contrast, comparing GFAP expression in cKO and control animals showed no significant changes in any of the investigated regions (see **Error! Reference source not found.** C b). Also activation of microglia cells did not iffer between GluN1 cKO and control mice (**Error! Reference source not found.** D). We concluded that the NMDAR knockout is also present at the protein level in astrocytes and that under pathological conditions the expression in astrocytes is increased to such an extent that it was possible to detect the minor differences after TAM application in cKO animals.

5.3 FACS of astroglial-specific NMDA receptor knockout cells

In addition, we applied the established FACS sorting procedure (see 4.2). We appointed GLAST$^{CreERT2/+}$ x tdTomato$^{fl/wt}$ as control, GLAST$^{CreERT2/+}$ x NRFL$^{fl/fl}$ x tdTomato$^{fl/wt}$ as cKO animals (see Figure 5. 7 a). Mice were injected with TAM at the age of 4 weeks and cortices were processed 21 d later. Two animals per group were sorted. As mentioned in 4. 6 three cell populations could be distinguished by fluorescence intensities, these populations were gated (see Figure 4. 12) and RNA and DNA was isolated. We tested on isolated cKO DNA the loss of the floxed sequences with primers flanking spacious the 3'- LoxP site. The forward primer was located in the intron region before exon 9 and the reverse primer stretched exon^{13}/intron$^{13/14}$ to circumvent RNA amplification. After the PCR reaction, amplified products were separated on an agarose gel. Representative samples are shown in Figure 5. 7 b. The non-fluorescent and less fluorescent populations showed a band of the expected amplicon size. In the highest fluorescent population the band intensity was strongly decreased. In conclusion and in line with former results (see Figure 4. 12) was the population with the highest red fluorescence identified as astrocytes and verified to be recombined. In additon we confirmed these results at the mRNA level. The mRNA expression of the astroglial marker protein GLT1 was enriched in population III, in control and cKO cortices, compared to population I. Furthermore, GluN1 expression was reduced in population III in cKO animals (0.24 ± 0.001) but not in control animals (1.45 ± 0.29). The GluN1 mRNA in population I was likewise not reduced (cKO: 2.25 ± 0.69, control: 1.46 ± 0.49). To verify that the whole NMDA receptor complex (4 subunits in total) is degraded, we tested mRNA expression of the GluN2C subunit which is thought to be enriched in astrocytes. As expected, we could observe an obvious reduction in average GluN2C expression in

population III in cKO, compared to population III of control animals (0.29 ± 0.46 and 2.49 ± 0.99, respectively), which did not reach significance since variance in control animals was too high. In addition, we supplied further evidence for specific enrichment of the GluN2C subunit in astrocytes. GluN2C mRNA in control sorted cells showed higher expression levels in population III, compared to population I (1.44 ± 0.55 and 2.49 ± 0.99, respectively, Figure 5. 7 c). In conclusion NMDAR knock out could be verified in FACS sorted astrocytes 21 d after TAM application at the mRNA level.

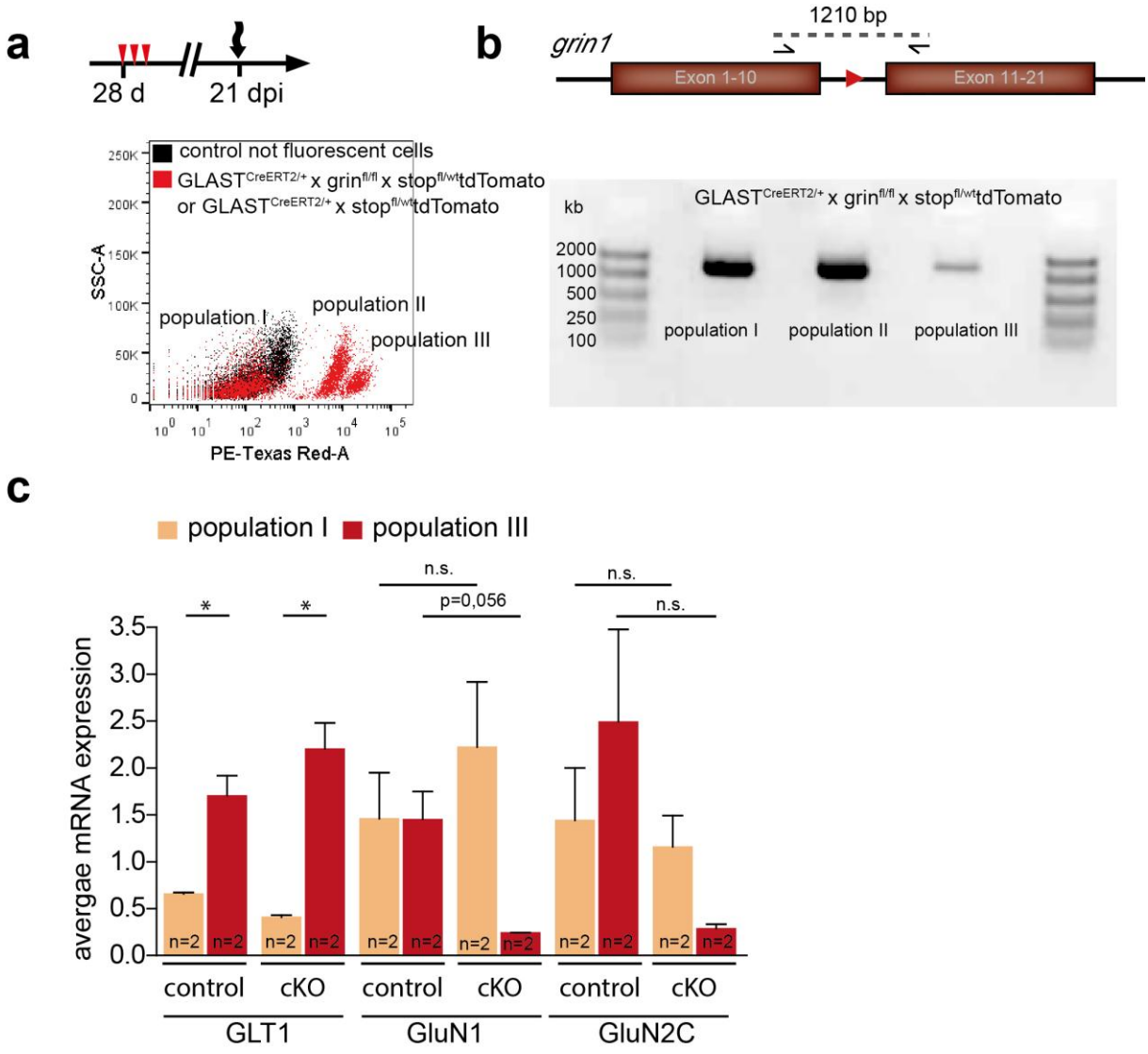

Figure 5. 7 FACS sorting of astroglial GluN1 cKO cells

A: Astrocytes of cortices of cKO animals (GLAST$^{CreERT2/+}$ x grin1$^{fl/fl}$ x tdTomato$^{fl/wt}$) and control animals GLAST$^{CreERT2/+}$ x tdTomato$^{fl/wt}$) were sorted. DNA and RNA were simultaneously isolated and investigated by qRT-PCR. **a:** Representative dot plots of investigated tdTomato+ animals. **b**: PCR results with primers flanking the DNA analysis of 3' LoxP site. Population I and II showed a band at the calculated amplicon size of 1210 bp. Population III, the potential knockout cells, showed a strongly diminished band intensity. **c**: mRNA analysis of population I and III showed an increase of astrocyte marker GLT1 in population III. GluN1 subunits were downregulated in astrocytic cKO population III, the same applies for the GluN2C subunit which was in contrast upregulated in the astrocytic control population. Data are shown as mean ± SEM of the natural replicates (n=2, per genotype, *p<0.05, unpaired t-test).

5.4 Evaluation of synaptically- activated glial currents in GluN1 mutants

So far, we followed changes at the DNA and mRNA level after TAM application in selective GluN1 mutants. In the following we asked about the functional aspect of the astroglial NMDARs. We first examined their electrophysiological properties and subsequently the influence of the conditional GluN1 ablation in astrocytes after TAM application. Therefore we patched cortical control and cKO cells in layer II, in acutely isolated slices and measured the response after stimulation of the according axons, originating from layer IV-VI. hGFAP-EGFP mice served as controls. Astrocytes were identified by the green fluorescence signal. GLAST$^{CreERT2/+}$ x grin1$^{fl/fl}$ x stop$^{fl/wt}$tdTomato mice were injected with P 8 and knockout cells were identified by tdTomato reporter expression 21 days after the first injection (GluN1 cKO). Previous data showed that measured astroglial currents after neuronal afferent stimulation were directly associated with synaptic transmission since application of TTX abolished glial responses (Lalo et al., 2011a; Lalo et al., 2006). Therefore, recorded responses are referred as glial synaptic currents (GSCs). Further, GSCs were analyzed similarly to previous data by Lalo et al., 2006 and 2011. Due to different decay times the responses could be separated into a fast and a slow component (see Figure 5. 8 and Figure 5. 9 red and blue traces, respectively).

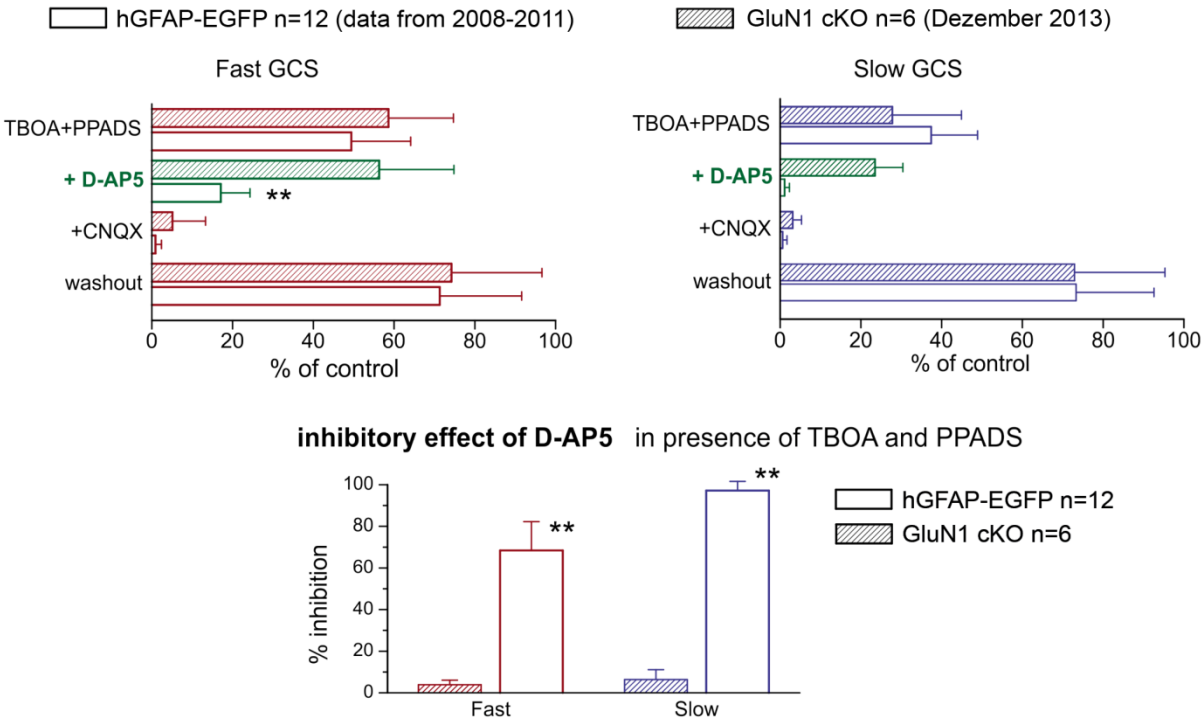

Figure 5. 8 Inhibition of glial synaptic currents

GSCs (fast and slow components) were analyzed similarly to previous data (Lalo et. al. 2008, 2011). Top panels show average amplitudes of fast and slow components of GSC, remained under drugs, relative to control. Data of GluN1 KO cells were gathered in December 2013 and compared to previously recorded astrocytes from hGFAP-EGFP mice of the same age group (4-6 weeks old). The data show significant difference in the sensitivity to D-AP5 in GluN1 cKO and hGFAP-EGFP mice. Final drug concentrations: TBOA mix DL-TBOA (30 µM) and TFB-TBOA (2 µM), PPADS (50 µM), CNQX (50 µM) and D-AP5 (30 µM)

Both components were sensitive to a combination of antagonists of EAAT1-5 glutamate transporters TBOA mix ((2S,3S) - 3 - [3-[4 -(trifluoromethyl) benzoylamino] benzyloxy] aspartate (TFB-TBOA) and DL-threo-b-benzyloxyaspartic acid (DL-TBOA)) and the broad antagonist of P2 receptors PPADS (pyridoxalphosphate-6–azophenyl-2',4'-disulfonic acid tetrasodium salt) in GluN1 cKO and control cells. But evoked GSCs in cKO cells were not further decreased by the selective antagonist of NMDARs D-(-)-2-amino-5-phosphonopentanoic acid (D-AP5). In contrast, D-AP5 had an inhibitory effect on EGFP+ control cells and decreased the current of the fast and slow component by around 60 % or even around 90 %, respectively (see Figure 5. 8). The antagonist of AMPA/kaniate receptors 6-cyano-7-nitroquinoxaline-2,3-dione (CNQX) was able to inhibit GSCs in GluN1 cKO cells.

In a second approach we likewise recorded control and GluN1 cKO cells. Here we applied first a combination of antagonists of glutamate transporters TBOA mix and PPADS. Application significantly reduced fast and slow components of the GSCs in both genotypes. Interestingly, we incubated slices next with the selective antagonist for GluN2C/D containing NMDA receptor UBP141. EGFP positive cells clearly showed further reduced GSCs almost to baseline levels. GSCs of GluN1 cKO cells in the presence of TBOA-mix and PPDAS were unchanged after application of the NMDAR blocker. In contrast, CNQX was able to reduce cKO currents (see Figure 5. 9). These results, together with the stainings and FACS data, supported previous data, suggesting that NMDRs in astrocytes constituted of the obligatory GluN1 and GluN2C subunits.

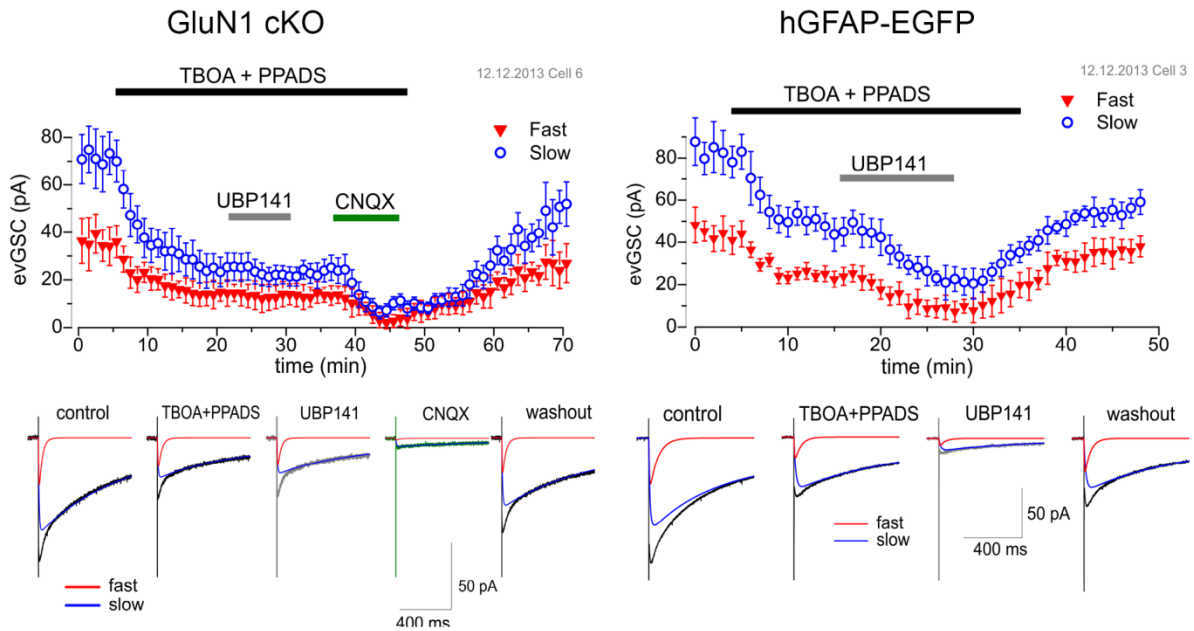

Figure 5. 9 Action of UBP141 on glial synaptic currents

GSCs (fast and slow components) were analyzed similarly to previous data (Lalo et. al. 2008, 2011). Representative recordings have been chosen since they were made on a same day and with identical experimental settings. Top panel: each point shows mean ± SD for 10 GSCs recorded within 1-min time window. Data show a significant difference in the sensitivity to the GluN2C/D subunits specific antagonist UBP141 in GluN1 cKO and hGFAP-EGFP mice. Used final drug concentrations: TBOA mix: DL-TBOA (30 µM) and TFB-TBOA (2 µM), PPADS (50 µM), CNQX (50 µM) and UBP141 (3 µM).

5.5 Generation of astroglial and inducible $P2Y_1$ receptor mutants

To investigate the impact of astroglial $P2Y_1$Rs in CNS function, conditional knockouts were generated to ablate $P2Y_1$Rs selectively in astrocytes in a temporally controlled fashion. We crossed mice, expressing the tamoxifen-sensitive Cre-recombinase CreERT2 under the astrocyte-specific, endogenous GLAST promoter (Mori et al., 2006) with mice carrying floxed *p2ry1* alleles (Leon et al., 1999). We injected conditional knock out ($GLAST^{CreERT2/+}$ x $p2ry1^{fl/fl}$) and control ($GLAST^{+/+}$ x $p2ry1^{fl/fl}$) mice with TAM at the age of 28 days for 3 d and studied the ablation of $P2Y_1$R mRNA 21 dpi in different brain regions by qRT-PCR for mRNA expression (see Figure 5. 10 a, b). Successful DNA recombination was already determined (see Figure 4. 5).

Primers flanked either exon 1 and 2 or lay within exon 1 and quantified to the same extent a reduction in every investigated brain region (see Figure 5. 10 a). Primers laying in exon 1 showed a better performance and were used in the following experiments. In detail, in brainstem a significant reduction to 75 (± 1) %, in the cerebellum to 39 (± 4) %, in the cortex to 57 (± 4) % and in the hippocampus to 64 (± 5) % of control expression levels were determined (see Figure 5. 10 b). Further, like for the NMDA receptor knockout mice, we applied FACS sorting to verify the knock down of $P2Y_1$R mRNA in isolated astrocytes. Here, cKO and control animals were heterozygous for the GLAST and tdTomato locus, since reporter expression was needed in both groups. Further, cKOs and controls were homozygous and heterozygous for the floxed *p2ry1* locus, respectively. Therefore just one intact *p2ry1* allele served as an mRNA template in control animals. Cortices and cerebelli were processed for FACS. The astroglial population (highest red fluorescence intensity) was gated, RNA was isolated and used for qRT-PCR for mRNA expression. For the analysis △CT values of cKOs were normalized to values of control animals. The results are depicted in Figure 5. 10 c. We could determine a reduction of $P2Y_1$R mRNA expression to 23 (± 5) % and 28 (± 1) % in cerebellum and cortex, respectively. As expected mRNA levels were further reduced as observed levels in homogenates. Remaining $P2Y_1$R expression is probably due to contamination of non-recombined neuronal cell types. We conclude that after successful DNA recombination, $P2Y_1$R mRNA is likewise efficiently degraded in all investigated brain regions in cKO animals.

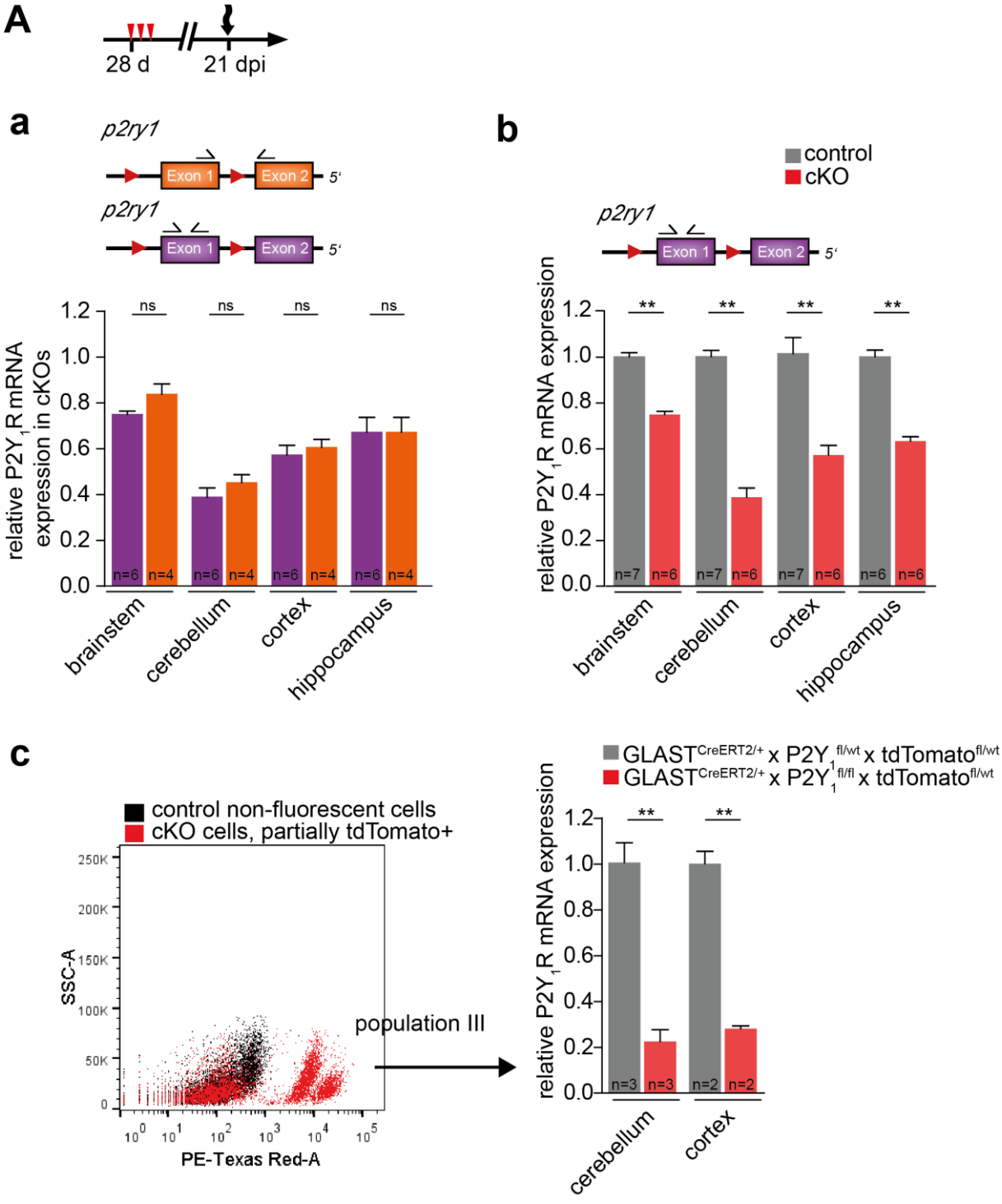

Figure 5. 10 P2Y$_1$R mRNA expression in P2Y$_1$ cKO mice is significantly reduced

A: Mice were injected with TAM at the age of 4 weeks for three days. RNA was isolated from brainstem, cerebellum, cortex and hippocampus 28 dpi. qRT PCR for mRNA expression was performed with two primers pairs, either stretching exon 1 and 2 or located in exon 1 **a:** Both primers show a reduction in P2Y$_1$R mRNA copies and no significant differences. **b:** Summarized qRT-PCR results for P2Y$_1$R mRNA expression in cKOs normalized to control values. **c:** Astrocytes were isolated from cerebellum and cortex from cKO and control animals with FACS. Obtained RNA was analyzed for P2Y$_1$R mRNA expression. ΔC_T-values of cKO animals were normalized to the mean of the respective control animals. Sorted cKO cells showed reduced P2Y$_1$R mRNA expression. Data are shown as mean ± SEM of the natural replicates (n = as indicated; *p<0.05, **p< 0.01, ***p<0.001, unpaired t-test)

5.6 Evaluation of commercially avaible $P2Y_1$ receptor antibodies

The $P2Y_1$ receptor is a seven pass transmembrane, G-protein-coupled, extracellular, nucleotide receptor (see Figure 5. 11) with several intra- and extracellular loops which served as epitopes for different, commercially available antibodies (AB). Two epitopes were intracellular and directed against the third internal loop (Alomone intracellular binding) or against the C-terminus (Abcam intracellular binding). One epitope was directed against the 2nd extracellular loop (Alomone extracellular binding). Publications commonly advice the use of antibodies from Alomone.

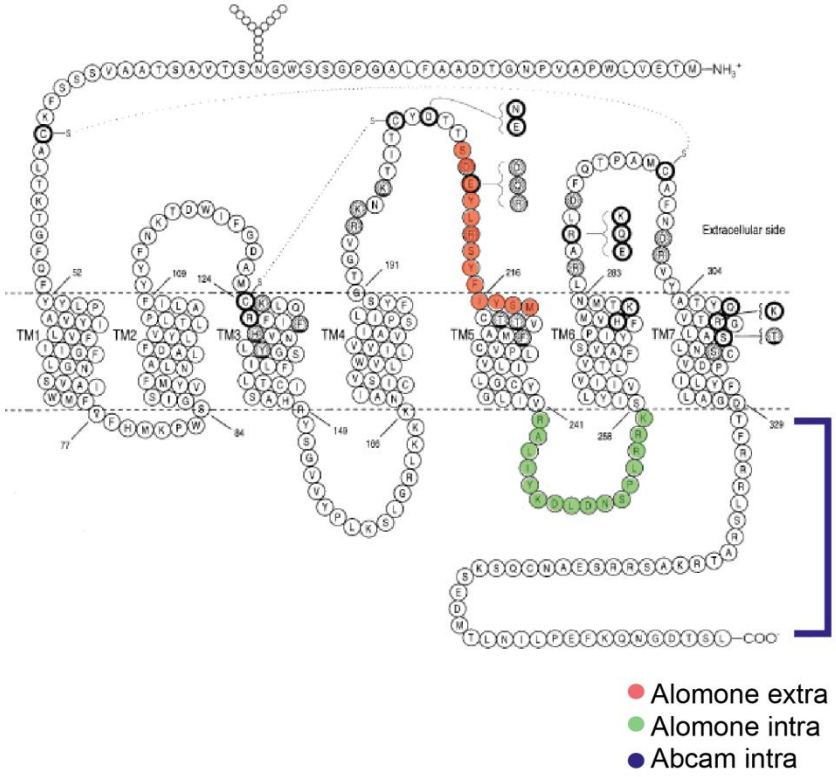

Figure 5. 11 Topology of the $P2Y_1$ receptor and epitopes used for AB production
The scheme shows the topology of the human $P2Y_1R$ protein. Epitopes used for antibody production are colored in green: Alomone intracellular binding (APR-009), red: Alomone extracellular binding (APR-021) and blue: Abcam intracellular binding (Ab85896). From human amino acid sequence used for the epitope, 12 of 14 are identical with the murine sequence. All antibodies are polyclonal and rabbits were used for immunization.

We first evaluated the intracellular binding antibody from Alomone. Therefore, 2 month old wild type (WT) and total $P2Y_1R$ knockout (tKO) mice were perfused. The ubiquitous knockout was achieved by crossbreeding a mouse line with Cre DNA recombinase expression driven by the human cytomegalovirus minimal promoter (CMV) (Schwenk et al., 1995) to the floxed $P2Y_1R$ mouse line. Sagittal brain slices of WT and tKO were stained against the $P2Y_1R$. Representative confocal images of the cerebellum (a, b), cortex (c, d), hippocampus (e, f) and brainstem (g, h) of WT and tKO are shown in Figure 5. 12 A and B, respectively. In Figure 5. 12 A i, B i epifluorescent overviews of a sagittal slice of a WT and tKO, respectively, are shown. Wild type brains showed typical punctuated receptor staining in all investigated brain regions. Total knockout brains displayed a strongly reduced staining

intensity when using the same imaging settings. Cell structures like somata of e.g. Purkinje cell somata could be easily identified.

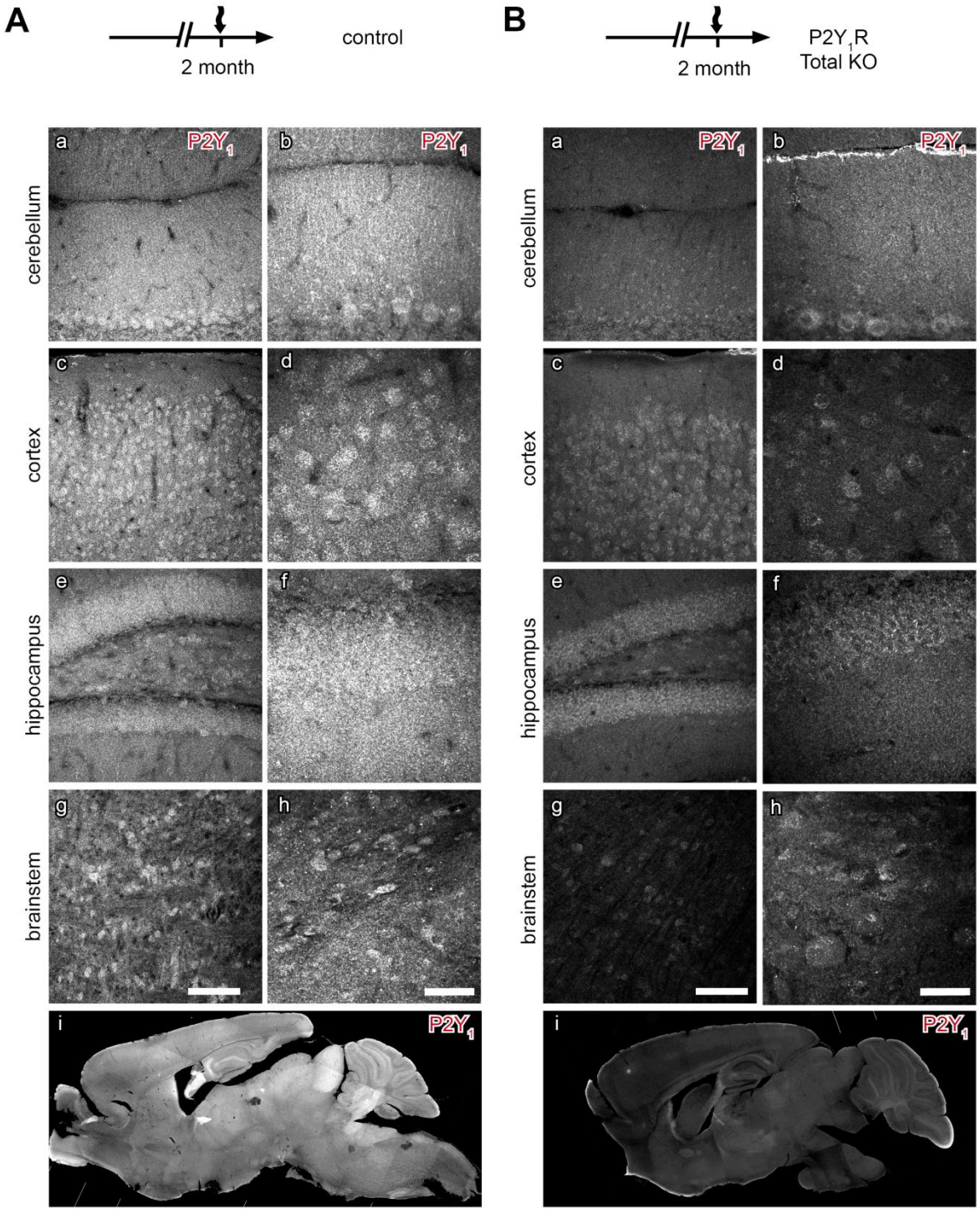

Figure 5. 12 Immunostaining in WT and P2Y$_1$R tKO brains using the APR-009 AB

The figure shows confocal images of brain sagittal slices, which have been stained against P2Y$_1$R (Alomone intracellular APR-009) in 2 month old wildtype (**A**) and total knockout mice for P2Y$_1$R (**B**). **a**, **c**, **e**, **g** show detailed images of cb, ctx, hp and bs. The scalebar in **g** and **h** corresponds to 100 µm. In **b**, **d**, **f**, **h** higher magnifications per regions are shown. In **i** overviews of sagittal slices of both genotypes are shown. Fluorescence intensity of the antibody is reduced in the total KO, but recognizes unspecific structures and cells based on the high background.

To address if we can also detect decreased fluorescence intensities in the astrocyte-specific $P2Y_1R$ knock outs, we injected control and cKO mice with tamoxifen at the age of 2 months and 21 dpi animals were perfused and vibratome brain sagittal slices stained following the same protocol with the intracellular binding antibody from Alomone (APR- 009).

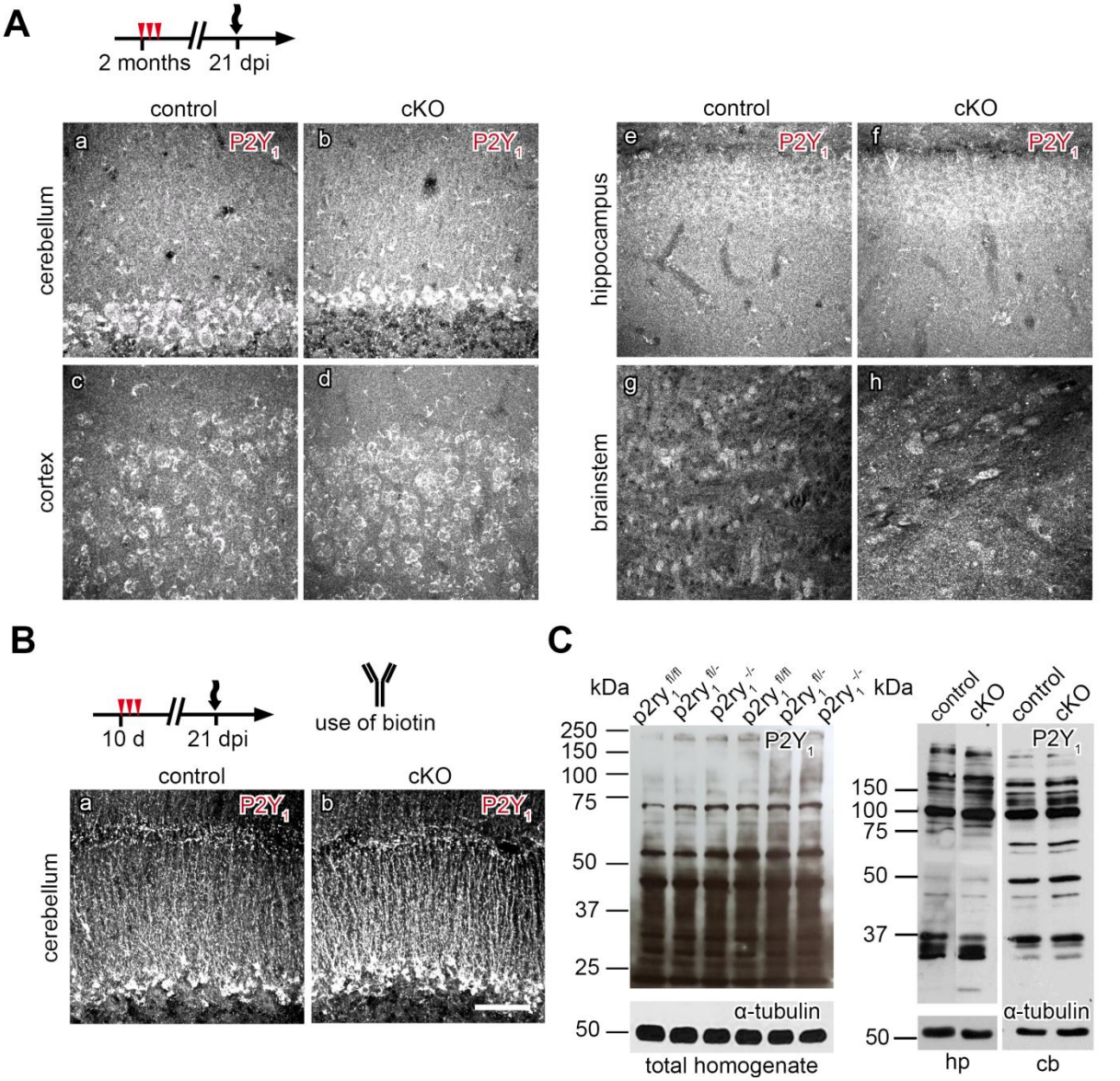

Figure 5. 13 Immunostaining and WB of control and $P2Y_1R$ c/tKO brains using APR-009 AB
Mice were injected at the age of 2 months (**A**) and 21 dpi sagittal slices were stained against the $P2Y_1R$. Confocal images show the cb, ctx, hp and bs of control and of $P2Y_1R$ cKO animals. **B:** Also the enhancement, using biotin and a streptadavin antibody did not emphasize differences as depicted in representative images of the cerebellum. The scalebar in **B** (**i**) correlates to 50 µm and applies for all images **C:** $P2Y_1R$ AB is not specific in Western blotting. The lanes represent recognized proteins of wildtype; heterozygous KO and total KO in whole brain homogenates. The pattern did not differ between genotypes. **C:** Band pattern of hippocampal and cerebellar homogenates differed from whole brain homogenates, but did not show differences between $P2Y_1R$ cKOs and controls.

In Figure 5. 13 A representative confocal images of the cerebellum, cortex, hippocampus and brainstem of a control (a, c, e, g) and cKO (b, d, f, h) animal are depicted. It was not possible to detect differences in the fluorescence intensity or staining pattern between control and cKO animals.

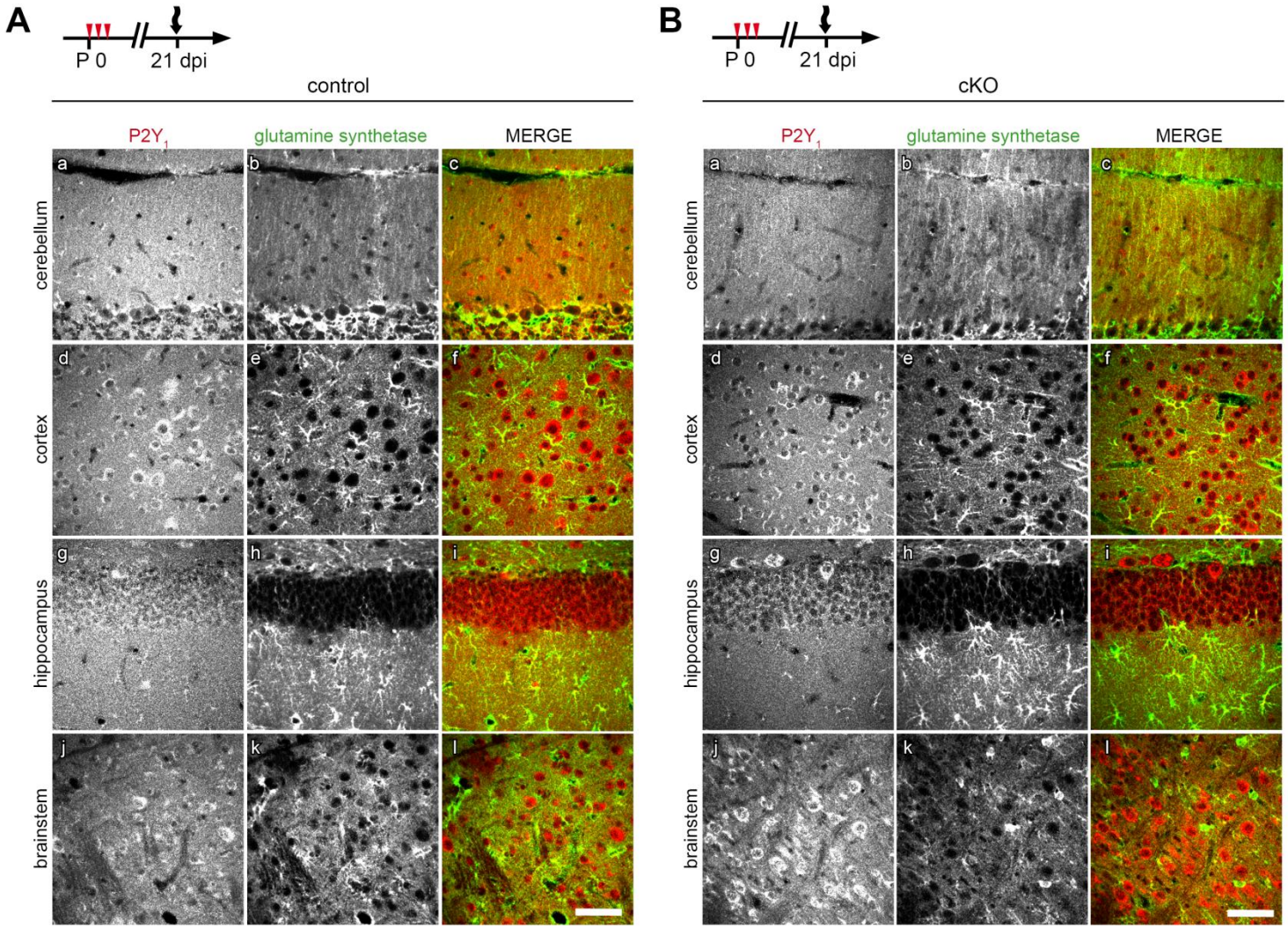

Figure 5. 14 Immunostaining of young control and $P2Y_1R$ cKO brain slices using APR-009 AB

In **A** and **B** representative confocal images are depicted of a control and cKO animal. The lactating mother was injected with TAM directly after birth and the pups were analyzed 21 dpi. Sagittal slices have been co-stained against $P2Y_1R$ (**A**, **B** left panel) and glutamine synthetase (**A**, **B**: middle panel). In control animals a co-localization of both fluorescent signals can be detected in cb (**A**, **B**: **a**-**c**), ctx (**A**, **B**: **d**-**f**), hp (**A**, **B**: **g**-**i**) and bs (**j**-**l**), predominantly at the processes of astrocytes, partially also in cKO animals. The scalebar in (**i**) corresponds to 50 µm and applies for all images.

Since staining intensity was also low in wild types, we intended to increase the signal of the first antibody by incubation with a biotin labeled antibody against the rabbit Fc (fragment crystallizable) region of the $P2Y_1R$ antibody.

In addition mice were injected at postnatal day 10, considering published data suggesting that at least in the cerebellum Bergmann glial cells express $P2Y_1Rs$ predominantly around postnatal day 7. Brain slices were stained 21 dpi (see Figure 5. 13 C). Indeed staining was predominantly enhanced on Bergmann glia processes in the molecular layer (a), but the staining pattern did not differ in the cKO animals (b). In addition we tested the antibody on whole brain homogenates by Western blotting of 2 months old animals homozygous (*p2ry1*$^{fl/fl}$), heterozygous (*p2yr1*$^{fl/wt}$) and null (*p2yr1*$^{-/-}$) for the *p2ry1* allele. Two samples per genotype were analyzed. In Figure 5. 13 D the Western blot immuno probed for the $P2Y_1R$ is depicted. Band patterns were identical for all investigated genotypes. Several bands could be identified, which is firstly evidence for unspecific binding properties of the antibody but in addition not a single band could be identified, which changed the intensity with regard to the $P2Y_1R$ genotype. We expected that blotted proteins of homogenates with only one functional *p2ry1* allele show at least one band with potentially less intensity compared to a band of the same size in homogenates with two functional alleles. Consequently this band would be missing in homogenates of $P2Y_1R$ null background.

We injected a lactating mother immediatly after birth and analyzed the pups (controls and cKOs) 21 dpi. We co-stained sagittal brain slices against the $P2Y_1R$ and the astrocyte marker protein glutamine synthetase. Representative confocal images of a control and cKO animal are depicted in Figure 5. 14 A and B, respectively. In the molecular layer of the cerebellum (A, B, a), the dentate gyrus (A, B g) and in the cortex (A, B d) a decreased $P2Y_1R$ fluorescence background intensity could be determined. This observation could not be verified for all investigated animals (n = 4) (data not shown). Based on the merge in control animals (A, c, f, i, l) co-localization of $P2Y_1Rs$ and glutamine synthetase was detected in every investigated brain region, predominantly at the processes of astrocytes. Somatic staining had neuronal character. But also in cKO animals, co-localization was still detectable (B, c, f, i, l). Remaining $P2Y_1R$ expression in 2 months and 10 days injected cKO animals might be due to unspecific AB binding which we showed by staining of $P2Y_1R$ total KOs.

The second antibody that we tested was from Abcam and detected an epitope intracellular at the C-terminus of the $P2Y_1R$ protein. The results are shown in Figure 5. 15. We co-stained sagittal slices against GFAP (A b, e, f) and the $P2Y_1R$ (A a, d, g) and performed Western blotting with the same samples mentioned above (B). Representative confocal images of the cerebellum (a-c), cortex (d-f) and hippocampus (g-i) showed co-localization of both fluorescent signals in the processes. Somatic staining was not from astroglial origin. Western blots probed for the $P2Y_1R$ with the antibody from Abcam, showed a different band pattern as the antibody from Alomone. But also here no specific $P2Y_1R$ band could be identified.

Finally, we tested an extracellular binding antibody from Alomone on vibratom slices. We changed the staining procedure (see 7.6.1) and co-stained GFAP and $P2Y_1R$. Representative images of the cerebellum, hippocampus and cortex are depicted in Figure 5. 16. $P2Y_1R$ staining was again present at the processes of astrocytes in the investigated brain regions.

However, we conclude that $P2Y_1R$ antibodies, recognizing an intracellular epitope of the

$P2Y_1R$ are partially specific for immunohistochemical methods but not sensitive enough to detect minor differences between control and astroglial $P2Y_1R$ cKOs. Further, the antibodies were not applicable for Western blotting under the tested conditions (see 7.5.2). The antibody, directed to an extracellular epitope (APR-0021), showed the most satisfying staining results, which appeard punctuated and clear and was used for further stainings (see 5.7).

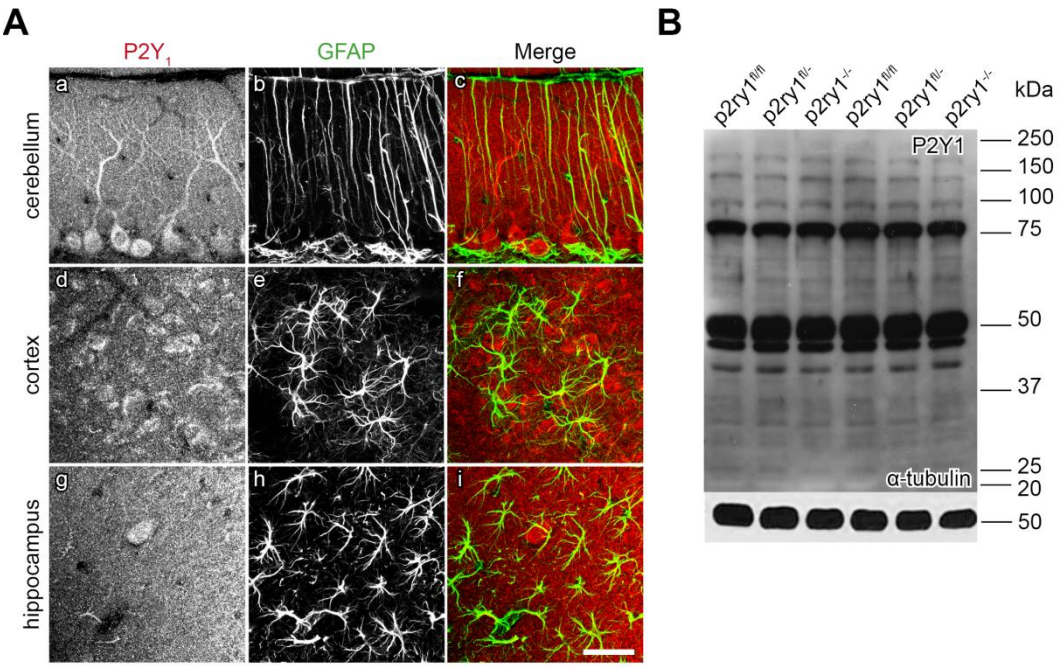

Figure 5. 15 Immunostaining and WB of control and $P2Y_1$ KO brains using the Abcam AB

In **A** representative images of sagittal brain slices of a 2 month old wild type animal are depicted co-stained for the $P2Y_1R$ (Abcam, left panel) and GFAP (middle panel). In the merge, co-localization of both fluorescent signals can be determined in cb (**A**, **B**, **a**-**c**), ctx (**A**, **B** **d**-**f**), hp (**A**, **B** **g**-**i**) predominantly at the processes. The scale bar in (**i**) corresponds to 50 µm and applies for all images. In **B** a Western blot was probed for the $P2Y_1R$ protein with the same antibody. The lanes show in doublets: wild type, heterozygous KO and total KO whole brain homogenates. The pattern does not differ.

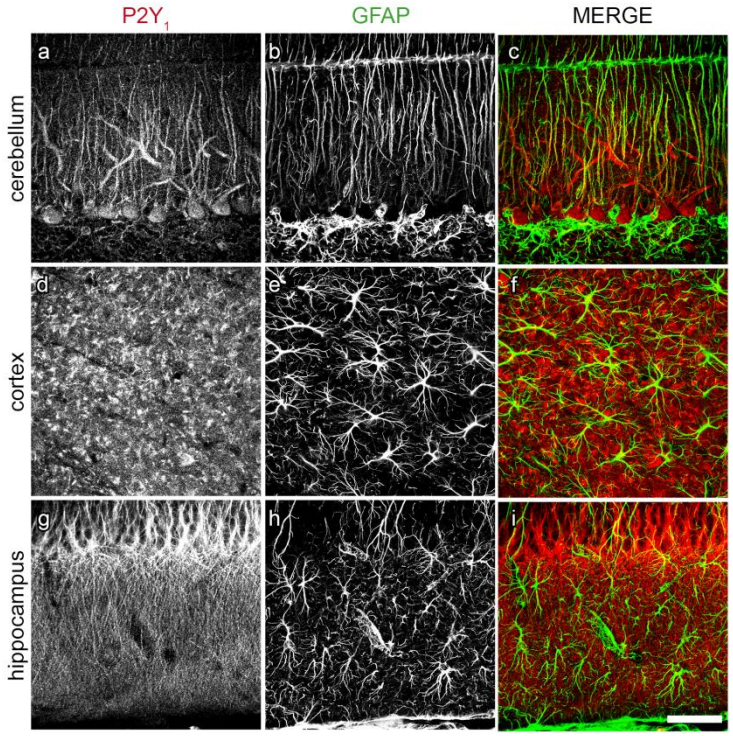

Figure 5. 16 Immunostaining of WT brains using the APR-0021 AB

Depicted are sagittal brain slices of 2 months old wild type mice co-stained for the $P2Y_1R$ (Alomone extracellular binding, left panel) and GFAP (middle panel). In the merge partial co-localization of both fluorescent signals can be determined in cb (**a**-**c**), ctx (**d**-**f**), hp (**g**-**i**).The scalebar in (**i**) corresponds to 50 µm and applies for all images.

5.7 Astroglial P2Y$_1$ receptor expression in the cerebellum

Further it was suggested by immunhistochemical methods that P2Y$_1$R expression would switch during cerebellar development (P 7) from glia cells (BG) to noradrenergic neurons (Purkinje cell) (P 21) (Amadio et al., 2007). In order to repeat this fundamental experiment, mice were perfused at P 9 and P 28 and we compared likewise the expression pattern of P2Y$_1$Rs. We could determine that Purkinje cells are not the predominant cerebellar cell type expressing the receptor at P 9. They started to express P2Y$_1$Rs later which was obvious by characteristic soma staining at the later time point (see Figure 5. 17 A e).

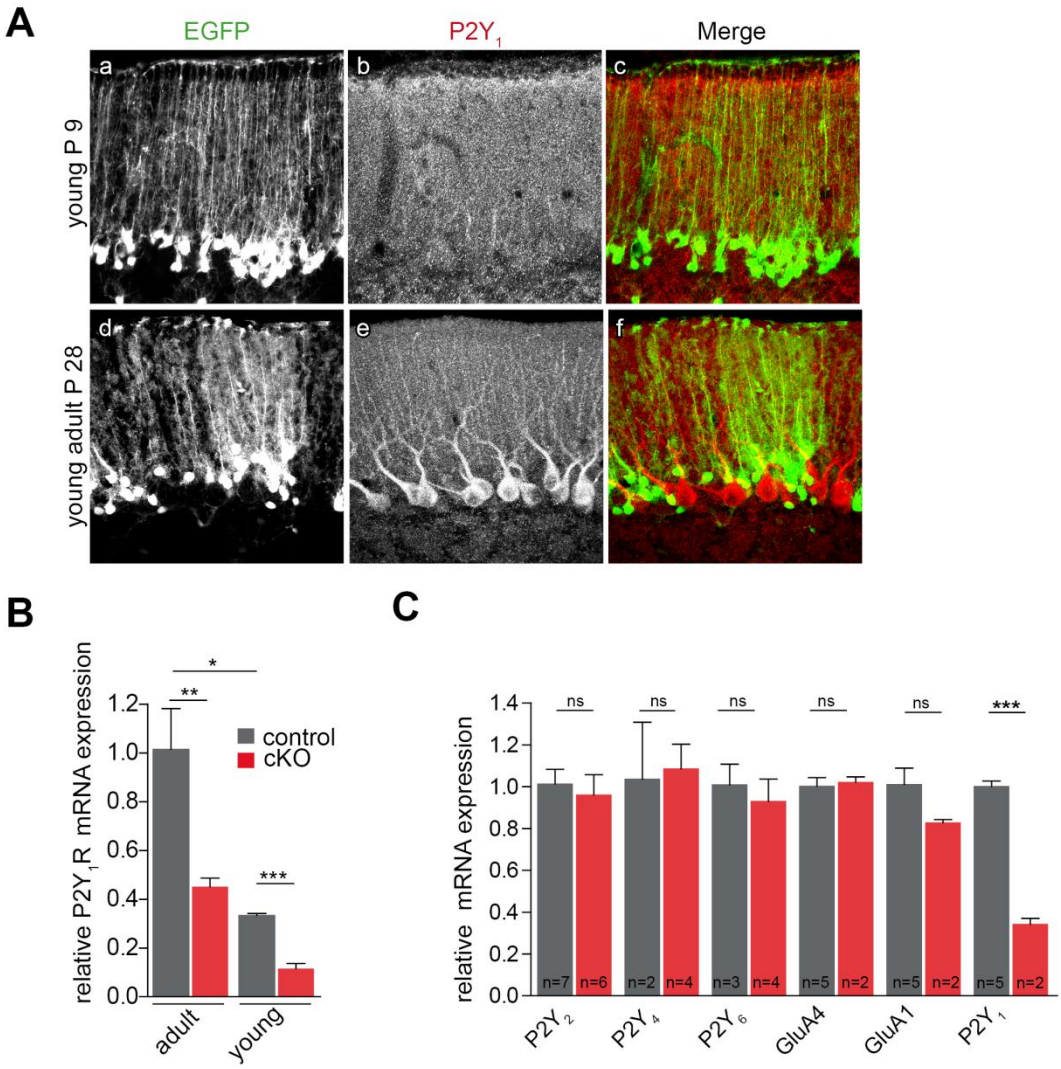

Figure 5. 17 P2Y$_1$R expression in the cerebellum of young and adult mice

In **A** sagittal vibratom slices of prenatal cerebelli at P 7 (**a**-**c**) and P 28 (**d**-**f**) of hGFAP-EGFP mice stained for P2Y$_1$R (**b**, **e**) are depicted. Bergmann glia cells express the EGFP reporter protein (**a**, **d**). In the merge (**c**, **f**) it is obvious that Purkinje cells expressed P2Y$_1$Rs at later stages, but co-localization of P2Y$_1$R and BG is detectable at both ages **B** shows 21 dpi, P2Y$_1$R mRNA expression levels in young (P 10) and adult (P 28) TAM injected control and cKO animals. P2Y$_1$ mRNA expression is increased with age, but at both ages reduced to the same extent in cKO animals. **C:** Homogenates of adult injected animals were analyzed for expression levels of P2Y$_1$, P2Y$_2$, P2Y$_4$ and P2Y$_6$ receptors and GluRA and GluRD AMPA receptor subunits. None of investigated receptors showed compensatory effects in P2Y$_1$R cKO animals. Only P2Y$_1$R expression was significantly changed.

But we could not confirm that $P2Y_1R$ expression in BG is diminished in animals from postnatal day 21. The characteristic long, fine BG processes were even more pronounced at P 28 (see Figure 5. 17 e). We investigated $P2Y_1R$ mRNA expression in young (P 10) and adult (P 28) injected control and cKO animals. 7 weeks old control animals showed 3 fold higher $P2Y_1R$ expression levels as 4 weeks old animals. In contrast, mRNA levels in young and adult injected animals showed the same relative reduction in mRNA expression (control 100 ± 16% → 45 ± 4 %; cKO: 33 ± 1 % → 11 ± 2 %). We conclude that $P2Y_1Rs$ are expressed in young and adult Bergmann glia cells and that they are likewise degraded to the same extent in cKO animals after TAM injection. However, for further studies it was important to exclude compensatory effects, especially by the three other P2Y subtypes, reported to be expressed in BG and of the AMPA subunits GluA1 and GluA4. We determined in 4 weeks old injected animals 21 dpi expression levels by qRT-PCR for mRNA expression. None of the analyzed receptor mRNAs was dysregulated in $P2Y_1R$ cKO animals (see Figure 5. 17).

5.7.1 No evidence for Bergmann glial process retractions from Purkinje cell synapses and changes in synapse density in $P2Y_1$ cKO animals

Ca^{2+} signaling of Bergmann glial AMPA receptors is important for synaptic transmission of Purkinje cell synapses (Iino et al., 2001; Saab et al., 2012). In young mice, deletion of BG AMPA receptors resulted in retraction of glial appendages from Purkinje cell (PC) synapses, increased amplitude and duration of evoked PC currents and a delayed formation of glutamatergic synapses. Here, we asked whether the selective loss of BG $P2Y_1Rs$ shows similar changes in the developing cerebellum. We injected mice at the age of 10 days with TAM and analyzed cerebellar slices 21 dpi. $P2Y_1R$ mRNA was significantly reduced. The gross cerebellar organization, like stratification of the granular cell, Purkinje cell and molecular layer, was not affected when Bergmann glial $P2Y_1$ receptors were lost in the second to third postnatal week of cerebellar development. There was neither an overt change in Purkinje cell morphology (see Figure 5. 18 A a, b). We also investigated, if Ca^{2+} signaling, induced by $P2Y_1Rs$ at this age, is required for the regulation of parallel fiber (PF)-Purkinje cell (PC) synapses. We analyzed PF-PC synapse density (in the upper third of the ML) at the ultrastructural level and did not detect a significant reduction of synapse number in cKO mice (Figure 5. 18 B). To exclude that the $P2Y_1Rs$ might be responsible at earlier stages, we injected a lactating mother at the first day after birth and analyzed synapse density of the pups 21 dpi. Sagittal slices were stained against the vesicular glutamate transporter VGlut1, a presynaptic marker protein and the astrocyte marker s100β. In total 2 controls and 6 cKO animals have been investigated. Representative confocal images of the cerebellum are shown in Figure 8. 11 and B (a-c), respectively. Densitometric quantification of confocal images determined no difference in VGlut1 fluorescence intensity between cKO and control animals; also S100β staining was unchanged compared to controls. We conclude that astroglial $P2Y_1R$ and PF-PC synapes were normally covered by BG lamellae and are disposable for synapse formation and/or maintenance in the developing brain. In addition, we analzyed the Bergmann glial surface area in the molecular layer. No abnormalities, as reduction in lamellar arborization, process complexity or swellings were observed in cKO mice. We determined no significant differences in the surface area between cKO and control animals (see Figure 5. 18 B a, b). Processes were not significantly retracted.

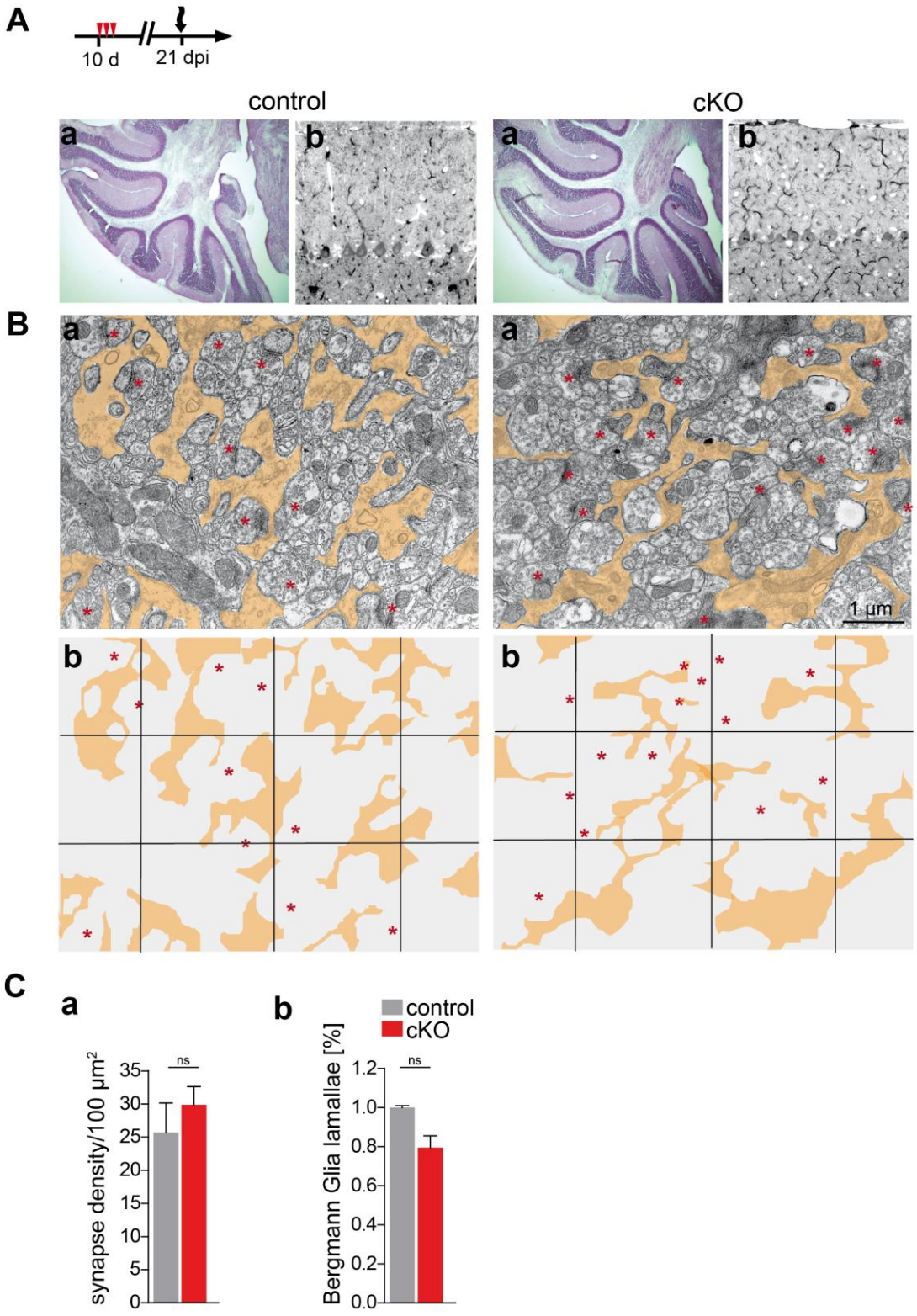

Figure 5. 18 Bergmann glial surface and density are not changed in cKO mice in the cb

A: Animals were injected with P 10 and processed 21 dpi. The gross cerebellar organization did not show abnormalities in cKO animals as seen in hematoxylin and eosin staining of the cerbellum (**a**) and semi section (500 nm) (**b**). PF-PC synapse density was quantified by counting synapses in randomly taken EM images from the upper third of the molecular layer (ML). 5-8 images per animal were counted blindly (**B a**) cKO mice revealed with 26 (±. 4) synapses per 100 µm^2 no reduction synapse density compared to controls (30 ± 3). Bergmann glial processes are false-colored brown and synapses are indicated with asterisks. Relative Bergmann glial process area was not reduced in cKOs compared to controls. Scale bar 1 µm.

6 Discussion

In Part I we investigated the GLAST-CreERT2/loxP system in regard to reliability and efficiency to knock out receptor proteins in mouse astrocytes. In Part II we started the functional analysis of astroglial $P2Y_1$ and NMDA receptors using respective knockout models. In the following sections results are discussed in the order presented in the results.

6.1 Pharmacokinetics of tamoxifen and recombination of loxP sites in mice

Tamoxifen (TAM) is used as an anti- breast cancer drug. Hence, pharmacokinetics of TAM in mice, rats and humans were mainly investigated in regard to compatibility of endocrine therapy for breast cancer in women. It was determined that mice, rats and humans show different metabolite profile after application of TAM. In general, metabolites formed by demethylation (e.g N-desmethyltamoxifen (NDMT)) are more abundant; whereas the concentrations of the more hydrophilic, hydroxylated metabolites (e.g 4-hydroxytamoxifen (4-OHT)) are generally lower. The metabolic disposition of TAM in rats resembles that in humans. In addition to TAM, NMDT in humans and rats, and 4-OHT in mice, are major serum metabolites (Kisanga et al., 2003; Robinson et al., 1991).

We were specifically interested in the efficiencies of 4-OHT to activate the CreERT2 fusion protein in the murine brain. For specific and effective Cre-loxP recombination *in vivo* the injected TAM dose and the duration of TAM activity is important. Therefore we studied TAM-metabolism in brain and serum of wild type mice after a single intraperitoneal injection (IP) of 100 mg/kg TAM.

We determined a fast decay of TAM and the potent metabolite 4-OHT in brain and serum. Serum concentrations were initially 8 fold lower than in the brain. This is in line with results obtained from tissue of rats and mice after oral dosages of TAM. They determined TAM concentrations to be 8- 200 fold higher in tissue than in serum (Lien et al., 1991a; Robinson et al., 1991). Furthermore, we measured peak levels in serum and brain after 8 h, our first time point. If we determined C_{maxTAM} and $C_{max4\text{-}OHT}$ to be after 8 h, half lifes in the serum were 22.3 h and 26.8 h for TAM and 4-OHT, respectively. In the brain it took 20.9 h and 25.3 h till concentrations of TAM and 4-OHT, respectively, were decreased to half of initial concentrations (see Table 1). In addition after the 5^{th} day, tamoxifen and 4-OHT residuals were hard to detect (see Table 17).

To our knowledge only one publication considered the distribution of TAM and metabolites in brain tissue (Lien et al., 1991a). Here, rats were fed with 1 mg/kg TAM with an esophageal tube for 3 or 14 days. They measured ~800 ng/ml TAM and ~200 ng/ml 4-OHT ~ 6 h after the last dose. Interestingly, the concentrations were not increased after 14 days of force feeding indicating a fast turnover of the drug. We determined 8 h after one single dose of 100 mg/kg TAM IP injecte a much higher concentration of 5750 ng/ml ± 667 ng/ml for TAM and 1005 ng/ml ± 169 ng/ml for 4-OHT in the brain of mice.

Studies in murine serum were often performed after subcutaneous injections or oral administration of the drug. Hereby oral administration was defined to achieve higher concentrations of metabolites (Reid et al., 2014; Robinson et al., 1989) (see Table 17). In general, obtained pharmacokinetics for TAM in serum of mice are difficult to compare. In

addition to the wide range of TAM doses reported in the literature, there are a variety of TAM administration methods, drug preparation protocols (oil suspensions vs. implanted pellets) and routes of administration (subcutaneous vs. intraperitoneal vs. oral). Further, different protocols to measure TAM and metabolites by HPLC techniques were used. The HPLC-MS used in this study was development to trustfully quantify TAM and 4-OHT concentrations in nM range in serum and brain tissue. Furthermore, mentioned studies were performed in either nude or CD1 or C57Bl6/N wild type mice. Taken together, our results are within the expected range, but we high likely missed peak levels of the drug, suggesting determined half lifes as too high (compare t_{50} values in Table 1).

Table 1 Summary of tamoxifen pharmacokinetic studies

TAM dose	Tissue/ species	adminis-tration	Peak level [h]	[TAM] ng/ml	[4-OHT] ng/ml	t_{50}:TAM/ 4-OHT [h]	reference
1 mg/kg	brain/ rat	oral for 3 or 14 days	6	800	200	-	(Lien et al., 1991a)
25 – 100 mg/kg	serum/ nude mice	IP	-	78 - 189	-	-	(DeGregorio et al., 1989)
0.8 mg	serum/ C57Bl6/N	IP	4	-	80	-	(Wilson et al., 2014)
200 mg/kg	serum/ nude mice	oral/ analysis after 24 h	3- 6	441 ± 208	628 ± 192	11.9/ 6	(Robinson et al., 1991; Robinson et al., 1989)
200 mg/kg	serum/ nude mice	subcutan/ analysis after 24h		120 ± 19	26 ± 5	-	(Robinson et al., 1991)
20 mg/kg	serum/ CD1 mice	oral	TAM: 1 4-OHT: 0.5	40.8 ± 51.9	26.4 ± 3.9	7.6/ 4.5	(Reid et al., 2014)
20 mg/kg	serum/ CD1 mice	subcutan	TAM: 4 4-OHT 2	49.4 ± 8.6	7.3 ± 3.4	11.2 / 11	(Reid et al., 2014)
100 mg/kg	**serum C57Bl6/N**	**IP**	**8**	**330 ± 39**	**284 ± 32**	**22.3 / 26.8**	**current study**
100 mg/kg	**brain/ C57Bl6/N**	**IP**	**8**	**2250 ± 485**	**515 ± 99**	**20.9 / 25.3**	**current study**

Subsequently, effective and especially specific recombination also depends on the promotor driven Cre expression. We investigated the recombination efficiency of two floxed target genes, *p2ry1* (coding for the $P2Y_1$ receptor) and *gria1* (coding for the GluA1 subunit), induced by the astrocyte-specific GLAST locus, by quantifying the increase of floxed alleles after different TAM injection protocols and determined that 3 injections of TAM at 3 consecutive days, are sufficient to obtain maximum number of recombined floxed alleles in cerebellum and cortex 21 days after the first injection of TAM.

The EC_{50} value for 4-OHT, to activate CreERT2 was determined to be 6 nM in F9 murine embryonal carcinoma cells (Feil et al., 1997). The EC_{50} value for TAM was not determined, since it exhibits a much lower affinity to the mutated receptor and whenever both compounds

are present, 4-OHT will bind. According to our data efficient levels to activate the Cre DNA recombinase were still determined at the 5th day after injection in the brain (2.5 ng/ml = 6 nM) 4-OHT). Interestingly, the interval protocol of in total 3 injections, with 2 days pause between each injection was not as efficient as 3 consecutive injections. This data demonstrate, regardless of determined concentrations, that *in vivo* after 2 days of a single injection of TAM, 4-OHT levels are not sufficient to activate Cre for DNA recombination in the brain.

Furthermore, in cerebellum and cortex the two chosen target genes showed different kinetics among themselves and among brain regions but reached same levels of recombined alleles 21 days after 3 daily injections of TAM. In the cerebellum, DNA recombination showed faster kinetics at the initial time points, 8 h and 21 d, after one injection of TAM compared to the cortex. In the cerebellum GLAST expression is reported to be much higher as in the cortex (Regan et al., 2007). The stronger promotor might therefore correlate to a higher number of CreERT2 molecules, leading to a greater possibility of successful recombination events in a given time window independent of TAM concentrations.

This result also indicates that the qRT-PCR approach, quantifying the gain of recombined alleles, is of high quality and able to detect these differences. In addition, recombination kinetics for *gria1* were already determined on a precise time scale, here we determined that 50 % of the maximal recombination occurred after ~11 h. In this study we determined after 8 h 37 % of recombined alleles, which is line with the already published data (Saab et al., 2012). In addition, the current study showed that one injection of TAM is not sufficient to achieve maximum recombination neither in the cortex nor in the cerebellum.

Taken together our results demonstrate that DNA recombination of target genes is reliably executed by the CreERT2 DNA recombinase as long as efficient levels of 4-OHT are present in the brain. Due to the fast turnover of the metabolite in the hour range, consecutive injections of tamoxifen for at least three days are needed. The actual amount of tamoxifen also depends on the brain regions, e.g. in the cerebellum, probably two consecutive injections are enough, in contrast to the cortex, here five injections are recommended to ensure maximum recombination. Furthermore, determination of serum concentrations was not meaningful for the actual concentration of TAM and 4-OHT in the brain of mice.

It is desirable to inject the least possible amount of TAM, since TAM has also severe side effects. Any other effects apart from the induction of DNA recombination should be prevented. Especially in developing mice (pups) but also in adult mice it was shown in several studies that TAM induced abnormalities in genitalia of female and male mice after administration of as little as micrograms of TAM (Newbold et al., 1997; Reinert et al., 2012; Taguchi and Nishizuka, 1985). Furthermore, it was shown that IP injections of comparable amounts of 5 mg/20 g for 3 days caused severe gastric toxicity (Huh et al., 2012). Further the incomplete absorption of injected oil, indicated by subcutaneous oil pockets found in the area of injection were shown (Reinert et al., 2012).

For inducible CreERT2/loxP recombination one critical parameter is the time line of TAM in a given tissue which is often not described. In our study we investigated, next to spatial extent of recombination in the target tissue (Ctx and Cb), also the temporal extent of recombination. Knowing the timeline of TAM-induced DNA recombination is important for lineage tracing experiments because unknowingly the labeling of newly generated cells is extended. In the pancreas the time line for TAM induced recombination was determined to be up to 4 weeks

after initial injection of 3 x 8 mg Tam and was reduced to one week after a lower dose of 3 x 1 mg TAM (Reinert et al., 2012). We can conclude, together with qRT-PCR data, that in the brain the temporal extent of TAM (100 mg/kg) to induce DNA recombination is restricted to one week maximally. Interval injections were not as efficient and after the 5th day it was difficult to detect 4-OHT in brain tissue.

Further, as mentioned in the introduction, newer studies revealed endoxifen as a highly efficient TAM metabolite to bind estrogen receptors. ENDX levels were lower than 4-OHT concentrations in serum of mice (Reid et al., 2014) but still present. ENDX should be investigated in regard to the efficiency to activate the CreERT2 fusion protein. To inject directly 4-OHT is albeit the cost an avantage since the number of metabolites of TAM and their storage in tissue is reduced. Predominantly, only the likewise potent endtoxifen is metabolized.

6.2 DNA recombination events as a quantitative measure of astrocytes

In addition, we quantified the loss of recombined alleles in cerebellum, cortex, hippocampus, brainstem and optic nerve for the floxed reporter gene *tdTomato* (coding for the red fluorescent reporter protein tdTomato) and target genes *p2ry1* and *gabbr1* (coding for the $GABA_{B1}$ receptor). All three alleles showed no significant differences in regard to DNA recombination efficiencies, 21 d after 3 injections of TAM and no differences between genders could be determined. As a consequence we equated the quantified loss of floxed alleles as a measure for astrocytes (GLAST+ cells) in a given brain tissue. We concluded that in a brain of a young adult mouse 20 % in the brainstem, 8 % in the cerebellum, 22 % in the cortex, 30 % in the hippocampus and 31 % in the optic nerve account for astrocytes. In support for these results, direct cell counting of tdTomato+ cells in the cortex concluded likewise that 21 % of all cells are astrocytes. These results indicate a high quality of the qRT-PCR approach to quantify the loss of recombined alleles.

Astrocytes are often considered as the most abundant cell type in the brain, but good references for this statement are missing. The work of Suzana Herculano-Houzel is unrivaled in investigating the ratio of neurons and glia in the brain of many species (Herculano-Houzel, 2014). They developed a non-stereological method, the isotropic fractionator (Herculano-Houzel and Lent, 2005), and determined total numbers of neuronal and non-neuronal cells, those expressing the neuronal marker NeuN or not, respectively. The isotropic fractionator is a cell counting technique that homogenizes fixed tissue, recovers cell nuclei in solution and samples and quantifies nuclei by extrapolation. Results of the new technique were validated and was at least as reliable as stereology (Bahney and von Bartheld, 2014; Tsai et al., 2009). They found in the mouse cerebral cortex the proportion of glial cells to vary around 55.4% (Fu et al., 2013; Herculano-Houzel, 2014). Herculana-Houzel further commented on their work “that it must be kept in mind that glial refers to a combination of astrocytes of various types, oligodendrocytes, and microglial cells and various precursor cells in the adult. The numbers and proportions of cell types in this heterogeneous population have yet to be determined across brain structures and species”. We provided here a method which can quantify the number of different glial cell types in the murine brain and which was likewise, at least in the cortex, validated to be as good as stereology. Furthermore, our method resembles closer the *in vivo* status; since we spare the isolation step, where a fraction of cell

nuclei are destroyed. The data could be upgraded by other suitable Cre driver lines for each cell type. We investigated already the non-inducible oligodendrocyte-specific CNP Cre driver (see Figure 5. 1), but could not use these data to correlate them with the actual number of oligodendrocytes in brain areas. CNP-Cre induced recombination occurred also in other cell types, like neurons. The PLP-CreERT2 line (Leone et al., 2003) was revealed to be restricted to oligodendrocytes and the recombination can be temporally controlled (unpublished data, Kirchhoff lab). To target loxP sites, specifically in microglia two Cre lines under the control of Cd11 promotor are available (Boillée et al., 2006; Ferron and Vacher, 2005) and an inducible CreERT2 mouse line under the control of the CX3CR1 (CXC chemokine receptor) promotor (Yona et al., 2013). For neuronal-specific recombination a whole battery of non- and inducible Cre variants are publicly available and listed at the Allen Brains Institute webpage (http://connectivity.brain-map.org/transgenic).

Our method is based on the simple fact that each cell contains the same genomic content, likewise loxP sites. After Cre activation only one cell population, astrocytes, looses this information. This loss is quantified. Primers for loxP sites should therefore simuationeuosly function as endogenes at the DNA level. We validated this assumption and indeed loxP primers for *gabbr1*, *p2y1*, *grin1* and *tdTomato* showed for each sample and also on average for each tissue the same tendency for a higher or lower DNA input (data not shown).

6.3 Efficiency of recombination depends on position of loxP sites

Furthermore, we investigated next to the three mentioned loxP sites, also the *grin1* locus. We quantified likewise the loss of floxed alleles after TAM application under control of the GLAST promoter. No significant differences in quantity of *grin1* loxP sites, between cKO and control animals, in every investigated brain region (ctx, hp, cb, opt. n., bs) was determined. This was independent of age when TAM injections started and also of the distance between loxP sites. The latter factor has been suggested to play a role for recombination efficiency (Collins et al., 2000; Koike et al., 2002; Liu et al., 2013; Zong et al., 2005). However, these publications dealed with interchromosomal recombination (loxP sites are located on different chromsomes or DNA strands) in which the Cre DNA recombinase has to bridge much bigger distances to form the synapse of loxP sites (Ghosh et al., 2007; Guo et al., 1997). Nagy and collegues successfully excised an almost 400 kb genomic region with 50% efficiency *in vitro,* utilizing likewise Cre-loxP mediated intrachromosomal recombination (loxP sites are located on the same DNA molecule). Also the removal of the selectable marker from targeted alleles (Meyers et al., 1998; Nagy et al., 1998) works reliable *in vivo* in spite of bigger distances as we described them. In summary, most reports validated the Cre DNA recombinase to work reliably between large distances within a chromosome or between different chromosomes.

In the current study, the GLAST-CreERT2 driver line recombined successfully the *p2ry1*, *gabbr1*, *gria1* and the reporter gene tdTomato; the distances between loxP sites ranged between 900 bp – 1700 bp. We investigated the *grin1* locus with a flanked sequence of 6800 and 2400 bp between loxP sites. In addition, a successful DNA recombination of the *grin1* locus (6800 bp) was inducible with an oligodendrocyte specific transgenic mouse line (CNP-Cre), which excludes technical problems. We conclude that the difficulty of DNA recombination of the floxed *grin1* gene is neither impaired because of the CreERT2 fusion protein nor the size of targeted locus. Nonetheless, we could show an increase of

recombined alleles in a non quantitative manner. The *grin1* locus in astrocytes is therefore recombined but with lower efficiency compared to other floxed loci.

The results draw the attention to cell type specific epigenetic context of floxed loci, meaning that the genomic *grin1* locus in astrocytes is not as well accessible for the DNA recombinase as other loci in astrocytes or the *grin1* locus in oligodendrocytes. Local chromatin structure and consequently, the potential for gene expression, are directly regulated by a number of post-translational, covalent modifications of histone-amino terminal tails, like methylation or acetylation. In general, within euchromatin structures the degree of condensation or DNA accessibility varies depending on gene activity (Allen, 2008). Dixon et al. could show that tissues (brain, testis) with the highest levels of Huntington's disease homolog (Hdh) mRNA in mice were at the same time the only tissues susceptible to Cre-mediated recombination between loxP sites at the Hdh locus. In contrast, the same Cre-expressing line caused recombination in every tissue for loxP sites at another genomic location (Dixon et al., 2004).

Long and Rossi (2009) studied three commonly used Cre-reporter strains, Z/AP, Z/EG and R26R-EYFP and demonstrated that although each reporter can be reliably activated by Cre during early development, exposure to Cre in adult hematopoietic cells resulted in a much lower frequency of reporter positive cells in the Z/AP or Z/EG strains than in the R26R-EYFP strain. In reporter negative cells, derived from the Z/AP and Z/EG strains, the transgenic promoter is methylated and Cre-mediated recombination of the locus is inhibited. Z/AP or Z/EG reporter cassettes were randomly inserted into the mouse genome and as such are more likely to be subjected to position effect variations than the R26R-EYFP reporter, which was inserted into the ubiquitously expressed Rosa26 genomic locus (Long and Rossi, 2009).

These explanantions are likewise possible for the *grin1* locus in astrocytes. NMDARs on astrocytes are expressed in low densities and their function is still under debate. In one of the first studies, it was shown by in situ hybridization together with immunohistochemistry (GFAP staining) that in adult rat cortical slices virtually no astrocytes contained mRNA transcripts of the GluN1 subunit (Conti et al., 1994). Minimal amounts of GluN1 transcripts, compared to other CNS cell types, in cultivated as well as acutely isolated astrocytes from 1-17 day-old mice were also confirmed by microarrays (Cahoy et al., 2008).

In this context we also investigated recombination kinetics of the AMPA receptor subunits GluA1 and GluA4 on a precise time scale in the cerebellum. Recombination within the *gria4* locus reached the time of maximal excision rate 24 h later as the g*ria1* locus. A comparable delay of 18 h is maintained at the mRNA level. GluA1 compared to GluA4 mRNA expression was determined to be two fold higher in the cerebellum. The differences between *gria1* and *gria4* recombination kinetics could be explained by affected chromatin structure, rendering the floxed sequences of *gria4* less accessible for the Cre recombinase.

Here, we could verify successful recombination for both genes also at the protein level. This was not possible for the GluN1 subunit on astrocytes (see 6.6 for further discussion).

6.4 Limitations of the GLAST-CreERT2 model to study astrocytes offers advantages to study the fate of progenitor cells in the adult neurogenesis

In the original publication, efficiency and specificity of the GLAST-CreERT2/loxP system was investigated throughout the brain using different tools (Mori et al., 2006). We aimed to

investigate this mouse line in regard to the reliable knockout of astroglial receptor proteins in the whole brain. The current study did not reveal any fundamental new functions of the GLAST-CreERT2 mouse but demonstrates the high potential to fulfill the requested function, by use of the highly sensitive tdTomato reporter mouse (Madisen et al., 2010).

First, we could show that the recombination efficiency of the reporter allele tdTomato correlates to the efficiency of targeted alleles. This statement holds for homogenates of investigated brain tissue, on average each cell is recombined for both alleles. Still, we can not state with this method that the recombination of reporter allele is accompanied by recombination of the target gene within the same cell. For this, a dual reporter approach linking recombination of a floxed allele directly with expression of a reporter protein is needed (Degen et al., 2012; Requardt et al., 2009).

Four weeks old mice that received TAM for 3 consecutive days showed widespread and strong expression of the tdTomato protein 3 days after TAM injection with little increase up to 5 months, demonstrating fast recombination kinetics. Just by morphology recombined cells revealed themselfes as astrocytes. They build a carpet like structure with non-overlapping domains of individual astrocytes, these is especially obvious in the cortex. Medulla, pons and midbrain showed different patterns with spots showing no recombined astrocytes. Albeit missing quantification the efficiency in the cortex should be far higher than 30 % quantified by (Mori et al., 2006) in adult GLAST-CreERT2 x Rosa26-reporter mice with β-galactosidase as reporter and S100β as a marker protein. However, by taking advantage of a second knock-in mouseline (GLAST-Cre-IRES-hrGFP), authors could show that GLAST driving Cre/GFP was expressed by a large subset (60–80%) of astrocytes (S100β+ and/or GS+) in cortex and striatum. This showed that the β-galactosidase reporter gene is not as sensitive as the tdTomato reporter gene to indicate recombination events. Long and Rossi, 2009 could show in their study that different efficiencies of reporter genes exist in spite of the same used R26 locus for transgene insertion. Furthermore, our results demonstrate that the GLAST promotor is active in the majority of astrocytes although GLT1 is validated to be the astroglial transporter of choice throughout the adult brain and especially in the cortex (Regan et al., 2007).

To investigate the origin of tdTomato+ cells, we predominantly used the astrocytic markers GFAP, GS and partially S100β 3 and 21 days, 3.5 and 5 month after the first TAM injection in the adult brain. We found that cells positive for GS or GFAP or S100β were also positive for tdTomato. In contrast, we found some tdTomoto+ cells that did not show any astrocytic marker expression, but cleary exhibit morphology of protoplasmic astrocytes. Mori et al also reported high diversity for astroglial marker expression of GS, S100β and Cx43 in reporter or Cre+ cells. Noteworthy, in the current study GFAP was not a sufficient marker, especially in cortex and brainstem. Cortices under physiological conditions virtualy lacked GFAP expression.

At no timepoint after the first injection, NeuN expression was found in tdTomato+ cells in the cerebellum, cortex and brainstem. Oligodendroglial (Olig2, MBP), NG2 glial (PDGFRα) and neuronal markers (NeuN, Vglut1) did not label tdTomato+ cells, 3.5 month after TAM injections in young adult (4 weeks) and old mice (6 months) in the cerebellum, cortex, hippocampus and brainstem. However, we found that neuronal markers were expressed by tdTomato+ cells in the OB and dentate gyrus. In addition, BLBP expression could be clearly

determined in a subpopulation of tdTomato+ cells in cortex and brainstem, radial glia cells (RGCs) in the SGZ and Bergmann glia 3.5 month after first TAM injection in young and adult mice. BLBP is a marker protein for radial glia cells during development (Feng et al., 1994; Kurtz et al., 1994) as well as astrocytes, and radia glial progenitor cells in adulthood (Schmid et al., 2006). Co-localization events were therefore expected.

Immunohistochemistry data have not yet been quantified and white matter areas in the cerebellum or the corpus callosum, hypothalamus, thalamus, striatum and septum, midbrain and pons have not been investigated in detail. Expression in other cell types apart from astrocytes in the mentioned brain regions can not be excluded.

In summary, these data support the view of a hetereogeneous astrocyte population and the GLAST promotor activity as efficient to target a large population of astrocytes. In the cortex we suggest that a larger population as described by the original publications is subject to DNA recombination.

There is no doubt that GLAST promotor activity is present in a subpopulation of astrocytes (B cells) in the SVZ and radial glia in the SGZ, which function as neural stem cells (NSCs) in the adult brain (Kriegstein and Alvarez-Buylla, 2009). Mori et al. described already the GLAST-CreERT2 system as highly efficient to target adult NSCs. They showed that 10 days after the last induction, many recombined cells were in the rostral migrating stream and few in the OB, were β-galatosidase positive, but after 4 months half of all interneurons in the OB were labeled. We confirmed these observations, using instead of the LaZ- the tdTomato reporter mouse line. The number of tdTomato+ cells increased dramatically from 3 days to 3.5 months after TAM injection in the OB.

More recently, the role of GLAST lineage cells to adult hippocampal neurogenesis was investigated (DeCarolis et al., 2013). The authors compared YFP labeled cells in two widely used TAM-inducible transgenic mouse lines: Nestin-CreERT2 x R26YFP and GLAST-CreERT2/R26YFP and analyzed their contribution to adult hippocampal neurogenesis. In GLAST-CreERT2/R26YFP (5-6 weeks) mice 12 dpi and 30 dpi, most YFP+ cells were RGCs and early progenitor cells, whereas at later times 100 dpi and 180 dpi, many cells matured into neurons (YFP+, NeuN+) with corresponding decreases in the proportions of RGCs and progenitors.

In the current study we also investigated the adult neurogenesis, by fate mapping tdTomato+ cells. We also found that after TAM application the number of tdTomato+ radial glial like cells (NeuN-) decreased and the number of granule cell neurons (displaying fine dendrites and axons) increased (NeuN+) to virtually 100 % in the DG. The advantage of the strong tdTomato+ reporter signal, compared to the YFP signal, was, that also the growth of dendrites and axons of newly born neurons were visible. However, in old mice (6 months), which were TAM injected 3.5 month before, far more tdTomato+ cells showed astroglial morphology and less newly generated granule cells were apparent in the hippocampus, indicating that in the aged hippocampus neurogenesis of GLAST+ progenitor cells is dramaticly decreased.

6.5 Promisis and limitations of sorting analysis tdTomato positive cells

Fluorescence activated cell sorting (FACS) to isolate murine astrocytes was established using transgenic mice expressing a green reporter protein specifically in astrocytes under control of the GFAP (Lovatt et al., 2007a), S100β (Cahoy et al., 2008), ALDH1l1 (Sun et al., 2013; Zhang et al., 2014) and GLT1 (Yang et al., 2011) promotor; the most used antibodies were GLT1 (Orre et al., 2014; Sun et al., 2013) and GLAST (Jungblut et al., 2012) in young animals. The protocols for the isolation procedure were similar. We adapted them to laboratory equipment and needs.

In this study we used tdTomato reporter mouse to establish FACS of young (1 month) and old (6 months) brain tissue and isolated astrocytes by the red fluorescence signal in recombined cells. We showed that the reporter expression is predominatly restricted to astrocytes and that labeling occurred with a high efficiency. Furthermore, no extra incubation steps with antibodies were needed and fluorescence intensity was more intense compared to EGFP (Srinivas et al., 2001) expression under control of the same promotor or EGFP labeled astrocytes under the hGFAP promotor (Hirrlinger et al., 2005) (data not shown). Owing to no significant differences in recombination efficiencies between reporter and target alleles (if the locus is accessible), we considered the use of this reporter mouse as the consequent step to isolate desired control and cKO populations and to be independent of antibody labeling.

Analysis of astrocyte-specific depletion of AMPA receptors demonstrated already that receptor expression in astrocytes is heterogeneous in regard to expression intensity and brain regions. Low receptor expression in the targeted cell type makes it in generally difficult to quantify the reduction in homogenates by Western blotting or immunohistochemistry due to higher expression by other cell types. Established FACS method was validated by proving sufficient reduction of targeted receptors in conditional $P2Y_1$-and NMDA receptor cKO models at the mRNA level.

Isolated cells showed high red fluorescence values which turned out to be a disadvantage, in brain areas, like cortex and hippocampus. Here, we identified two flurescent populations with either high or lower fluorescencent properties. The latter one was determined by marker expression to contain a high number of microglia cells, which was further verified by FACS experiments with mice expressing specifically in microglia cells the green fluorescent protein (CX3CR1-EGFP, (Jung et al., 2000)). Astrocytes were labeled here with an antibody against GLAST. A high proportion of microglial cells, isolated by the green fluorescent signal, were positive for both fluorescent dyes (data not shown).

The ability of microglial cells to phagocytize dying cells was established long ago and has been studied quite extensively. In this case it is quite likely that during the harsch isolation procedure to obtain a single cell suspension, cells dye, next to more sensitive neurons also astroctyes which are phagocytized by microglia cells. Furthermore, it was reported that microglia cells are capable of de novo expression of glutamate transporter protein within 4 h after brain injury (van Landeghem, 2001). In this case microglia cells are labeled due to their own GLAST expression by the antibody. In addition these circumstances might also explain that in the cerebellum only one fluorescent population was observed. The density of microglial cells in the cerebellum is 3x times lower as in the cortex (Yang et al., 2013). It is

also possible that leaked tdTomato protein of dying astrocytes or parts of astrocytes, like processes, stick to other cells and label them likewise.

However, further experiments have to be executed to evaluate the containing cell types in these two populations, like culturing of obtained cells and stainings of respective marker proteins. For the quality of transcriptome analysis the avoidance of contaminaton of other cell types has high priority. Marker gene expression of other cell types, like neurons and oligodendrocytes was decreased in isolated astroglial population, but not diminished.

The main goal is the transcriptome analysis between astroglial receptor knockout and control cells. The performed qRT-PCRs, to validate decreased amount of respective receptor mRNA for the conditional $P2Y_1$ and NMDA receptor knockout mice, were initial experiments. Desired are microarray analyses, in which transcript abundance is indirectly derived from fluorescence signal intensities or the more cost intensive RNA sequencing, in which also absolute amounts of mRNA molecules and unknown transcripts could be identified (Zhang et al., 2014). Single cell sequencing would be the method of choice to identify the receptor profile, expressed by individual cells and to help to reveal questions of hetereogenous populations. Next generation sequencing could be helpful to discover signaling pathways.

6.6 Heterogeneity of astroglial receptors

We showed in published data that GluA1 and GluA4 are intensively expressed in Bergmann Glia cells of the cerebellum (Saab et al., 2012). After TAM application we were able to show the degradation of both subunits by immunohistochemical stainings in a timely controlled manner. The staining of one subunit is able to outline the morphology of one BG cell.

Wwe investigated also changes at the mRNA and protein level in other brain regions and failed to show the timeline of DNA recombination, mRNA expression and finally protein degradation of astroglial AMPA receptors.

The results revealed one unique example of an optimized symbiosis between a specialized astrocyte, the Bergmann glial cell and a specialized neuron, the Purkinje cell. In this sense, astroglial heterogeneity closely reflects neuronal heterogeneity or more simple neuronal demands. It is a demanding task to reveal the function of various receptors expressed on astrocytes also of the AMPA type in different brain regions besides the cererbellum.

We demonstrated by immunohistochemical methods of $P2Y_1$ and NMDA receptors on vibratome slices difficulties to determine the exact localization of these receptors. Cell bodies of astrocytes mostly lacked receptor expression, whereas cell bodies of other cell types clearly showed expression of the respective receptor. Co-localization events were found preferably at the processes. However, functional studies validate the existence of both receptors (see introduction).

In general, different receptor expression profiles on astrocytes are possible, considering different brain regions (see Figure 6. 1): Astrocytes with homogenous expression of several receptors over their membranes (A), astrocytes with specialized microdomains, expressing only one type of receptor (B) or astrocytes which just express one type of receptor (C).

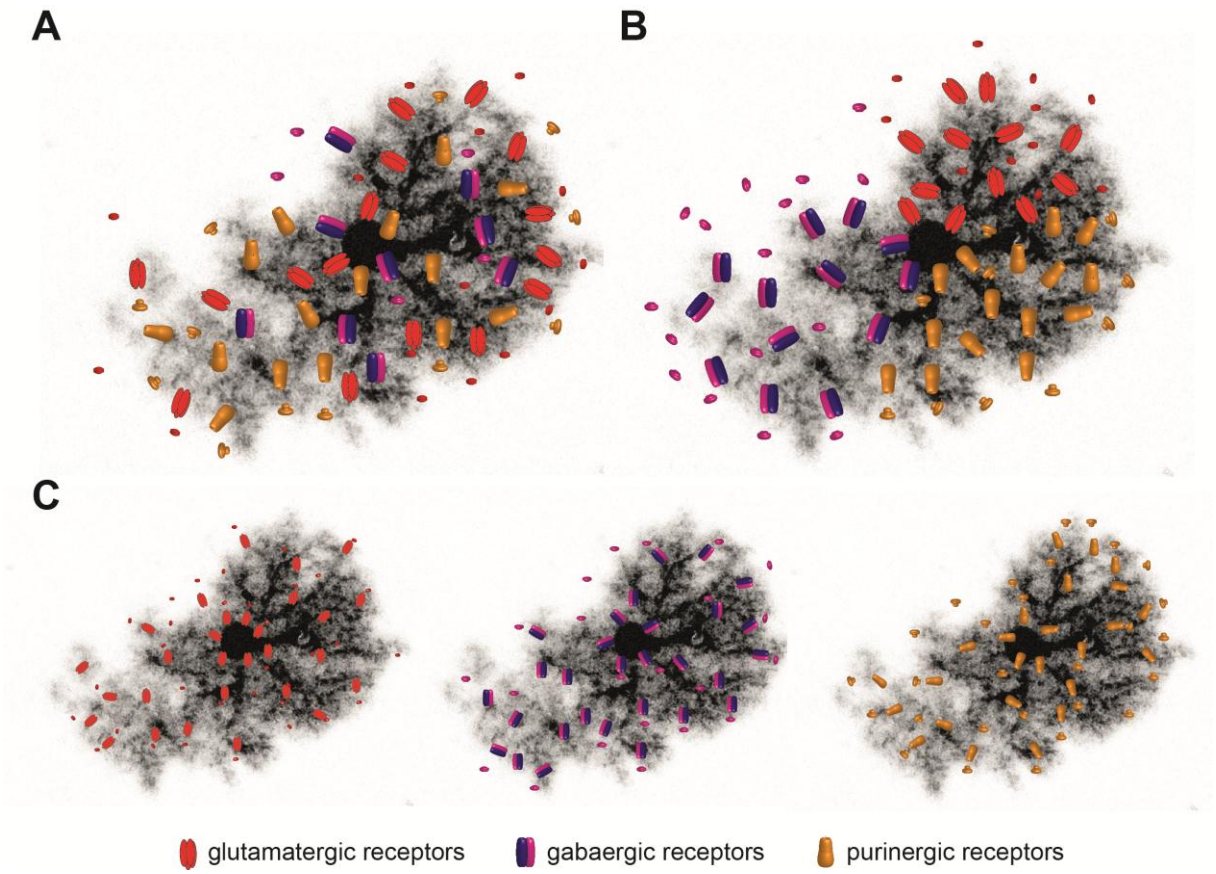

Figure 6. 1. Heterogeneity of astroglial receptor expression profiles

Astrocytes express indisputable receptors, but the concept of expression patterns is under debate. **A:** Do they express receptors equally distributed over soma and cell body? **B:** Do exist specialized microdomains for each receptor? **C:** Or does a single astrocyte only express one type of receptor?

6.7 NMDA receptors on astrocytes

We addressed the role of astroglial, glutamate NMDARs in the central nervous system of mice with special emphasis on the cortex by generating conditional mutants where the obligatory GluN1 subunit is ablated. In general, Ca^{2+} signals evoked by ionotropic receptors are less investigated by imaging techniques since they do not activate the massive release of Ca^{2+} from internal stores. Especially astroglial NMADR function is under debate. More recently controversial results in different brain regions since 1980 were summarized (Dzamba et al., 2013). To investigate the functional impact of astroglial NMDARs *in vivo* should help to clarify these issues.

In general, the verification of the GluN1 subunit, was difficult to detect on astrocytes. In fixed brain slices, astrocytes in cerebellum, brainstem and cortex lacked the GluN1 subunit at the soma and showed little co-localization at the processes. These results are in line with ultrastructural analysis showing subcellular localization of the GluN1 subunit on cortical astrocytes to be restriced to distal processes (Conti et al., 1996; Conti et al., 1997). Furthermore, NMDA-triggered Ca^{2+} signals were restricted to peripheral parts of processes and were not observed in the soma (Schipke et al., 2001). In summary, the conditional and temporally controlled delation of the GluN1 subunit in astrocytes was difficult to quantify with immunohistochemical techniques since detection was aleready difficult in control animals.

On the other hand, cultured hippocampal astrocytes showed NMDARs at GFAP positive processes when using the same antibody, a brain region, where NMDARs were rather reported to lack NMDARs (Matthias et. al, 2003, Höft et al., 2014). This fact demonstrated that circumstances *in vitro* do not correlate to the circumstances *in vivo.*

We further suggested that the chromatin structure for the *grin1* locus in astrocytes is difficult to access by the Cre DNA recombinase *in vivo*. The low expression of NMDARs on astrocytes might lead to methylation, closed chromatin structure and silencing of the gene. It is possible that only subpopulations of astrocytes express NMDARs which can be targeted by DNA recombination. However, DNA recombination could be determined but not to the same extent as quantified for other loci. In addition, FACS sorted cortical GluN1 cKO cells showed significantly reduced levels of GluN1 mRNA and glial synaptic currents in cortical slices of cKO mice showed no sensitivity to NMDAR antagonists.

Staining of the GluN2C subunit showed a decent expression even in the cell soma of cortical astrocytes. Further, we verified that synaptic evoked currents in astrocytes are sensitive to the NR2C/D specific antagonist UDP141 besides to Palygin et al., 2011 and showed enriched NR2C subunit expression in FACS sorted astrocytes, which is supported by (Cahoy et al., 2008; Zhang et al., 2014).

The biological importance of the GluN1 subunit in CNS function and behavior is highlighted by GluN1 null-mutant mice. They are not viable and shortly die after birth most likely due to respiratory failure (Forrest et al., 1994). Even a single point mutation in only one allele of the *grin1* locus is dominant lethal (Single et al., 2000). Conditional GluN1 mutants, restricting gene deletion to the hippocampal CA1 region, provided the first direct evidence that NMDARs are involved in synaptic plasticity (induction of LTP) and that they are essential for spatial memory and proper representation of space (McHugh et al., 1996; Tsien et al., 1996a; Tsien et al., 1996b) and revealed the absence of functional NMDARs in the membrane as the GluN2 subunits are retained in the ER (Fukaya et al., 2003).

The assembly of NMDAR subunits has been investigated in the late 90s in cell culture experiments with recombinant proteins (Béhé et al., 1995; McIlhinney et al., 2003; Monyer et al., 1992). The more recently resolved X-ray structure of GluN1/GluN2B NMDAR (Karakas et al., 2011; Lee et al., 2014) tightened the view of the incooperation of two GluN1 subunits. Since functional astroglial NMDARs showed the lack of Mg^{2+} block, together with lower Ca^{2+} permeability, also the incoopertion of a GluN3 sunbunit next to a GluR2C or D was suggested (Palygin et al., 2011). Assuming the incooperation of two GluN1 subunits, the expression of GluN1 in astroglial membranes should be at least equally intense and it should co-localize with GluN2C subunit. Therefore, against all odds it is tempting to speculate that astroglial receptors might have different stochastics than neuronal receptors containg only one GluN1 subunit next to three or two GluN2C subunits. Although (Palygin et al., 2011) exclude already the heteromeric composition of GluN2C due to the lacking Mg^{2+} block in astrocytes. But it would explain why the GluN2C can be visalized and not the GluN1 subunit.

In conclusion, it might be reasonble to use double knockouts for the GluN1 and GluN2C subunit to target astrocytes. Co-localization studies of GluN1, GluN2 and GluN3 subunits on astrocytes and neurons have not been performed with high resolution microscopy techniques avaible today since the interest of NMDARs increased in the early 90s (Conti et al., 1997).

Staining of the GluN1 units is accepted to demonstrate the whole complex. The actual subunit composition is derived from pharmacological properties.

It was also reported that, GluN2C-containing NMDARs exhibit unique properties, like low conductance, low open probability, and low sensitivity to Mg^{2+} (Farrant et al., 1994; Ishii et al., 1993; Monyer et al., 1992). The latter allowed GluN2C containing NMDARs to be activated without the requirement of postsynaptic depolarization, at least in the barrel cortex (Binshtok et al., 2006). GluN2C elsewhere is predominatly expressed in granule cells of the cerebellum. The properties of GluN1/GluN2D (Qian et al., 2005; Qian and Johnson, 2006) and GluN1/GluN2C (Dravid et al., 2008) are suggested to be similar, but less intense studied than the functional impact of GluN1/GluN2A or B at the synapse (Paoletti et al., 2013).

After cortical stab wound injury, GluN1 expression was increased at the lesion site and cKO animals showed hereby significantly reduced expression levels, verifying the protein degradation of astroglial NMDARs and upregualtion in case of CNS injury. We concluded that under pathological conditions NMDAR expression is increased in astrocytes to such an extent that is was possible to detect minor differences in cKO animals.

Conditional ablation of the GluN1 subunit in oligodendrocytes is condsiered to contribute to axonal energy metabolism. Stimulation of NMDARs on oligodendrocytes caused glucose transporter 1 (GLUT1) trafficking to the cell surface, which was followed by enhanced glucose uptake. They suggested that fast spiking axons activate oligodendroglial glutamate receptors to match GLUT1 incoorporation into myelin and metabolic support to the levels of neuronal activity. They supported this model by monitoring optic nerve conduction under oxygen-glucose deprivation. The subsequent recovery of function following oxygen-glucose reperfusion is severely reduced in GluN1 mutant nerves. In contrast, functional recovery is identical to controls when reperfusion is with oxygen-lactate (Saab et. al, 2015, unpublished).

The increase of astroglial NMDARs under pathological conditions might likewise serve a neuroprotective role. The metabolic coupling of neurons and astrocytes is known as the lactate shuttle. During signaling, glutamate is taken up by astrocytes, a process operated by GLAST and GLT1, which use the electrochemical gradient of Na^+ as the driving force. Glutamate is cotransported with Na^+, which results in an increase in the intracellular concentration of Na^+ and the activation of the Na^+-K^+ ATPase, which then triggers aerobic glycolysis. Glutamate is ATP dependent converted to glutamine by glutamine synthase. Lactate, produced by the glutamate-stimulated glycolysis is released from astrocytes and can be taken up by neurons as an energy source (Magistretti, 2006, 2009; Pellerin et al., 2007). We speculate that under physiological conditions "Na^+ signaling" is efficient to regulate operations and metabolic needs of astrocytes and neurons. Under pathological condition neurons tend to downregulate NMDAR expression, since excessive activation leads to Ca^{2+} influx and cell death. Astroglial NMDARs might be upregulated to directly sense the increased amount of glutmate. The additional Ca^{2+} entry through NMDARs might regulate compensatory mechanisms as suggested by Saab et al., 2015, like increase of glucose transporters or glutamine synthetase to adapt processes to maintain physiological conditions.

Furthermore, it was shown that anesthesia rapidly and selectively impaired astrocytic Ca^{2+} signaling in awake animals. Among the drugs tested was ketamine which acts preferentialy on NR2D/C containing NMDARs, suggested to be expressed on astrocytes. This effect also occured if synaptic activity is blocked, suggesting a direct effect on astrocytes of the

anesthestic drug. It was also shown that IP_3 receptor deletion completely suppressed astrocytic signaling. A significant proportion of the anesthetic effect on astrocytes must therefore be mediated by internal release of Ca^{2+} (Thrane et al., 2012). However, there is evidence of a subtype specific regulation of NMDARs by G-protein coupled receptors (GPCRs) (Yang et al., 2014). There might be a feedback loop of blocked NMDARs to GPCRs, responsibel for Ca^{2+} release in astrocytes. However, it would be from great interest to image the Ca^{2+} signals in GluN1 cKO animals.

6.8 $P2Y_1$ receptors on astrocytes

We investigated the function of purinergic astroglial $P2Y_1$Rs in the brain by generating conditional knockout mice, where the receptor could be ablated in a timely controlled manner. Successful DNA recombination for the floxed *p2yr1* gene was determined; likewise $P2Y_1$R mRNA was reduced in homogenates of cerebellum, cortex, hippocampus and brainstem in $P2Y_1$R cKO animals. Reduction in $P2Y_1$R mRNA expression in cerebellum and cortex could be further verified by FACS experiments. High CT values in qRT-PCR experiments, compared to CT values of other receptors, indicated low levels of the $P2Y_1$R mRNA in the brain. To prove reduced levels of protein specifically on astrocytes after tamoxifen application failed since tested antibodies were not useful (see 6.8.1). The functional role of astroglial $P2Y_1$Rs was studied in more detail in Bergmann glial cells in the cerebellum (see 6.8.2).

However, to access recombination kinetics at the mRNA level, half of the cerebellum, the cortex, brainstem and hippocampus were homogenized. Recombination resulted in a maximal reduction to 75 (± 1) % in the brainstem, to 39 (± 4) % in the cerebellum, to 57 (± 4) % in the cortex and to 64 (± 5) % in the hippocampus remaining $P2Y_1$R mRNA expression. Apart from astrocytes also other cell types express the $P2Y_1$ subtype and knowing that maximal recombination is reached 21 d after first expression (see 6.1 and (Saab et al., 2012), the remaining gene expression should originate from other neural cell types (neurons, oligodendrocytes, microglia). The exact extent, how many cell types per brain regions express this subtype, is not easy to state. It exists a diversity of pharmacological studies per brain region and cell type *in vitro*, *in situ* and *in vivo*. In contrast, probably also due to the lack of reliable and specifc antibodies, (see 6.8.1) rather a low number of immunohistochemical studies clarify the localization of the receptor.

However, the quantified percentage of astroglial gene expression of the receptor is high. Together with DNA recombination data we can conclude that in the brainstem 20 % of all cells (astrocytes) express 25 % of the $P2Y_1$R mRNA, likewise in the cerebellum 8% of all cells express 61 %, in the cortex 22 % of all cells express 43 % and in the hippocampus 30 % astrocytes/ radial/ newly born granule cells express 36 % of the total $P2Y_1$ mRNA. These results further support the outstanding role of astroglial $P2Y_1$Rs in the brain of mice.

A recent study investigated the mRNA profile of FACS sorted and isolated cortical cell types (Zhang et al., 2014). Here neurons and oligodendrocyte precursor cells, OPCs, are the two main cell types, expressing the *p2ry1* gene followed by astrocytes. Other cell types can be neglected.

In the hippocampus, $P2Y_1Rs$ are expressed by neurons and astrocytes, although not homogeneously. In the area CA1, they are present in astrocytes of the stratum radiatum, pyramidal neurons and GABAergic interneurons (Bowser and Khakh, 2004; Guzman et al., 2010; Kawamura et al., 2004; Morán-Jiménez and Matute, 2000), whereas it was reported that in the dentate gyrus $P2Y_1Rs$ are mostly expressed in astrocytes (Domercq et al., 2006). At least in the molecular layer of the dentate gyrus immunohistochemical stainings showed $P2Y_1R$ positive granule cells. In the brainstem e. g. modulation of preBötzinger complex inspiratory rhythm by ATP is $P2Y_1$ receptor dependent (Zwicker et al., 2011) and involved both neurons (Lorier et al., 2008) and astrocytes (Huxtable et al., 2010). The cellular distribution of $P2Y_1Rs$ in the cerebellum is discussed in 6.8.2.

Furthermore, the knockout of one of eight closely related receptor subtypes always bails the risk of compensatory mechanism of other subytypes in the living organism. Next to $P2Y_1R$ also $P2Y_2R$, $P2Y_4R$, $P2Y_6R$, $P2Y_{12}$ and $P2Y_{14}$ are reported to be expressed in astrocytes. P2YR subtypes, such as $P2Y_2R$, $P2Y_4R$, $P2Y_6R$, are activated most likely by UTP and $P2Y_{14}$ by UDP-glucose. In physiological context $P2Y_{12}$ would be most likely upregulated, since ADP is also the most potent agonist. But this receptor is known to couple to Gi/o, leading to inhibition of the adenlyate cyclase. The main pathway upon $P2Y_1R$ is mediated by Gq/G_{11} coupling and PLC activation (Fields and Burnstock, 2006; Franke et al., 2012). In any case this question should be kept in mind and addressed in the future.

However, albeit the fact that one important pathway for IP_3 mediated Ca^{2+} release in astrocytes was prevented, $P2Y_1R$ cKO mice showed at the first glance no apparent morphological or physiological abnormalities, and display normal development, survival, and reproduction compared to littermate controls. This accounts likewise for total $P2Y_1$ knockout animals, which were predominatly generated for the investigation of platelet function (Fabre et al., 1999; Leon et al., 1999). Interestingly, functional aspects, using $P2Y_1$ knockouts in every cell type for studies in the brain, were often reduced to the lack of receptor function in astrocytes (Chin et al., 2013; Noguchi et al., 2013; Pascual et al., 2012; Shinozaki et al., 2014)

In summary, we own a highly useful tool to investigate the function of astroglial $P2Y_1Rs$, which have been suggested to play an important role throughout the brain. It can help e. g. to reveal the role in purinergic modulation of pre-Bötzinger complex activity in the brainstem, in the immune response in cortical layers after injury, in memory function in the hippocampus, in the modulation of neural circuits in the cerebellum or migration and neuronal differention in the developing brain or adult neurogenesis. Furthermore, the GLAST-CreERT2 system was highly efficient to recombine radial glia cells and progenitor cells. The purinergic neuron-glia interactions in sensory system, like the retina and olfactory bulb, were also defined to involve $P2Y_1Rs$ (Lohr et al., 2014).

6.8.1 $P2Y_1$ receptor antibodies lack specificity

We chose to test three commercially available antibodies, first the intracellular binding antibody (APR-009) and later also the extracellular binding antibody (APR-021) from Alomone, Israel based on publications referring without any further specification to the company Alomone. In addition, we tested the antibody against an intracellular epitop from Abcam (ab85896). All are polyclonal from immunized rabbits.

Selectivity of an antibody is likely if its staining disappears in immunohistochemical studies or Western blots of tissues from animals genetically engineered to lack that receptor. Based on the more or less specific staining pattern in tissue of APR-009 in brain slices, containing no $P2Y_1R$, we concluded that the antibody did not identify another cellular antigen. However, in Western blots the antibody bound similar proteins in both, wild type and $P2Y_1R$ total knockout tissue. Furthermore, Western blots of conditional and control animals failed as well. Recognized bands looked similar in both genotypes.

Likewise the antibody from Abcam showed a similar band pattern in total $P2Y_1$ KO (tKO) brain homogenates, albeit the receptor-like staining in wild type mice. Herewith, attempts to correlate any of the bands to the actual $P2Y_1R$ protein failed. The predicted molecular weight is ~42 kDa for the $P2Y_1R$. Published Western blots claimed from ~40 kDa (Siow et al., 2010) over ~60 (Pinheiro et al., 2013) up to high molecular weights of ~200 kDa (Suadicani et al., 2003) specific for the $P2Y_1R$ by use of the same antibody. To validate the specificity of APR-021 antibody by performing the same assays on brains from $P2Y_1R$ tKO mice, remain to be done. Immunohistochemical stainings looked most promising.

Taken together, tested antibodies might recognize (among other subtypes?) the right receptor in fixed brain slices. Thereby it can be questioned if the antibodies are sensitive enough to detect minor differences in conditional knockouts. But clearly, none of the two tested antibodies (APR-009 and ab85896) can be considered to be specific on immunoblots. It is possible that the antibodies do not recognize the denaturated epitope of the receptor. Therefore non-denaturated gels might lead to better results.

Finally, it seems to be a systemic difficulty in creating antibodies for this important class of signaling proteins. The lack of selectivity of GPCR antibodies, appeared to be the rule rather than the exception (Michel et al., 2009; Yu and Hill, 2013), and antibody based data need to be rigorous controls as described in (Seifert et al., 2013).

6.8.2 Function of glial $P2Y_1$- and AMPA receptors in the cerebellum

Local molecular layer stimulation elicited large and slowly decaying currents in patched Bergmann glia cells (BG). These currents were associated with transient increases in Ca^{2+} that were composed of a small-amplitude, relatively fast rising increase, followed by a slower rising, larger-amplitude phase. Due to pharmacological approaches Bergmann glia Ca^{2+} transients were separated into a first AMPA- dependent (blue) and a second P2Y (red) receptor dependent phase (see Figure 6. 2 A) (Piet and Jahr, 2007). Ca^{2+} signals in BGs were IP_3 dependent and highest potency to liberate Ca^{2+} from internal stores was determined to be ADP (Beierlein and Regehr, 2006; Kirischuk et al., 1995), thus $P2Y_1$ receptors were suggested as the main effector subtype in BG.

We already investigated Bergmann glial AMPA receptors (AMPARs) in the cerebellum. BG AMPARs are essential to optimize synaptic integration and cerebellar output function throughout life (Saab et al., 2012). Using conditional gene inactivation, via GLAST-CreERT2/loxP system, we found that the majority of cerebellar Ca^{2+}-permeable GluA1/A4-type AMPA recepotors, are expressed in a high density in BG in the cerebellum. The intracellular change of $[Ca^{2+}]$, induced by AMPA receptors is hereby relatively small. The Ca^{2+} rise via internal stores by $P2Y(_1)R$ activation was significantly higher (compare red and blue colored area in Figure 6. 2 A), but $P2Y_1R$ expression levels seemed low (see 5.6). We

determined therefore mRNA expression levels of the AMPA receptor subunits GluA1 and GluA4 and of the $P2Y_1$ receptor in homogenates of wild type cerebelli by qRT-PCR (Figure 6. 2 B). The GluA1 and GluA4 subunits were 53 (± 3) and 18 (± 1) fold higher expressed, respectively, as the $P2Y_1R$, supporting the impression of low expression levels in the membrane determined by $P2Y_1R$ staining in ML of the cerebellum.

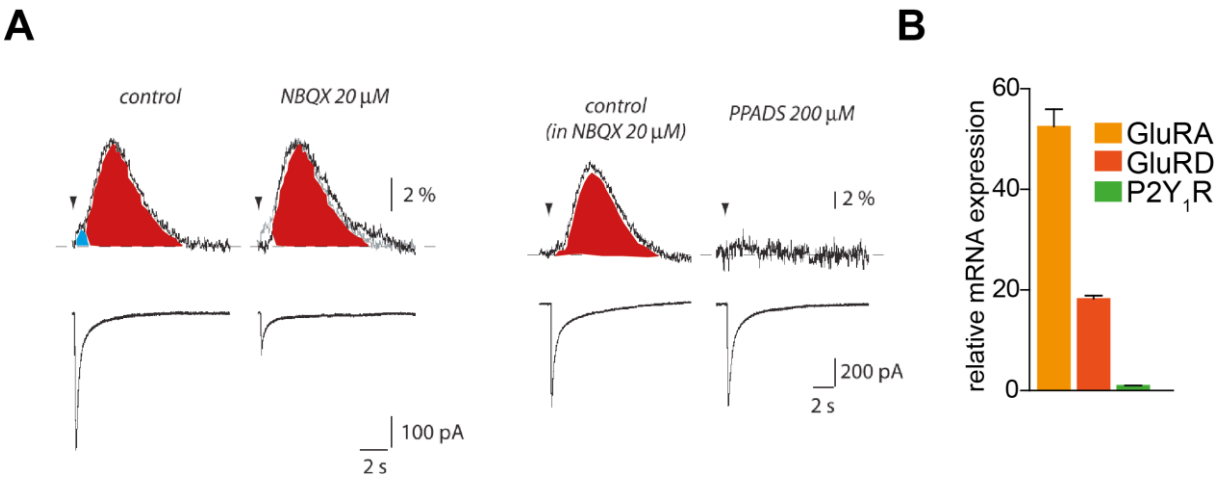

Figure 6. 2. Ca^{2+} transients in BG and expression profile of AMPA and $P2Y_1$ receptors

A: Modified after Piet and Jahr, 2007. Bath application of 20 µM NBQX inhibited the current and the first phase of the Ca^{2+} transient (blue colored) evoked in a BG by local ML stimulation. PPADS (200 µM) blocked the second Ca^{2+} transient (red colored) recorded in the presence of NBQX. **B:** Depicted are mRNA expression levels of GluA1, GluA4 and $P2Y_1R$ relative to $P2Y_1R$.

Furthermore, since Bergmann glial cells just account for about 8 % of the total cells in the cerebellum the determined percentage of 61 % of astroglial $P2Y_1R$ mRNA expression in cerebellar homogenates is extremely high. The remaining expression should originate from granule cells and Purkinje cells (Morán-Jiménez and Matute, 2000; Santiago and Scemes, 2012). Furthermore, other cell types in the white matter or in the deep nuclei of the cerebellum could contribute to gene expression levels. Our findinds suggest that BGs are the predominant cell type in the cerebellum, expressing the $P2Y_1$ subtype at the mRNA level.

In addition, we showed that astroglial $P2Y_1R$ expression is not restricted to young ages (<P 7) as suggested by immunohistological staining, using likewise an antibody from Alomone (Amadio et al., 2007). We demonstrated successful $P2Y_1R$ mRNA reduction in cerebelli of cKO mice, injected with P 10 and likewise with P 28 (see above). If BGs do not express $P2Y_1Rs$ after P 7, the contribution of astroglial mRNA expression should be reduced.

Furthermore, the developmental regulation of the ATP-mediated Ca^{2+} signaling was studied in (Kirischuk et al., 1995). They used Bergmann glial cells, obtained from mice of three age groups (P 6, P 16-20 and P 40-45). There was no significant difference with respect to the amplitude and shape of ATP-induced $[Ca^{2+}]_{intra}$ transients.

In addition, Ramona Rudolph could show in her PhD thesis that $P2Y_1$- and AMPA receptors in BG modulate spontaneous inhibitory postsynaptic currents (sIPSC) at the interneuron-Purkinje cell synapse in 4 weeks old animals. It was further shown that hereby rather activation of BG $P2Y_1Rs$ led to Ca^{2+} dependant release of glutamate which binds to NMDA receptors on interneurons, enhancing GABA release which leaded to the measured

enhancement of Purnkinje cell sIPSC frequency (unpublished data from collaborating laboratory, Kaiserslautern, Joachim Deitmer).

We showed that loss of BG AMPARs lead to process retraction of BG processes, leading to an increased amplitude, half-width and decay time of parallel fiber (PF)-evoked PC currents (PF-EPSCs) in dKO mice, probably due to an impaired clearance of synaptically released glutamate. Furthermore, miniature EPSC frequency was decreased in PCs of dKO mice which could be explained by decreased synapse density in the ML in dKO mice. We concluded that during cerebellar development PF-PC synapse formation is, at least partially, regulated by BG AMPAR signaling. We tested if we see a similar or even more pronounced phenotype in the developing cerebellum of $P2Y_1R$ cKO mice, in which the actual higher Ca^{2+} entry should be diminished. We showed that loss of Bergmann glial $P2Y_1Rs$ signaling at young ages did not reduce glial coverage of Purkinje cell synapses or altered synapse density in the cerebellar cortex. These results demonstrated that BG $P2Y_1Rs$ and AMPAR receptors have different not overlapping functions at the PF-PC cell synapse. In contrast, Ramona Rudolph showed that $P2Y_1$- and AMPA receptors interact to convey signals between two synapses, the interneuron and the Purkinje cell (unpublished data).

6.8.3 Knock-in mouse expressing fluorescent $P2Y_1$ receptors in astrocytes

G-protein coupled receptors (GPCRs), like $P2Y_1Rs$, regulate a wide variety of cellular functions by converting extracellular signals into intracellular signals via the production of second messengers, i.e. cAMP and Ca^{2+}. GPCRs are notoriously difficult to study, because they are expressed in nearly every cell type; many respond to the same ligand, and some activate the same G protein, while others stimulate multiple G proteins. To overcome these limitations and to visualize the respective receptor, researchers worked successfully already with GPCR-GFP chimeras in the cell culture system (Kallal and Benovic, 2000).

In addition, BAC transgenic mice were designed; expressing fluorescent protein, driven by the promoter of respective GPCRs. The fluorescent protein is expressed in appropriate cells, but the precise subcellular localization and function of the receptor cannot be examined. To closer resemble physiological conditions in knock-in animals, in which a fluorescent protein is introduced at the locus of interest by homologous recombination, were made. Furthermore, the consequence of homozygous animals is the absence of the functional GPCR and equivalent to a knock-out phenotype. Therefore, GPCR-FP fusion proteins were considered for the knock-in strategy for functional studies *in vivo*. Constructs were first tested in cell culture experiments with either appropriate behavior of recombined proteins or deleterious effects like defective targeting to the cell surface or overexpression. Cell lines used for heterologous expression may provide a different intracellular machinery for complex protein folding or post-translational modifications compared to naturally producing cells.

As a consequence knock-in mouse models were designed. Despite the concerns about the *in vivo* use of GPCR-FP fusion proteins, developed mouse lines proved to be useful in many aspects and helped to study receptor neuroanatomy throughout the nervous system, real-time receptor trafficking in live cells, and receptor movements *in vivo*. They gave new insights of GPCR function under physiological conditions (Masotte and Ceredig, 2015). The best characterized GPCR-FP knock-in model is a mouse where the enhanced GFP (EGFP) is knocked into δ-opioid receptor gene (*Oprd1*) and produced mice, expressing a functional

DOR-EGFP C-terminal fusion in place of the native DOR (Bardoni et al., 2014; Erbs et al., 2012; Faget et al., 2012; Pradhan et al., 2009; Scherrer et al., 2009; Scherrer et al., 2006).

The same research group recently generated a second knock-in mouse where the μ-opiod receptor (MOR) is fused with red fluorescent protein mCherry. The mCherry cDNA was introduced into exon 4 of the MOR gene in frame and 5' from the stop codon (Erbs et al., 2014). In both mouse lines, expression pattern and receptor properties, like agonist binding are more or less comparable to the native forms. Actually, the first generated GPCR-FP knock-in mice produced the fluorescent human rhodopsin. Here, expression was five fold-reduced from the transgenic locus and led to retinal degeneration.

However, the comparison of the different homozygous mouse lines enabled the correlation of the decrease in human rhodopsin–EGFP expression to the increased rate of retinal degeneration, providing a model of human diseases (Chan et al., 2004). The generation of a conditional and inducible mouse line which expresses a $P2Y_1R$-EGFP fusion instead of the native form upon TAM inj., specifically in astrocytes is not reported yet (see Figure 6. 3).

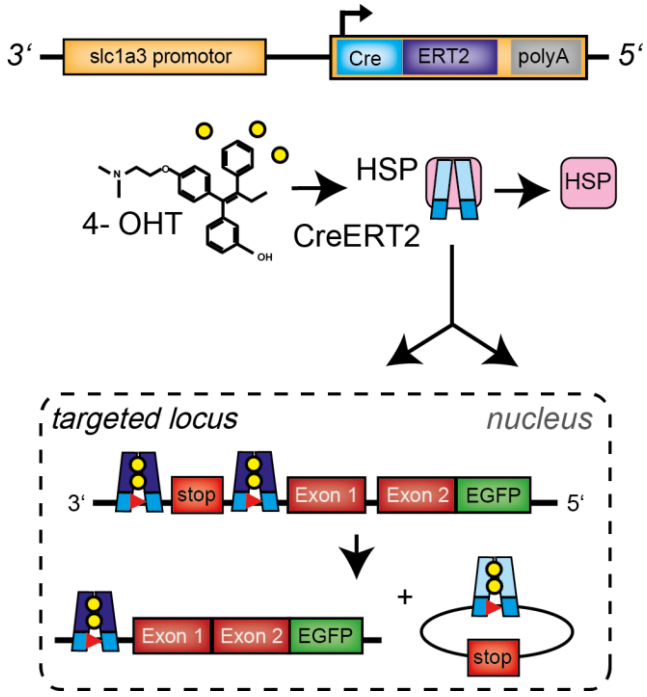

Figure 6. 3. Knock-in mouse expressing fluorescent $P2Y_1$ receptors in astrocytes

At top the genetic modified gene section of the mouse line used for inducible depletion of floxed target sequences in astrocytes is illustrated. After expression, controlled by the astrocyte-specific GLAST promotor, CreERT2 remains bound to the heat shock protein (HSP90) in the cytosol. After binding of 4-hydroxytamoxifen (4-OHT), the complex is released and CreERT2 is transported to the nucleus. Two molecules bind to each loxP site (red arrow heads) and the stop codon is excised. After DNA recombination the GPCR-EGFP fusion protein is specifally expressed in astrocytes.

The direct visualization of astroglial $P2Y_1R$ to decipher the functional role in neuronal networks and to understand the complex relation between behavior and receptor subcellular distribution and signaling would mean a big success towards the molecular understanding of the tripartite synapse. A chimeric rat GFP-tagged $P2Y_1R$ was tested in HEK cells and validated to be fully active and to show regular signal transduction coupling (Vöhringer et al., 2000).

7 Materials and Methods

All buffers and aqueous solutions were prepared with deionized water ($_dH_2O$) from the water facility TKA GenPure (Thermo Scientific TKA). All stated concentrations are final concentrations. Any materials and buffers needed for a particular method are stated in the method section directly. The same applies for any special devices and the respective statistical analysis.

7.1 Manipulation, breeding and genotyping of mice

7.1.1 Genetically modified mice and administration

For the administration of mice the database Pyrat (Python based Relational Animal Tracking) from Scionics Computer Innovation GmbH was used. In this database all relevant information like mouse number (=earmark), date of birth, sex, pedigree, genotype and breeding behavior are saved. Used mouse lines are listed below (Table 2).

Table 2 Mouse lines

Genetic modification	Reference	Provided by
TgH (GLAST-Cre^{ERT2})$_{GLAC}$	(Mori et al., 2006)	Magdalena Götz, München
TgH(CNP^{Cre})$_{CNCE}$	(Lappe-Siefke et al., 2003)	Klaus Armin Nave, Göttingen
TgH (P2Y1$^{fl/fl}$)$_{P2Y1fl}$	(Leon et al., 1999)	Christian Gachet, Straßburg
TgH (GABA$_{B1}$$^{fl/fl}$)$_{GABA}$	(Haller et al., 2004)	Christian Steinhäuser, Bonn
TgH (GluN1$^{fl/fl}$)$_{NRFL}$	(Tsien et al., 1996b)	Jackson Laboratory, Bar Habor, USA
TgH(GluN1$^{fl/fl}$)$_{NRFL2}$	(Bannerman et al., 2012)	Rolf Sprengel, Heidelberg
TgH (GluA1$^{fl/fl}$)$_{GLRA}$	(Fuchs et al., 2007)	Daniel Zamanillo, Rolf Sprengel, Heidelberg
TgH(GluA4$^{fl/fl}$)$_{GLRD}$	(Zamanillo et al., 1999)	Elke Fuchs, Hannah Monyer, Heidelberg
TgH(tdTomato)$_{RATO}$	(Madisen et al., 2010)	Hongkui Zeng, Seattle, USA
Tgh (Ubi Cre)$_{CMV}$	(Schwenk et al., 1995)	Rolf Sprengel, Heidelberg
TgN(hGFAP-EGFP)$_{GFEA/GFEC}$	(Nolte et al., 2001)	Frank Kirchoff, Homburg

7.1.2 Tail biopsy

Tail biopsies of mice were taken at three weeks of age. The obtained DNA was used for routine genotyping of transgenic mice through PCR (7.1.4). Per mouse one piece of tail tissue (~ 0.5 cm) was removed and stored at -20 °C till digestion.

7.1.3 Preparation of genomic DNA from mouse tail tissue

Tail digestion for DNA extraction and subsequent PCR reactions (7.3) were performed with the Extract-N-Amp^{TM} Tissue PCR kit from Sigma-Aldrich. Extraction solution and tissue preparation solution were pre-mixed in a ratio of 4:1. The tails were placed in collection microtubes (Qiagen) and 63.5 µl of the mixture was added to each tail. Through centrifugation it was ensured that the tails were in solution. After incubation for 10 min at room temperature (RT) the collection microtubes were placed for 10 min in another heat block preheated to 95 °C. Following cooling down to room temperature (RT) 50 µl of neutralization buffer was given to the samples. With this method the tissue was not

completely digested. After centrifugation the extracts were transferred to new collection microtubes and used for PCR reactions. Tissue left over was stored by -20 °C.

7.1.4 Polymerase chain reaction and genotyping of mice

The isolated DNA from tail tissue of the experimental animals was used for genotyping PCR. The reaction consists of a cyclic repetition of the following steps: **At 95 °C** the DNA strands are separated. **At 50 - 60 °C** the binding of the primers on the DNA strands takes place (annealing). The exact temperature in this phase is based on the sequence dependent melting temperature of the primers. **At 72 °C** the synthesis of the complementary DNA strand is accomplished by Red Taq DNA polymerase (Sigma-Aldrich) which fills up the missing nucleotides starting from the 3' end of the primer in 5' - 3' direction. The required time is dependent the length of the DNA fragment that has to be amplified. The reactions took place in a volume of 20 µl (see Table 3) and were performed in 96-well-PCR-reaction-tubes in a peqSTAR Thermo Cycler (peqlab).

Table 3 Standard PCR setup

Component	µl
$_{d}$H20	6.0 respectively 5.0 or 4.0 if Primer 3/4 are needed
DNA	2.0
Primer 1 (10 pM)	1.0
Primer 2 (10 pM)	1.0
Primer 3 (not mandatory)	1.0
Primer 4 (not mandatory)	1.0
Mastermix (Sigma-Aldrich)	10.0

In experiments using the **GLAST-CreERT2** driver line, animals termed conditional knockouts (cKO) were heterozygous for the GLAST locus and for the CreERT2 construct ($GLAST^{CreERT2/+}$), respectively, to maintain physiological function of the transporter. Animals homozygous for GLAST allele were thus negative for the CreERT2 construct and used as controls ($GLAST^{+/+}$). Both groups were injected with tamoxifen. Oil controls were excluded since in we determined no significant differences between them in Saab et al., 2012. Likewise for experiments using the **CNP-Cre** driver line, animals heterozygous for the CNP locus $CNP^{Cre/+}$ were considered as knockout animals (KO), animals homozygous for this locus as controls $CNP^{+/+}$.

These Cre driver lines were crossbred to mice carrying different floxed receptor genes and/or the floxed reporter gene for tdTomato. Primers flank one of the two LoxP sites and allowed the distinction of floxed or wild type alleles (see Table 4 for further information). Knockout and control animals were usually homozygously floxed for one or more receptor genes or/and the reporter gene ($^{fl/fl}$). For immunochemical recombination studies animal were heterozygous for the floxed reporter locus. In case of **FACS experiments** control and cKO animals were positive for the CreERT2 transgene ($GLAST^{CreERT2/+}$), heterozygous for the floxed reporter gene tdTomato ($stop^{flwt}$tdTomato) and control animals were heterozygously floxed the respective receptor gene or not floxed.

Table 4 Genotyping primer and respective amplicon size of PCR products

Name	Sequence	Product size [bp]
11984 GLAST fwd	5' -GAGGCACTTGGCTAGGCTCTGAGGA- 3'	KI: 400 bp, wt: 700 bp
11985 GLAST rev	5' -GAGGAGATCCTGACCGATCAGTTGG- 3'	
11986 Cre^{ERT2} rev	5' -GGTGTACGGTCAGTAAATTGGACAT- 3'	
1955 CNP	5' -CATAGCCTGAAGAACGAGA- 3'	KI: 357 bp, wt: 643 bp
7315 CNP	5 '-CCCAGCCCTTTTATTACCAC- 3'	
2016 CNP	5' -GCCTTCAAACTGTCCATCTC- 3'	
4192 Ubi Cre fwd	5'- GCTGGAGCCCGTGCAGTTCCTCAG- 3'	KI: 339 bp
4193 Ubi Cre rev	5' -CCGGGGGCTGCCATCTTCCAGC- 3'	
23982 p2ry1 LoxP fwd	5' -CCTGCGCGTCCTGTTGTGTAAC-3'	loxP: 304 bp, wt: 228 bp
23983 p2ry1 LoxP rev	5'- CAGCAGCGGCGAGAGACTCAGC- 3'	
24233 grin1 ^{NRFL} LoxP fwd	5 '-CTGTCAGTTCAAGGCCAGCAT- 3'	loxP: 350 bp, wt: 300 bp
24234 grin1 ^{NRFL} LoxP rev	5' -GTGCTGGGATCCACATTCATG- 3'	
24392 gabbr1 fwd	5' -GCTCTTCACCTTTCAACCCAGCCTCAGGCAGGC-3'	loxP: 742 bp, wt: 526 bp
24393 gabbr1 rev	5' -CCTCTGCCTTCCTCCACATGTTTCTCCT-3'	
32881 grin1^{NRFL2} LoxP fwd	5' -CTCAAGTGAGTCTGCCCCATGCTG – 3'	loxP: 369 bp, wt: 315 bp
32883 grin1 ^{NRFL2} LoxP rev	5' -CACAGGGGAGGCAACACTGTGGAC- 3'	
Sigma grin1 ^{NRFL} LoxP fwd	5'-GGCCCCGGCTAGTTCTTATC-3'	wt: 1200 bp
Sigma grin1 ^{NRFL} LoxP rev	5'-GGCTTAACCTCACCTTCCCC-3'	
Sigma grin1 ^{NRFL2} LoxP fwd	5'-GCTTTGGAAAGGACACAGCC-3'	Gain PCR : 419 bp
32847 grin1 ^{NRFL2} LoxP rev	5'-AGGCTGTTGTACCACACCAT-3'	
27488 WT tdTomato rev	5' -AAGGGAGCTGCAGTGGAGTA- 3'	loxP: 196 bp, wt: 297 bp
27489 WT tdTomato fwd	5 '-CCGAAAATCTGTGGGAAGTC- 3'	
27490 tdTomato rev	5 '-GGCATTAAAGCAGCGTATCC- 3'	
27491 tdTomato fwd	5' -CTGTTCCTGTACGGCATGG- 3'	

7.1.5 Agarose gel electrophoresis for the separation of DNA fragments

PCR products ranging from 200 to 700 bp of size were separated in 1.5 - 3.0 % (w/v) agarose gels. The desired amount of agarose was dissolved in 1xTAE buffer by heating in a microwave. After cooling ethidiumbromide diluted 1:5000 was added and the warm agarose was slowly poured into a gel tank in which combs were inserted. Following polymerization the combs were lifted gently and DNA marker (Easy ladder 100 bp, Bioline) and DNA samples were loaded into the well. The gel was run at 180 V in 1x TAE until desired separation was achieved. For documentation, snapshots of UV-transilluminated gels were taken with the Quantum gel documentation device from peqlab. Gel chambers, combs und sleighs were produced at the workshop of the institute.

Tris acetate EDTA buffer (TAE, 50x, 1000 ml)

Tris	2	mM
Acetic acid	2	mM
EDTA (Ethylendiamintetraacetate, 0,5 M, pH 8)	57.1	ml

Agarose gel		
Agarose powder in TAE buffer	1.8	% (w/v)
Ethidiumbromide in 1x TAE agarose	0.015	% (v/v)

7.1.6 Treatment of mice with tamoxifen

Tamoxifen (Sigma, T5648) was dissolved in corn oil (Sigma, C8267) at concentration of 10 mg/ml, aliquoted and stored at -20 °C. Mice were intraperitoneal (IP) injected with a tamoxifen dosage of 100 mg/kg bodyweight (e.g: 20 g mice receives 200 µl tamoxifen) once a day for three consecutive days. Of note wild type mice, for the tamoxifen metabolism study (see 4.1), received just one dose of tamoxifen and samples were collected at different time points. For investigations of the gene recombination efficiencies mice were injected also five times and in an interval fashion (1^{st} x tam, 2 d pause, 2^{nd} x tam, 2 d pause and 3rd x tam). The age of mice and time point of analysis after the first injection are always indicated in the text and figures. The IP injections were done by the animal care taker Daniel Rhode and Tamara Vogelgesang.

7.1.7 Perfusion of mice

Mice were anesthetized with ketamine/xylazine (ketamine 28 mg/ml, xylazine 2 mg/ml in 0.9 % NaCl; 100 µl/20 g body weight) and fixed on a rubber plate by use of pins in paws and feet. A skin incision was made below the sternum and the musculature of the abdomen and the peritoneum were severed from caudal to cranial until reaching the sternum. Subsequently, the peritoneum was cut from medial to lateral. Ongoing, the diaphragm was cut through beneath the costal arch and the pericardium was released carefully from the thorax. This led to a pulmonary collapse. The ribs were loosened to the collarbone and the thorax was removed. In the following a vein canula (butterfly) was placed into the left ventricle and the perfusion with a peristaltic pump was started and mice were perfused with ice cold HBSS (Hank's balanced salt solution w/o Ca^{2+} or Mg^{2+}; Sigma) for 2-3 min. Simultaneously, an incision of the vena cava superior was made so that the blood could drain off. The color change of the liver indicated the successful exchange of blood to buffer.

In case of **FACS experiments,** the brain was dissected and immediately used for the further treatment (see 4.2 and 7.4).

To study the **tamoxifen metabolism**, a canula connected to a syringe was placed in the left ventricle to obtain blood (400 - 600 µl) before perfusion started. In the following the brain was immediately cut sagittal and transferred into a tube filled with 500 µl 0.9 % NaCl solution and around 20 precellys beads (peqlab). Brains were homogenized for 2x10 sec, 5500 rpm, 10 sec pause in between in the Precellys 24 (peqlab). Blood and brain samples were kept in light protected 2 ml tubes at -80 °C till further analysis (see 4.1 and 7.2)

Mice used for **immunochemical analysis** were perfused 2 - 3 min with ASCF, followed by ~15 ml of 4 % formaldehyde solution to fix the brain tissue. Brains were dissected, cut sagittally and post-fixed in the same fixative for 2 h or over night at 4 °C (see 7.6).

ACSF (artificial cerebrospinal fluid)		
NaCl	126	mM
KCl	3	mM
NaH_2PO_4	1.25	mM
$NaHCO_3$	26	mM
$MgSO_4$	2	mM
Glucose	10	mM
$CaCl_2$	2	mM
Carbogen gas		
Oxygen	95	%
Carbon dioxide	5	%
Sucrose in ACSF		
Sucrose	30	% (w/v)
4 % PFA in PB (200 ml)		
NaH_2PO_4 (20 ml)	0.2	M
Na_2HPO_4 (80 ml)	0.2	M
Paraformaldehyde (50 ml)	16	% (w/v)

Deionized H_2O was added to a final volume of 200 ml. 16 % PFA solution was freshly prepared and filtered through a paper filter.

Ketamine	Ketavet®, Pfizer, Germany
Xylazine	Rumpon®, Bayer Healthcare

7.2 HPLC-MS analysis

Homogenated brain and blood samples (see 7.1.7) were processed for high-performance liquid chromatography mass spectrometry (HPLC-MS) as followed. 250 µl of brain and serum were mixed with 25 µl of an internal standard (Risperidon 1 mg/L spikesolution) and 750 µl of zinc sulfacte ($ZnSO_4$) solution. Samples were vortexed for 2 min and stored for additional 5 min at -20 °C in an aluminium block. Subsequently samples were centrifuged at 14000 rpm. 900 µl of the supernatant were transferred to brown glas vials for the analysis. The HPLC-MS and the stated protocol were established by Andreas Helfer and Julian Michely, Research group of Prof. Hans Maurer, Department of Experimental und Clinical Toxicology, University of Saarland. They also performed the HPLC-MS experiments and analyzed row data in Excel. The results (± SD) were depicted in graphs generated by GraphPad Prism5 and processed with Adobe Illustrator CS6.

7.3 Quantitative real time PCR

7.3.1 Isolation of DNA and RNA

Genomic DNA was isolated from brainstem (half), cerebellum (half), cortex, hippocampus and the optic nerve of individual animals at 7 weeks of age using either the Invisorb Spin Tissue Mini Kit **(I)** or the Qiagen, AllPrep RNA/DNA mini kit **(II)** following the manufacturer's instructions.

Notably for **(I)**: the optic nerve was digested in 200 µl lysis buffer and binding buffer was consequently reduced to 100 µl. All other tissues were prior to 1 h digestion, homogenized in 400 µl lysis buffer in Precellys Ceramic tubes using the Precellys 24 homogenizer (Peqlab) 2x (10 s, 5500 rpm, 10 s pause in between) After short centrifugation, samples were mixed with binding buffer and processed as suggested.

Notable for **(II)**: brainstem, cerebellum, cortex and hippocampus were homogenized in 600 µl and 300 µl sucrose buffer, respectively, containing protease inhibitors (Complete tablets, Roche) in Precellys Ceramic tubes using the Precellys 24 homogenizer (10 s, 5500 rpm, 10 s pause in between). After short centrifugation, 100 µl of the homogenate was mixed with 500 µl RLT plus buffer and DNA and mRNA was isolated following the manufactures instructions.

FACS sorted cells were pelleted by centrifugation (300xg, 15 min) and then resuspended in 800 µl Trisure. RNA was isolated following the manufacturer's instructions with chloroform and isopropanol. If experiments asked for RNA and DNA, nucleic acids were isolated with the all prep RNA/DNA micro KIT from Qiagen.

Sucrose buffer

Sucrose	320	mM
Tris (pH 7.4)	10	mM
$MgCl_2$	1	mM
$NaHCO_3$	1	mM

7.3.2 Determination of DNA and RNA concentrations

For working purposes the following OD_{260} -concentration relations were used: 1 OD_{260} for dsDNA: 50 µg/µl; 1 OD_{260} for RNA: 44 µg/µl. To determine the concentration, DNA/RNA was either diluted 1:50 with ${}_dH_2O$ and pipetted into a 70 µl cuvette for measurement in a common photometer (Eppendorf) or 2 µl of the undiluted solution was directly used for measurement with the Nanodrop System from Thermo scientific. The purity of the DNA preparation was estimated by calculating the ratio of absorbance's at 260 nm and 280 nm (A_{260}/A_{280}). A ratio of 1.8 - 2.0 is desired when purifying nucleic acids. If the ratio is less than 1.7 the solution is probably contaminated by protein.

7.3.3 Precipitation of RNA

In order to obtain a specific amount of RNA in 12 µl volume for cDNA synthesis, RNA had to be precipitated in some cases. Respective to the concentration of the sample 50 ng -1 µg RNA was diluted in 50 µl ${}_dH_20$ and was well mixed with 1.3 µl Pellet paint. Next, 25 µl of 7.5 M NH_4Ac was added and vortexed. Subsequently 180 µl 100 % EtOH were given to the

samples, vortexed and inverted. After centrifugation for 15 min the supernatants were carefully discarded. The pellet was washed with 200 µl of 70 % EtOH. After centrifugation for 5 min the supernatant was carefully removed. Subsequently the pellets were dried for 10 min at room temperature and resolved in 12 µl RNase free water prior to putting the tubes 10 min on ice.

7.3.4 First strand cDNA synthesis

For the cDNA synthesis 50 ng - 1 µg of RNA and the Omniscript Kit from Qiagen were used. The reaction was performed in a final volume of 20 µl in a peqSTAR Thermocycler (peqlab). RNA in 12 µl RNase free water from the precipitation step was transferred into 96-well-PCR-plate and incubated for 5 min at 65 °C. Next, 8 µl master mix were added to the RNA template, containing Omniscript Reverse Transcriptase, dNTPs, buffer RT, rRNase inhibitor (Promega) and RNase free water. Next, the RNA template was incubated for 60 min at 37 °C with the master mix. The amplified cDNA was directly diluted 1:10 with RNase free water and stored at -20 °C. For quantitative real time PCR the cDNA solution was further diluted 1:4. The reaction took place in a volume of 19.5 µl and was performed in a peqSTAR Thermo Cycler (Peqlab). The setup of a single PCR reaction and the temperature program are stated in Table 5.

Table 5 Setup for reverse transcriptase PCR

Component	µl
RNA	12
dt-mix Primer (0.6 pol/µl)	1
N9 Primer (120 pmol/µl)	1
Incubation at 70 °C for 2 min, afterwards on ice	
10 x RT buffer	2.0
DTT (0.1 M)	1.0
dNTPs (5 mM each)	0.5
RNase Inhibitor [10 U/µl]	1.0
Omniscript (200 U/µl)	1.0
Incubation at 37 °C for 60 min	

7.3.5 Primer design for quantitative real time PCR

Primers were designed using the NCBI primer blast software or the Universal Probe Library Assay Design Center from Roche. Primer pairs with the least probabilities of amplifying nonspecific products as predicted by the software were selected. Primers for qRT-PCR for mRNA expression were designed to amplify products that span exon–exon junctions to avoid amplification of genomic DNA at the mRNA level. Primers for qRT-PCR for DNA recombination laid in most cases in “transgenic” sequences or were designed to span exon-intron stretches to avoid amplification of RNA sequences. All primers were tested for their specificity by analyzing their dissociation curve and examining the PCR product by agarose gel electrophoresis. If necessary PCR efficiency of a primer pair were determined (7.3.8). Primers that passed the quality check were used for PCR reactions.

7.3.6 Real time quantitative PCR for genomic recombination

Real time quantitative PCR for genomic recombination was performed to enable the relative quantification of the loss of floxed intact alleles after tamoxifen application **(loss)** in various brain regions and to quantify the relative increase of recombined alleles after tamoxifen injection **(gain)** in cortex and cerebellum.

In the first approach primers were located closely upstream and downstream of the 5' LoxP site (*grin1* Tsien, *p2ry1*, *gabbr1*, *stop tdTomato* and 3' prime loxP site (*grin1* Sprengel). Only non-recombined alleles would be amplified whereas after successful recombination the anti-sense primer could not anneal to its complementary strand impeding the PCR amplification (see 4.3). Here, values (△CT) of cKO animals were normalized to values of control animals. In the second approach primers flank the 3' and 5' LoxP sites. Only after successful recombination PCR products can be amplified. Without activation of the Cre recombinase the floxed locus remains unaltered and the DNA polymerase is prevented from synthesizing a much longer PCR product (see 4.2). Here, only cKO animals were considered and △CT values were normalized to the mean △CT values of animals that received 5x tamoxifen.

For quantification of the PCR products, the fluorescent dye EvaGreen (Axon) was used. Primers for qRT-PCR for DNA recombination and respective sequences are listed in Table 6. The setup of a single reaction and the temperature program are given in Table 7 and Table 8. DNA Samples (20 ng/µl) were pipetted into 96 well plates (Axon) and the reactions were performed in the CFX96 Real-Time PCR Detection System (BioRad). All reactions were carried out in triplicates.

Neuregulin 1 type III (*NrgIII*) and β-actin (*bact*) were used as endogenous gene controls. Data normalization and analysis were performed with the qbase+ real time PCR data analysis software (Biogazelle) based on the $\Delta\Delta C_T$-method. Statistical analyses were conducted through GraphPad Prism 5. Inter-group comparisons were done by two-tailed Student *t* test after testing that a normal distribution is given. The levels of significance were set as * $P < 0.05$; ** $P < 0.01$; *** $P < 0.001$. Data are represented as means ± SEM of natural replicates (mice).

Table 6 Primers qRT-PCR for DNA recombination

Name		Sequence	Product size [bp]	name
4767	Neuregulin fwd	5'-GTGTGCGGAGAAGGAGAAAACT-3'	120	endogene
4805	Neuregulin rev	5'-AGGCACAGAGAGGAATTCATTTCTTA-3'		
29472	β-actin fwd	5'-CTGCTCTTTCCCAGACGAGG-3'	137	endogene
29473	β-actin rev	5'-AAGGCCACTTATCACCAGCC-3'		
15160	grin1$^{fl/fl}$ fwd	5'-GTCAAGCTTAGGATCCGGAACCC-3'	184	loss Tsien
15161	grin1$^{fl/fl}$ rev	5'-GACCTTCGGAAGAGCAGTTGG-3'		
32844	grin1$^{fl/fl}$ fwd	5'-AAGAGCCTCCCACAAAGTTGAGA-3'	168	loss Sprengel
Sigma	grin1$^{fl/fl}$ rev	5'-GGCTGTTGTACCACACCATAC-3'		
23518 3	gabbr1$^{fl/fl}$ fwd	5'-CAGTCGACAAGCTTAGTGGATCC -3'	82	loss
235193	gabbr1$^{fl/fl}$ rev	5'-TCCTCGACTGCAGAATTCCTG -3'		
23996	p2yr1$^{fl/fl}$ fwd	5'-CTTAGATCGGTCGCAGCTCC-3'	129	loss
23997	p2yr1$^{fl/fl}$ rev	5'-GCGCTTTTGTCGCGTTAATTA-3'		

32844	grin1$^{fl/fl}$ fwd	5'-AAGAGCCTCCCACAAAGTTGAGA-3'	168	loss
Sigma 90	grin1$^{fl/fl}$ rev	5'-GGCTGTTGTACCACACCATAC-3'		
Sigma	tdTomato$^{fl/fl}$ fwd	5'-ATCATGTCTGGATCCCCATC-3'	218	loss
Sigma	tdTomato$^{fl/fl}$ rev	5'-CGTGGCCGTTCATGGAGCCC-3'		
23996	p2yr1$^{fl/fl}$ fwd	5'-CTTAGATCGGTCGCAGCTCC-3'	202	gain
23997	p2yr1$^{fl/fl}$ rev	5'-TGGCCAGTTTTCTTGGAGACA-3'		
10466	gria1$^{fl/fl}$ fwd	5'-GTTCAGACAGGGACCCTCTCA-3'	129	gain
10467	gria1$^{fl/fl}$ rev	5'-GCCTGCCTGGGTAAAGTGACT-3'		

Table 7 Setup for qRT-PCR for genomic recombinaton

Component	µl
DNA	4
5x Eva green Mastermix	2
Forward primer (10 µM)	0.1
Reverse primer (10 µM)	0.1
$_{d}$H20	3.8

Table 8 qRT-PCR for DNA recombination program for the light cycler

stage/repetition	temperature [°C]	time [min]
1/ 1	95	10
2/ 42	95	0: 15
3/ 42	60 and 62 (p2ry1 loss)	0: 25
3/ 42 → data collection	72	0: 42

7.3.7 Real time quantitative PCR for mRNA expression

qRT-PCRs for mRNA expression were performed to quantify RNA molecules in brain homogenates or isolated cells after FACS. For quantification of the PCR products, the fluorescent dye EvaGreen (Axon) or SybrGreen (Biorad) were used. Primers for qRT-PCR for mRNA expression analysis and respective sequences are listed in Table 9. The setup of a single reaction and the temperature program are given in Table 10 and Table 11. cDNA samples were pipetted into 96 well plates (Axon) and the reactions were performed in the CFX96 Real-Time PCR Detection System (BioRad). All reactions were carried out in triplicates.

β-actin and ATP-synthase subunit β (ATP5B), in addition phosphoglycerate kinase (PGK) and glyceraldehyde 3-phosphate dehydrogenase (GAPDH) for analysis of FACS data, served as endogenous gene control to compensate variation in starting material of cDNA. Data normalization and analysis were performed with the qbase+ real time PCR data analysis software (Biogazelle). If cKO and control animals were compared values (△CT) of cKO animals were normalized to values of control animals. Marker gene expression data of FACS sorted cell populations are presented as average expressions after normalization to endogene expression.

Statistical analyses were conducted through GraphPad Prism 5. Inter-group comparisons were done by two-tailed Student *t* test after testing that a normal distribution is given. The levels of significance were set as * $P < 0.05$; ** $P < 0.01$; *** $P < 0.001$. The results (± SEM)

were depicted in graphs generated by GraphPad Prism5 and processed with Adobe Illustrator CS6.

Table 9 Primers for qRT-PCR for mRNA expression

Name		Sequence	Product size [bp]	Project
11282	ATP5b fwd	5' -GGATCTGCTGGCCCCATAC- 3'	?	endogene
11283	ATP5b rev	5' -CTTTCCAACGCCAGCACCT- 3'		
9146	ß-actin fwd	5 '-CTTCCTCCCTGGAGAAGAGC- 3'	124	endogene
9147	ß-actin rev	5' -ATGCCACAGGATTCCATACC- 3'		
29502	GAPDH fwd	5'-GGGTCCCTATAAATACGGACTGC- 3'	112	endogene
30535	GAPDH rev	5' -CCATTTTGTCTACGGGACGA- 3'		
23424	PGK fwd	5 '-TACCTGCTGGCTGGATGG- 3'		endogene
23425	PGK rev	5' -CACAGCCTCGGCATATTTCT- 3'		
24001	P2Y1 fwd	5' -CACGAGTTTGTGAAGGCACG- 3'	100	$P2Y_1$
24003	P2Y1 rev	5 '-GCTTCTTCTTGACCTGTGTATGCA-3'		
28467	P2Y1 Roche fwd	5' -CATCTCCGTGTACATGTTCAATTT- 3'	73	$P2Y_1$
30533	P2Y1 Roche rev	5' -GAAGATGAGGGCTGGTAGGG- 3'		
26449	P2Y2 fwd	5' -GGCCTGTGCATATGTGAGTG- 3'	127	$P2Y_1$
26450	P2Y2 rev	5 '-CCATTGATGGTGCTATTCCA- 3'		
26453	P2Y4 fwd	5' -CCACATCAGGGGGAACTAAG- 3'	125	$P2Y_1$
26454	P2Y4 rev	5' -GGAGGCAGTCAATGGTGTTC- 3'		
26457	P2Y6 fwd	5' -AAAACAACGAGGAACACCAAA- 3'	94	$P2Y_1$
26458	P2Y6 rev	5' -CCTGTCAGCCTTTCCTATGC- 3'		
14921	GluA1 fwd	5' -TCATGCAGCAAGGATGTGAC- 3'	138	$P2Y_1$
14922	GluA1 rev	5' -CCATCCTTTCCACAGTCAGG- 3'		
14913	GluA4 fwd	5' -GGGATGGTAGGAGAGCTTGTGT- 3'	61	$P2Y_1$
14914	GluA4 rev	5' -TGATTGTCAGAGGTGCAATGG- 3'		
30576	Itgam fwd	5' -CAATAGCCAGCCTCAGTGC- 3'	65	FACS
30577	Itgam rev	5' -GAGCCCAGGGGAGAAGTG- 3'		
30531	Glutamine synthetase	5' -CTCGCTCTCCTGACCTGTTC- 3'	94	FACS
30532	Glutamine synthetase	5' -TTCAAGTGGGAACTTGCTGA- 3'		
29474	NeuN	5' -GAAGAGAATGGCGAGACACTG- 3'	67	FACS
30580	NeuN	5' -GGCCCATAGACTGTTCCTACC- 3'		
29513	Aldh1l1	5' -GAGGAAGCAGCCACCTATGA- 3'	66	FACS
30582	Aldh1l1	5' -TGGCTGGTCCCAGTTGAT- 3'		
30529	Mbp	5' -CCTCAGAGGACAGTGATGTGTTT- 3'	62	FACS
30530	Mbp	5' -AGCCGACGTCCCATTGTT- 3'		
30525	PDGFRα	5' -AAGACCTGGGCAAGAGGAAC- 3'	67	FACS
30526	PDGFRα	5' -GAACCTGTCTCGATGGCACT- 3'		
29519	GLT1	5' -GATGCCTTCCTGGATCTCATT- 3'	93	FACS
30583	GLT1	5' -CAGAACTTTCTTTGTCACTGTCTGA- 3'		
30574	Aquaporin4	5' -TGGAGGATTGGGAGTCACC- 3'	92	FACS
30575	Aquaporin4	5' -TGAACACCAACTGGAAAGTGA- 3'		
23780	VGlut1	5'-CACGTGGTGGTGCAGAAA- 3'	104	FACS

23781 VGlut1	5' –CCTCCAGGAATCTGAGTGACA- 3'		
ST01357785 tdTomato	5' -CCCATGGTCTTCTTCTGCAT- 3'	190	reporter
ST01357786 tdTomato	5' -TCCCCGATTACAAGAAGCTG- 3'		
14455 GluN1 ex2_3 fwd	5' -TCTCCTACACAGCTGGCTTCT- 3'		NMDA
14456 GluN1 ex 2_3 rev	5' -AAGCTCAGGTGGATGCTCTT- 3'		
14451 GluN1 ex19_20 fwd	5' -CATTTAGGGCTATCACCTCCA- 3'		NMDA
14452 GluN1 ex19_20 fwd	5' -CACTGTGTCTTTTTGGTTTTGC- 3'		
14453 GluN1 ex8_9 fwd	5' -TGTCATCCCAAATGACAGGA- 3'		NMDA
14454 GluN1 ex8_9 fwd	5' -GGGTTCTTGGTGGATTGTCA- 3'		
14878 GluN2C ex9_10 fwd	5' -ATGGTGGCAAGGAGCAAC- 3'	84	NMDA
14879 GluN2C ex9_10 fwd	5' -CAAACATCATCACCCACACG- 3'		

Table 10 Setup for qRT-PCR for mRNA expression

Component	µl
DNA	4
5x EvaGreen Mastermix/ 2x SybrGreen Mastermix	2/ 5
Forward primer (10 µM)	0.1
Reverse primer (10 µM)	0.1
$_dH_20$	3.8/ 0.8

Table 11 qRT-PCR for mRNA expression program for the light cycler

stage/repetition	temperature [°C]	time [min]
1/1	50	2
2/1	95	15
3/42	95	0:15
3/42 → data collection	60	1

7.3.8 Determination of PCR efficiency for qRT-PCR at the DNA and mRNA level

To address questions concerning absolute amounts of DNA or cDNA amplicons, it is absolutely essential to determine the PCR efficiencies to consider possible differences in the performance for the analysis. After running the respective PCR reactions on a dilution series of DNA and cDNA, respectively, threshold cycle were plotted against the logarithm of dilution in relative units. The slope of the standard curve can be used to determine the exponential amplification and efficiency of the PCR reaction by the following equations:

Exponential amplification = $10^{(-1/slope)}$ and efficiency = $[10^{(-1/slope)}]–1$

The results show a robust performance of endogenes and target genes correlating to reliable data concerning the evaluation of qRT- PCR experiments. The determined efficiencies were applied in the analysis with the qbase+ real time PCR data analysis software (Biogazelle). In Figure 7. 1 and Figure 7. 2 are the determined efficiencies for endogenes and target genes for qRT-PCR for DNA recombination and mRNA expression, respectively, depicted.

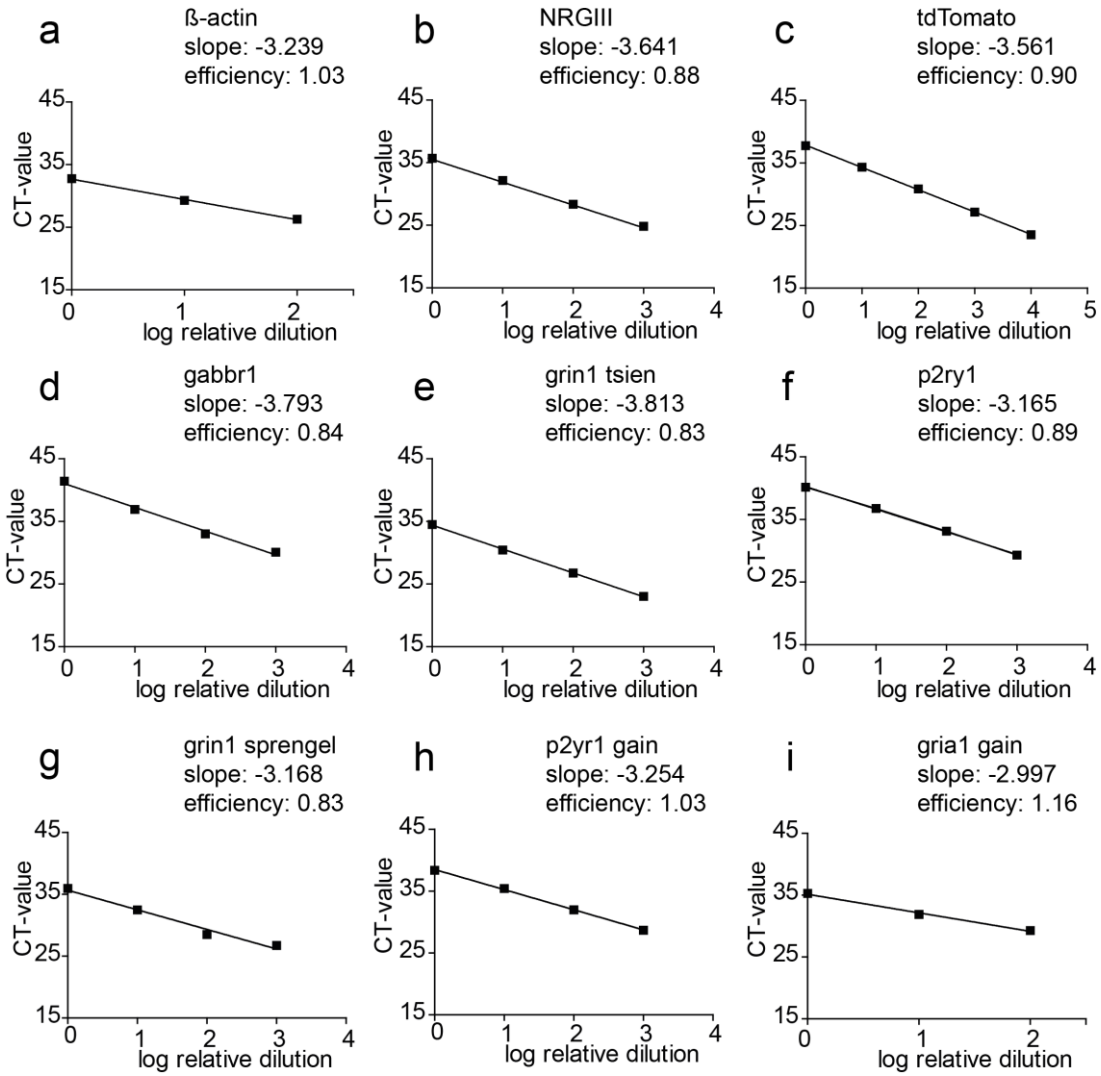

Figure 7. 1 Assessment of PCR efficacies for qRT-PCR DNA recombination
Efficiencies were determined for β-actin **(a)**, NRGIII **(b)**, tdTomato **(c)**, gabbr1 **(d),** grin1 Tsien **(e)**, p2ry1 **(f)**, grin1 Sprengel **(g)**, p2ry1 gain **(h)** and gria1 gain **(i)**. PCRs were run on undiluted, 1:10, 1:100 and 1:1000 diluted samples. Threshold cycles of the dilution were determined and plotted inversy against the logarithm of the dilution. Data were fitted with a linear regression. The slope was used to determine exponential amplification $10^{(-1/slope)}$ and efficiency $[10^{(-1/slope)}]–1$ of the PCRs.

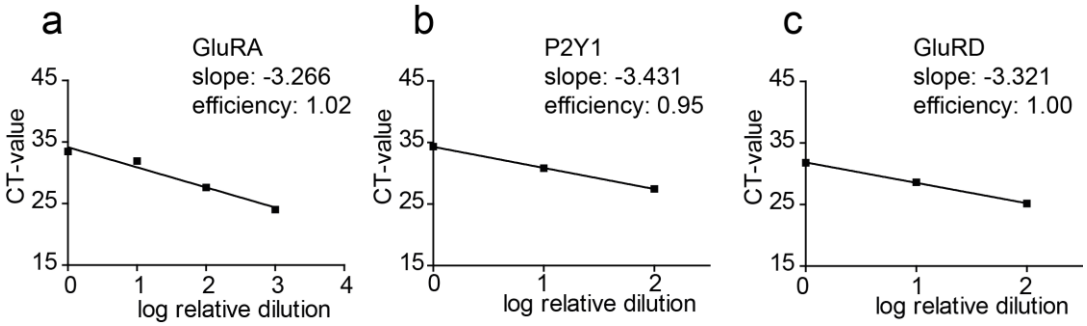

Figure 7. 2 Assessment of PCR efficacies for qRT-PCR mRNA expression
Efficiencies were determined for GluRA **(a)**, P2Y1 **(b)** and GluRD **(c)**. PCR were run on undiluted, 1:10, 1:100 and 1:1000 diluted samples. Threshold cycles of the dilution were determined and plotted inversy against the logarithm of the dilution. Data were fitted with a linear regression. The slope was used to determine exponential amplification $10^{(-1/slope)}$ and efficiency $[10^{(-1/slope)}]–1$ of the PCRs.

7.4 Fluorescence activated cell sorting (FACS)

To isolate astrocytes from brain tissue for mRNA analysis fluorescent activated cell sorting for different brain regions of young and adult mice were established. All analyzed reporter mice were heterozygous for the reporter locus and for the GLAST locus (tdTomato$^{fl/wt}$, GLAST$^{CreERT2/+}$). Control animals were negative for the CreERT2 DNA recombinase (GLAST$^{+/+}$). For the analysis of conditional $P2Y_1$ KO mouse line heterozygously floxed receptor mice were mated (*p2ry1*$^{fl/wt}$). Male and/or female were hereby also heterozygously for the GLAST locus. Ideally one gender was homozygously floxed for the tdTomato locus (stop$^{fl/fl}$tdTomato). Pubs were genotyped and grouped into control (p2ry1$^{fl/wt}$, GLAST$^{CreERT2/+}$, tdTomato$^{fl/wt}$) and cKO animals (p2ry1$^{fl/fl}$, GLAST$^{CreERT2/+}$, tdTomato$^{fl/wt}$). For the analysis of the conditional NMDA reporter knockout mouse line, mice heterozygously for the GLAST and tdTomato reporter gene were set as controls (GLAST$^{CreERT2/+}$, tdTomato$^{fl/wt}$). Animals considered as cKOs were additionally floxed for the grin locus (grin$^{fl/fl}$). In summary, for $P2Y_1$ experiments control and cKOs were littermates and in case of the NRFL mouse two different mouse lines were used. In Figure 7. 3 the experimental design of FACS is depicted. In the following paragraphs the sample processing and procedure is described in more detail

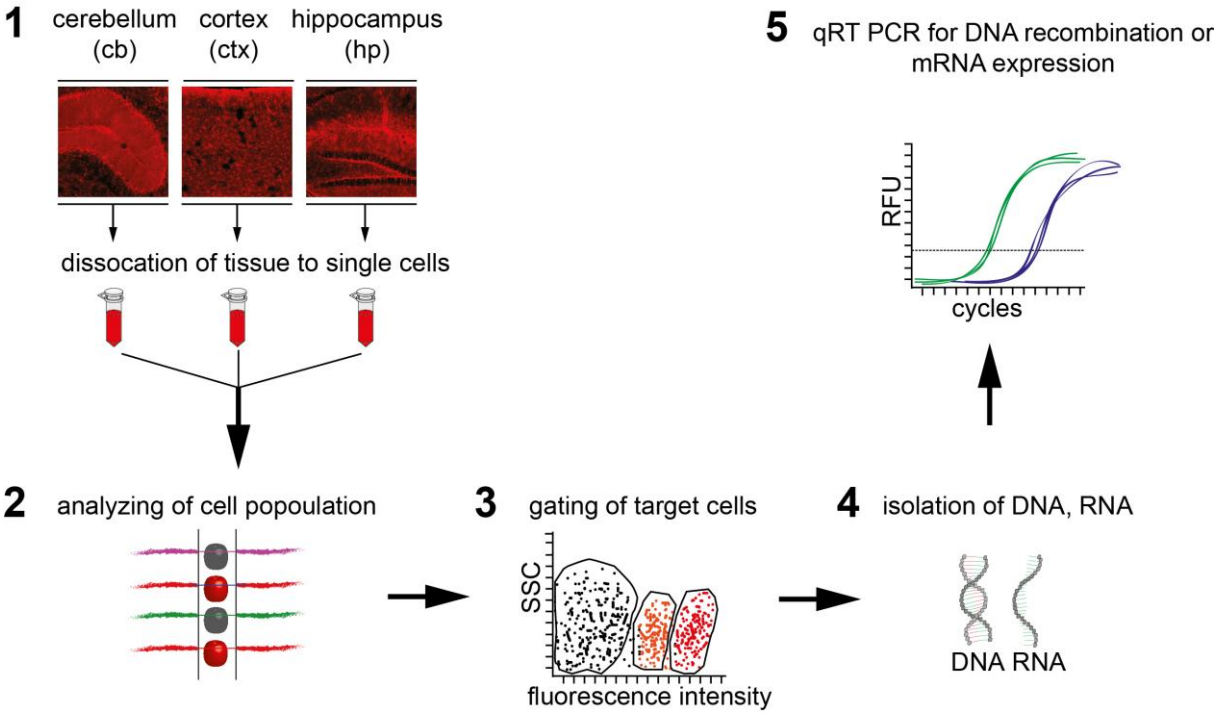

Figure 7. 3 Schematic outline of FACS of astrocytes
Brain tissue was dissected in cerebellum, cortex, hippocampus and dissociated (**1.)**, followed by fluorescence activated cell sorting (FACS) to measure properties of single events (**2**). Due to different properties and red fluorescence populations were identified and gated (**3**), followed by isolation of RNA and DNA (**4**), which were used for qRT-PCR analysis (**5**).

FACS glossary

Area, width and height

When a particle is analyzed by flow cytometry it passes through the laser beam. Therefore the signal for each individual particle can be described by three basic parameters: The height (**H**) measures the maximum intensity of the signal. The width (**W**) measures the time over which the signal was recorded and the area (**A**) measures the integrated signal over the time.

FSC

FSC refers to “forward scatter” and measures scattering of laser light at low (forward) angles. Even though this is a simplification, for practical purposes the FSC signal is often referred to as the size of a particle.

SSC

SSC refers to “side scatter” and measures scattering of laser light at a 90°-angle. The SSC signal is related to the internal complexity of a particle. For example, a cell that contains a lot of internal membranes, such as a granulocyte, scatters more light at a 90° -angle than a comparable particle of less internal complexity.

Gates

Gates are used in flow-cytometry and flow-sorting to select data/events of certain signal ranges for further analyses or sorting.

7.4.1 Isolation of astrocytes from brain tissue for FACS

Preparation of single cell suspension was adapted to our purposes on earlier protocols (Lovatt et al., 2007b; Orre et al., 2014) and is described here in detail since the method was established in this laboratory for the first time. Mice were anesthetized and perfused with ice cold HBSS without Mg^{2+} and Ca^{2+} for 2 to 3 min. Cortex, hippocampus (after coronal slicing of forebrain) and cerebellum were dissected and kept in ice cold HBSS. After mechanical dissociation into smaller pieces with a scalpel, tissue was transferred to a 15 ml falcon filled with HBSS.

In parallel activated papain was prepared. For digestion of two cortices 500 µl of papain activation solution and 156 µl papain (Sigma) were added to 4.5 ml of pipes working solution and incubated for 20 min at 37°C. After incubation 100 µl DNAse I (Roche, 200 Units) was added and the solution was filtered (Satorius, 0.45 µm, single unit).

After tissue pieces had sunken to the bottom HBSS was removed to a rest volume of 2.5 ml, filled up to 5 ml with pipes workings solution und mixed carefully. After tissue pieces sunk again, solution was removed to a rest volume of 2.5 ml and filled up to 5 ml with the activated papain solution (f. c. 6 U/ml). Falcon tubes were encircled with parafilm to balance the lid for a stable horizontal lay, fixed in a suitable box and incubated for 40 min at 37° C, 40 rpm. Subsequently 3 ml wash buffer containing 100 µl DNase (200 Units) were added to each sample and incubated another 15 min. The mix was spun at 200xg for 5 min and the pellet was triturated with a 1 ml pipette in 2 ml wash medium to obtain a single-cell suspension. Single cells were filtered through a pre-wet 70 mm single-cell strainer (BD Bioscience), and washed in 15 ml wash medium. Cells were pelleted at 200xg for 10 min. Supernatant was carefully removed. The pellet was resuspended in 800 µl PBS, 0.5 % BSA (MACS buffer)

and incubated for 15 min with 80 µl of Myelin Removal Beads II (Miltenyi Biotec). Cells were washed in 10 ml MACS buffer and centrifuged, followed by magnetic separation of bound myelin from single cells. Without myelin removal the number of duplets and debri in the suspension was much higher (compare Figure 7. 4 a, b and Figure 7. 6 b) The flow through was collected and centrifuged once more at 200xg for 10 min. Pellet was resuspended in 1 ml GKN media and proceeded with the FACS sorting procedure.

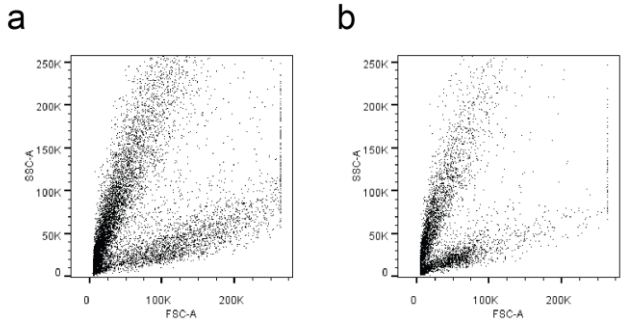

Figure 7. 4 FACS of cortical and hippocampal cells without myelin beads
Cortex (**a**) and hippocampus (**b**) were processed for FACS without myelin beads. Number of debri and duplets is increased, recognized by events that possessed lower FSC and higher SSC values (dots on the left part of each plot)

Washmedia

Dulbeco's modified eagles medium, 4.5 mg/glucose/L, 500 ml (Sigma)

Open bottle, add ~30 ml medium to dissolve 5 g of BSA (Sigma), filter it through single unit filter (Satorius, 0.45 µm) to transfer it back.

PIPES stock buffer		
PIPES	0.5	M
NaOH	1	M
NaCl + KCl solution		
NaCl	1.2	M
KCl	50	mM
PIPES working solution		
PIPES Stock buffer	2	ml
NaCl + KCl solution	5	ml
50 % Glucose	0.45	ml
Adjust to pH 7.4		
Papain activation buffer		
L-Cystein HCl	55	mM
EDTA	11	mM
Adjust to pH 7.2		
GKN medium 10x		
NaCl	1.37	M
KCl	54	mM

Na_2HPO_4 x $7H_2O$	114	mM
NaH_2PO_4 x $2H_2O$	50	mM
D(+)-glucose monohydrat	111	mM

MACS buffer

1xPBS (pH 7.2)

BSA	0.5	%

Topro3 life/dead cell solution

TO-PRO-3® (1 mM Invitrogen)	1	µM

7.4.2 FACS instrumentation

The FACS Aria-I was maintained according to recommendations of the supplier and regularly checked by the technical service. The Drop Delay was determined before each experiment. Throughout this study the instrument was operated in the following configurations:

70 or 85 µm nozzle

488 nm laser:	tdTomato detector
633 nm laser	TO-PRO-3® detector
Sheath fluid:	PBS
Sort Precision:	Purity

To analyze recorded FACS events the BD FACSDiva software was used. 10.000 events were recorded to set first SSC and FSC conditions. All events should be visible in the plot window. The laser intensity (voltage) of the 488 nm laser was set according to the fluorescent properties of control and tdTomato+ cells (see Figure 7. 5 a-c, black and red dots respectively) of the cerebellum (a), cortex (b) and hippocampus (c). For detecting the signal the PE filter settings were used (585/42, 556LP) and the side scatter was plotted against the fluorescence intensity. The same accounted for the setup of 633 nm laser for TO-PRO-3® detection for life and dead cell dicrimination. Cells with (blue dots in Figure 7. 5 d) and without (black dots) TO-PRO-3® incubation were analyzed, signal intensities here were collected with the AlexaFluor 700 filter settings (730/45, 690LP).

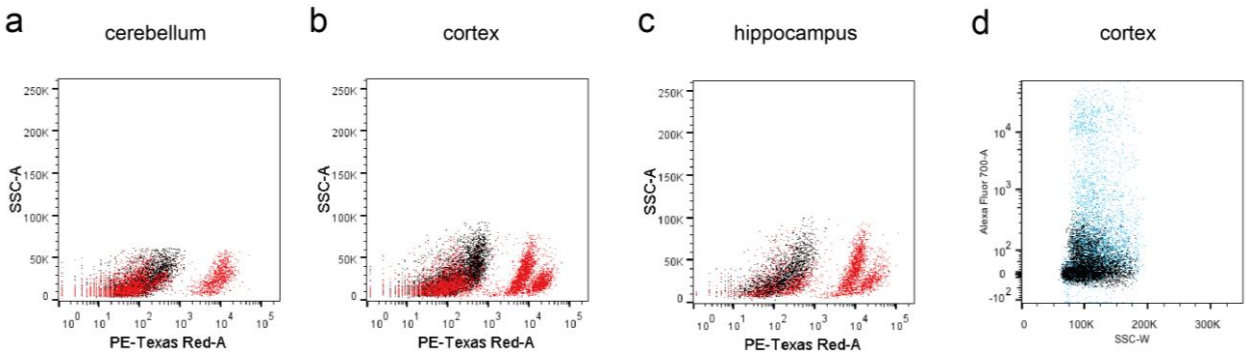

Figure 7. 5 Positive and negative controls for FACS settings.
The pictures depicts 10.000 events of a single cell suspension of non (black) and tdTomato fluorescent cells (red) of cb (**a**), ctx (b) and hp (**c**) of GLAST$^{CreERT2/+}$ x stop^{flwt}tdTomato animals. In (**d**) approximately 5000 events after gating are presented. Cell suspensions were stained with TO-PRO-3® (blue dots) for life and dead cell discrimination. Black dots represent unstained control cells to set the settings.

In the following figure the gating strategy is depicted in representative images: Accudrops have a size of exactly 6 µm, they serve as a control to set gate debri at the right position (1. and 2.). Subsequently single cells were gated with help of the side (SSW) and forward scatter (FSC) (**3**. and **4**.). Duplets show different optic properties and can be distinguished from single cells. Finally single cells were investigated in regard to their health status; nuclei of dead cells were stained by the dye TO-PRO-3® and can be distinguished from alive and apoptotic cells (**5.**). At last, tdTomato+ cells were gated for the sort process (**6.**)

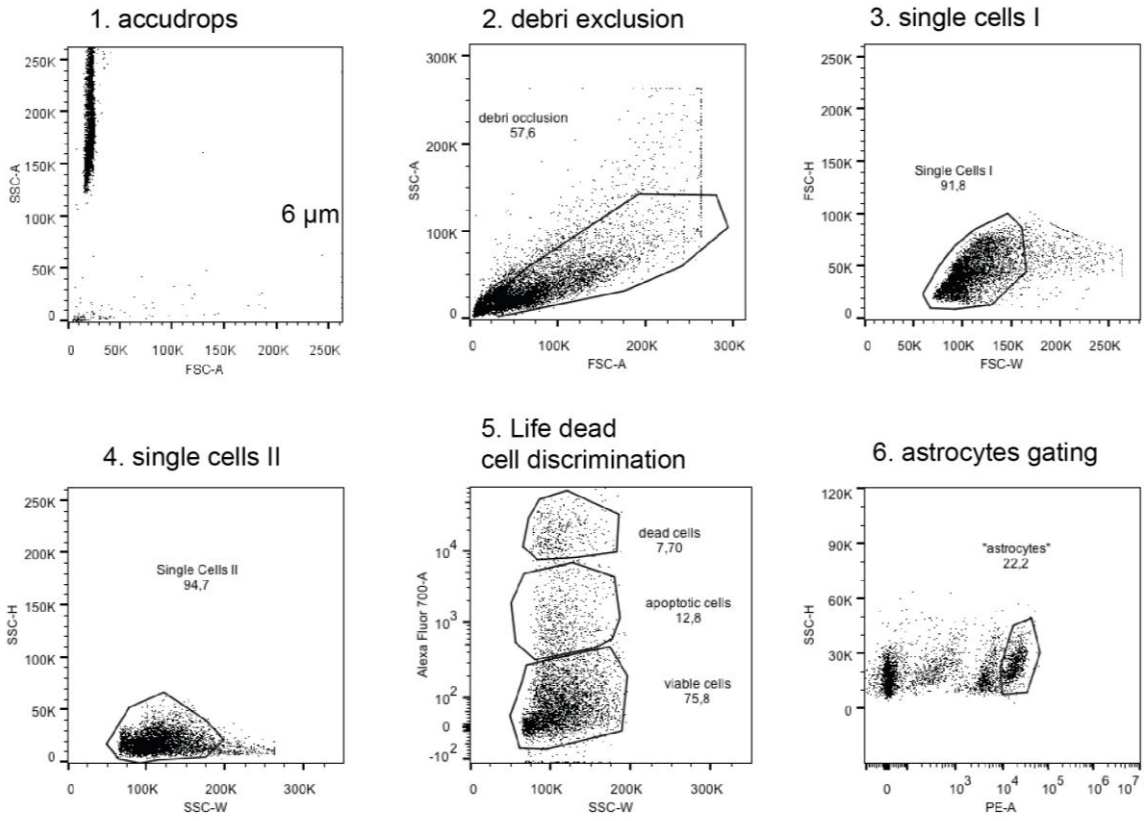

Figure 7. 6 Gating strategy for FACS of tdTomato+ astrocytes
In 6 steps cells were gated to obtain alive cells and highest possible purity in the tdTomato+ population.

FACS data of each experiment were exported as fsc.3 files and analyzed with the FlowJo_V10 software. Statistics were realized with GraphPad Prism5. Inter-group comparisons were done by two-tailed Student *t* test after testing that a normal distribution is given. The levels of significance were set as * $P < 0.05$; ** $P < 0.01$; *** $P < 0.001$. Data are represented as means ± SEM of natural replicates (mice) or experiments per brain tissue (e.g. 26 cortices).

7.5 Protein biochemical methods

7.5.1 Protein concentration measurement by the BCA method

The protein concentration was measured by using the Thermo Scientific Pierce BCA Protein Assay Kit according to manufacture's "microplate procedure" protocol. The absorbance was read at 620 nm in a Mithras LB 940 microplate reader (Berthold Technologies), exported with the MikroWin 2000 software (Mikrotek) and processed with Excel 3.0. To determine the concentrations of unknown samples, measured values were compared with values of protein solutions with known concentrations. Here bovine serum albumin (BSA) was used as a standard (100, 200, 400, 600, 800, 1000 µg). Protein solutions were diluted 1:5 and 1:20 in $_{d}H_2O$. 10 µl of the samples and standard solutions were pipetted in duplicates into a 96 microtiter plate (Falcon). Next 200 µl of reagent A and B premixed in a ratio of 50:1 containing 4 % cupric sulphate (Cu^{2+}) and bicinchoninic acid were given into wells. After incubation for 30 min at 37°C the samples were measured and the protein concentrations were calculated with the aid of the determined standard curve.

7.5.2 SDS-PAGE, Western blotting and immuno detection

Proteins were separated by use of discontinuous SDS-polyacrylamide gel electrophoresis (SDS-PAGE) using the system from BioRad or Serva. From the protein lysates to be analyzed 1 µg/µl solutions mixed with 4x SDS sample buffer were prepared, 1 % β-ME was freshly added and the samples were incubated for 10 min on ice. Samples were loaded on the gel (SERVA*Gel*™ TG PRiME™ 10 % or self-made gels, see Table 12). The control wells were loaded with 7 µl molecular weight standard (MagicMarkTM XP Western Protein standard, Invitrogen). An equal volume of 1x SDS sample buffer was added to any empty well to prevent spreading of adjoining lanes The gel was run in a chamber (BlueVertical™ PRiME™, Serva or the Mini-Protein III system, BioRad) filled with running buffer at 250 V (50 mA, 150 W) for 45 min.

After the run was finished, the gel was removed from the plates and separated proteins were electrophoretically transferred to a nitrocellulose membrane (Protran, Nitrocellulose BA 85, Schleicher & Schüll). The transfer took place in a vertically orientation under wet conditions. The chromatography paper (Whatman), the nitrocellulose membrane and the sponges were pre-soaked with ice cold transfer buffer and assembled in a Biorad adapter cassette in the following order: 1 sponge, 2 Whatman paper, gel, nitrocellulose membrane, 2 Whatman paper and 1 sponge. The blotting was performed for 2 h at a constant voltage of 100 V (200 mA, 150 W) in a Biorad Mini-Trans-Blot Cell wet chamber filled with transfer buffer.

After electrophoretic transfer, the NC membrane was immediately placed in blocking buffer (5 % milk powder in PBS) and was incubated for 1 h to block remaining protein binding sites to avoid unspecific binding of the detection reagents. The blocked membrane was cut into stripes corresponding to the molecular weight of the protein to be detected. The stripes were placed into 50 ml microtubes (Falcon) and incubated with the primary antibody over night at 4°C (for dilutions see Table 13). The next day the membrane stripes were washed three times with PBST (PBS; 0,05 % Tween) and the appropriate secondary HRP conjugated antibody diluted in 5 % milk powder in PBS was then applied to the membrane. The incubation was carried out for 1 h at RT followed by three washes for 10 min in PBST. All

steps were performed by continuous shaking or turning to achieve homogeneous binding of antibodies, washing or blocking of the membrane. After the washing steps, the membrane was incubated for 2 min in Enhanced Chemilumniescent Detection (ECL) solution according to the manufacturer's recommendations (Western Lightning™, Western Blot Chemiluminescence Reagent Plus, PerkinElmer Life Sciences, Inc.). The membrane was placed in a cassette impermeable to light and covered with transparent foil. In the dark room an ECL photographic film (Hyperfilm™, Amersham Biosciences) was exposed to the membrane. The time of exposure varied from 1 s to 30 min depending on the signal intensity.

For re-probing of the membrane with a second primary antibody, the membrane was placed into stripping buffer for 30 min, washed two times for 5 min with $_dH_20$ followed by incubation in TRIS-HCL pH 8.8 for 10 min and two washing steps in $_dH_20$. Afterwards the membrane was washed for 10 min in PBST, blocked for 1 h in blocking buffer and incubated with the desired second primary antibody over night at 4°C. All steps were performed by continuous shaking or turning.

Table 12 Solutions for 10% SDS-PA-gel

10 % separation gel	[ml] (for one gel)	Stack	[ml] (for one gel)
$_dH20$	4.0	$_dH20$	1.4
30 % acrylamide mix (Sigma)	3.3	30 % acrylamide mix (Sigma)	0.33
1.5 M Tris-HCL (pH 8.8)	2.5	1 M Tris-HCL (pH 6.8)	0.25
10 % SDS	0.1	10 % SDS	0.02
10 % APS	0.1	10 % APS	0.02
TEMED	0.004	TEMED	0.002

Sucrose buffer

Sucrose	320	mM
Tris (pH 7.4)	10	mM
$NaHCO_3$	1	mM
MgCl2	1	mM

Buffer was prepared freshly each time and protease inhibitor aliquots (Complete Mini protease inhibitor tablets, (Roche) were added before use.

10x SDS running buffer

Tris	250	mM
Glycine	1.92	M
SDS	1	%

4x SDS sample buffer (10 ml)

$_dH_20$	3.8	ml
1 M Tris HCL	1	ml
Glycerol	0.8	ml
10 % SDS	1.6	ml
β-mercaptoethanol	0.4	ml
1 % bromphenol blue	0.4	ml

Phosphate buffered saline (PBS, 10x concentrated)		
NaCl	1.7	M
KCl	0.034	M
Na_2HPO_4	0.04	M
KH_2PO_4	0.018	M

Table 13 Primary antibodies for Western blotting

antibody/ordernumber	dilution	company
rabbit anti $P2Y_1R$ polyclonal intra/ APR 009	1: 300	Alomone
rabbit anti $P2Y_1R$ polyclonal/ ab85896	1: 300	Abcam
mouse anti NMDAR subunit1 monoclonal/ 32-0500	1: 500	Invitrogen
mouse anti α-tubulin monoclonal/ T6074	1: 5000	Sigma

Table 14 Secondary antibodies for Western blotting

antibody	dilution	company
goat anti-rabbit IgG HRP-conjugated	1: 2000	Dianova
goat anti-mouse IgG HRP-conjugated	1: 2000	Dianova

1x transfer buffer		
Glycine	3.9	mM
Tris	4.8	mM
Methanol	20	% (v/v)
Stripping buffer		
Acetic acid	60	ml
NaCl	28.2	mg
H_20	900	ml
Blocking buffer		
Nonfat milk powder in PBS	5	% (w/v)
Washing buffer		
Tween 20 in PBS	0.05	% (v/v)
Protein marker		
MagicMarkTM XP Western Protein standard		Invitrogen

7.5.3 Densitometric quantification of band intensity and illustration of Western blots

For densitometric analyses only films exposed at non-saturating levels were used. These films were scanned at greyscale (300 dpi resolution) using a regular horizontal scanner (Hewlett Packard ScanJet 6300C). These images were then exported as tiff files for band intensity analysis using ImageJ. The integrated density (=area*mean grey value) for the band of interest was normalized to the integrated density of the respective α-tubulin band. Finally the determined values of GluN1 cKO animals were normalized to the mean value of control animals (n=3). Results (±SEM) were depicted as histograms generated with GraphPad Prism5 and processed with Adobe Illustrator CS6. Figures with images of representative Western blot films were arranged with Adobe InDesign CS6.

7.6 Histological and immunochemical methods

7.6.1 Fluorescent immunodetection on vibratome sections and histology

Common protocol: Fixed brains were cut into sagittal sections 40 µm sections in ice cold PBS at a Leica VT1000S vibratom. The sections were collected in 24 wells tissue culture plates (Falcon) containing 1x PBS. Vibratome sections were incubated for 1 h in 500 µl of 0.3 % Triton X-100 and 5 % horse serum (HS) in 1x PBS for 1 h at RT. Sections were then incubated over night at 4 °C with 200 µl of the primary antibody diluted in the same solution stated above. The next day the sections were rinsed three times for 5 min each in 1x PBS. To visualize the site of binding of primary antibodies, sections were incubated with 200 µl of the according fluorescent labeled secondary antibodies (1: 2000) in 2 % HS in 1x PBS for 2 h at RT. For nuclei staining DAPI (1: 40000) or TO-PRO-3® (1: 10000) was added to the sections and incubated for 5 min before rinsing sections twice with 1x PBS for 5 min to remove any non-specifically bound antibody. Finally, sections were placed in a water bath and mounted in Immo-Mount (Shandon) or Aquapoly mount (Polysciences).

In case of the $P2Y_1R$ extracellular binding antibody (Alomone) brains were cut 2 h after post fixation and blocked with 10 % HS and 0.5 % Triton X-100 in 1x PBS, followed by incubation of the primary antibodies in 0.3 % Triton X-100 overnight. Further P2Y1 intracellular binding antibodies (Alomone, Abcam) were incubated for 1 h after the first antibody with biotin labeled antibody against rabbit in 4 % HS and 0.1 % Trition X-100 to increase primary antibody signal. Subsequent washing steps were followed by incubation for 30 min with streptavidin texas red antibody (1: 1300 in PBS).

For haematoxylin and eosin (H&E) counterstaining of the cerebellum of $P2Y_1$ cKO and control mice, sections were put on superfrost object slides, rehydrated and then successively incubated for 3-5 min in 0.1 % haematoxylin (color blue; basic tissue compartments) and 0.1 % eosin (color red, acidic tissue compartments).

Table 15 Primary antibodies for immunhistochemistry

antibody/ordernumber	dilution	producer
rabbit anti $P2Y_1R$ polyclonal intra/ APR 009	1: 300	Alomone
rabbit anti P2Y1R polyclonal extra/ APR 021	1: 300	Alomone
rabbit anti $P2Y_1R$ polyclonal/ ab85896	1: 300	Abcam
rabbit anti GFAP polyclonal/ Z0334	1: 500	Dako Cytomation
mouse anti GFAP monoclonal	1: 100	Novocastra
mouse anti GluN1 subunit monoclonal/ 32-0500	1: 200	Invitrogen
rabbit anti GluN2C subunit polyclonal AGC 018	1: 200	Alomone
rabbit anti GluA1 polyclonal clone C3 T 04-855	1: 500	Millipore
rabbit anti PDGFRα polyclonal/ 558774	1: 500	Cell Signaling
rabbit anti Olig2 polyclonal	1: 200	Stiles laboratory
rabbit ant S100β monoclonal/ ab52642	1: 500	Abcam
mouse anit NeuN monoclonal clone A60/ MAB377	1: 500	Millipore
mouse anti BLBP polyclonal/ ABN14	1: 500	Millipore
mouse anti MPB monoclonal	1: 500	Novocastra
mouse glutamine synthetase/ 610518	1: 500	BD

guinea pig anti VGlut1 polyclonal AB5905	1: 1000	Millipore

Table 16 Secondary antibodies for immunohistochemistry

antibody	dilution	producer
donkey anti rabbit Alexa 488-conjugated	1: 2000	Invitrogen
donkey anti mouse Alexa 488 conjugated	1: 2000	Invitrogen
donkey anti mouse Alexa 633-conjugated	1: 2000	Invitrogen
donkey anti rabbit Alexa 555-conjugated	1: 2000	Invitrogen
donkey anti mouse Alexa 555 conjugated	1: 2000	Invitrogen
donkey anti guinea pig Alexa 555 conjugated	1: 2000	Invitrogen
Streptadivin TEXAS RED®	1: 1000	Millipore
goat ant rabbit IgG biotin labeled	1: 1000	Millipore

7.7 Microscopy

7.7.1 Epifluorescence microscopy

For detection of fluorescent signals from vibratome sections an Zeiss AxioImager.Z2 microscope equipped with a Stereo Investigator system (MicroBrightField) was used for image acquisition. The software enabled imaging of overviews of selected regions of interest, like whole brain or just parts by encircling the contour. Images were taken automatically with a 5x objective and stitched together. Images were saved as tiff files and processed with Adobe Photoshop. Representative images were documented with Adobe InDesign CS6 and Adobe Illustrator CS6.

7.7.2 Confocal microscopy

Confocal images were taken using a laser-scanning microscope (LSM-710, Zeiss) with appropriate excitation and emission filters. Z-stack images were taken at 0.5–2 µm intervals with the 10x and 40x (oil) objectives. The argon/krypton (488 nm) - and helium/neon (543 nm and 633 nm) - lasers were used as exciting sources. For final analysis, captured LSM images were processed with ImageJ and saved as tiff files. Figures of representative images were arranged with Adobe InDesign CS6.

7.7.2.1 Densitometric quantification of confocal images

GFAP and GluN1

For the analysis GluN1 cKO and control animals were utilized (n=2). Confocal z-stacks of the GluN1 and GFAP staining at the stabwound, next to the lesion and contralateral site were processed using customized macros written with Tinn-R and run by ImageJ. Here channels of images were split, brightness and contrast was adjusted per single image and subsequently integrated fluorescence density (=area*mean grey value fluoresce) were measured. Images per channel were treated in the same way. Averaged values of cKO animals were normalized to the mean value of control animals. The results (± SEM) were depicted as histograms generated by GraphPad Prism5 and processed with Adobe Illustrator CS6.

VGlut1

Per animal confocal images of the cb, ctx, hp and bs were processed using customized macros written with Tinn-R and run by ImageJ. Briefly, maximum intensity was projected and brightness and contrast was adjusted. Images of control and inducible cKO animals (cKO n=4, control n=2) were treated in the same way. Stained regions were selected with the ImageJ seclection tool and integrated fluorescence density (=area*mean grey value) were measured. Averaged values of cKO animals were normalized to the mean value of control animals. The analysis for statistical significance (unpaired t-test) was performed using GraphPad Prism5.

tdTomato

The fluorescence intensity of tdTomato (area*mean grey value) of male (n=2) and female (n=3) brain were measured in sagittal overviews using ImageJ. Mean values of male brains were normalized to mean value of females.

TO-PRO-3®/ tdTomato

For the determination of tdTomato+ cells in the cortex two parasagittal slices per animal were considered (n=3, per gender). 3 detailed images (40x) in the cortex per slice were taken. In total in 6 images per animals tdTomato+- and TO-PRO-3®+ cells were counted. Finally determined number of tdTomato+- was normalized to the total number of TO-PRO-3®+ cells and area.

7.7.3 Electronen Microscopy

Following anesthesia, mice were perfused with ACSF containing in mM: 124 NaCl, 3.0 KCl, 2.0 $CaCl_2$, 2.0 $MgSO_4$, 1.25 NaH_2PO_4, 23 $NaHCO_3$, and 10 glucose, and subsequently with a fixative solution containing 4 % formaldehyde, 0.5 % glutaraldehyde in phosphate buffer with 0.5 % NaCl. Brains were isolated and post fixed in the same fixative for 24 h. Tissue was washed 3x times for 30 min in 0.1 M PB, incubated for 1 h in 1 % osmium tetraoxid, followed by dehydration in a graded series of ethanol with a final step in 100 % isopropanol (each for ≈ 30 min. Subsequently tissue pieces were incubated for 1 h in propylenoxide, in 2: 1 propylenoxide and epon, 1: 1 propylenoxide and epon, 1: 2 propylenoxide and epon and finally in pure epon (the embedding was done by Gabriele Kiefer, Research group of Prof. Dr. med. Frank Schmitz, Department of Anatomy, University of Saarland).

Tissue pieces were transferred to plastic capsule filled with epon and baked for 24 h in the oven. All cerebellar samples were trimmed to focus only on lobe 5 of the cerebellar cortex. Ultrathin sections (50 nm) were cut using a Ultracut S ultramicrotome (Leica), dried on 100 mesh grids (plano GmbH) coated with a thin film of formvar and contrasted with an aqueous solution of 2 % uranyl acetate (Merck) followed by lead citrate. EM images from the upper third of the molecular layer were taken at a Tecnai Biotwin digital transmission electron microscope (FEI). Per genotype 2 animals were processed and 5-8 images (16.8 x 12.6 µm) were taken randomly. For analysis, the experimenter was blinded for all images that were studied. The area of BG processes was analyzed with the point-hit method. The method is generally used to determine the surface of an object. The electro micrographs were virtually intersected with the ImageJ plugin “grid”: Bergmann glial processes falling within the

boundaries of the intersections were count as a “hit”. The “hits” per picture were multiplied by the area of an intersection. The determined BG process area per picture was summed up per animal and normalized to the total area of the respective number of pictures. The area of BG processes was finally determined by normalizing the cKO values to controls. Synapses were visually counted per picture (5 x 6.9 x 5.2 µm and 5 x 16.8 x 12.6 µm per animal), summed up per animal and converted per area. cKO values per normalized to control values. Inter-group comparisons were done by two-tailed Student *t* test. The levels of significance were set as * $P < 0.05$; ** $P < 0.01$; *** $P < 0.001$. Data are represented as means ± SEM of natural replicates (mice).

7.8 Stab wound experiment

Mice were anesthetized and placed on a heating plate to keep the body temperature at 36.5-37.5 °C. An incision along the midline of the scalp was made and a craniotomy with 3 mm diameter was executed with a hand drill (0.7 mm). The center of the craniotomy is approximately located (bregma considered as 0) laterally 1.5 mm and longitudinally 2 mm. The center was stabbed with a surgical scapel till 1 mm depth from the pial. After the bleeding was stopped, the wound was closed and mice were treated with Buprenorphin (100 µl / 30g body weight). Stab wound injuries (SWI) were performed in adult mice (12 weeks old). Experiments were performed by Xanshiu Bai.

7.9 Recordings of glial synaptic currents

Experiments performed in Homburg, Saar, Germany were conducted at room temperature (22–24 °C). Mice were decapitated, the brain was dissected and placed in ice-cooled, carbogen-saturated (5 % CO_2-95 % O_2, pH~7.4) preparation solution without calcium containing (in mM) 126 NaCl, 3 KCl, 25 $NaHCO_3$, 1.2 NaH_2PO_4, 3 $MgCl_2$ and 15 glucose. Sections were cut with a vibratome (Leica VT 1200S) and transferred to a nylon-basket as slice holder for incubation in artificial cerebral spinal fluid (aCSF) containing (in mM) 126 NaCl, 3 KCl, 25 $NaHCO_3$, 15 glucose, 1.2 NaH_2PO_4, 2 $CaCl_2$, and 2 $MgCl_2$ at 35°C. The slices recovered in ACSF with continuous oxygenation for at least 1 hour before recording. Subsequently, slices were transferred to a recording chamber and kept submerged by a platinum grid with nylon threads for mechanical stabilization. The chamber was mounted on an upright microscope (Axioscope 2 FSmot, Zeiss, Germany) and continuously perfused with ACSF with 1 $MgCl_2$ and 2.5 $CaCl_2$ (room temperature; 20–23 °C) at a flow rate of 2–5 ml/min. Astrocytes were identified by their respective fluorescence using conventional epifluorescence illumination (with a 40x water immersion objective and filter sets for EGFP/EYFP and DsRed1). Whole-cell voltage-clamp recordings were obtained with an EPC10 patch-clamp amplifier (HEKA). Data acquisition was controlled by Patchmaster software (HEKA). Patch electrodes were pulled from borosilicate capillaries (OD: 1.5 mm; Hilgenberg GmbH) using a Micropipette Puller (Model P-97, Sutter Instrument Co., CA). Patch pipettes were filled with a solution containing (in mM) 120 KCl, 5 $MgCl_2$, 5 EGTA, 10 HEPES and 5 Na_2ATP (pH~ 7.2). The resistance of the pipettes was between 4 and 7 MΩ. The stimulation and recording protocol and analysis were performed by Dr. Yuriy Pankratov as described in (Lalo et al., 2011a; Lalo et al., 2006). Data presented from

patched GFAP-EGFP mice were performed and analysed likewise by Dr. Ulyana Lalo and Dr. Yuriy Pankratov at the University of Warwick, UK. Chemicals obtained in Homburg were purchased from Tocris Bioscience.

7.10 Primary astrocyte culture

Preparation of the flasks: 5 mg of the collagen stock were diluted to 0.5 mg/ml collagen. 350 µl of the 0.5 mg/ml collagen solution was pipetted into a T-75 cm^2 cell culture flask, where the collagen was equally distributed over the surface. **Preparation of astrocytes:** Mice were killed with CO^2 and quickly decapitated. The embryonic mouse was placed into a petri dish, the decapitated and fixed with forceps while the skin and skull is carefully cut away using a small scissor. The cut should be directed from dorsal to frontal. The brain was taken with a spatula and transferred in a petri dish filled with ice cold HBSS. The dissection and preparation of the hippocampus was done under a stereomicroscope (Zeiss, Stemi 2000). The meninges and other connective tissue were removed with fine forceps. The hippocampi were transferred into an Eppendorf tube and stored on ice until all needed hippocampi were prepared. Following, they were put onto a cell stainer on top of a 50 ml falcon tube. With a sterile spreader the hippocampi were dissociated through the cell stainer with 20 ml ice-cold DMEM. The suspension is centrifuged at 1700 rpm for 7 min at RT. The excess medium was removed up to the visible pellet. The pellet was resuspended carefully first with a blue, then yellow tip in 3 ml 10 % FCS Medium. The previously prepared flask was filled with 15 ml 10% FCS Medium. The 3 ml cell suspension is transferred into the flask and incubated at 37°C/5 % CO^2. The next day the medium was replaced with fresh medium. The astrocytes were grown for 5 d and the subcultured onto collagen-covered coverslips and processed for immunohistochemical methods. Culture and immunostaining was performed by Dr. Yvonne Schwarz, Research group of Prof. Dr. Dieter Bruns, Department of Physiology, Unversity of Saarland.

8 Supplements

Table 17 TAM and 4-OHT concentrations in serum and brain of wild type mice

	serum				brain			
	TAM [ng/µl]		4-OHT [ng/µl]		TAM [ng/µl]		4-OHT [ng/µl]	
time	mean	SEM	mean	SEM	mean	SEM	mean	SEM
8 h	778.550	92.796	483.361	36.175	5748.707	667.442	1005.812	169.638
1 d	330.011	39.161	284.756	31.776	2249.945	484.543	515.767	98.988
2 d	39.511	28.518	39.179	29.111	308.899	196.692	83.425	57.311
5 d	6.170	3.872	0.168	0.056	2.422	0.761	0.551	0.169
7 d	0.799	0.377	0.346	0.286	0.449	0.007	1.132	0.970
14 d	0.440	0.008	0.000	0.000	0.153	0.007	0.187	0.019
21 d	0.833	0.383	0.000	0.000	0.218	0.061	0.238	0.013

In the following figures marker stainings of recombined tdTomato+ cells after different time points after tamoxifen injection in GLAST-CreERT2 x tdTomato$^{fl/wt}$ are depicted.

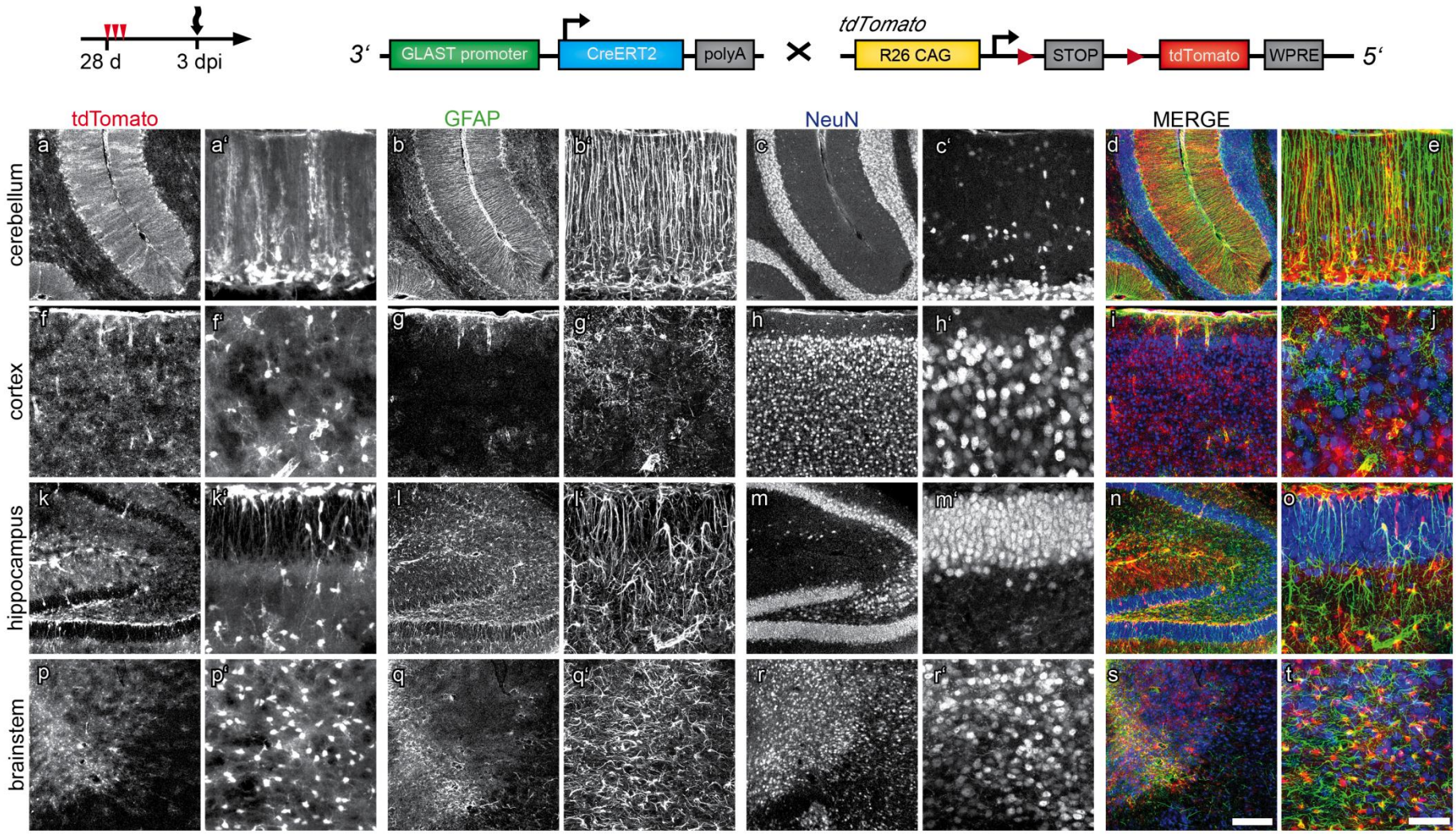

Figure 8. 1 Neuronal marker expression in tdTomato+ cells 3 days after TAM injections in young mice

Depicted are confocal images of sagittal slices of tdTomato reporter animals 3 d after TAM injections to a 4 weeks old animal (**a, a’, f, f’**, **k, k’, p, p’**). Slices were in addition stained against the astroglial marker protein GFAP (**b, b’, g, g’, l, l’, q, q’**) and the neuronal marker protein NeuN (**c, c’, h, h’, m, m’, r, r’**). In **a-c, f-h, k-m, p-r** overview images and in **a’-c’, f’-h’, k’-m’, p’-r’** detailed confocal images of cb (**a**, **a’-c**, **c’**), ctx (**f**, **f’- h**, **h’**), hp (**k**, **k’- m**, **m’**) and bs (**p**, **p’ – r**, **r’**) are shown. Based on the merge of the fluorescent signals (**d, e, i, j, n, o, s, t**) co-localization of tdTomato and GFAP can be detected for each brain regions. In contrast NeuN+ cells do not co-localize with tdTomato. The scale bar in (**s**) corresponds to 200 µm and applies for images (**a-c, f-h, k-m, p-r**). The bar in (**t**) correlates to 50 µm and holds for images (**a’-c’, f’-h’, k’-m’, p’-r’**).

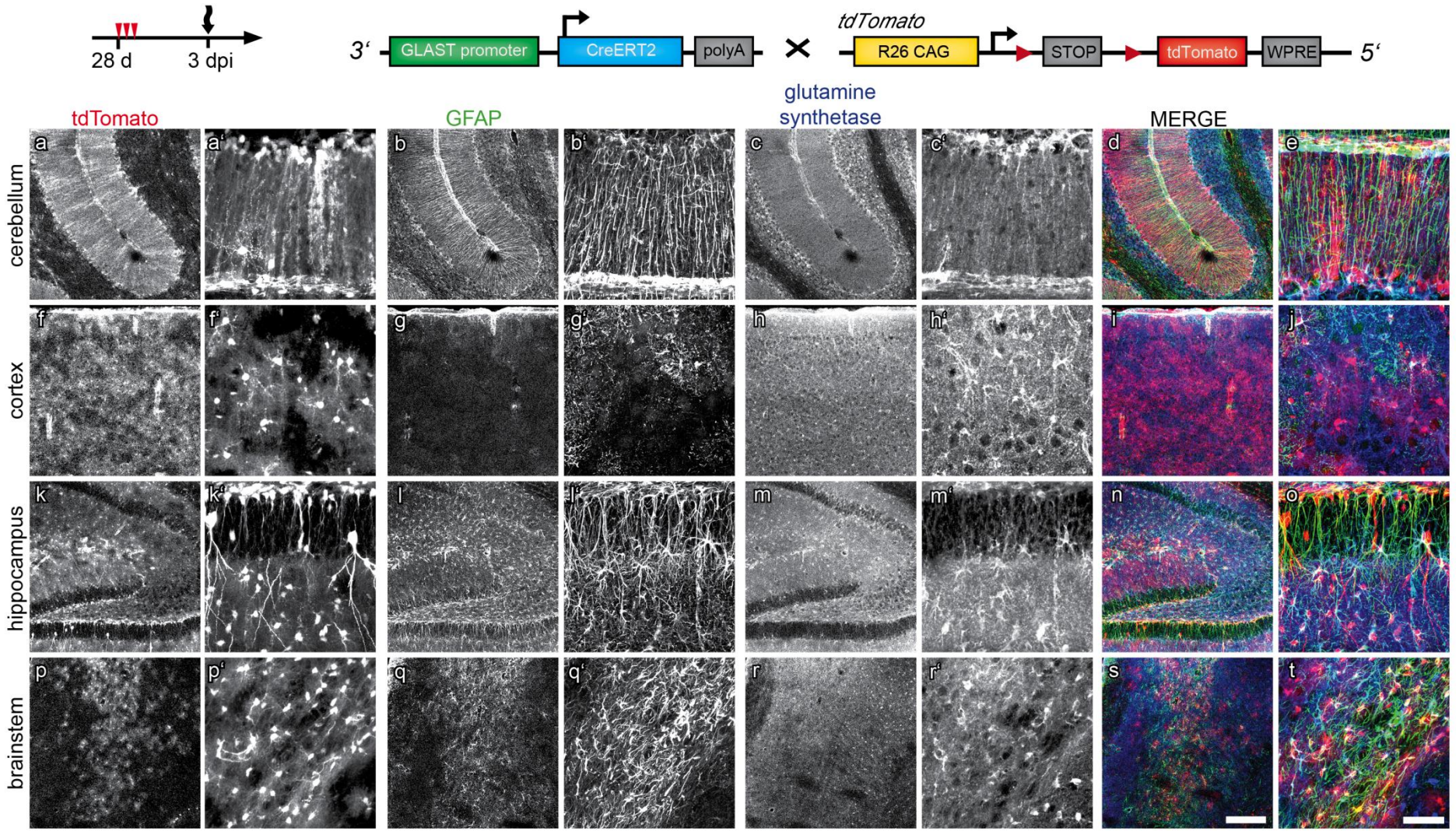

Figure 8. 2 Astroglial marker expression in tdTomato+ cells 3 days after TAM injections in young mice

Depicted are confocal images of sagittal slices of tdTomato reporter animals 3 d after TAM injections to a 4 weeks old animal (**a, a’, f, f’**, **k, k’, p, p’**). Slices were in addition stained against the astroglial marker protein GFAP (**b, b’, g, g’, l, l’, q, q’**) and GS (**c, c’, h, h’, m, m’, r, r’**). In **a-c, f-h, k-m, p-r** overview images and in **a’-c’, f’-h’, k’-m’, p’-r’** detailed confocal images of cb (**a**, **a’**-**c**, **c’**), ctx (**f**, **f’**- **h**, **h’**), hp (**k**, **k’**- **m**, **m’**) and bs (**p**, **p’** – **r**, **r’**) are shown. Based on the merge of the fluorescent signals (**d, e, i, j, n, o, s, t**) co-localization of tdTomato and GFAP or GS can be detected for each brain regions. The scale bar in (**s**) corresponds to 200 µm and applies for images (**a-c, f-h, k-m, p-r**). The bar in (**t**) correlates to 50 µm and holds for images (**a’-c’, f’-h’, k’-m’, p’-r’**).

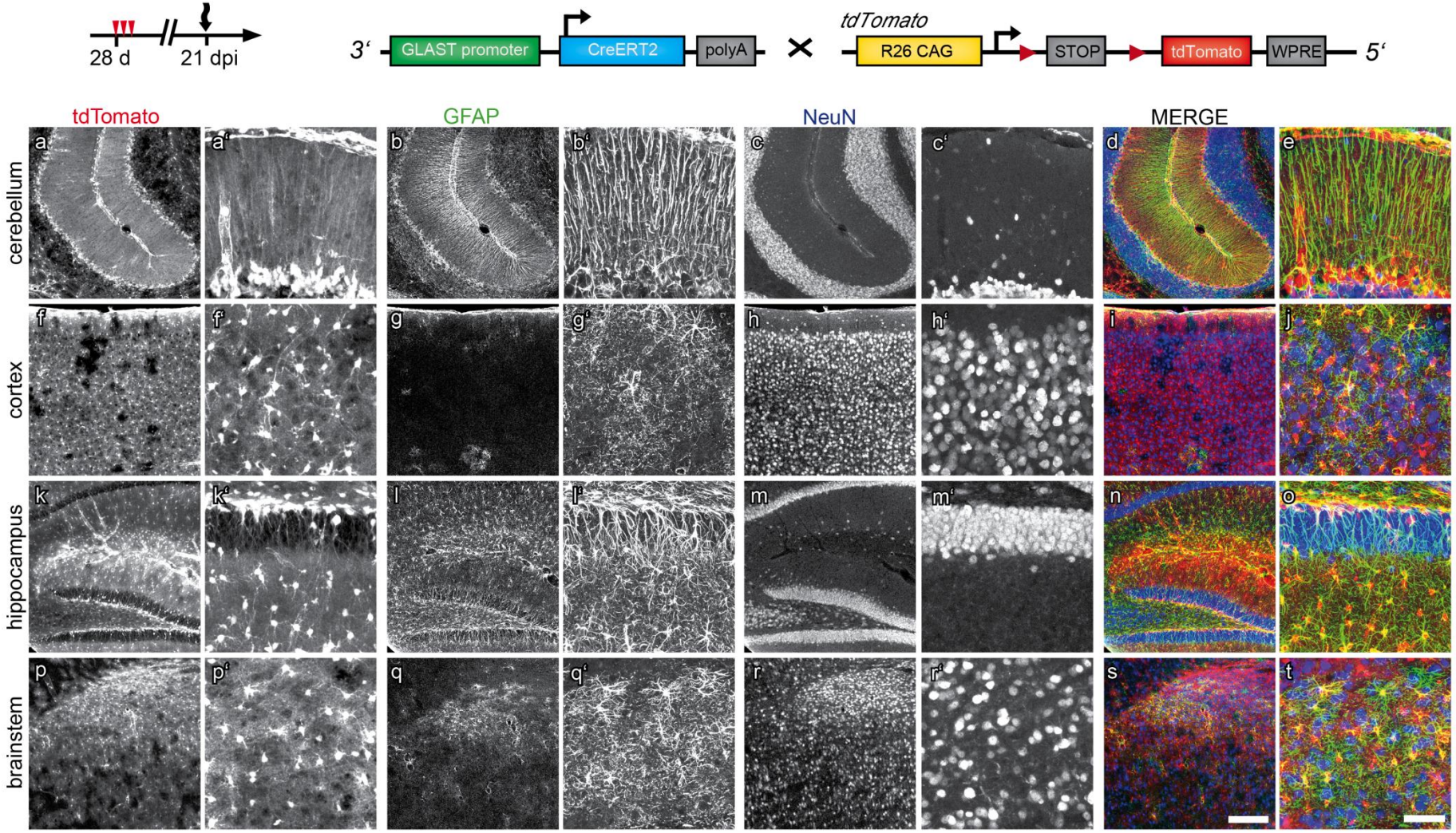

Figure 8. 3 Neuronal marker expression in tdTomato+ cells 21 days after TAM injections in young mice

Depicted are confocal images of sagittal slices of tdTomato reporter animals 21 d after TAM injections to a 4 weeks old animal (**a, a’, f, f’**, **k, k’, p, p’**). Slices were in addition stained against the astroglial marker protein GFAP (**b, b’, g, g’, l, l’, q, q’**) and the neuronal marker protein NeuN (**c, c’, h, h’, m, m’, r, r’**). In **a-c, f-h, k-m, p-r** overview images and in **a’-c’, f’-h’, k’-m’, p’-r’** detailed confocal images of cb (**a**, **a’-c**, **c’**), ctx (**f**, **f’- h**, **h’**), hp (**k**, **k’- m**, **m’**) and bs (**p**, **p’ – r**, **r’**) are shown. Based on the merge of the fluorescent signals (**d, e, i, j, n, o, s, t**) co-localization of tdTomato and GFAP can be detected for each brain regions. In contrast NeuN+ cells do not co-localize with tdTomato in cb, ctx and bs but the DG of the hp (**n**, **o**). The scale bar in (**s**) corresponds to 200 µm and applies for images (**a-c, f-h, k-m, p-r**). The bar in (**t**) correlates to 50 µm and holds for images (**a’-c’, f’-h’, k’-m’, p’-r’**).

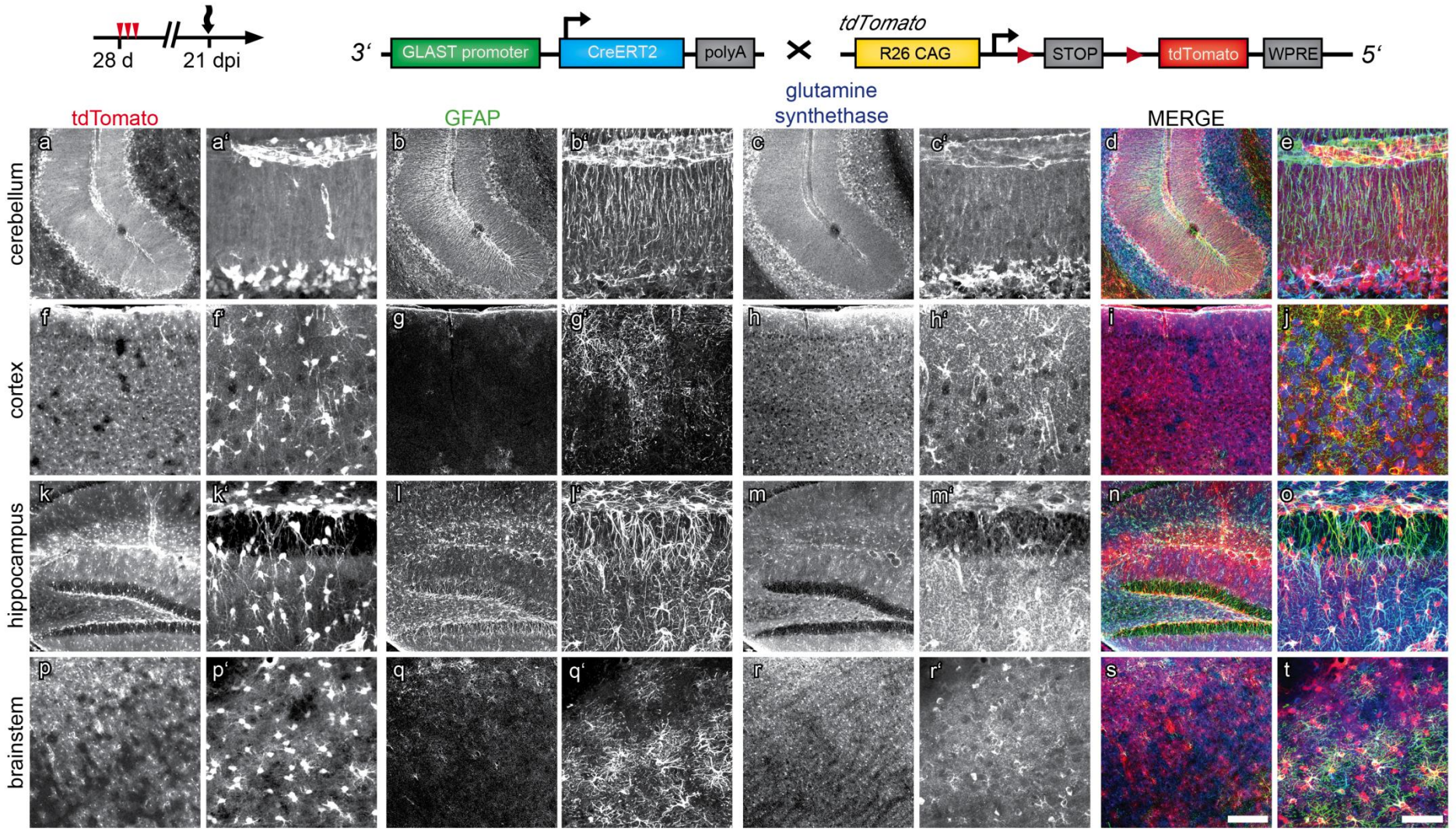

Figure 8. 4 Astroglial marker expression in tdTomato+ cells 21 days after TAM injections in young mice

Depicted are confocal images of sagittal slices of tdTomato reporter animals 21 d after TAM injections to a 4 weeks old animal (**a, a', f, f'**, **k, k', p, p'**). Slices were in addition stained against the astroglial marker protein GFAP (**b, b', g, g', l, l', q, q'**) and GS (**c, c', h, h', m, m', r, r'**). In **a-c, f-h, k-m, p-r** overview images and in **a'-c', f'-h', k'-m', p'-r'** detailed confocal images of cb (**a**, **a'-c**, **c'**), ctx (**f**, **f'- h**, **h'**), hp (**k**, **k'- m**, **m'**) and bs (**p**, **p'** – **r**, **r'**) are shown. Based on the merge of the fluorescent signals (**d, e, i, j, n, o, s, t**) co-localization of tdTomato and GFAP or GS can be detected for each brain regions. The scale bar in (**s**) corresponds to 200 µm and applies for images (**a-c, f-h, k-m, p-r**). The bar in (**t**) correlates to 50 µm and holds for images (**a'-c', f'-h', k'-m', p'-r'**).

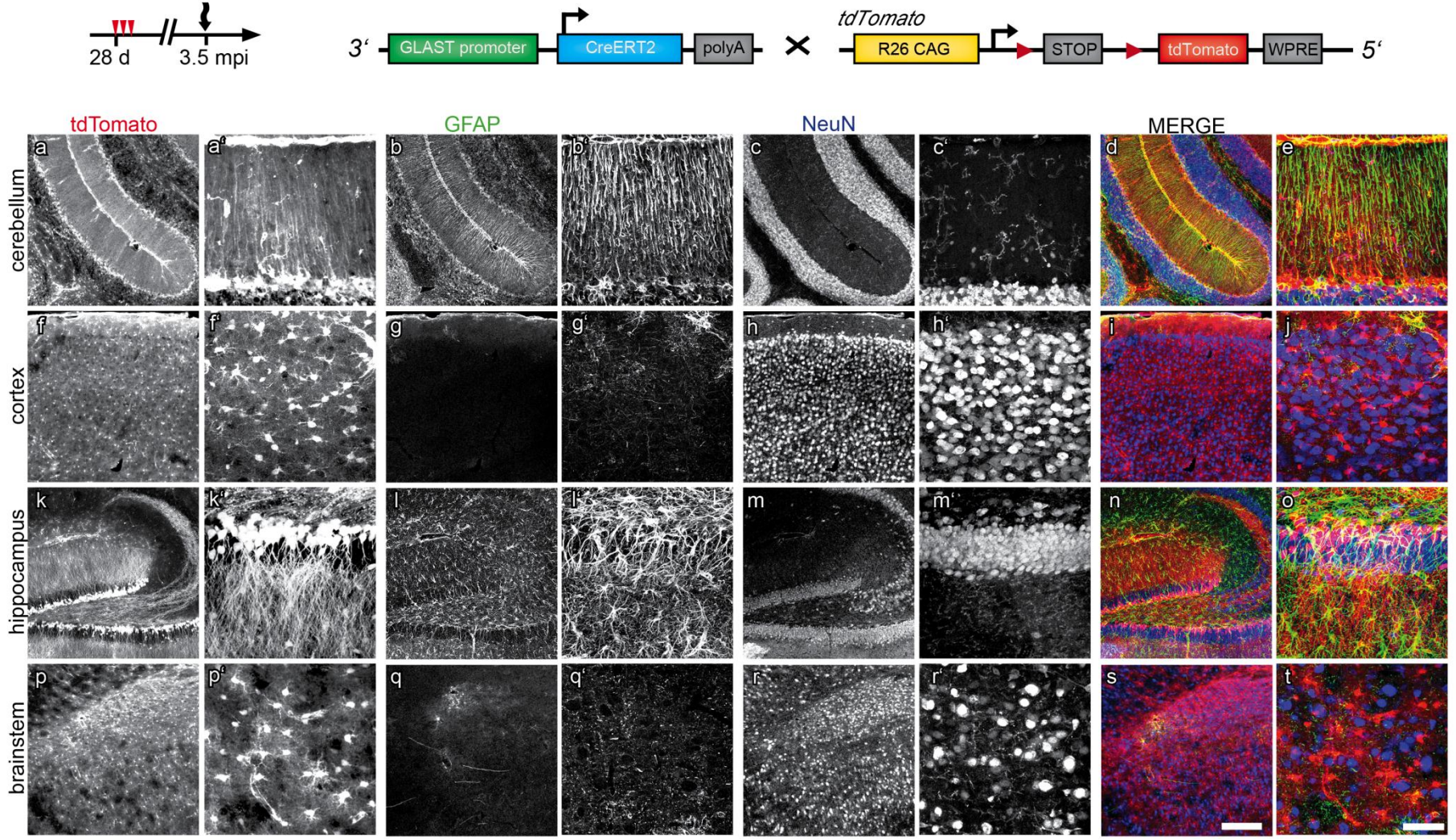

Figure 8. 5 Neuronal marker expression in tdTomato+ cells 3.5 months after TAM injections in young mice

Depicted are confocal images of sagittal slices of tdTomato reporter animals 3.5 mpi after TAM injections to a 4 weeks old animal (**a, a', f, f'**, **k, k', p, p'**). Slices were in addition stained against the astroglial marker protein GFAP (**b, b', g, g', l, l', q, q'**) and the neuronal marker protein NeuN (**c, c', h, h', m, m', r, r'**). In **a-c, f-h, k-m, p-r** overview images and in **a'-c', f'-h', k'-m', p'-r'** detailed confocal images of cb (**a**, **a'**-**c**, **c'**), ctx (**f**, **f'**- **h**, **h'**), hp (**k**, **k'**- **m**, **m'**) and bs (**p**, **p' – r**, **r'**) are shown. Based on the merge of the fluorescent signals (**d, e, i, j, n, o, s, t**) co-localization of tdTomato and GFAP can be detected for each brain regions. In contrast NeuN+ cells do not co-localize with tdTomato in cb, ctx and bs but the DG of the hp (**n**, **o**). The scale bar in **s)** corresponds to 200 µm and applies for images (**a-c, f-h, k-m, p-r**). The bar in **t)** correlates to 50 µm and holds for images (**a'-c', f'-h', k'-m', p'-r'**).

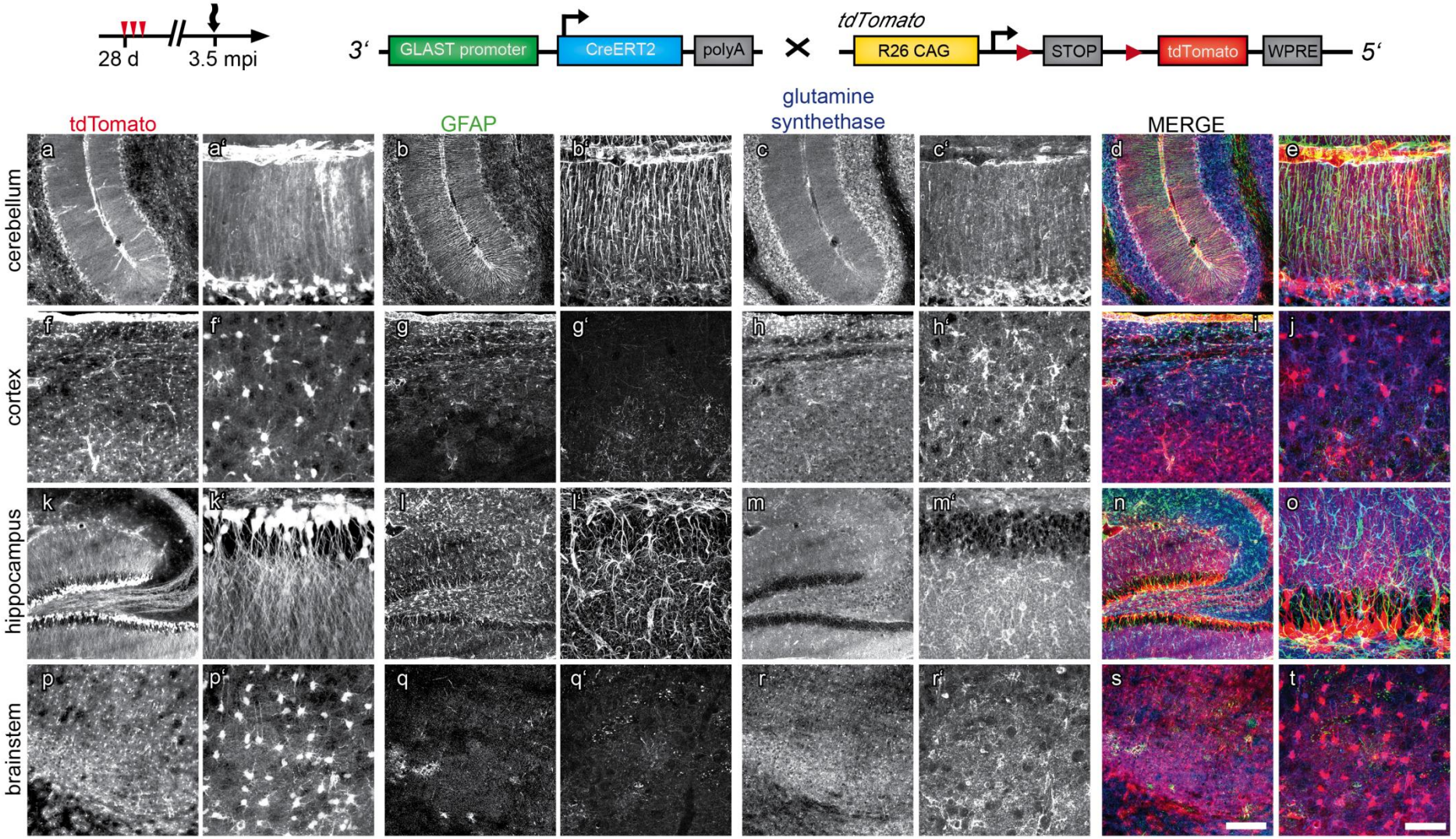

Figure 8. 6 Astroglial marker protein in tdTomato+ cells 3.5 months after TAM injections in young mice

Depicted are confocal images of sagittal slices of tdTomato reporter animals 3.5 mpi after TAM injections to a 4 weeks old animal (**a, a', f, f'**, **k, k', p, p'**). Slices were in addition stained against the astroglial marker protein GFAP (**b, b', g, g', l, l', q, q'**) and GS (**c, c', h, h', m, m', r, r'**). In **a-c, f-h, k-m, p-r** overview images and in **a'-c', f'-h', k'-m', p'-r'** detailed confocal images of cb (**a**, **a'**-**c**, **c'**), ctx (**f**, **f'**- **h**, **h'**), hp (**k**, **k'**- **m**, **m'**) and bs (**p**, **p'** – **r**, **r'**) are shown. Based on the merge of the fluorescent signals (**d, e, i, j, n, o, s, t**) co-localization of tdTomato and GFAP or GS can be detected for each brain regions. The scale bar in (**s**) corresponds to 200 µm and applies for images (**a-c, f-h, k-m, p-r**). The bar in (**t**) correlates to 50 µm and holds for images (**a'-c', f'-h', k'-m', p'-r'**).

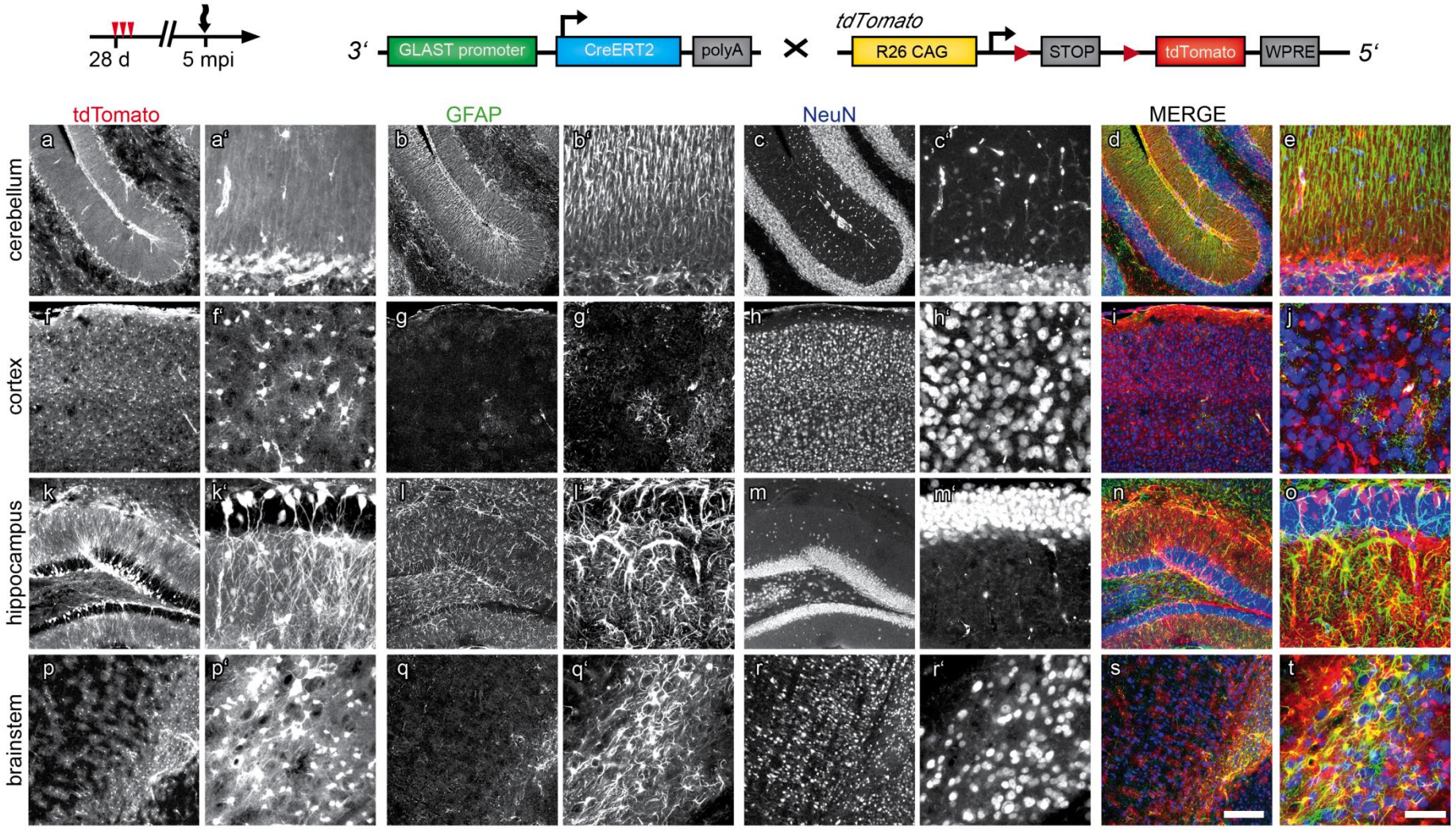

Figure 8. 7 Neuronal marker expression in tdTomato+ cells 5 months after TAM injections in young mice

Depicted are confocal images of sagittal slices of tdTomato reporter animals 5 mpi after TAM injections to a 4 weeks old animal (**a, a’, f, f’**, **k, k’, p, p’**). Slices were in addition stained against the astroglial marker protein GFAP (**b, b’, g, g’, l, l’, q, q’**) and the neuronal marker protein NeuN (**c, c’, h, h’, m, m’, r, r’**). In **a-c, f-h, k-m, p-r** overview images and in **a’-c’, f’-h’, k’-m’, p’-r’** detailed confocal images of cb (**a**, **a’**-**c**, **c’**), ctx (**f**, **f’**- **h**, **h’**), hp (**k**, **k’**- **m**, **m’**) and bs (**p**, **p’** – **r**, **r’**) are shown. Based on the merge of the fluorescent signals (**d, e, i, j, n, o, s, t**) co-localization of tdTomato and GFAP can be detected for each brain regions In contrast NeuN+ cells do not co-localize with tdTomato in cb, ctx and bs but the DG of the hp.The scale bar in (**s**) corresponds to 200 µm and applies for images (**a-c, f-h, k-m, p-r**). The bar in (**t**) correlates to 50 µm and holds for images (**a’-c’, f’-h’, k’-m’, p’-r’**).

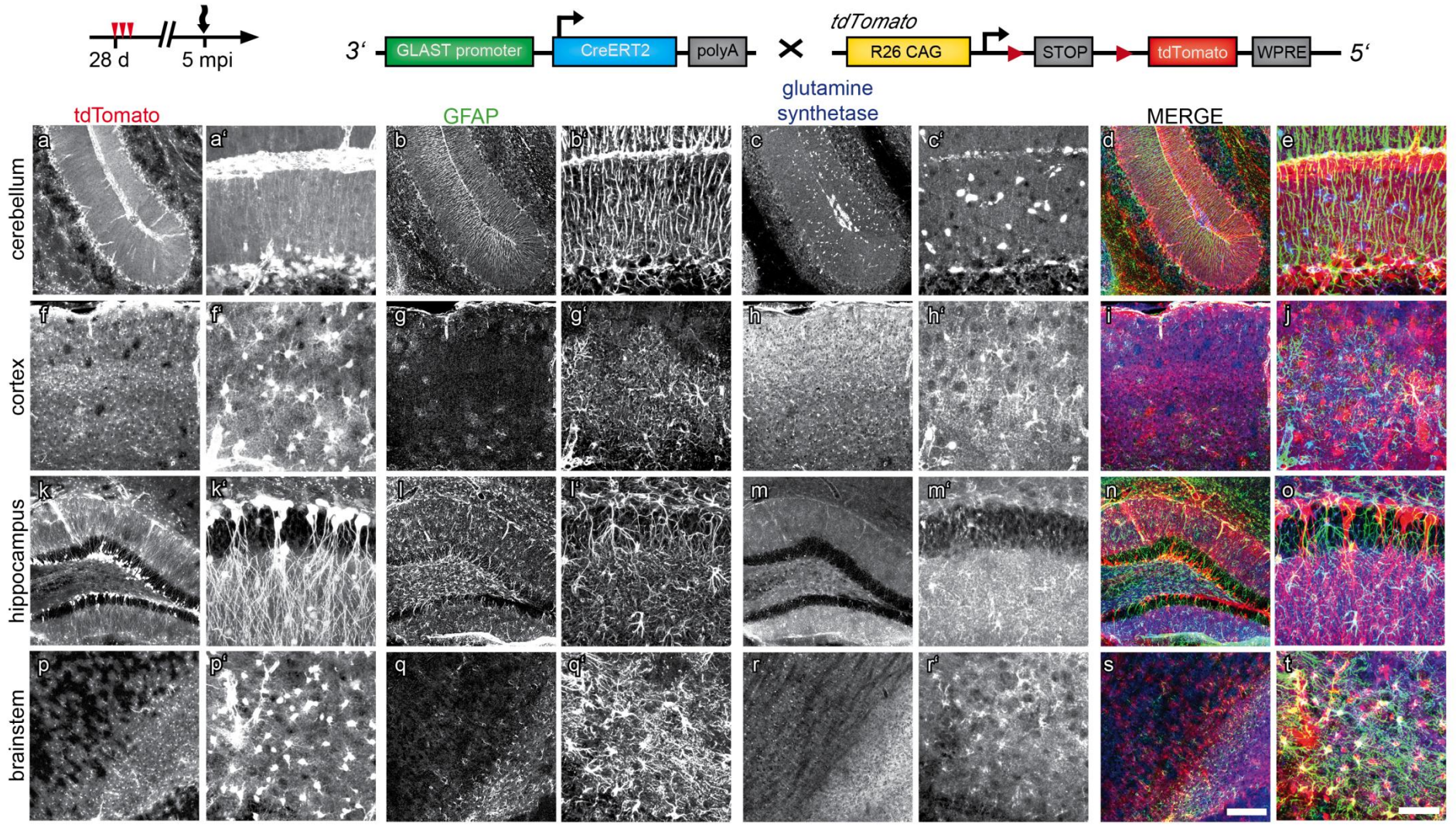

Figure 8. 8 Astroglial marker expression in tdTomato+ cells 5 months after TAM injections in young mice

Depicted are confocal images of sagittal slices of tdTomato reporter animals 5 mpi after TAM injections to a 4 weeks old animal (**a, a', f, f'**, **k, k', p, p'**). Slices were in addition stained against the astroglial marker protein GFAP (**b, b', g, g', l, l', q, q'**) and GS (**c, c', h, h', m, m', r, r'**). In **a-c, f-h, k-m, p-r** overview images and in **a'-c', f'-h', k'-m', p'-r'** detailed confocal images of cb (**a**, **a'**-**c**, **c'**), ctx (**f**, **f'**- **h**, **h'**), hp (**k**, **k'**- **m**, **m'**) and bs (**p**, **p'** – **r**, **r'**) are shown. Based on the merge of the fluorescent signals (**d, e, i, j, n, o, s, t**) co-localization of tdTomato and GFAP or GS can be detected for each brain regions. The scale bar in **s)** corresponds to 200 µm and applies for images (**a-c, f-h, k-m, p-r**). The bar in (**t**) correlates to 50 µm and holds for images (**a'-c', f'-h', k'-m', p'-r'**).

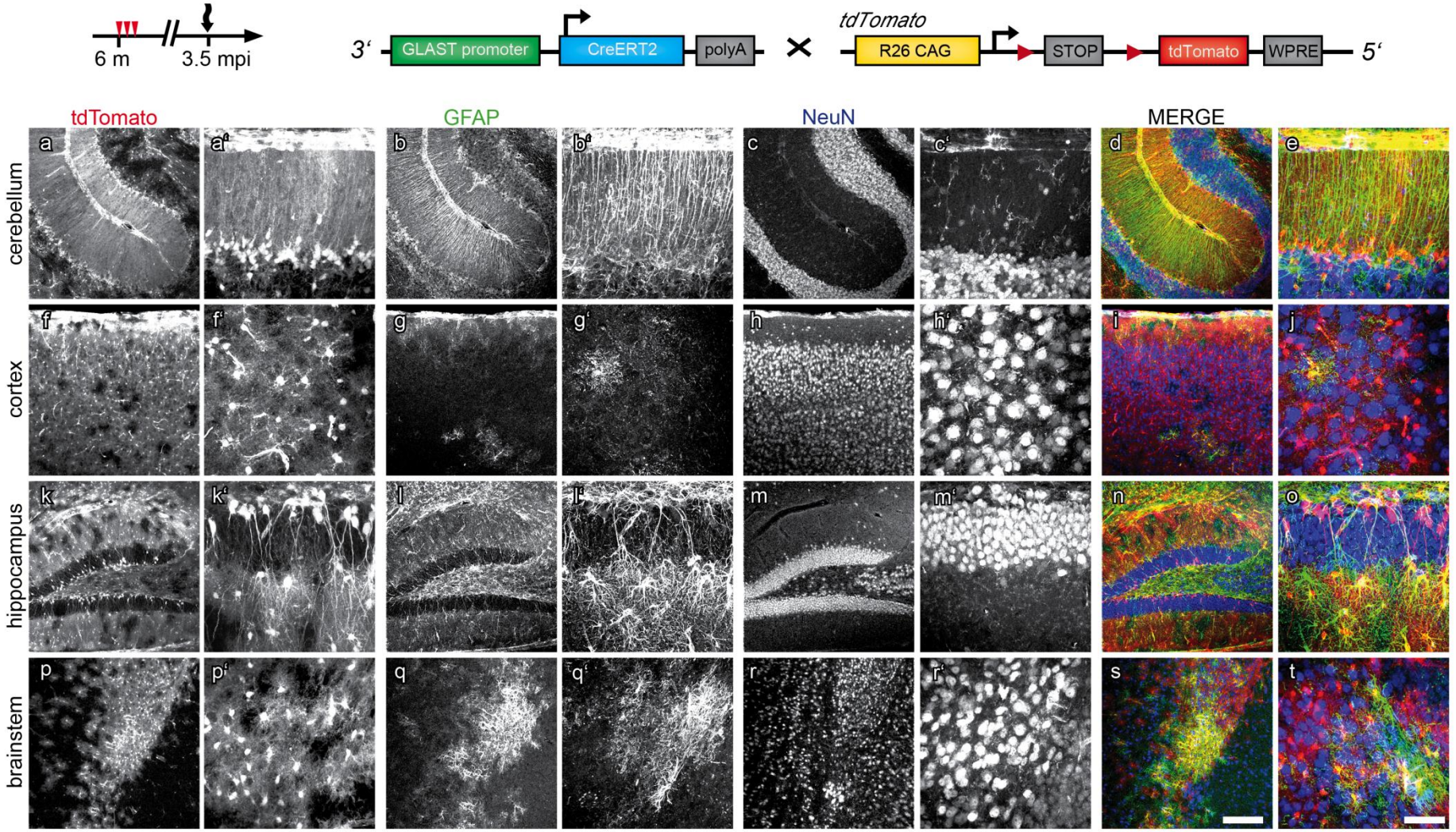

Figure 8. 9 Neuronal marker expression in tdTomato+ cells 3.5 months after TAM injections in old mice

Depicted are confocal images of sagittal slices of tdTomato reporter animals 3.5 mpi after TAM injections to a 6 months old animal (**a, a', f, f'**, **k, k', p, p'**). Slices were in addition stained against the astroglial marker protein GFAP (**b, b', g, g', l, l', q, q'**) and the neuronal marker protein NeuN (**c, c', h, h', m, m', r, r'**). In **a-c, f-h, k-m, p-r** overview images and in **a'-c', f'-h', k'-m', p'-r'** detailed confocal images of cb (**a**, **a'**-**c**, **c'**), ctx (**f**, **f'**- **h**, **h'**), hp (**k**, **k'**- **m**, **m'**) and bs (**p**, **p'** – **r**, **r'**) are shown. Based on the merge of the fluorescent signals (**d, e, i, j, n, o, s, t**) co-localization of tdTomato and GFAP can be detected for each brain regions. In contrast NeuN+ cells do not co-localize with tdTomato in cb, ctx and bs but the DG of the hp. The scale bar in (**s)** corresponds to 200 µm and applies for images (**a-c, f-h, k-m, p-r**). The bar in **t)** correlates to 50 µm and holds for images (**a'-c', f'-h', k'-m', p'-r'**).

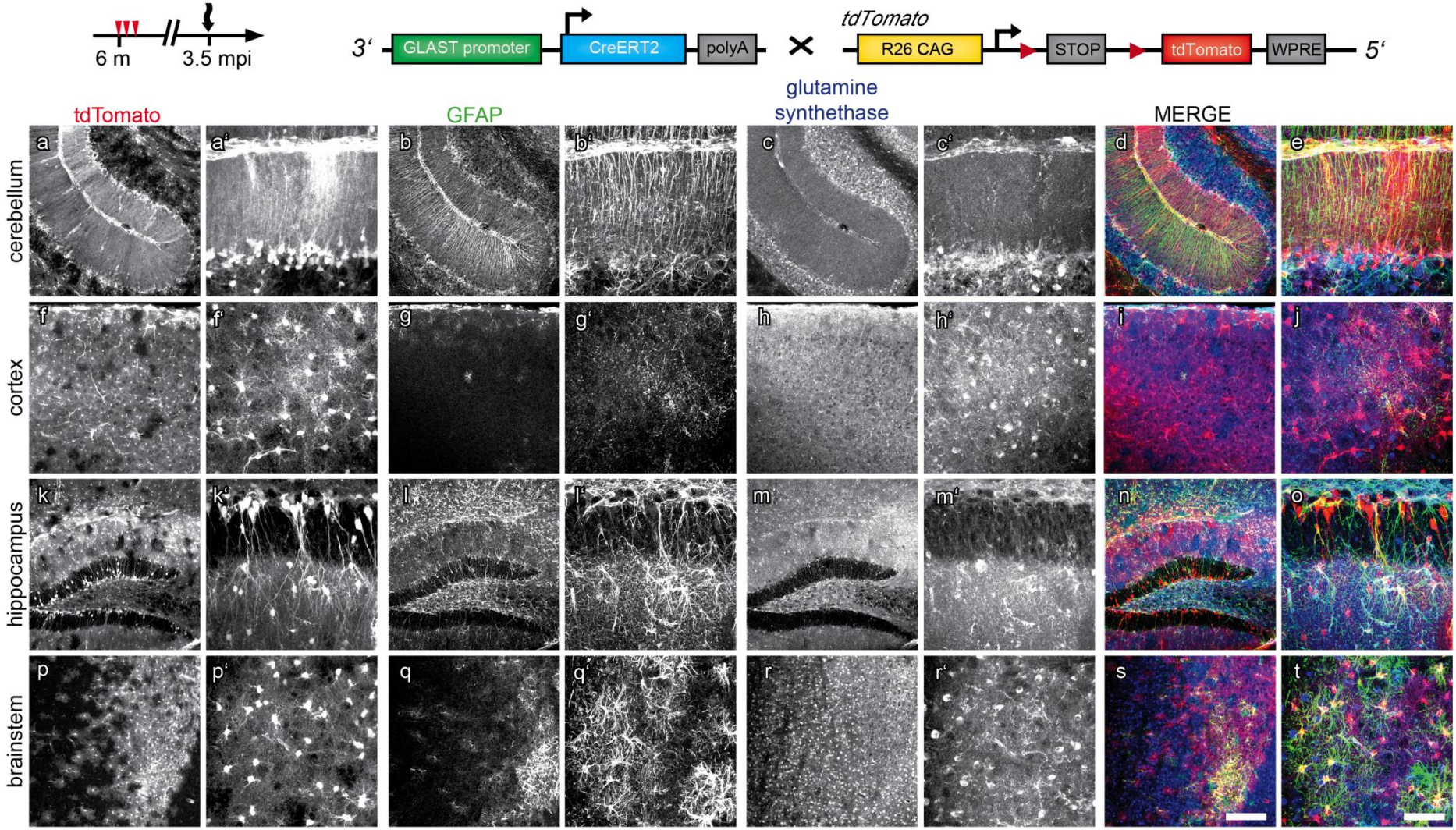

Figure 8. 10 Astroglial marker expression in tdTomato+ cells 3.5 months after TAM injections in old mice

Depicted are confocal images of sagittal slices of tdTomato reporter animals 3 days after TAM injections to a 6 months old animal (**a, a', f, f'**, **k, k', p, p'**). Slices were in addition stained against the astroglial marker protein GFAP (**b, b', g, g', l, l', q, q'**) and GS (**c, c', h, h', m, m', r, r'**). In **a-c, f-h, k-m, p-r** overview images and in **a'-c', f'-h', k'-m', p'-r'** detailed confocal images of cb (**a**, **a'**-**c**, **c'**), ctx (**f**, **f'**- **h**, **h'**), hp (**k**, **k'**- **m**, **m'**) and bs (**p**, **p'** – **r**, **r'**) are shown. Based on the merge of the fluorescent signals (**d, e, i, j, n, o, s, t**) co-localization of tdTomato and GFAP or GS can be detected for each brain regions. The scale bar in **s)** corresponds to 200 µm and applies for images (**a-c, f-h, k-m, p-r**). The bar in (**t**) correlates to 50 µm and holds for images (**a'-c', f'-h', k'-m', p'-r'**).

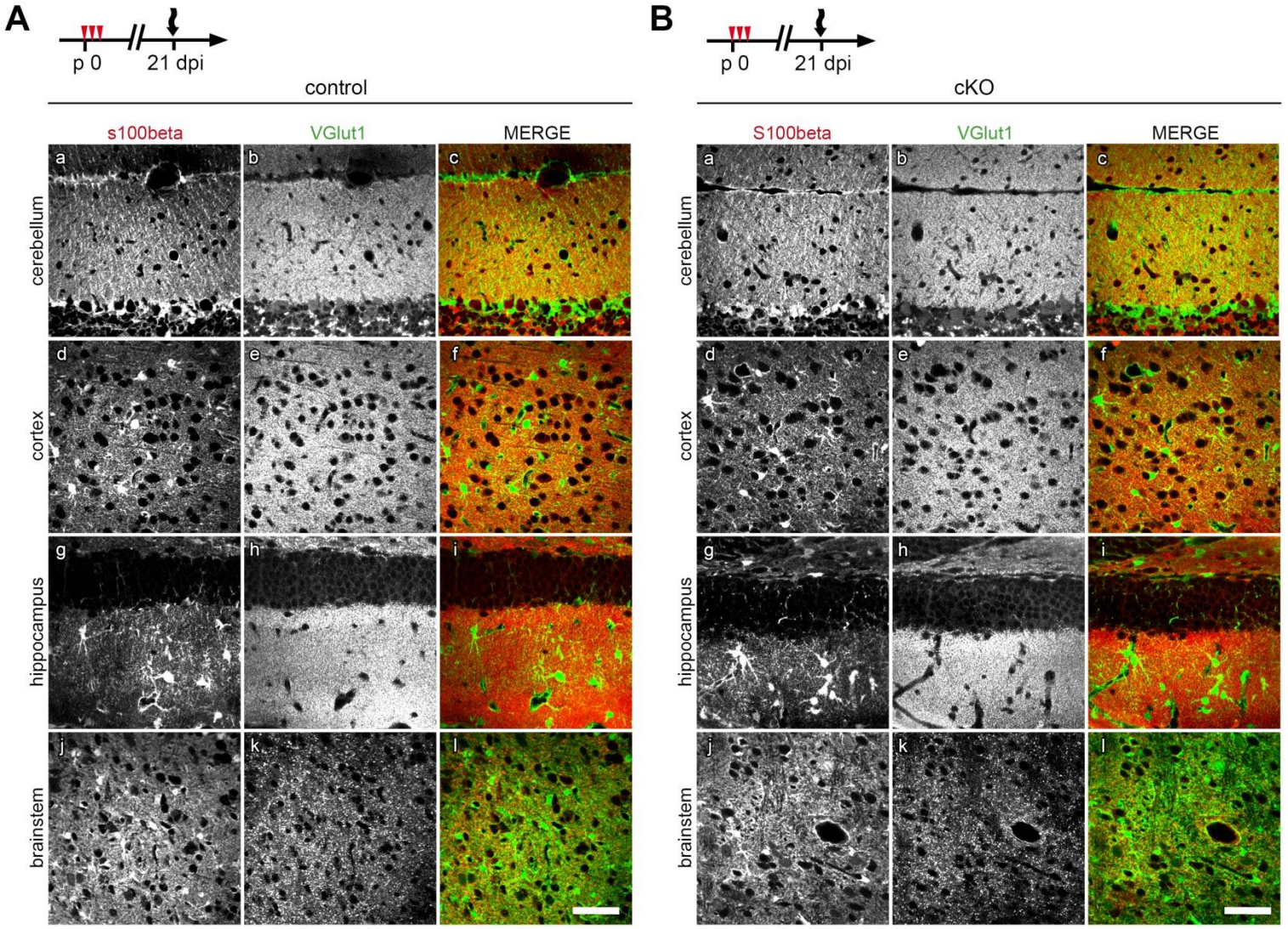

Figure 8. 11 Astroglial P2Y$_1$Rs are disposable for synapse formation

In **A** and **B** representative confocal images are depicted of control and cKO animals, respectively. The lactating mother was injected with TAM directly after birth and the pubs analyzed 21 dpi. Sagittal slices have been co-stained for S100β (**A**, **B** left panel) and VGlut1 (A, B: middle panel). The merge of both fluorescent signals is shown in the right panel. S100β and VGlut1 fluorescence intensity in the cb (**A**, **B**: **a**, **b**), ctx (**A**, **B**: **d**, **e**), hp (**A**, **B**: **g**, **h**) and bs (**A**, **B**: **i**, **k**) did not differ in control and cKO animals. The scalebar in (**i**) corresponds to 50 µm and applies for all images.

9 References

Abremski, K., R. Hoess, and N. Sternberg, 1983, Studies on the properties of P1 site-specific recombination: evidence for topologically unlinked products following recombination: Cell, v. 32, p. 1301-11.

Ahmed, Z., C. A. Lewis, and D. S. Faber, 1990, Glutamate stimulates release of Ca2+ from internal stores in astroglia: Brain Res, v. 516, p. 165-9.

Al-Hallaq, R. A., T. P. Conrads, T. D. Veenstra, and R. J. Wenthold, 2007, NMDA di-heteromeric receptor populations and associated proteins in rat hippocampus: J Neurosci, v. 27, p. 8334-43.

Amadio, S., F. Vacca, A. Martorana, G. Sancesario, and C. Volonté, 2007, P2Y1 receptor switches to neurons from glia in juvenile versus neonatal rat cerebellar cortex: BMC Dev Biol, v. 7, p. 77.

Anderson, C. M., and R. A. Swanson, 2000, Astrocyte glutamate transport: review of properties, regulation, and physiological functions: Glia, v. 32, p. 1-14.

Araque, A., G. Carmignoto, P. G. Haydon, S. H. Oliet, R. Robitaille, and A. Volterra, 2014, Gliotransmitters travel in time and space: Neuron, v. 81, p. 728-39.

Araque, A., V. Parpura, R. P. Sanzgiri, and P. G. Haydon, 1999, Tripartite synapses: glia, the unacknowledged partner: Trends Neurosci, v. 22, p. 208-15.

Bahney, J., and C. S. von Bartheld, 2014, Validation of the isotropic fractionator: comparison with unbiased stereology and DNA extraction for quantification of glial cells: J Neurosci Methods, v. 222, p. 165-74.

Bannerman, D. M., T. Bus, A. Taylor, D. J. Sanderson, I. Schwarz, V. Jensen, O. Hvalby, J. N. Rawlins, P. H. Seeburg, and R. Sprengel, 2012, Dissecting spatial knowledge from spatial choice by hippocampal NMDA receptor deletion: Nat Neurosci, v. 15, p. 1153-9.

Bardoni, R., V. L. Tawfik, D. Wang, A. François, C. Solorzano, S. A. Shuster, P. Choudhury, C. Betelli, C. Cassidy, K. Smith, J. C. de Nooij, F. Mennicken, D. O'Donnell, B. L. Kieffer, C. J. Woodbury, A. I. Basbaum, A. B. MacDermott, and G. Scherrer, 2014, Delta opioid receptors presynaptically regulate cutaneous mechanosensory neuron input to the spinal cord dorsal horn: Neuron, v. 81, p. 1312-27.

Beierlein, M., and W. G. Regehr, 2006, Brief bursts of parallel fiber activity trigger calcium signals in bergmann glia: J Neurosci, v. 26, p. 6958-67.

Berger, U. V., and M. A. Hediger, 1998, Comparative analysis of glutamate transporter expression in rat brain using differential double in situ hybridization: Anat Embryol (Berl), v. 198, p. 13-30.

Binshtok, A. M., I. A. Fleidervish, R. Sprengel, and M. J. Gutnick, 2006, NMDA receptors in layer 4 spiny stellate cells of the mouse barrel cortex contain the NR2C subunit: J Neurosci, v. 26, p. 708-15.

Boccazzi, M., C. Rolando, M. P. Abbracchio, A. Buffo, and S. Ceruti, 2014, Purines regulate adult brain subventricular zone cell functions: contribution of reactive astrocytes: Glia, v. 62, p. 428-39.

Boillée, S., K. Yamanaka, C. S. Lobsiger, N. G. Copeland, N. A. Jenkins, G. Kassiotis, G. Kollias, and D. W. Cleveland, 2006, Onset and progression in inherited ALS determined by motor neurons and microglia: Science, v. 312, p. 1389-92.

Bonfanti, L., and P. Peretto, 2007, Radial glial origin of the adult neural stem cells in the subventricular zone: Prog Neurobiol, v. 83, p. 24-36.

Borges, S., Z. Desta, L. Li, T. C. Skaar, B. A. Ward, A. Nguyen, Y. Jin, A. M. Storniolo, D. M. Nikoloff, L. Wu, G. Hillman, D. F. Hayes, V. Stearns, and D. A. Flockhart, 2006, Quantitative effect of CYP2D6 genotype and inhibitors on tamoxifen metabolism: implication for optimization of breast cancer treatment: Clin Pharmacol Ther, v. 80, p. 61-74.

Borgna, J. L., and H. Rochefort, 1981, Hydroxylated metabolites of tamoxifen are formed in vivo and bound to estrogen receptor in target tissues: J Biol Chem, v. 256, p. 859-68.

Bowser, D. N., and B. S. Khakh, 2004, ATP excites interneurons and astrocytes to increase synaptic inhibition in neuronal networks: J Neurosci, v. 24, p. 8606-20.

Bowser, D. N., and B. S. Khakh, 2007, Vesicular ATP is the predominant cause of intercellular calcium waves in astrocytes: J Gen Physiol, v. 129, p. 485-91.

Brocard, J., X. Warot, O. Wendling, N. Messaddeq, J. L. Vonesch, P. Chambon, and D. Metzger, 1997, Spatio-temporally controlled site-specific somatic mutagenesis in the mouse: Proc Natl Acad Sci U S A, v. 94, p. 14559-63.

Brothwell, S. L., J. L. Barber, D. T. Monaghan, D. E. Jane, A. J. Gibb, and S. Jones, 2008, NR2B- and NR2D-containing synaptic NMDA receptors in developing rat substantia nigra pars compacta dopaminergic neurones: J Physiol, v. 586, p. 739-50.

Burnstock, G., 2007, Purine and pyrimidine receptors: Cell Mol Life Sci, v. 64, p. 1471-83.

Bushong, E. A., M. E. Martone, Y. Z. Jones, and M. H. Ellisman, 2002, Protoplasmic astrocytes in CA1 stratum radiatum occupy separate anatomical domains: J Neurosci, v. 22, p. 183-92.

Butt, A. M., 2011, ATP: a ubiquitous gliotransmitter integrating neuron-glial networks: Semin Cell Dev Biol, v. 22, p. 205-13.

Béhé, P., P. Stern, D. J. Wyllie, M. Nassar, R. Schoepfer, and D. Colquhoun, 1995, Determination of NMDA NR1 subunit copy number in recombinant NMDA receptors: Proc Biol Sci, v. 262, p. 205-13.

Cahoy, J. D., B. Emery, A. Kaushal, L. C. Foo, J. L. Zamanian, K. S. Christopherson, Y. Xing, J. L. Lubischer, P. A. Krieg, S. A. Krupenko, W. J. Thompson, and B. A. Barres, 2008, A transcriptome database for astrocytes, neurons, and oligodendrocytes: a new resource for understanding brain development and function: J Neurosci, v. 28, p. 264-78.

Cai, Z., and H. K. Kimelberg, 1997, Glutamate receptor-mediated calcium responses in acutely isolated hippocampal astrocytes: Glia, v. 21, p. 380-9.

Caldas, C., and I. F. Tannock, 2013, Breast cancer: Tamoxifen--when more might be better: Nat Rev Clin Oncol, v. 10, p. 125-6.

Cao, X., L. P. Li, X. H. Qin, S. J. Li, M. Zhang, Q. Wang, H. H. Hu, Y. Y. Fang, Y. B. Gao, X. W. Li, L. R. Sun, W. C. Xiong, T. M. Gao, and X. H. Zhu, 2013, Astrocytic adenosine 5'-triphosphate release regulates the proliferation of neural stem cells in the adult hippocampus: Stem Cells, v. 31, p. 1633-43.

Cauli, O., R. Rodrigo, M. Llansola, C. Montoliu, P. Monfort, B. Piedrafita, N. El Mlili, J. Boix, A. Agustí, and V. Felipo, 2009, Glutamatergic and gabaergic neurotransmission and neuronal circuits in hepatic encephalopathy: Metab Brain Dis, v. 24, p. 69-80.

Chan, F., A. Bradley, T. G. Wensel, and J. H. Wilson, 2004, Knock-in human rhodopsin-GFP fusions as mouse models for human disease and targets for gene therapy: Proc Natl Acad Sci U S A, v. 101, p. 9109-14.

Charles, K. J., J. Deuchars, C. H. Davies, and M. N. Pangalos, 2003, GABA B receptor subunit expression in glia: Mol Cell Neurosci, v. 24, p. 214-23.

Charron, G., E. Doudnikoff, M. H. Canron, Q. Li, C. Véga, S. Marais, J. Baufreton, A. Vital, S. H. Oliet, and E. Bezard, 2014, Astrocytosis in parkinsonism: considering tripartite striatal synapses in physiopathology?: Front Aging Neurosci, v. 6, p. 258.

Chatterton, J. E., M. Awobuluyi, L. S. Premkumar, H. Takahashi, M. Talantova, Y. Shin, J. Cui, S. Tu, K. A. Sevarino, N. Nakanishi, G. Tong, S. A. Lipton, and D. Zhang, 2002, Excitatory glycine receptors containing the NR3 family of NMDA receptor subunits: Nature, v. 415, p. 793-8.

Chaudhry, F. A., K. P. Lehre, M. van Lookeren Campagne, O. P. Ottersen, N. C. Danbolt, and J. Storm-Mathisen, 1995, Glutamate transporters in glial plasma membranes: highly differentiated localizations revealed by quantitative ultrastructural immunocytochemistry: Neuron, v. 15, p. 711-20.

Chin, Y., M. Kishi, M. Sekino, F. Nakajo, Y. Abe, Y. Terazono, O. Hiroyuki, F. Kato, S. Koizumi, C. Gachet, and T. Hisatsune, 2013, Involvement of glial $P2Y_1$ receptors in cognitive deficit after focal cerebral stroke in a rodent model: J Neuroinflammation, v. 10, p. 95.

Choo, A. M., W. J. Miller, Y. C. Chen, P. Nibley, T. P. Patel, C. Goletiani, B. Morrison, M. K. Kutzing, B. L. Firestein, J. Y. Sul, P. G. Haydon, and D. F. Meaney, 2013, Antagonism of purinergic signalling improves recovery from traumatic brain injury: Brain, v. 136, p. 65-80.

Ciabarra, A. M., J. M. Sullivan, L. G. Gahn, G. Pecht, S. Heinemann, and K. A. Sevarino, 1995, Cloning and characterization of chi-1: a developmentally regulated member of a novel class of the ionotropic glutamate receptor family: J Neurosci, v. 15, p. 6498-508.

Coco, S., F. Calegari, E. Pravettoni, D. Pozzi, E. Taverna, P. Rosa, M. Matteoli, and C. Verderio, 2003, Storage and release of ATP from astrocytes in culture: J Biol Chem, v. 278, p. 1354-62.

Collins, E. C., R. Pannell, E. M. Simpson, A. Forster, and T. H. Rabbitts, 2000, Inter-chromosomal recombination of Mll and Af9 genes mediated by cre-loxP in mouse development: EMBO Rep, v. 1, p. 127-32.

Conti, F., P. Barbaresi, M. Melone, and A. Ducati, 1999, Neuronal and glial localization of NR1 and NR2A/B subunits of the NMDA receptor in the human cerebral cortex: Cereb Cortex, v. 9, p. 110-20.

Conti, F., S. DeBiasi, A. Minelli, and M. Melone, 1996, Expression of NR1 and NR2A/B subunits of the NMDA receptor in cortical astrocytes: Glia, v. 17, p. 254-8.

Conti, F., A. Minelli, S. DeBiasi, and M. Melone, 1997, Neuronal and glial localization of NMDA receptors in the cerebral cortex: Mol Neurobiol, v. 14, p. 1-18.

Conti, F., A. Minelli, M. Molnar, and N. C. Brecha, 1994, Cellular localization and laminar distribution of NMDAR1 mRNA in the rat cerebral cortex: J Comp Neurol, v. 343, p. 554-65.

Cull-Candy, S. G., and D. N. Leszkiewicz, 2004, Role of distinct NMDA receptor subtypes at central synapses: Sci STKE, v. 2004, p. re16.

Danbolt, N. C., J. Storm-Mathisen, and B. I. Kanner, 1992, An [Na+ + K+]coupled L-glutamate transporter purified from rat brain is located in glial cell processes: Neuroscience, v. 51, p. 295-310.

Das, S., Y. F. Sasaki, T. Rothe, L. S. Premkumar, M. Takasu, J. E. Crandall, P. Dikkes, D. A. Conner, P. V. Rayudu, W. Cheung, H. S. Chen, S. A. Lipton, and N. Nakanishi, 1998, Increased NMDA current and spine density in mice lacking the NMDA receptor subunit NR3A: Nature, v. 393, p. 377-81.

De Biase, L. M., S. H. Kang, E. G. Baxi, M. Fukaya, M. L. Pucak, M. Mishina, P. A. Calabresi, and D. E. Bergles, 2011, NMDA receptor signaling in oligodendrocyte progenitors is not required for oligodendrogenesis and myelination: J Neurosci, v. 31, p. 12650-62.

DeCarolis, N. A., M. Mechanic, D. Petrik, A. Carlton, J. L. Ables, S. Malhotra, R. Bachoo, M. Götz, D. C. Lagace, and A. J. Eisch, 2013, In vivo contribution of nestin- and GLAST-lineage cells to adult hippocampal neurogenesis: Hippocampus, v. 23, p. 708-19.

Degen, J., P. Dublin, J. Zhang, R. Dobrowolski, M. Jokwitz, K. Karram, J. Trotter, R. Jabs, K. Willecke, C. Steinhäuser, and M. Theis, 2012, Dual reporter approaches for identification of Cre efficacy and astrocyte heterogeneity: FASEB J, v. 26, p. 4576-83.

DeGregorio, M. W., E. Coronado, and C. K. Osborne, 1989, Tumor and serum tamoxifen concentrations in the athymic nude mouse: Cancer Chemother Pharmacol, v. 23, p. 68-70.

Delekate, A., M. Füchtemeier, T. Schumacher, C. Ulbrich, M. Foddis, and G. C. Petzold, 2014, Metabotropic P2Y1 receptor signalling mediates astrocytic hyperactivity in vivo in an Alzheimer's disease mouse model: Nat Commun, v. 5, p. 5422.

Desta, Z., B. A. Ward, N. V. Soukhova, and D. A. Flockhart, 2004, Comprehensive evaluation of tamoxifen sequential biotransformation by the human cytochrome P450 system in vitro: prominent roles for CYP3A and CYP2D6: J Pharmacol Exp Ther, v. 310, p. 1062-75.

Dimou, L., and M. Gotz, 2014, Glial Cells as Progenitors and Stem Cells: New Roles in the Healthy and Diseased Brain, Physiol Rev, v. 94, Copyright (c) 2014 the American Physiological Society., p. 709-737.

Dingledine, R., K. Borges, D. Bowie, and S. F. Traynelis, 1999, The glutamate receptor ion channels: Pharmacol Rev, v. 51, p. 7-61.

Domercq, M., L. Brambilla, E. Pilati, J. Marchaland, A. Volterra, and P. Bezzi, 2006, P2Y1 receptor-evoked glutamate exocytosis from astrocytes: control by tumor necrosis factor-alpha and prostaglandins: J Biol Chem, v. 281, p. 30684-96.

Dravid, S. M., A. Prakash, and S. F. Traynelis, 2008, Activation of recombinant NR1/NR2C NMDA receptors: J Physiol, v. 586, p. 4425-39.

Dzamba, D., P. Honsa, and M. Anderova, 2013, NMDA Receptors in Glial Cells: Pending Questions: Curr Neuropharmacol, v. 11, p. 250-62.

Erbs, E., L. Faget, G. Scherrer, P. Kessler, D. Hentsch, J. L. Vonesch, A. Matifas, B. L. Kieffer, and D. Massotte, 2012, Distribution of delta opioid receptor-expressing neurons in the mouse hippocampus: Neuroscience, v. 221, p. 203-13.

Erbs, E., L. Faget, G. Scherrer, A. Matifas, D. Filliol, J. L. Vonesch, M. Koch, P. Kessler, D. Hentsch, M. C. Birling, M. Koutsourakis, L. Vasseur, P. Veinante, B. L. Kieffer, and D. Massotte, 2014, A mu-delta opioid receptor brain atlas reveals neuronal co-occurrence in subcortical networks: Brain Struct Funct.

Fabre, J. E., M. Nguyen, A. Latour, J. A. Keifer, L. P. Audoly, T. M. Coffman, and B. H. Koller, 1999, Decreased platelet aggregation, increased bleeding time and resistance to thromboembolism in P2Y1-deficient mice: Nat Med, v. 5, p. 1199-202.

Faget, L., E. Erbs, J. Le Merrer, G. Scherrer, A. Matifas, N. Benturquia, F. Noble, M. Decossas, M. Koch, P. Kessler, J. L. Vonesch, Y. Schwab, B. L. Kieffer, and D. Massotte, 2012, In vivo visualization of delta opioid receptors upon physiological activation uncovers a distinct internalization profile: J Neurosci, v. 32, p. 7301-10.

Fam, S. R., C. J. Gallagher, L. V. Kalia, and M. W. Salter, 2003, Differential frequency dependence of P2Y1- and P2Y2- mediated Ca 2+ signaling in astrocytes: J Neurosci, v. 23, p. 4437-44.

Farrant, M., D. Feldmeyer, T. Takahashi, and S. G. Cull-Candy, 1994, NMDA-receptor channel diversity in the developing cerebellum: Nature, v. 368, p. 335-9.

Feil, R., J. Brocard, B. Mascrez, M. LeMeur, D. Metzger, and P. Chambon, 1996, Ligand-activated site-specific recombination in mice: Proc Natl Acad Sci U S A, v. 93, p. 10887-90.

Feil, R., J. Wagner, D. Metzger, and P. Chambon, 1997, Regulation of Cre recombinase activity by mutated estrogen receptor ligand-binding domains: Biochem Biophys Res Commun, v. 237, p. 752-7.

Feng, L., M. E. Hatten, and N. Heintz, 1994, Brain lipid-binding protein (BLBP): a novel signaling system in the developing mammalian CNS: Neuron, v. 12, p. 895-908.

Ferron, M., and J. Vacher, 2005, Targeted expression of Cre recombinase in macrophages and osteoclasts in transgenic mice: Genesis, v. 41, p. 138-45.
Fields, R. D., and G. Burnstock, 2006, Purinergic signalling in neuron-glia interactions: Nat Rev Neurosci, v. 7, p. 423-36.
Fischer, W., K. Appelt, M. Grohmann, H. Franke, W. Nörenberg, and P. Illes, 2009, Increase of intracellular Ca2+ by P2X and P2Y receptor-subtypes in cultured cortical astroglia of the rat: Neuroscience, v. 160, p. 767-83.
Flores-Soto, M. E., V. Chaparro-Huerta, M. Escoto-Delgadillo, M. E. Ureña-Guerrero, A. Camins, and C. Beas-Zarate, 2013, Receptor to glutamate NMDA-type: the functional diversity of the nr1 isoforms and pharmacological properties: Curr Pharm Des, v. 19, p. 6709-19.
Forrest, D., M. Yuzaki, H. D. Soares, L. Ng, D. C. Luk, M. Sheng, C. L. Stewart, J. I. Morgan, J. A. Connor, and T. Curran, 1994, Targeted disruption of NMDA receptor 1 gene abolishes NMDA response and results in neonatal death: Neuron, v. 13, p. 325-38.
Franke, H., and P. Illes, 2014, Nucleotide signaling in astrogliosis: Neurosci Lett, v. 565, p. 14-22.
Franke, H., H. Kittner, J. Grosche, and P. Illes, 2003, Enhanced P2Y1 receptor expression in the brain after sensitisation with d-amphetamine: Psychopharmacology (Berl), v. 167, p. 187-94.
Franke, H., U. Krügel, J. Grosche, C. Heine, W. Härtig, C. Allgaier, and P. Illes, 2004, P2Y receptor expression on astrocytes in the nucleus accumbens of rats: Neuroscience, v. 127, p. 431-41.
Franke, H., U. Krügel, R. Schmidt, J. Grosche, A. Reichenbach, and P. Illes, 2001, P2 receptor-types involved in astrogliosis in vivo: Br J Pharmacol, v. 134, p. 1180-9.
Franke, H., C. Sauer, C. Rudolph, U. Krügel, J. G. Hengstler, and P. Illes, 2009, P2 receptor-mediated stimulation of the PI3-K/Akt-pathway in vivo: Glia, v. 57, p. 1031-45.
Franke, H., A. Verkhratsky, G. Burnstock, and P. Illes, 2012, Pathophysiology of astroglial purinergic signalling: Purinergic Signal, v. 8, p. 629-57.
Fu, Y., Z. Rusznák, S. Herculano-Houzel, C. Watson, and G. Paxinos, 2013, Cellular composition characterizing postnatal development and maturation of the mouse brain and spinal cord: Brain Struct Funct, v. 218, p. 1337-54.
Fuchs, E. C., A. R. Zivkovic, M. O. Cunningham, S. Middleton, F. E. Lebeau, D. M. Bannerman, A. Rozov, M. A. Whittington, R. D. Traub, J. N. Rawlins, and H. Monyer, 2007, Recruitment of parvalbumin-positive interneurons determines hippocampal function and associated behavior: Neuron, v. 53, p. 591-604.
Fujita, T., H. Tozaki-Saitoh, and K. Inoue, 2009, P2Y1 receptor signaling enhances neuroprotection by astrocytes against oxidative stress via IL-6 release in hippocampal cultures: Glia, v. 57, p. 244-57.
Fukaya, M., A. Kato, C. Lovett, S. Tonegawa, and M. Watanabe, 2003, Retention of NMDA receptor NR2 subunits in the lumen of endoplasmic reticulum in targeted NR1 knockout mice: Proc Natl Acad Sci U S A, v. 100, p. 4855-60.
Fumagalli, M., R. Brambilla, N. D'Ambrosi, C. Volonté, M. Matteoli, C. Verderio, and M. P. Abbracchio, 2003, Nucleotide-mediated calcium signaling in rat cortical astrocytes: Role of P2X and P2Y receptors: Glia, v. 43, p. 218-03.
Funfschilling, U., L. M. Supplie, D. Mahad, S. Boretius, A. S. Saab, J. Edgar, B. G. Brinkmann, C. M. Kassmann, I. D. Tzvetanova, W. Mobius, F. Diaz, D. Meijer, U. Suter, B. Hamprecht, M. W. Sereda, C. T. Moraes, J. Frahm, S. Goebbels, and K. A. Nave, 2012, Glycolytic oligodendrocytes maintain myelin and long-term axonal integrity: Nature, v. 485, p. 517-21.
Gallagher, C. J., and M. W. Salter, 2003, Differential properties of astrocyte calcium waves mediated by P2Y1 and P2Y2 receptors: J Neurosci, v. 23, p. 6728-39.
Ghosh, K., F. Guo, and G. D. Van Duyne, 2007, Synapsis of loxP sites by Cre recombinase: J Biol Chem, v. 282, p. 24004-16.
Glasgow, N. G., B. Siegler Retchless, and J. W. Johnson, 2014, Molecular bases of NMDA receptor subtype-dependent properties: J Physiol.
Glass, M. J., D. M. Hegarty, M. Oselkin, L. Quimson, S. M. South, Q. Xu, V. M. Pickel, and C. E. Inturrisi, 2008, Conditional deletion of the NMDA-NR1 receptor subunit gene in the central nucleus of the amygdala inhibits naloxone-induced conditioned place aversion in morphine-dependent mice: Exp Neurol, v. 213, p. 57-70.
Goetz, M. P., A. Kamal, and M. M. Ames, 2008, Tamoxifen pharmacogenomics: the role of CYP2D6 as a predictor of drug response: Clin Pharmacol Ther, v. 83, p. 160-6.
Grindley, N. D., K. L. Whiteson, and P. A. Rice, 2006, Mechanisms of site-specific recombination: Annu Rev Biochem, v. 75, p. 567-605.
Gu, H., Y. R. Zou, and K. Rajewsky, 1993, Independent control of immunoglobulin switch recombination at individual switch regions evidenced through Cre-loxP-mediated gene targeting: Cell, v. 73, p. 1155-64.

Guo, F., D. N. Gopaul, and G. D. van Duyne, 1997, Structure of Cre recombinase complexed with DNA in a site-specific recombination synapse: Nature, v. 389, p. 40-6.
Guzman, S. J., H. Schmidt, H. Franke, U. Krügel, J. Eilers, P. Illes, and Z. Gerevich, 2010, P2Y1 receptors inhibit long-term depression in the prefrontal cortex: Neuropharmacology, v. 59, p. 406-15.
Haller, C., E. Casanova, M. Muller, C. M. Vacher, R. Vigot, T. Doll, S. Barbieri, M. Gassmann, and B. Bettler, 2004, Floxed allele for conditional inactivation of the GABAB(1) gene: Genesis, v. 40, p. 125-30.
Hamilton, D. L., and K. Abremski, 1984, Site-specific recombination by the bacteriophage P1 lox-Cre system. Cre-mediated synapsis of two lox sites: J Mol Biol, v. 178, p. 481-6.
Harsing, L. G., and P. Matyus, 2013, Mechanisms of glycine release, which build up synaptic and extrasynaptic glycine levels: the role of synaptic and non-synaptic glycine transporters: Brain Res Bull, v. 93, p. 110-9.
Henneberger, C., T. Papouin, S. H. Oliet, and D. A. Rusakov, 2010, Long-term potentiation depends on release of D-serine from astrocytes: Nature, v. 463, p. 232-6.
Herculano-Houzel, S., 2014, The glia/neuron ratio: how it varies uniformly across brain structures and species and what that means for brain physiology and evolution: Glia, v. 62, p. 1377-91.
Herculano-Houzel, S., and R. Lent, 2005, Isotropic fractionator: a simple, rapid method for the quantification of total cell and neuron numbers in the brain: J Neurosci, v. 25, p. 2518-21.
Hertz, L., R. Dringen, A. Schousboe, and S. R. Robinson, 1999, Astrocytes: glutamate producers for neurons: J Neurosci Res, v. 57, p. 417-28.
Hirrlinger, J., S. Hülsmann, and F. Kirchhoff, 2004, Astroglial processes show spontaneous motility at active synaptic terminals in situ: Eur J Neurosci, v. 20, p. 2235-9.
Hirrlinger, P. G., A. Scheller, C. Braun, J. Hirrlinger, and F. Kirchhoff, 2006, Temporal control of gene recombination in astrocytes by transgenic expression of the tamoxifen-inducible DNA recombinase variant CreERT2: Glia, v. 54, p. 11-20.
Hirrlinger, P. G., A. Scheller, C. Braun, M. Quintela-Schneider, B. Fuss, J. Hirrlinger, and F. Kirchhoff, 2005, Expression of reef coral fluorescent proteins in the central nervous system of transgenic mice: Mol Cell Neurosci, v. 30, p. 291-303.
Hoess, R. H., and K. Abremski, 1984, Interaction of the bacteriophage P1 recombinase Cre with the recombining site loxP: Proc Natl Acad Sci U S A, v. 81, p. 1026-9.
Hollmann, M., and S. Heinemann, 1994, Cloned glutamate receptors: Annu Rev Neurosci, v. 17, p. 31-108.
Huang, W., N. Zhao, X. Bai, K. Karram, J. Trotter, S. Goebbels, A. Scheller, and F. Kirchhoff, 2014, Novel NG2-CreERT2 knock-in mice demonstrate heterogeneous differentiation potential of NG2 glia during development: Glia, v. 62, p. 896-913.
Huh, W. J., S. S. Khurana, J. H. Geahlen, K. Kohli, R. A. Waller, and J. C. Mills, 2012, Tamoxifen induces rapid, reversible atrophy, and metaplasia in mouse stomach: Gastroenterology, v. 142, p. 21-24.e7.
Huxtable, A. G., J. D. Zwicker, T. S. Alvares, A. Ruangkittisakul, X. Fang, L. B. Hahn, E. Posse de Chaves, G. B. Baker, K. Ballanyi, and G. D. Funk, 2010, Glia contribute to the purinergic modulation of inspiratory rhythm-generating networks: J Neurosci, v. 30, p. 3947-58.
Höft, S., S. Griemsmann, G. Seifert, and C. Steinhäuser, 2014, Heterogeneity in expression of functional ionotropic glutamate and GABA receptors in astrocytes across brain regions: insights from the thalamus: Philos Trans R Soc Lond B Biol Sci, v. 369, p. 20130602.
Iino, M., K. Goto, W. Kakegawa, H. Okado, M. Sudo, S. Ishiuchi, A. Miwa, Y. Takayasu, I. Saito, K. Tsuzuki, and S. Ozawa, 2001, Glia-synapse interaction through Ca2+-permeable AMPA receptors in Bergmann glia: Science, v. 292, p. 926-9.
Indra, A. K., X. Warot, J. Brocard, J. M. Bornert, J. H. Xiao, P. Chambon, and D. Metzger, 1999, Temporally-controlled site-specific mutagenesis in the basal layer of the epidermis: comparison of the recombinase activity of the tamoxifen-inducible Cre-ER(T) and Cre-ER(T2) recombinases: Nucleic Acids Res, v. 27, p. 4324-7.
Ishii, T., K. Moriyoshi, H. Sugihara, K. Sakurada, H. Kadotani, M. Yokoi, C. Akazawa, R. Shigemoto, N. Mizuno, and M. Masu, 1993, Molecular characterization of the family of the N-methyl-D-aspartate receptor subunits: J Biol Chem, v. 268, p. 2836-43.
Jacobs, S., Z. Cui, R. Feng, H. Wang, D. Wang, and J. Z. Tsien, 2014, Molecular and genetic determinants of the NMDA receptor for superior learning and memory functions: PLoS One, v. 9, p. e111865.
Jiang, R., M. D. Haustein, M. V. Sofroniew, and B. S. Khakh, 2014, Imaging Intracellular Ca2+ Signals in Striatal Astrocytes from Adult Mice Using Genetically-encoded Calcium Indicators: J Vis Exp.

John, G. R., E. Scemes, S. O. Suadicani, J. S. Liu, P. C. Charles, S. C. Lee, D. C. Spray, and C. F. Brosnan, 1999, IL-1beta differentially regulates calcium wave propagation between primary human fetal astrocytes via pathways involving P2 receptors and gap junction channels: Proc Natl Acad Sci U S A, v. 96, p. 11613-8.

Johnson, M. D., H. Zuo, K. H. Lee, J. P. Trebley, J. M. Rae, R. V. Weatherman, Z. Desta, D. A. Flockhart, and T. C. Skaar, 2004, Pharmacological characterization of 4-hydroxy-N-desmethyl tamoxifen, a novel active metabolite of tamoxifen: Breast Cancer Res Treat, v. 85, p. 151-9.

Jordan, V. C., and K. E. Allen, 1980, Evaluation of the antitumour activity of the non-steroidal antioestrogen monohydroxytamoxifen in the DMBA-induced rat mammary carcinoma model: Eur J Cancer, v. 16, p. 239-51.

Jordan, V. C., M. M. Collins, L. Rowsby, and G. Prestwich, 1977, A monohydroxylated metabolite of tamoxifen with potent antioestrogenic activity: J Endocrinol, v. 75, p. 305-16.

Jourdain, P., L. H. Bergersen, K. Bhaukaurally, P. Bezzi, M. Santello, M. Domercq, C. Matute, F. Tonello, V. Gundersen, and A. Volterra, 2007, Glutamate exocytosis from astrocytes controls synaptic strength: Nat Neurosci, v. 10, p. 331-9.

Jung, S., J. Aliberti, P. Graemmel, M. J. Sunshine, G. W. Kreutzberg, A. Sher, and D. R. Littman, 2000, Analysis of fractalkine receptor CX(3)CR1 function by targeted deletion and green fluorescent protein reporter gene insertion: Mol Cell Biol, v. 20, p. 4106-14.

Jungblut, M., M. C. Tiveron, S. Barral, B. Abrahamsen, S. Knöbel, S. Pennartz, J. Schmitz, M. Perraut, F. W. Pfrieger, W. Stoffel, H. Cremer, and A. Bosio, 2012, Isolation and characterization of living primary astroglial cells using the new GLAST-specific monoclonal antibody ACSA-1: Glia, v. 60, p. 894-907.

Kallal, L., and J. L. Benovic, 2000, Using green fluorescent proteins to study G-protein-coupled receptor localization and trafficking: Trends Pharmacol Sci, v. 21, p. 175-80.

Karakas, E., N. Simorowski, and H. Furukawa, 2011, Subunit arrangement and phenylethanolamine binding in GluN1/GluN2B NMDA receptors: Nature, v. 475, p. 249-53.

Kawamura, M., C. Gachet, K. Inoue, and F. Kato, 2004, Direct excitation of inhibitory interneurons by extracellular ATP mediated by P2Y1 receptors in the hippocampal slice: J Neurosci, v. 24, p. 10835-45.

Kettenmann, H., F. Kirchhoff, and A. Verkhratsky, 2013, Microglia: new roles for the synaptic stripper: Neuron, v. 77, p. 10-8.

Kimelberg, H. K., 2010, Functions of mature mammalian astrocytes: a current view: Neuroscientist, v. 16, p. 79-106.

Kirischuk, S., T. Möller, N. Voitenko, H. Kettenmann, and A. Verkhratsky, 1995, ATP-induced cytoplasmic calcium mobilization in Bergmann glial cells: J Neurosci, v. 15, p. 7861-71.

Kirischuk, S., V. Parpura, and A. Verkhratsky, 2012, Sodium dynamics: another key to astroglial excitability?: Trends Neurosci, v. 35, p. 497-506.

Kisanga, E. R., J. Gjerde, J. Schjøtt, G. Mellgren, and E. A. Lien, 2003, Tamoxifen administration and metabolism in nude mice and nude rats: J Steroid Biochem Mol Biol, v. 84, p. 361-7.

Kiyotani, K., T. Mushiroda, Y. Nakamura, and H. Zembutsu, 2012, Pharmacogenomics of tamoxifen: roles of drug metabolizing enzymes and transporters: Drug Metab Pharmacokinet, v. 27, p. 122-31.

Koch, H. P., and H. P. Larsson, 2005, Small-scale molecular motions accomplish glutamate uptake in human glutamate transporters: J Neurosci, v. 25, p. 1730-6.

Koike, H., K. Horie, H. Fukuyama, G. Kondoh, S. Nagata, and J. Takeda, 2002, Efficient biallelic mutagenesis with Cre/loxP-mediated inter-chromosomal recombination: EMBO Rep, v. 3, p. 433-7.

Kriegstein, A., and A. Alvarez-Buylla, 2009, The glial nature of embryonic and adult neural stem cells: Annu Rev Neurosci, v. 32, p. 149-84.

Kuboyama, K., H. Harada, H. Tozaki-Saitoh, M. Tsuda, K. Ushijima, and K. Inoue, 2011, Astrocytic P2Y(1) receptor is involved in the regulation of cytokine/chemokine transcription and cerebral damage in a rat model of cerebral ischemia: J Cereb Blood Flow Metab, v. 31, p. 1930-41.

Kurtz, A., A. Zimmer, F. Schnütgen, G. Brüning, F. Spener, and T. Müller, 1994, The expression pattern of a novel gene encoding brain-fatty acid binding protein correlates with neuronal and glial cell development: Development, v. 120, p. 2637-49.

Lai, T. W., S. Zhang, and Y. T. Wang, 2014, Excitotoxicity and stroke: identifying novel targets for neuroprotection: Prog Neurobiol, v. 115, p. 157-88.

Lalo, U., O. Palygin, R. A. North, A. Verkhratsky, and Y. Pankratov, 2011a, Age-dependent remodelling of ionotropic signalling in cortical astroglia: Aging Cell, v. 10, p. 392-402.

Lalo, U., Y. Pankratov, F. Kirchhoff, R. A. North, and A. Verkhratsky, 2006, NMDA receptors mediate neuron-to-glia signaling in mouse cortical astrocytes: J Neurosci, v. 26, p. 2673-83.

Lalo, U., Y. Pankratov, V. Parpura, and A. Verkhratsky, 2011b, Ionotropic receptors in neuronal-astroglial signalling: what is the role of "excitable" molecules in non-excitable cells: Biochim Biophys Acta, v. 1813, p. 992-1002.

Lappe-Siefke, C., S. Goebbels, M. Gravel, E. Nicksch, J. Lee, P. E. Braun, I. R. Griffiths, and K. A. Nave, 2003, Disruption of Cnp1 uncouples oligodendroglial functions in axonal support and myelination: Nat Genet, v. 33, p. 366-74.

Latour, I., C. E. Gee, R. Robitaille, and J. C. Lacaille, 2001, Differential mechanisms of Ca2+ responses in glial cells evoked by exogenous and endogenous glutamate in rat hippocampus: Hippocampus, v. 11, p. 132-45.

Lecca, D., S. Ceruti, M. Fumagalli, and M. P. Abbracchio, 2012, Purinergic trophic signalling in glial cells: functional effects and modulation of cell proliferation, differentiation, and death: Purinergic Signal, v. 8, p. 539-57.

Lee, C. H., W. Lü, J. C. Michel, A. Goehring, J. Du, X. Song, and E. Gouaux, 2014, NMDA receptor structures reveal subunit arrangement and pore architecture: Nature, v. 511, p. 191-7.

Lee, M. C., K. K. Ting, S. Adams, B. J. Brew, R. Chung, and G. J. Guillemin, 2010, Characterisation of the expression of NMDA receptors in human astrocytes: PLoS One, v. 5, p. e14123.

Lee, Y., B. M. Morrison, Y. Li, S. Lengacher, M. H. Farah, P. N. Hoffman, Y. Liu, A. Tsingalia, L. Jin, P. W. Zhang, L. Pellerin, P. J. Magistretti, and J. D. Rothstein, 2012, Oligodendroglia metabolically support axons and contribute to neurodegeneration: Nature, v. 487, p. 443-8.

Lehre, K. P., L. M. Levy, O. P. Ottersen, J. Storm-Mathisen, and N. C. Danbolt, 1995, Differential expression of two glial glutamate transporters in the rat brain: quantitative and immunocytochemical observations: J Neurosci, v. 15, p. 1835-53.

Leon, C., B. Hechler, M. Freund, A. Eckly, C. Vial, P. Ohlmann, A. Dierich, M. LeMeur, J. P. Cazenave, and C. Gachet, 1999, Defective platelet aggregation and increased resistance to thrombosis in purinergic P2Y(1) receptor-null mice: J Clin Invest, v. 104, p. 1731-7.

Leone, D. P., S. Genoud, S. Atanasoski, R. Grausenburger, P. Berger, D. Metzger, W. B. Macklin, P. Chambon, and U. Suter, 2003, Tamoxifen-inducible glia-specific Cre mice for somatic mutagenesis in oligodendrocytes and Schwann cells: Mol Cell Neurosci, v. 22, p. 430-40.

Lewandoski, M., 2001, Conditional control of gene expression in the mouse: Nat Rev Genet, v. 2, p. 743-55.

Lien, E. A., E. Solheim, and P. M. Ueland, 1991a, Distribution of tamoxifen and its metabolites in rat and human tissues during steady-state treatment: Cancer Res, v. 51, p. 4837-44.

Lien, E. A., K. Wester, P. E. Lønning, E. Solheim, and P. M. Ueland, 1991b, Distribution of tamoxifen and metabolites into brain tissue and brain metastases in breast cancer patients: Br J Cancer, v. 63, p. 641-5.

Lim, D., V. Ronco, A. A. Grolla, A. Verkhratsky, and A. A. Genazzani, 2014, Glial calcium signalling in Alzheimer's disease: Rev Physiol Biochem Pharmacol, v. 167, p. 45-65.

Lipton, S. A., 2006, NMDA receptors, glial cells, and clinical medicine: Neuron, v. 50, p. 9-11.

Liu, J., S. G. Willet, E. D. Bankaitis, Y. Xu, C. V. Wright, and G. Gu, 2013, Non-parallel recombination limits Cre-LoxP-based reporters as precise indicators of conditional genetic manipulation: Genesis, v. 51, p. 436-42.

Lohr, C., A. Grosche, A. Reichenbach, and D. Hirnet, 2014, Purinergic neuron-glia interactions in sensory systems: Pflugers Arch, v. 466, p. 1859-72.

Long, M. A., and F. M. Rossi, 2009, Silencing inhibits Cre-mediated recombination of the Z/AP and Z/EG reporters in adult cells: PLoS One, v. 4, p. e5435.

Lorier, A. R., J. Lipski, G. D. Housley, J. J. Greer, and G. D. Funk, 2008, ATP sensitivity of preBötzinger complex neurones in neonatal rat in vitro: mechanism underlying a P2 receptor-mediated increase in inspiratory frequency: J Physiol, v. 586, p. 1429-46.

Lovatt, D., U. Sonnewald, H. S. Waagepetersen, A. Schousboe, W. He, J. H. Lin, X. Han, T. Takano, S. Wang, F. J. Sim, S. A. Goldman, and M. Nedergaard, 2007a, The transcriptome and metabolic gene signature of protoplasmic astrocytes in the adult murine cortex: J Neurosci, v. 27, p. 12255-66.

Lovatt, D., U. Sonnewald, H. S. Waagepetersen, A. Schousboe, W. He, J. H.-C. Lin, X. Han, T. Takano, S. Wang, F. J. Sim, S. A. Goldman, and M. Nedergaard, 2007b, The Transcriptome and Metabolic Gene Signature of Protoplasmic Astrocytes in the Adult Murine Cortex.

Löfgren, S., A. L. Hagbjörk, S. Ekman, R. Fransson-Steen, and Y. Terelius, 2004, Metabolism of human cytochrome P450 marker substrates in mouse: a strain and gender comparison: Xenobiotica, v. 34, p. 811-34.

Mack, A., B. Sauer, K. Abremski, and R. Hoess, 1992, Stoichiometry of the Cre recombinase bound to the lox recombining site: Nucleic Acids Res, v. 20, p. 4451-5.

Madisen, L., T. A. Zwingman, S. M. Sunkin, S. W. Oh, H. A. Zariwala, H. Gu, L. L. Ng, R. D. Palmiter, M. J. Hawrylycz, A. R. Jones, E. S. Lein, and H. Zeng, 2010, A robust and high-throughput

Cre reporting and characterization system for the whole mouse brain: Nat Neurosci, v. 13, p. 133-40.
Madlensky, L., L. Natarajan, S. Tchu, M. Pu, J. Mortimer, S. W. Flatt, D. M. Nikoloff, G. Hillman, M. R. Fontecha, H. J. Lawrence, B. A. Parker, A. H. Wu, and J. P. Pierce, 2011, Tamoxifen metabolite concentrations, CYP2D6 genotype, and breast cancer outcomes: Clin Pharmacol Ther, v. 89, p. 718-25.
Magistretti, P. J., 2006, Neuron-glia metabolic coupling and plasticity: J Exp Biol, v. 209, p. 2304-11.
Magistretti, P. J., 2009, Role of glutamate in neuron-glia metabolic coupling: Am J Clin Nutr, v. 90, p. 875S-880S.
Mahgoub, A., J. R. Idle, L. G. Dring, R. Lancaster, and R. L. Smith, 1977, Polymorphic hydroxylation of Debrisoquine in man: Lancet, v. 2, p. 584-6.
Maragakis, N. J., and J. D. Rothstein, 2004, Glutamate transporters: animal models to neurologic disease: Neurobiol Dis, v. 15, p. 461-73.
Masubuchi, Y., T. Iwasa, S. Hosokawa, T. Suzuki, T. Horie, S. Imaoka, Y. Funae, and S. Narimatsu, 1997, Selective deficiency of debrisoquine 4-hydroxylase activity in mouse liver microsomes: J Pharmacol Exp Ther, v. 282, p. 1435-41.
Matthias, K., F. Kirchhoff, G. Seifert, K. Hüttmann, M. Matyash, H. Kettenmann, and C. Steinhäuser, 2003, Segregated expression of AMPA-type glutamate receptors and glutamate transporters defines distinct astrocyte populations in the mouse hippocampus: J Neurosci, v. 23, p. 1750-8.
McHugh, T. J., K. I. Blum, J. Z. Tsien, S. Tonegawa, and M. A. Wilson, 1996, Impaired hippocampal representation of space in CA1-specific NMDAR1 knockout mice: Cell, v. 87, p. 1339-49.
McIlhinney, R. A., E. Philipps, B. Le Bourdelles, S. Grimwood, K. Wafford, S. Sandhu, and P. Whiting, 2003, Assembly of N-methyl-D-aspartate (NMDA) receptors: Biochem Soc Trans, v. 31, p. 865-8.
McLaughlin, L. A., L. J. Dickmann, C. R. Wolf, and C. J. Henderson, 2008, Functional expression and comparative characterization of nine murine cytochromes P450 by fluorescent inhibition screening: Drug Metab Dispos, v. 36, p. 1322-31.
Metzger, D., and P. Chambon, 2001, Site- and time-specific gene targeting in the mouse: Methods, v. 24, p. 71-80.
Metzger, D., J. Clifford, H. Chiba, and P. Chambon, 1995, Conditional site-specific recombination in mammalian cells using a ligand-dependent chimeric Cre recombinase: Proc Natl Acad Sci U S A, v. 92, p. 6991-5.
Meyers, E. N., M. Lewandoski, and G. R. Martin, 1998, An Fgf8 mutant allelic series generated by Cre- and Flp-mediated recombination: Nat Genet, v. 18, p. 136-41.
Michel, M. C., T. Wieland, and G. Tsujimoto, 2009, How reliable are G-protein-coupled receptor antibodies?: Naunyn Schmiedebergs Arch Pharmacol, v. 379, p. 385-8.
Monyer, H., R. Sprengel, R. Schoepfer, A. Herb, M. Higuchi, H. Lomeli, N. Burnashev, B. Sakmann, and P. H. Seeburg, 1992, Heteromeric NMDA receptors: molecular and functional distinction of subtypes: Science, v. 256, p. 1217-21.
Moore, D., J. Chambers, H. Waldvogel, R. Faull, and P. Emson, 2000, Regional and cellular distribution of the P2Y(1) purinergic receptor in the human brain: striking neuronal localisation: J Comp Neurol, v. 421, p. 374-84.
Mori, T., K. Tanaka, A. Buffo, W. Wurst, R. Kuhn, and M. Gotz, 2006, Inducible gene deletion in astroglia and radial glia--a valuable tool for functional and lineage analysis: Glia, v. 54, p. 21-34.
Moriyoshi, K., M. Masu, T. Ishii, R. Shigemoto, N. Mizuno, and S. Nakanishi, 1991, Molecular cloning and characterization of the rat NMDA receptor: Nature, v. 354, p. 31-7.
Morán-Jiménez, M. J., and C. Matute, 2000, Immunohistochemical localization of the P2Y(1) purinergic receptor in neurons and glial cells of the central nervous system: Brain Res Mol Brain Res, v. 78, p. 50-8.
Müller, T., J. Grosche, C. Ohlemeyer, and H. Kettenmann, 1993, NMDA-activated currents in Bergmann glial cells: Neuroreport, v. 4, p. 671-4.
Mürdter, T. E., W. Schroth, L. Bacchus-Gerybadze, S. Winter, G. Heinkele, W. Simon, P. A. Fasching, T. Fehm, M. Eichelbaum, M. Schwab, H. Brauch, and G. T. a. A. C. Group, 2011, Activity levels of tamoxifen metabolites at the estrogen receptor and the impact of genetic polymorphisms of phase I and II enzymes on their concentration levels in plasma: Clin Pharmacol Ther, v. 89, p. 708-17.
Nagy, A., C. Moens, E. Ivanyi, J. Pawling, M. Gertsenstein, A. K. Hadjantonakis, M. Pirity, and J. Rossant, 1998, Dissecting the role of N-myc in development using a single targeting vector to generate a series of alleles: Curr Biol, v. 8, p. 661-4.
Nakazawa, K., T. J. McHugh, M. A. Wilson, and S. Tonegawa, 2004, NMDA receptors, place cells and hippocampal spatial memory: Nat Rev Neurosci, v. 5, p. 361-72.

Nebert, D. W., R. A. McKinnon, and A. Puga, 1996, Human drug-metabolizing enzyme polymorphisms: effects on risk of toxicity and cancer: DNA Cell Biol, v. 15, p. 273-80.
Neves, G., S. F. Cooke, and T. V. Bliss, 2008, Synaptic plasticity, memory and the hippocampus: a neural network approach to causality: Nat Rev Neurosci, v. 9, p. 65-75.
Newbold, R. R., W. N. Jefferson, E. Padilla-Burgos, and B. C. Bullock, 1997, Uterine carcinoma in mice treated neonatally with tamoxifen: Carcinogenesis, v. 18, p. 2293-8.
Nishizaki, T., T. Matsuoka, T. Nomura, T. Kondoh, N. Tamaki, and Y. Okada, 1999, Store Ca2+ depletion enhances NMDA responses in cultured human astrocytes: Biochem Biophys Res Commun, v. 259, p. 661-4.
Noguchi, Y., Y. Shinozaki, K. Fujishita, K. Shibata, Y. Imura, Y. Morizawa, C. Gachet, and S. Koizumi, 2013, Astrocytes protect neurons against methylmercury via ATP/P2Y(1) receptor-mediated pathways in astrocytes: PLoS One, v. 8, p. e57898.
Nolte, C., M. Matyash, T. Pivneva, C. G. Schipke, C. Ohlemeyer, U. K. Hanisch, F. Kirchhoff, and H. Kettenmann, 2001, GFAP promoter-controlled EGFP-expressing transgenic mice: a tool to visualize astrocytes and astrogliosis in living brain tissue: Glia, v. 33, p. 72-86.
Obara-Michlewska, M., J. Ruszkiewicz, M. Zielińska, A. Verkhratsky, and J. Albrecht, 2014, Astroglial NMDA receptors inhibit expression of Kir4.1 channels in glutamate-overexposed astrocytes in vitro and in the brain of rats with acute liver failure: Neurochem Int.
Oka, M., M. Wada, Q. Wu, A. Yamamoto, and T. Fujita, 2006, Functional expression of metabotropic GABAB receptors in primary cultures of astrocytes from rat cerebral cortex: Biochem Biophys Res Commun, v. 341, p. 874-81.
Oliet, S. H., and J. P. Mothet, 2009, Regulation of N-methyl-D-aspartate receptors by astrocytic D-serine: Neuroscience, v. 158, p. 275-83.
Orellana, J. A., and J. Stehberg, 2014, Hemichannels: new roles in astroglial function: Front Physiol, v. 5, p. 193.
Orre, M., W. Kamphuis, L. M. Osborn, J. Melief, L. Kooijman, I. Huitinga, J. Klooster, K. Bossers, and E. M. Hol, 2014, Acute isolation and transcriptome characterization of cortical astrocytes and microglia from young and aged mice: Neurobiol Aging, v. 35, p. 1-14.
Pachernegg, S., N. Strutz-Seebohm, and M. Hollmann, 2012, GluN3 subunit-containing NMDA receptors: not just one-trick ponies: Trends Neurosci, v. 35, p. 240-9.
Palygin, O., U. Lalo, and Y. Pankratov, 2011, Distinct pharmacological and functional properties of NMDA receptors in mouse cortical astrocytes: Br J Pharmacol, v. 163, p. 1755-66.
Palygin, O., U. Lalo, A. Verkhratsky, and Y. Pankratov, 2010, Ionotropic NMDA and P2X1/5 receptors mediate synaptically induced Ca2+ signalling in cortical astrocytes: Cell Calcium, v. 48, p. 225-31.
Panatier, A., D. T. Theodosis, J. P. Mothet, B. Touquet, L. Pollegioni, D. A. Poulain, and S. H. Oliet, 2006, Glia-derived D-serine controls NMDA receptor activity and synaptic memory: Cell, v. 125, p. 775-84.
Paoletti, P., C. Bellone, and Q. Zhou, 2013, NMDA receptor subunit diversity: impact on receptor properties, synaptic plasticity and disease: Nat Rev Neurosci, v. 14, p. 383-400.
Papouin, T., L. Ladépêche, J. Ruel, S. Sacchi, M. Labasque, M. Hanini, L. Groc, L. Pollegioni, J. P. Mothet, and S. H. Oliet, 2012, Synaptic and extrasynaptic NMDA receptors are gated by different endogenous coagonists: Cell, v. 150, p. 633-46.
Parsons, M. P., and L. A. Raymond, 2014, Extrasynaptic NMDA receptor involvement in central nervous system disorders: Neuron, v. 82, p. 279-93.
Pascual, O., S. Ben Achour, P. Rostaing, A. Triller, and A. Bessis, 2012, Microglia activation triggers astrocyte-mediated modulation of excitatory neurotransmission: Proc Natl Acad Sci U S A, v. 109, p. E197-205.
Paukert, M., A. Agarwal, J. Cha, V. A. Doze, J. U. Kang, and D. E. Bergles, 2014, Norepinephrine controls astroglial responsiveness to local circuit activity: Neuron, v. 82, p. 1263-70.
Pellerin, L., A. K. Bouzier-Sore, A. Aubert, S. Serres, M. Merle, R. Costalat, and P. J. Magistretti, 2007, Activity-dependent regulation of energy metabolism by astrocytes: an update: Glia, v. 55, p. 1251-62.
Pellerin, L., and P. J. Magistretti, 1994, Glutamate uptake into astrocytes stimulates aerobic glycolysis: a mechanism coupling neuronal activity to glucose utilization: Proc Natl Acad Sci U S A, v. 91, p. 10625-9.
Perea, G., M. Navarrete, and A. Araque, 2009, Tripartite synapses: astrocytes process and control synaptic information: Trends Neurosci, v. 32, p. 421-31.
Perez-Alvarez, A., and A. Araque, 2013, Astrocyte-neuron interaction at tripartite synapses: Curr Drug Targets, v. 14, p. 1220-4.

Perez-Alvarez, A., M. Navarrete, A. Covelo, E. D. Martin, and A. Araque, 2014, Structural and functional plasticity of astrocyte processes and dendritic spine interactions: J Neurosci, v. 34, p. 12738-44.

Piet, R., and C. E. Jahr, 2007, Glutamatergic and purinergic receptor-mediated calcium transients in Bergmann glial cells: J Neurosci, v. 27, p. 4027-35.

Pilli, J., and S. S. Kumar, 2012, Triheteromeric N-methyl-D-aspartate receptors differentiate synaptic inputs onto pyramidal neurons in somatosensory cortex: involvement of the GluN3A subunit: Neuroscience, v. 222, p. 75-88.

Pinheiro, A. R., D. Paramos-de-Carvalho, M. Certal, M. A. Costa, C. Costa, M. T. Magalhães-Cardoso, F. Ferreirinha, J. Sévigny, and P. Correia-de-Sá, 2013, Histamine induces ATP release from human subcutaneous fibroblasts, via pannexin-1 hemichannels, leading to Ca2+ mobilization and cell proliferation: J Biol Chem, v. 288, p. 27571-83.

Piña-Crespo, J. C., M. Talantova, I. Micu, B. States, H. S. Chen, S. Tu, N. Nakanishi, G. Tong, D. Zhang, S. F. Heinemann, G. W. Zamponi, P. K. Stys, and S. A. Lipton, 2010, Excitatory glycine responses of CNS myelin mediated by NR1/NR3 "NMDA" receptor subunits: J Neurosci, v. 30, p. 11501-5.

Platel, J. C., V. Gordon, T. Heintz, and A. Bordey, 2009, GFAP-GFP neural progenitors are antigenically homogeneous and anchored in their enclosed mosaic niche: Glia, v. 57, p. 66-78.

Pradhan, A. A., J. A. Becker, G. Scherrer, P. Tryoen-Toth, D. Filliol, A. Matifas, D. Massotte, C. Gavériaux-Ruff, and B. L. Kieffer, 2009, In vivo delta opioid receptor internalization controls behavioral effects of agonists: PLoS One, v. 4, p. e5425.

Qian, A., A. L. Buller, and J. W. Johnson, 2005, NR2 subunit-dependence of NMDA receptor channel block by external Mg2+: J Physiol, v. 562, p. 319-31.

Qian, A., and J. W. Johnson, 2006, Permeant ion effects on external Mg2+ block of NR1/2D NMDA receptors: J Neurosci, v. 26, p. 10899-910.

Rajewsky, K., H. Gu, R. Kühn, U. A. Betz, W. Müller, J. Roes, and F. Schwenk, 1996, Conditional gene targeting: J Clin Invest, v. 98, p. 600-3.

Regan, M. R., Y. H. Huang, Y. S. Kim, M. I. Dykes-Hoberg, L. Jin, A. M. Watkins, D. E. Bergles, and J. D. Rothstein, 2007, Variations in promoter activity reveal a differential expression and physiology of glutamate transporters by glia in the developing and mature CNS: J Neurosci, v. 27, p. 6607-19.

Reichenbach, A., A. Derouiche, and F. Kirchhoff, 2010, Morphology and dynamics of perisynaptic glia: Brain Research Reviews, v. 63, p. 11-25.

Reid, J. M., M. P. Goetz, S. A. Buhrow, C. Walden, S. L. Safgren, M. J. Kuffel, K. E. Reinicke, V. Suman, P. Haluska, X. Hou, and M. M. Ames, 2014, Pharmacokinetics of endoxifen and tamoxifen in female mice: implications for comparative in vivo activity studies: Cancer Chemother Pharmacol, v. 74, p. 1271-8.

Reinert, R. B., J. Kantz, A. A. Misfeldt, G. Poffenberger, M. Gannon, M. Brissova, and A. C. Powers, 2012, Tamoxifen-Induced Cre-loxP Recombination Is Prolonged in Pancreatic Islets of Adult Mice: PLoS One, v. 7, p. e33529.

Requardt, R. P., L. Kaczmarczyk, P. Dublin, A. Wallraff-Beck, T. Mikeska, J. Degen, A. Waha, C. Steinhäuser, K. Willecke, and M. Theis, 2009, Quality control of astrocyte-directed Cre transgenic mice: the benefits of a direct link between loss of gene expression and reporter activation: Glia, v. 57, p. 680-92.

Robertson, D. W., J. A. Katzenellenbogen, D. J. Long, E. A. Rorke, and B. S. Katzenellenbogen, 1982, Tamoxifen antiestrogens. A comparison of the activity, pharmacokinetics, and metabolic activation of the cis and trans isomers of tamoxifen: J Steroid Biochem, v. 16, p. 1-13.

Robinson, S. P., S. M. Langan-Fahey, D. A. Johnson, and V. C. Jordan, 1991, Metabolites, pharmacodynamics, and pharmacokinetics of tamoxifen in rats and mice compared to the breast cancer patient: Drug Metab Dispos, v. 19, p. 36-43.

Robinson, S. P., S. M. Langan-Fahey, and V. C. Jordan, 1989, Implications of tamoxifen metabolism in the athymic mouse for the study of antitumor effects upon human breast cancer xenografts: Eur J Cancer Clin Oncol, v. 25, p. 1769-76.

Rose, C. F., A. Verkhratsky, and V. Parpura, 2013, Astrocyte glutamine synthetase: pivotal in health and disease: Biochem Soc Trans, v. 41, p. 1518-24.

Rose, C. R., and C. Karus, 2013, Two sides of the same coin: sodium homeostasis and signaling in astrocytes under physiological and pathophysiological conditions: Glia, v. 61, p. 1191-205.

Rose, E. M., J. C. Koo, J. E. Antflick, S. M. Ahmed, S. Angers, and D. R. Hampson, 2009, Glutamate transporter coupling to Na,K-ATPase: J Neurosci, v. 29, p. 8143-55.

Rothstein, J. D., L. Martin, A. I. Levey, M. Dykes-Hoberg, L. Jin, D. Wu, N. Nash, and R. W. Kuncl, 1994, Localization of neuronal and glial glutamate transporters: Neuron, v. 13, p. 713-25.

Rudolph, Ramona: Phd Thesis "Purinerge und glutameterge Modulation von inhibitorischen synaptischen Eingängen an Purkinje-Neuronen im Kleinhirn der Maus. Universität Kaiserslautern

Saab, A. S., A. Neumeyer, H. M. Jahn, A. Cupido, A. A. Šimek, H. J. Boele, A. Scheller, K. Le Meur, M. Götz, H. Monyer, R. Sprengel, M. E. Rubio, J. W. Deitmer, C. I. De Zeeuw, and F. Kirchhoff, 2012, Bergmann glial AMPA receptors are required for fine motor coordination: Science, v. 337, p. 749-53.

Saab, A. S., I. D. Tzvetanova, and K. A. Nave, 2013, The role of myelin and oligodendrocytes in axonal energy metabolism: Curr Opin Neurobiol, v. 23, p. 1065-72.

Saab, A. S., Tzvetavona I. D., Selva B., Trevisiol A., Dibaj P., Möbius W., Kusch K., Goetze B., Jahn H. M., Huang W., Steffens H., Schomburg E. D., Pérez-Samartín A., Pérez-Cerdá F., Bakhtiari D., Matute C., Löwel S., Griesinger C., Hirrlinger J., Kirchhoff F. and Nave K. A. (2015): Oligodendroglial NMDA receptors regulate axonal energy metabolism. (Research article, in preparation)

Sakamoto, M., R. Kageyama, and I. Imayoshi, 2014, The functional significance of newly born neurons integrated into olfactory bulb circuits: Front Neurosci, v. 8, p. 121.

Sakry, D., K. Karram, and J. Trotter, 2011, Synapses between NG2 glia and neurons: J Anat, v. 219, p. 2-7.

Santello, M., P. Bezzi, and A. Volterra, 2011, TNFα controls glutamatergic gliotransmission in the hippocampal dentate gyrus: Neuron, v. 69, p. 988-1001.

Santiago, M. F., and E. Scemes, 2012, Neuroblast migration and P2Y(1) receptor mediated calcium signalling depend on 9-O-acetyl GD3 ganglioside: ASN Neuro, v. 4, p. 357-69.

Sanz-Clemente, A., R. A. Nicoll, and K. W. Roche, 2013, Diversity in NMDA receptor composition: many regulators, many consequences: Neuroscientist, v. 19, p. 62-75.

Sauer, B., and N. Henderson, 1989, Cre-stimulated recombination at loxP-containing DNA sequences placed into the mammalian genome: Nucleic Acids Res, v. 17, p. 147-61.

Scherrer, G., N. Imamachi, Y. Q. Cao, C. Contet, F. Mennicken, D. O'Donnell, B. L. Kieffer, and A. I. Basbaum, 2009, Dissociation of the opioid receptor mechanisms that control mechanical and heat pain: Cell, v. 137, p. 1148-59.

Scherrer, G., P. Tryoen-Tóth, D. Filliol, A. Matifas, D. Laustriat, Y. Q. Cao, A. I. Basbaum, A. Dierich, J. L. Vonesh, C. Gavériaux-Ruff, and B. L. Kieffer, 2006, Knockin mice expressing fluorescent delta-opioid receptors uncover G protein-coupled receptor dynamics in vivo: Proc Natl Acad Sci U S A, v. 103, p. 9691-6.

Schipke, C. G., C. Ohlemeyer, M. Matyash, C. Nolte, H. Kettenmann, and F. Kirchhoff, 2001, Astrocytes of the mouse neocortex express functional N-methyl-D-aspartate receptors: FASEB J, v. 15, p. 1270-2.

Schmid, R. S., Y. Yokota, and E. S. Anton, 2006, Generation and characterization of brain lipid-binding protein promoter-based transgenic mouse models for the study of radial glia: Glia, v. 53, p. 345-51.

Schwenk, F., U. Baron, and K. Rajewsky, 1995, A cre-transgenic mouse strain for the ubiquitous deletion of loxP-flanked gene segments including deletion in germ cells: Nucleic Acids Res, v. 23, p. 5080-1.

Schwenk, F., R. Kuhn, P. O. Angrand, K. Rajewsky, and A. F. Stewart, 1998, Temporally and spatially regulated somatic mutagenesis in mice: Nucleic Acids Res, v. 26, p. 1427-32.

Seibler, J., B. Zevnik, B. Küter-Luks, S. Andreas, H. Kern, T. Hennek, A. Rode, C. Heimann, N. Faust, G. Kauselmann, M. Schoor, R. Jaenisch, K. Rajewsky, R. Kühn, and F. Schwenk, 2003, Rapid generation of inducible mouse mutants: Nucleic Acids Res, v. 31, p. e12.

Seifert, G., and C. Steinhäuser, 1995, Glial cells in the mouse hippocampus express AMPA receptors with an intermediate Ca2+ permeability: Eur J Neurosci, v. 7, p. 1872-81.

Seifert, R., A. Strasser, E. H. Schneider, D. Neumann, S. Dove, and A. Buschauer, 2013, Molecular and cellular analysis of human histamine receptor subtypes: Trends Pharmacol Sci, v. 34, p. 33-58.

Sellers, L. A., J. Simon, T. S. Lundahl, D. J. Cousens, P. P. Humphrey, and E. A. Barnard, 2001, Adenosine nucleotides acting at the human P2Y1 receptor stimulate mitogen-activated protein kinases and induce apoptosis: J Biol Chem, v. 276, p. 16379-90.

Shaner, N. C., G. H. Patterson, and M. W. Davidson, 2007, Advances in fluorescent protein technology: J Cell Sci, v. 120, p. 4247-60.

Shao, Y., and K. D. McCarthy, 1997, Responses of Bergmann glia and granule neurons in situ to N-methyl-D-aspartate, norepinephrine, and high potassium: J Neurochem, v. 68, p. 2405-11.

Sheldon, A. L., and M. B. Robinson, 2007, The role of glutamate transporters in neurodegenerative diseases and potential opportunities for intervention: Neurochem Int, v. 51, p. 333-55.

Shelton, M. K., and K. D. McCarthy, 1999, Mature hippocampal astrocytes exhibit functional metabotropic and ionotropic glutamate receptors in situ: Glia, v. 26, p. 1-11.
Shimizu, E., Y. P. Tang, C. Rampon, and J. Z. Tsien, 2000, NMDA receptor-dependent synaptic reinforcement as a crucial process for memory consolidation: Science, v. 290, p. 1170-4.
Shinozaki, Y., M. Nomura, K. Iwatsuki, Y. Moriyama, C. Gachet, and S. Koizumi, 2014, Microglia trigger astrocyte-mediated neuroprotection via purinergic gliotransmission: Sci Rep, v. 4, p. 4329.
Single, F. N., A. Rozov, N. Burnashev, F. Zimmermann, D. F. Hanley, D. Forrest, T. Curran, V. Jensen, O. Hvalby, R. Sprengel, and P. H. Seeburg, 2000, Dysfunctions in mice by NMDA receptor point mutations NR1(N598Q) and NR1(N598R): J Neurosci, v. 20, p. 2558-66.
Siow, N. L., R. C. Choi, H. Q. Xie, L. W. Kong, G. K. Chu, G. K. Chan, J. Simon, E. A. Barnard, and K. W. Tsim, 2010, ATP induces synaptic gene expressions in cortical neurons: transduction and transcription control via P2Y1 receptors: Mol Pharmacol, v. 78, p. 1059-71.
Sofroniew, M. V., 2005, Reactive astrocytes in neural repair and protection: Neuroscientist, v. 11, p. 400-7.
Sofroniew, M. V., 2009, Molecular dissection of reactive astrogliosis and glial scar formation: Trends Neurosci, v. 32, p. 638-47.
South, S. M., T. Kohno, B. K. Kaspar, D. Hegarty, B. Vissel, C. T. Drake, M. Ohata, S. Jenab, A. W. Sailer, S. Malkmus, T. Masuyama, P. Horner, J. Bogulavsky, F. H. Gage, T. L. Yaksh, C. J. Woolf, S. F. Heinemann, and C. E. Inturrisi, 2003, A conditional deletion of the NR1 subunit of the NMDA receptor in adult spinal cord dorsal horn reduces NMDA currents and injury-induced pain: J Neurosci, v. 23, p. 5031-40.
Srinivas, S., T. Watanabe, C. S. Lin, C. M. William, Y. Tanabe, T. M. Jessell, and F. Costantini, 2001, Cre reporter strains produced by targeted insertion of EYFP and ECFP into the ROSA26 locus: BMC Dev Biol, v. 1, p. 4.
Stearns, V., K. L. Beebe, M. Iyengar, and E. Dube, 2003, Paroxetine controlled release in the treatment of menopausal hot flashes: a randomized controlled trial: JAMA, v. 289, p. 2827-34.
Stearns, V., and J. M. Rae, 2008, Pharmacogenetics and breast cancer endocrine therapy: CYP2D6 as a predictive factor for tamoxifen metabolism and drug response?: Expert Rev Mol Med, v. 10, p. e34.
Sternberg, N., and D. Hamilton, 1981, Bacteriophage P1 site-specific recombination. I. Recombination between loxP sites: J Mol Biol, v. 150, p. 467-86.
Storck, T., S. Schulte, K. Hofmann, and W. Stoffel, 1992, Structure, expression, and functional analysis of a Na(+)-dependent glutamate/aspartate transporter from rat brain: Proc Natl Acad Sci U S A, v. 89, p. 10955-9.
Suadicani, S. O., M. H. De Pina-Benabou, M. Urban-Maldonado, D. C. Spray, and E. Scemes, 2003, Acute downregulation of Cx43 alters P2Y receptor expression levels in mouse spinal cord astrocytes: Glia, v. 42, p. 160-71.
Sucher, N. J., S. Akbarian, C. L. Chi, C. L. Leclerc, M. Awobuluyi, D. L. Deitcher, M. K. Wu, J. P. Yuan, E. G. Jones, and S. A. Lipton, 1995, Developmental and regional expression pattern of a novel NMDA receptor-like subunit (NMDAR-L) in the rodent brain: J Neurosci, v. 15, p. 6509-20.
Sun, J. J., Y. Liu, and Z. R. Ye, 2008, Effects of P2Y1 receptor on glial fibrillary acidic protein and glial cell line-derived neurotrophic factor production of astrocytes under ischemic condition and the related signaling pathways: Neurosci Bull, v. 24, p. 231-43.
Sun, W., E. McConnell, J. F. Pare, Q. Xu, M. Chen, W. Peng, D. Lovatt, X. Han, Y. Smith, and M. Nedergaard, 2013, Glutamate-dependent neuroglial calcium signaling differs between young and adult brain: Science, v. 339, p. 197-200.
Suyama, S., T. Sunabori, H. Kanki, K. Sawamoto, C. Gachet, S. Koizumi, and H. Okano, 2012, Purinergic signaling promotes proliferation of adult mouse subventricular zone cells: J Neurosci, v. 32, p. 9238-47.
Taguchi, O., and Y. Nishizuka, 1985, Reproductive tract abnormalities in female mice treated neonatally with tamoxifen: Am J Obstet Gynecol, v. 151, p. 675-8.
Talley Watts, L., S. Sprague, W. Zheng, R. J. Garling, D. Jimenez, M. Digicaylioglu, and J. Lechleiter, 2013, Purinergic 2Y1 receptor stimulation decreases cerebral edema and reactive gliosis in a traumatic brain injury model: J Neurotrauma, v. 30, p. 55-66.
Tanaka, K., K. Watase, T. Manabe, K. Yamada, M. Watanabe, K. Takahashi, H. Iwama, T. Nishikawa, N. Ichihara, T. Kikuchi, S. Okuyama, N. Kawashima, S. Hori, M. Takimoto, and K. Wada, 1997, Epilepsy and exacerbation of brain injury in mice lacking the glutamate transporter GLT-1: Science, v. 276, p. 1699-702.
Terunuma, M., P. G. Haydon, M. N. Pangalos, and S. J. Moss, 2015, Purinergic receptor activation facilitates astrocytic GABAB receptor calcium signalling: Neuropharmacology, v. 88, p. 74-81.

Thrane, A. S., V. Rangroo Thrane, D. Zeppenfeld, N. Lou, Q. Xu, E. A. Nagelhus, and M. Nedergaard, 2012, General anesthesia selectively disrupts astrocyte calcium signaling in the awake mouse cortex: Proc Natl Acad Sci U S A, v. 109, p. 18974-9.

Tonazzini, I., M. L. Trincavelli, J. Storm-Mathisen, C. Martini, and L. H. Bergersen, 2007, Co-localization and functional cross-talk between A1 and P2Y1 purine receptors in rat hippocampus: Eur J Neurosci, v. 26, p. 890-902.

Tsai, P. S., J. P. Kaufhold, P. Blinder, B. Friedman, P. J. Drew, H. J. Karten, P. D. Lyden, and D. Kleinfeld, 2009, Correlations of neuronal and microvascular densities in murine cortex revealed by direct counting and colocalization of nuclei and vessels: J Neurosci, v. 29, p. 14553-70.

Tsien, J. Z., 2000, Linking Hebb's coincidence-detection to memory formation: Curr Opin Neurobiol, v. 10, p. 266-73.

Tsien, J. Z., D. F. Chen, D. Gerber, C. Tom, E. H. Mercer, D. J. Anderson, M. Mayford, E. R. Kandel, and S. Tonegawa, 1996a, Subregion- and cell type-restricted gene knockout in mouse brain: Cell, v. 87, p. 1317-26.

Tsien, J. Z., P. T. Huerta, and S. Tonegawa, 1996b, The essential role of hippocampal CA1 NMDA receptor-dependent synaptic plasticity in spatial memory: Cell, v. 87, p. 1327-38.

Tu, J., and L. P. Wang, 2009, Therapeutic potential of extracellular ATP and P2 receptors in nervous system diseases: Neurosci Bull, v. 25, p. 27-32.

Verkhratsky, A., and G. Burnstock, 2014, Purinergic and glutamatergic receptors on astroglia: Adv Neurobiol, v. 11, p. 55-79.

Verkhratsky, A., and F. Kirchhoff, 2007, NMDA Receptors in glia: Neuroscientist, v. 13, p. 28-37.

Verkhratsky, A., M. Nedergaard, and L. Hertz, 2014, Why are Astrocytes Important?: Neurochem Res.

Verkhratsky, A., J. J. Rodríguez, and V. Parpura, 2013, Astroglia in neurological diseases: Future Neurol, v. 8, p. 149-158.

Verkhratsky, A., A. Verkhrasky, O. A. Krishtal, and G. Burnstock, 2009, Purinoceptors on neuroglia: Mol Neurobiol, v. 39, p. 190-208.

Volterra, A., N. Liaudet, and I. Savtchouk, 2014, Astrocyte Ca^{2+} signalling: an unexpected complexity: Nat Rev Neurosci, v. 15, p. 327-35.

Volterra, A., and J. Meldolesi, 2005, Astrocytes, from brain glue to communication elements: the revolution continues: Nat Rev Neurosci, v. 6, p. 626-40.

von Kügelgen, I., 2006, Pharmacological profiles of cloned mammalian P2Y-receptor subtypes: Pharmacol Ther, v. 110, p. 415-32.

Vöhringer, C., R. Schäfer, and G. Reiser, 2000, A chimeric rat brain P2Y1 receptor tagged with green-fluorescent protein: high-affinity ligand recognition of adenosine diphosphates and triphosphates and selectivity identical to that of the wild-type receptor: Biochem Pharmacol, v. 59, p. 791-800.

Washburn, K. B., and J. T. Neary, 2006, P2 purinergic receptors signal to STAT3 in astrocytes: Difference in STAT3 responses to P2Y and P2X receptor activation: Neuroscience, v. 142, p. 411-23.

Watase, K., K. Hashimoto, M. Kano, K. Yamada, M. Watanabe, Y. Inoue, S. Okuyama, T. Sakagawa, S. Ogawa, N. Kawashima, S. Hori, M. Takimoto, K. Wada, and K. Tanaka, 1998, Motor discoordination and increased susceptibility to cerebellar injury in GLAST mutant mice: Eur J Neurosci, v. 10, p. 976-88.

Weissman, T. A., P. A. Riquelme, L. Ivic, A. C. Flint, and A. R. Kriegstein, 2004, Calcium waves propagate through radial glial cells and modulate proliferation in the developing neocortex: Neuron, v. 43, p. 647-61.

Wilson, C. H., I. Gamper, A. Perfetto, J. Auw, T. D. Littlewood, and G. I. Evan, 2014, The kinetics of ER fusion protein activation in vivo: Oncogene, v. 33, p. 4877-80.

Yang, K., M. F. Jackson, and J. F. MacDonald, 2014, Recent progress in understanding subtype specific regulation of NMDA receptors by G Protein Coupled Receptors (GPCRs): Int J Mol Sci, v. 15, p. 3003-24.

Yang, T. T., C. Lin, C. T. Hsu, T. F. Wang, F. Y. Ke, and Y. M. Kuo, 2013, Differential distribution and activation of microglia in the brain of male C57BL/6J mice: Brain Struct Funct, v. 218, p. 1051-60.

Yang, Y., S. Vidensky, L. Jin, C. Jie, I. Lorenzini, M. Frankl, and J. D. Rothstein, 2011, Molecular comparison of GLT1+ and ALDH1L1+ astrocytes in vivo in astroglial reporter mice: Glia, v. 59, p. 200-7.

Yona, S., K. W. Kim, Y. Wolf, A. Mildner, D. Varol, M. Breker, D. Strauss-Ayali, S. Viukov, M. Guilliams, A. Misharin, D. A. Hume, H. Perlman, B. Malissen, E. Zelzer, and S. Jung, 2013, Fate mapping reveals origins and dynamics of monocytes and tissue macrophages under homeostasis: Immunity, v. 38, p. 79-91.

Yu, W., and W. G. Hill, 2013, Lack of specificity shown by P2Y6 receptor antibodies: Naunyn Schmiedebergs Arch Pharmacol, v. 386, p. 885-91.

Zamanillo, D., R. Sprengel, O. Hvalby, V. Jensen, N. Burnashev, A. Rozov, K. M. Kaiser, H. J. Koster, T. Borchardt, P. Worley, J. Lubke, M. Frotscher, P. H. Kelly, B. Sommer, P. Andersen, P. H. Seeburg, and B. Sakmann, 1999, Importance of AMPA receptors for hippocampal synaptic plasticity but not for spatial learning: Science, v. 284, p. 1805-11.

Zerangue, N., and M. P. Kavanaugh, 1996, Flux coupling in a neuronal glutamate transporter: Nature, v. 383, p. 634-7.

Zhang, Y., K. Chen, S. A. Sloan, M. L. Bennett, A. R. Scholze, S. O'Keeffe, H. P. Phatnani, P. Guarnieri, C. Caneda, N. Ruderisch, S. Deng, S. A. Liddelow, C. Zhang, R. Daneman, T. Maniatis, B. A. Barres, and J. Q. Wu, 2014, An RNA-sequencing transcriptome and splicing database of glia, neurons, and vascular cells of the cerebral cortex: J Neurosci, v. 34, p. 11929-47.

Zheng, W., L. Talley Watts, D. M. Holstein, J. Wewer, and J. D. Lechleiter, 2013, P2Y1R-initiated, IP3R-dependent stimulation of astrocyte mitochondrial metabolism reduces and partially reverses ischemic neuronal damage in mouse: J Cereb Blood Flow Metab, v. 33, p. 600-11.

Ziak, D., A. Chvátal, and E. Syková, 1998, Glutamate-, kainate- and NMDA-evoked membrane currents in identified glial cells in rat spinal cord slice: Physiol Res, v. 47, p. 365-75.

Zong, H., J. S. Espinosa, H. H. Su, M. D. Muzumdar, and L. Luo, 2005, Mosaic analysis with double markers in mice: Cell, v. 121, p. 479-92.

Zorec, R., A. Araque, G. Carmignoto, P. G. Haydon, A. Verkhratsky, and V. Parpura, 2012, Astroglial excitability and gliotransmission: an appraisal of Ca2+ as a signalling route: ASN Neuro, v. 4.

Zwicker, J. D., V. Rajani, L. B. Hahn, and G. D. Funk, 2011, Purinergic modulation of preBötzinger complex inspiratory rhythm in rodents: the interaction between ATP and adenosine: J Physiol, v. 589, p. 4583-600.

10 Acknowledgements

First I would like to thank Prof. Frank Kirchhoff for his support and guidance during the last years. Thank you for the calmness and patience in the moments I lost it. Thank you for wanting the best for all of us. In addition, I owe my gratitude to Prof. Alexei Verkhratsky who took over the supervision during my stays at the University of Manchester. Thank you for your help and support in scientific and bureaucratic issues. Not all students are privileged to be accompanied by a professor to open a bank account. You will stay as my „Doktorväter“ in my mind.
In addition I thank our collaborators Dr. Ulyana Lalo and Dr. Yuriy Pankratov for teaching me the basics in electrophysiology and initial experiments in regard to the NMDAR project.
Furthermore, I really appreciated being part of the EduGlia family. I enjoyed our meetings and travels a lot. I thank the PIs for their open ears and spirits and especially the fellows for their loving support and the believe in each others strengths. I owe an extra big hug to my special fellow and friend Cai (Xianshu Bai): Thank you so much for our time together in the lab and outside in this world - best roommate I could wish for ;) and for the corrections of my never ending writing.
Furthermore, I am deeply thankful to Dr. Anja Scheller: Thank you for keeping us togehter, thank you for the discussions, your suggestions and corrections of my thesis and especially for your comfortable warmth and trust.
I thank from the heart all members of the Kirchhoff lab for our team spirit. Frank Rhode: Thank you so much for your help in the lab and even more for your mental support, you are a great psychologist. Daniel Rhode: Thank you so much for taking care of my mice, drawing attention to weird requests and being the reliable backbone of my experiments. Laura Schlosser: Thank you for your optimistic character and your motivation to get things done for the lab. Dr. Fei (Wenhui) Huang and Na Zhao: thank you for our efficient mensa runs and even more for your delicious chinese cooking at your places. Fei, thanks for listening, thanks for your corrections, your believe in me and scientific input. Na, thanks for being my desk neighbour, I love your attitude and your talent to cheer me up.
I am still thankful to Dr. Aiman Saab. It takes a lot of efforts to be a good mentor and teacher. You did a great job in being mine. In retrospect I am even more thankful that you filtered my chaotic thoughts and gave me a red line to work for. In this context I am deeply thankful to Carmen Bohn who allowed me to be her mentor. Thank you for dealing with me and my confusion the one or other day ;). Thank you for your trust, your skilled manual work and corrections. It makes it easier to leave knowing that you will be the one who continues to fight for an happy end of our $P2Y_1R$ and NMDAR story.
I don‘t want to forget Dr. Alexander Cupido and Dr. Bogdan Catalin: Thank you for your company and humor during working and pub hours. I missed you guys here.
I am likewise thankful to the „Hoths“ next door for scientific help and the nice working atmosphere.
And I want to thank two lovely ladies, Anna Schneider und Hélène Lyrmann: Thank you so much that you have been there for me the last three years. Thank you for your friendship, it means a lot to me!
I am further deeply thankful that I got the chance to meet my Göttinger MPI Mädels: Theresa Kungl, Lotti Supplie, Sarah Richert, Ulrike Gerwig and Elina Ott. We went through a lot - bad and so much more good moments, we traveled, partied, laughed, loved and hated science togehter. I look up to everyone of you as great humun beings. I missed you so much in Saarbrücken.
Isolde Hoberg, Hase: I am so happy to have you in my life! You kept me rocking this world in so many uncountable moments already. Thank you for your straight words. I appreciate them a lot!
And I am not less thankful to Sandra Oetjen, Kambulakwao Chakanga, Sarah Narkus, Katja Kühbach und Mareike Volkenandt for our joint task force when we started our scientific career at the University of Oldenburg. Great memories and great friends. Thank you so much girls.
Ich danke Andreas Weber, Carolin Walther und Thorsten Klimeck: Ihr habt mich so herzlich in Saarbrücken aufgenommen und es zu meinem zu Hause gemacht, auch wenn wir das letzte Jahr eigene Wege gegangen sind. Danke für die tollen Momente, die ich mit euch erlebt habe.

Danke, dass ich bei euch die Arbeit vergessen oder diskutieren konnte. Danke, dass ihr wirklich da wart, auch in Momenten, die für mich nicht leicht waren. Eurer Rückhalt und Verständnis war sehr viel wert und keine Selbstverständlichkeit. Ebenfalls danke ich den Jungs und Mädels der „Pokerrunde“ für viele tolle Abende in der WG und Nächte in Saarbrücken.
Mein ganz besonderer Dank gilt zudem den Wassernballern des SV08 Saarbrücken. In vielen Aspekten wart ihr wichtiger für mich als ihr es vermutet. Danke, für die Montag- und Mittwoch-abende und Wochenenden die wir zusammen im Wasser oder am Land verbracht haben. Ihr seid ein wahnsinniges sympathisches Team mit einem tollem Zusammenhalt. Ihr seid ein Grund warum ich dieses kleine Bundesland sehr vermissen werde!
Zudem bin ich meinen Freunden in meiner Heimatstadt Salzgitter-Bad sehr dankbar! Danke, dass ich immer zurückkehren darf, im Besonderem Florian Gorsolke, Meike Tworowski, Carina Vahldieck, und Carina Schulz.
Und auch wenn alles nur mit einem Jahr in NYC begann, Doreen Kittler und Florian Türke, ich danke euch ebenso für die jahrlange Unterstützung und Freundschaft, die uns mittlerweile verbindet.
Und ich danke all den Menschen, die mir ebenso wichtig sind, die ich hier allerdings nicht gesondert erwähnt habe.
Mein ganz besonderer Dank gilt meiner Familie: Mama, Papa, ihr habt mich bei jedem Schritt begleitet und unterstützt. Ihr habt mir den Freiraum und die Stärke für eigene Entscheidungen, Fehler und Träume gegeben. Eurer bedingsloser Halt ist unersetzbar! Ihr seid Teil meines Erfolges und ich verdanke euch, wer ich heute bin. Alina + Holger, Milena + Florian und Jonas, ihr akzeptiert mich mit meinen ganzen Fehlern, als wären diese nicht existent ;) Ich danke euch vom tiefsten Herzen, dass ihr mich und mein Handeln versteht. Dieses Verständnins und Mitgefühl war die beste Unterstützung in diesen auch zugegeben etwas anstrengenden vier Jahren. Oma Mommel (Wilma) ich danke dir für deinen messerscharfen Verstand, du findest für jede Situation die richtigen Worte. Sie sind gespeichert ;) Oma Bringfriede, ich danke dir für unsere gemeinsame Zeit und Liebe. Ihr seid meine Lieblingsmenschen und mein Zuhause. Danke, dass es euch gibt!

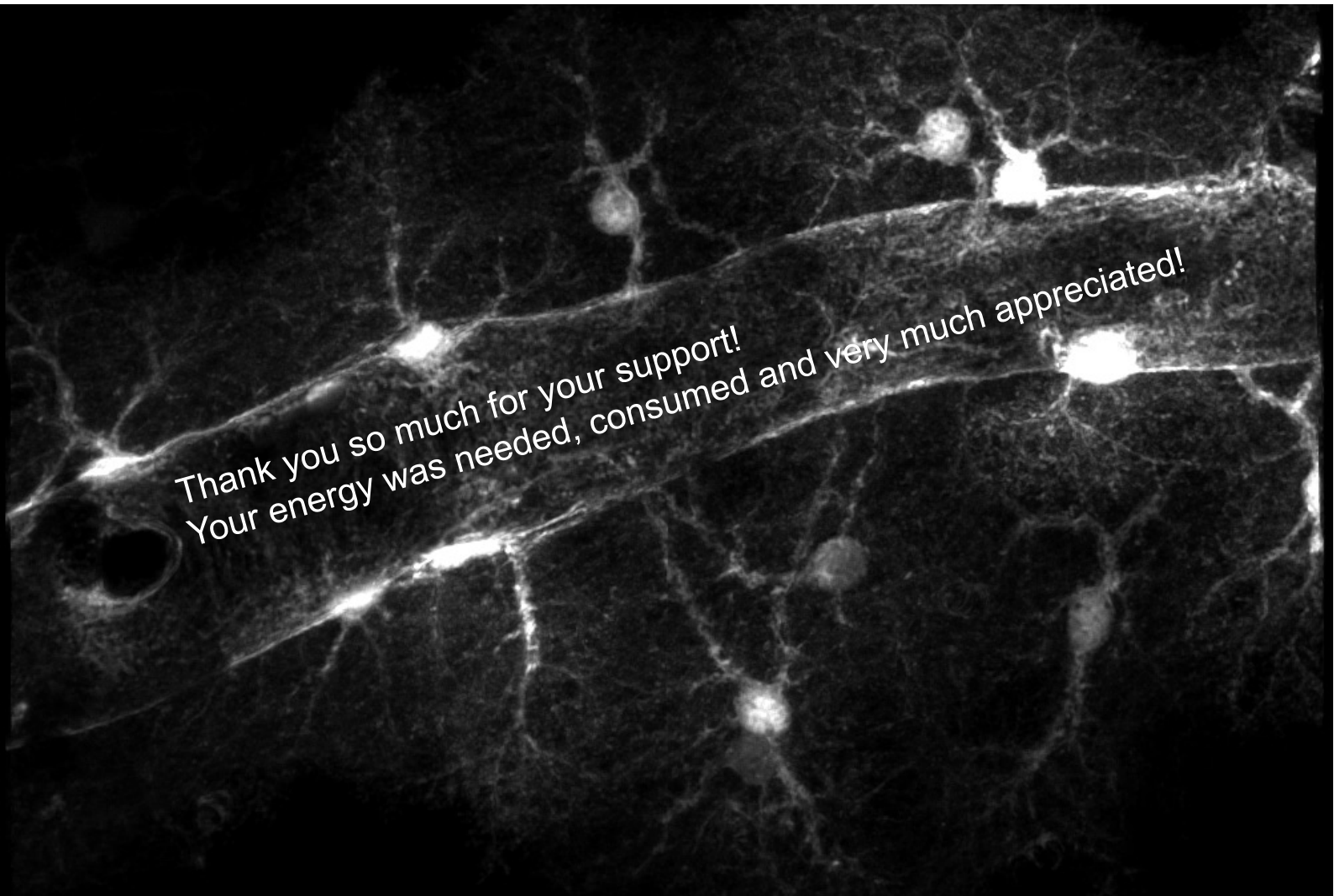

11 CV, Publications and Presentation

Aus Datenschutzgründen wird der Lebenslauf in der hier veröffentlichten elektronischen Version nicht gezeigt.

These informations are excluded in the published electronic version due to data security issues.